TARGETING SPLICE FACTOR KINASES IN CHRONIC MYELOID LEUKAEMIA

by

Hanan A. Alabouh

A thesis submitted in partial fulfilment of the requirements of the University of the West of England, Bristol for the degree of Doctor of Philosophy

January 2017

Supervisors:

Dr. Michael Ladomery

Dr. Sebastian Oltean

Dr. Ruth Morse

Prof. John Hancock

DECLARATION

I, Hanan AbdulAziz Alabouh, confirm that the work presented in this thesis is my entirely my own work. I have exercised reasonable care to ensure that the work is original, and does not to the best of my knowledge brech any law copyright.

ACKNOWLEDGEMENT

This PhD journey has been one of memorable encounters, valuable lessons and self-discovery. I am very thankful to the Government of Kuwait for the scholarship that has allowed me to undertake an MSc and PhD at University of West of England, Bristol. I am grateful to the Kuwait Cultural Office (KCO) for taking me in with open arms and hearts; Dr. Fawzan AlFares (head of office), Mrs. Wafa Alkharji, Amina McCulloch, Saif Basheer and Mahasin El-Gaddal.

I would like to thank UWE and my supervisors for this opportunity to do this project. Special thanks to my friends in UWE for their support, tears, and the laughter. Thank you Kannan Vembu for his technical support. Special thanks to Dr. Yasmine Asi and Sezab Idris for their support and advices.

I am grateful to my second supervisor Dr. Sebastian Oltean and all of my friends in UoB, especially Dr. Maryam Hamdollah-Zadeh and Dr. Hesham Elhegni for their positive encouragement and support. I am grateful for the opportunity of joining their lab.

Last but not least ─ I would like to thank my family. To my parents and my sister, Manal Alabouh for their unwavering support and love.

I would like also to take this oppourtunity to thank my lovely daughter Latifah Alasfour who always believes that I could finish this thesis.

DEDICATION

For my aunt, Khalti Mothi Al-Omair (2016)

خالتي موضي العمير

For my sister from a different mother, Pam Knox (2016)

May their souls rest in peace.

TABLE OF CONTENTS

LIST OF FIGURES

LIST OF TABLES

ABBREVIATIONS

3’ SS selection	Alternative 3’ splice site selection
5’ SS selection	Alternative 5’ splice site selection
ABL1	Abelson murine leukaemia viral oncogene homology
aCML	Atypical chronic myeloid leukemia
AIF	Apoptosis-inducing factor
AKT	Phosphatidylinositol 3-kinase
AML	Acute myeloid leukaemia
AML1	Acute myeloid leukaemia 1
Annexin V-FITC+ and PI-	Annexin V-FITC positive and PI negative
Annexin V-FITC+ and PI+	Annexin V-FITC positive and PI positive
AO	Acridine orange
AP	Accelerated phase
APAF-1	Apoptotic caspase activating factor-1
Apo	Apoptosis
AS	Alternative splicing
asHTF	Alternative spliced human TF
ATP	Adenosine triphosphate
BC	Blast crisis
Bcl-2	B-cell lymphoma-2

Bcl-xL	B-cell lymphoma extra large
BCR	Breakpoint cluster region
BM	Bone marrow
BMT	Bone marrow transplantation
BP	Branchpoint
bp	Base pairs
CBF	Core binding factor
CBFα2	Core-binding factor α2
Cdc-like-kinase	Cycline dependent like kinase
cDNA	Complementary DNA
CHR	Complete haematologic response
Clk1	Cdc2-like kinase 1
CLPs	Common lymphoid progenitors
CML	Chronic myeloid leukaemia
CMML	Chronic myelomonocytic leukaemia
CMPs	Common myeloid progenitors
CNL	Chronic neutrophilic leukaemia
CP	Chronic phase
CQ	Chloroquine
DISC	Death initiation signalling complex
DMEM	Dolbecco's Modified Eagle Medium
DMSO	Dimethyl sulfoxide

ECL	Enhanced chemoluminiscence
EGF	Epidermal growth factor
EGFR	Epidermal growth factor receptor
EMA	European medicines agency
ESE	Exonic splicing enhancer
ESEs	Exonic splicing enhancers
ESSs	Exonic splicing silencers
ET	Essential thrombocythemia
EtBr	Ethidium bromide
FDA	US Food and Drug Administration
FGFR	Fibroblast growth factor receptor
flTF	Full-length TF
GFP	Green fluorescent protein
GMPs	Granulocytes and macrophages progenitors
Grb2	Growth factor receptor-bound protein 2
GvHD	Graft versus host disease
HATs	Histone acetyltransferases
Hck	Haemopoietic cell kinase
HCV	Hepatitis C virus
HDACs	Histone deacetyleases
HGF	Hepatocyte growth factor

HGFR	Hepatocyte growth factor
Hh	Hedgehog
HIV	Human immunodeficiency virus
HL	Hodgkin lymphoma
HMEC-1	Human microvascular endothelial cells
hnRNPs	Heterogeneous nuclear ribonucleoprotein
HRS	Hodgkin/reed-Sternberg
HSC	Haematopoietic stem cell
IAPs	Inhibitory of apoptosis proteins
IFN	Interferon
IgG	Immunoglobulin g
IM	Imatinib mesylate
IM-Gleevec	Imatinib mesylate
InsR	Insulin receptor
ISEs	Intronic splicing enhancers
ISSs	Introns splicing silencers
JAK	Janus kinase
JMML	Juvenile myelomonocytic leukaemia
m-BCR	Minor breakpoint cluster region
M-BCR	Major breakpoint cluster region
MAPKK or MEX or MAPK2	MEK, MAP kinase kinase

Mcl-1	Myeloid cell leukaemia-1
MDS	Myelodysplastic syndromes
MDS-RS	MDS with ring sideroblasts
MDS/MPN	Myelodysplastic/myeloproliferative neoplasms
MDS/MPN-RS-T	MDS/MPN with ring sideroblasts and thrombocytosis
MEPs	Megakaryocyte/erythrocyte progenitors
Met	Hepatocyte growth factor (HGFR)
MPAL	Mixed phenotype acute leukaemia
MPN	Myeloproliferative neoplasms
MPNs	Myeloproliferative neoplasms
MPPs	Multipotent progenitors
MSP	Macrophage-stimulating protein
MST1R	Macrophage stimulating protein receptor
mTOR	Mammalian target of rapamycin
NC	Necrotic cells
NKC	Natural killer cells
NMD	Nonsense-mediated mRNA decay
NOS	Not otherwise specified
nRTKs	Non-receptor tyrosine kinases
NXF1/TAP	Nuclear RNA export factor 1/Tip-associated protein
OMM	Outer mitochondrial membrane

PC-3	Prostate cancer cell line
PCR	Polymerase chain reaction
PDGF	Platelet Derived Growth Factor
PEBP2αB	Polymavirus enhancer binding protein 2αb
PH	Pleckstrin homology
Ph+	Philadelphia chromosome (page number 9)
Ph+	Philadelphia positive
PMF	Primary myelofibrosis
PP1	Protein phosphatase 1
PP2A	Protein phosphatase 2A
pre-mRNAs	Precursor messenger RNAs
PRMT1	Protein arginine methyltransferase 1
proMSP	proteolytic cleavage of a single chain
PTCs	Premature termination codons
PTMs	Post-translational modifications
PV	Polycythemia vera
Py	Polypyrimidine
qRT-PCR	Quantitative real-time PCR
Ras	Rat sarcoma viral oncogene homolog
RNAP II	RNA polymerase II
RON	Recepteur d’origine nantais

RRM	RNA recognition motif
RRMH	RNA recognition motif homology
RS	Arginine/serine-rich domain
RT-PCR	Reverse transcription polymerase chain reaction
RT-VE	Reverse transcriptase negative control
RTK	Receptor tyrosine kinase
RTKs	Receptor tyrosine kinases
Runx1	Runt-related transcription factor 1
RUNX1-ETO	Runt-related transcription factor 1- eight twenty-one
SF1	Splice factor 1
sh-CTRL	scrambled shRNA
si-CTRL	Scrambled control siRNA
siRNA	Small interfering RNA
snRNPs	Small nuclear ribonucleoproteins.
Sos	Son of sevenless
SPHINX	SR protein Inhibitor X
SR proteins	Serine/arginine-rich proteins
SRPIN340	Specific serine/threonine protein kinase inhibitor 340
SRPIN349	Negative SR protein inhibitor 349
SRPK1	Serine arginine protein kinase-1

SRPKs	Serine/arginine protein kinase family
SRSF1	Serine/arginine-rich splicing factor 1
STAT	Signal transducers and activators of transcription
Stem cell factor	(c-kit)
TAM	Transient abnormal myelopoiesis
TKI	Tyrosine kinase inhibitor
TKIs	Tyrosine kinase inhibitors
TRN-SR	Transportin-SR
U2AF-35 and U2AF-65	Heterodimeric splice factor U2 auxiliary factor
VC	Viable cells
VEGF	Vascular endothelial growth factor
VEGFA	Vascular endothelial growth factor A
WBC	White blood cell
WHO	World Health Organization
Zn	Zinc
α- tubulin	Alpha tubulin
μ-BCR	Micro breakpoint cluster region

ABSTRACT

Alternative splicing of pre-mRNA is a ubiquitous and versatile mechanism controlling the expression of human genes. In humans, approximately 93% of multi-exonic genes are alternatively spliced, producing functionally distinct proteins. Dysregulation of alternative splicing results in the overexpression of the oncogene splice factor SRSF1, which has been implicated in various types of tumours. Initial research has shown that the alternatively spliced isoforms of vascular endothelial growth factor (VEGF) (pro-angiogenic) promotes tumorigenesis. VEGF is regulated through serine-arginine (SR)-specific protein kinase SRPK1 and SRSF1. Additionally, the activity and intracellular localisation of the SRSF1 is regulated by the kinases SRPK1 and Clk1. Therefore, it is worthly to target SRPK1 and SRSF1 in chronic myelogenous leukaemia cell line (K562 cells).

Chronic myeloid leukaemia (CML) is a myeloproliferative disorder of stem cell origin. It arises from *BCR-ABL1* fusion forming the Philadelphia chromosome. This fusion leads to a constitutively activated tyrosine kinase. Treatment of CML was revolutionised by tyrosine kinase inhibitors (TKIs). Despite the success of TKI in eliminating CML, drug resistance develops in patients over time. Allogenic bone marrow transplantation (BMT) is the only curative therapy, however the mortality rates increase due to infection.

The precise role of SRPK1 and Clk1 in haematological malignancies is unclear. This study has sought to target SRPK1, Clk1, TK and SRSF1 through inhibition or knockdown to identify the effects of alternative splicing on the expression of *CASPASE-9*, *RON* and *RUNX1* in K562 cells. Additionally, this study would

investigate the drug efficacy of imatinib (TK inhibitor) used in conjunction with either SPHINX (SRPK1 inhibitor) or TG003 (Clk1 inhibitor) in K562 cells. In this study, it may identify novel therapeutic targets that could be beneficial for patients with leukaemia.

This study demonstrated that targeting SRPK1 and SRSF1 through inhibition or knockdown had little or no significant positive effect on the alternative splicing of *CASPASE-9*, *RON* and *RUNX1* in K562 cells. Comparatively, targeting Clk1 with the selective inhibitor TG003, resulted in significantly positive effects on the alternative splicing for both *CASPASE-9* and *RON* and *RUNX1*. This was confirmed by increased apoptosis of K562 cells. Knockdown studies of Clk1, showed a significant effect on *RUNX1* only, eliciting the production of the Runx1 isoform. Finally, co-treatment of imatinib (TK inhibitor) and SPHINX elicited an effect on alternative splicing resulting in an overall shift to the pro-apoptotic isoforms using minimal doses of the drugs. Additionally, combinations of kinase inhibitors (imatinib and TG003) exhibited a more effective shift in *RON* splicing towards Ron isoforms. This suggests that co-therapy may offer a potential therapy for CML patients.

The introduction of tyrosine kinase inhibitors has successfully improved the prognosis of CML. However, intrinsic and acquired resistance to imatinib is becoming an ever-increasing clinical problem. This study, for the first time, has demonstrated novel therapeutic target to Clk1 that affects the alternative splicing of *CASPASE-9*, *RON* and *RUNX1* in K562 cells. Targeting of the genes is essential in the treatment of CML as cell differentiation, migration, invasion and apoptosis are

affected. This study not only shows that the Clk1 selective inhibitor TG003 is beneficial on alternative splicing of *CASPASE-9* but conjucated inhibitors of imatinib and SPHINX induce a greater effect on the splicing of *CASPASE-9* in K562 cells. Compared to the use of imatinib alone, co-treatment using both drugs maybe more effective in the treatment of CML and therefore may circumvent acquired drug resistance seen in patients with leukaemia.

CHAPTER 1. INTRODUCTION

1.1 Haematopoiesis and haemopoietic stem cells

Haematopoiesis is a hierarchical process in bone marrow whereby all mature blood cells are generated from haematopoietic stem cells (HSCs) (Figure 1.1), which are multipotent cells that located in bone marrow. HSCs can self-renew to produce more HSCs and they can differente into many cell types through multipotent progenitors (MPPs) (Morrison, Uchida and Weissman, 1995). HSCs differentiate into common myeloid progenitors (CMPs) and common lymphoid progenitors (CLPs) terminating mature myeloid and lymphoid cells. The CMPs can differentiate into all myeloid lineages through megakaryocyte/erythrocyte progenitors (MEPs) and granulocytes and macrophages progenitors (GMPs). MEPs can differentiate further into mature red blood cells and platelets, while monocytes and granulocytes resulted from GMPs. In addition, CLPs can differentiate to lymphocytes (T- or B-cells) and natural killer cells (NKCs) (Morrison, Uchida and Weissman, 1995).

The proliferation and differentiation of MPPs, along with GMPs and CLPs leads to the production of differentiated and functional haematopoietic cells, allowing the cells to react to haematopoietic crises, including blood loss or infection (Shao *et al.*, 2013) HSCs are regulated by several growth factors (Zhang and Lodish, 2008), for example, the development of megakaryocytes and platelet formation are regulated by interleukins (IL-3, IL-6 and IL-11) along with thrombopoietin (TPO) (Buza-Vidas *et al.*, 2006; Fortunel, Hatzfeld and Hatzfeld, 2000).

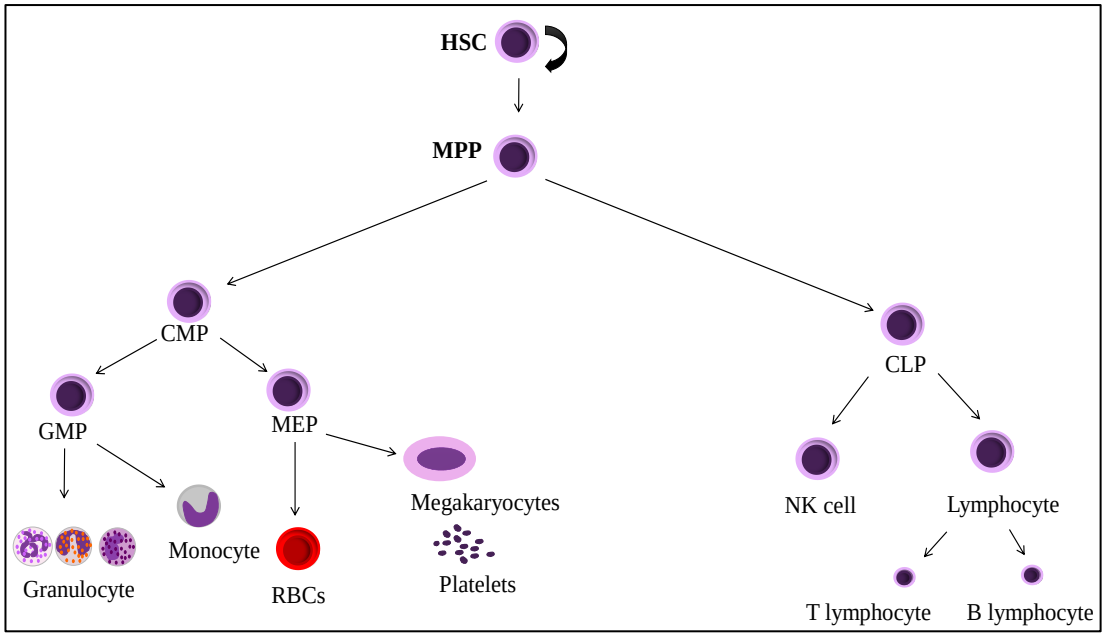

Figure 1.1. A diagram of normal haematopoietic system
The development of blood cells from haematopoietic stem cells (HSCs) to mature blood cells through multipotent progenitors (MPPs). CMPs, common myeloid progenitors; CLPs, common lymphoid progenitors; GMP, macrophages progenitors; MEP, megakaryocyte/erythrocyte progenitors.

1.1.1. Leukaemia

Leukaemia or haematologic malignancy refers to an overproduction of immature leukocytes in the bone marrow leading an inhibition in the production of mature blood cells, causing anaemia, fatigue and other symptoms (Hoffbrand *et al.*, 2011). The incidence of chronic myeloid leukaemia (CML) is estimated at approximately 10 in 1,000,000 each year (Warmuth, Danhauser-Riedl and Hallek, 1999); in 2013 in the UK, approximately 710 individuals were diagnosed with CML (Cancer Research UK, 2016). The disorder can be diagnosed using several methods including blood tests, bone marrow (BM) aspiration, BM trephine biopsy, cytochemistry, histology, flow cytometeric immunophenotyping, immunohistochemistry, cytogenetic analysis, fluorescence in situ hypbridisation (FISH) and other molecular genetic analyses (Hoffbrand *et al.*, 2011). The factors leading to an increase in the risk of developing leukaemia are listed in Table1.1.

Table 1.1. Genetic or environmental risk factors identified in leukaemia

Congenital and inherited syndromes
Inherited bone marrow hypoplasia syndromes Fanconi anaemia Schwachman–Diamond syndrome Dyskeratosis congenita DNA repair defects Bloom syndrome (DNA helicase mutations) Ataxia telangiectasia Inherited predisposition to haematological malignancies Chronic lymphocytic leukaemia Acute myeloid leukaemia Lymphoma Myeloma Polycythaemia vera Essential thrombocythaemia Down syndrome
Environmental risk factors
Exposure to genotoxic mutagens Atomic bombs Chemotherapy Radiotherapy Benzene Infections HTLV-1 HIV Epstein-Barr virus Helicobacter pylori Immunosuppressive drugs

According to the French-American-British (FAB) classification system, leukaemia can be classified as acute or chronic and is further classified depending on cell lineage as myeloid and lymphoid. This generates four major types of leukaemia: 1) acute myeloid leukaemia (AML), 2) acute lymphocytic leukaemia (ALL), 3) chronic myeloid leukaemia (CML) and 4) chronic lymphocytic leukaemia (CLL) (Jones, 2010). The World Health Organization (WHO) also classifies leukaemia into

myeloproliferative neoplasms (MPNs) and acute myeloid leukaemia (AML) (Arber *et al.*, 2016), Table 1.2.

Table 1.2. The WHO myeloid neoplasm and acute leukaemia classification system

Myeloproliferative neoplasms (MPN)
Chronic Myeloid Leukaemia (CML), BCR-ABL1^{+}
Chronic Neutrophilic Leukaemia (CNL)
Polycythemia Vera (PV)
Primary MyeloFibrosis (PMF)
PMF, prefibrotic/early stage
PMF, overt fibrotic stage
Essential Thrombocythemia (ET)
Chronic Eosinophilic Leukaemia, Not Otherwise Specified (NOS)
MPN, unclassifiable
Mastocytosis
Myeloid/lymphoid neoplasms with eosinophilia and rearrangement of PDGFRA, PDGFRB, or FGFR1, or with PCM1-JAK2
Myeloid/Lymphoid Neoplasms with PDGFRA rearrangement
Myeloid/Lymphoid Neoplasms with PDGFRB rearrangement
Myeloid/Lymphoid Neoplasms with FGFR1 rearrangement
Provisional entity: Myeloid/Lymphoid Neoplasms with PCM1-JAK2
Myelodysplastic/myeloproliferative neoplasms (MDS/MPN)
Chronic Myelomonocytic Leukaemia (CMML)

Atypical Chronic Myeloid Leukaemia (aCML), BCR-ABL1
Juvenile Myelomonocytic Leukaemia (JMML)
MDS/MPN with Ring Sideroblasts and Thrombocytosis (MDS/MPN-RS-T)
MDS/MPN, unclassifiable
Myelodysplastic syndromes (MDS)
MDS with single lineage dysplasia
MDS with Ring Sideroblasts (MDS-RS)
MDS-RS and single lineage dysplasia
MDS-RS and multilineage dysplasia
MDS with multilineage dysplasia
MDS with excess blasts
MDS with isolated del(5q)
MDS, unclassifiable
Provisional entity: Refractory cytopenia of childhood
Myeloid neoplasms with germ line predisposition
Acute myeloid leukemia (AML) and related neoplasms
AML with recurrent genetic abnormalities
AML with t(8;21)(q22;q22.1); RUNX1-RUNX1T1
AML with inv(16)(p13.1q22) or t(16;16)(p13.1;q22);CBFB-MYH11
APL with PML-RARA
AML with t(9;11)(p21.3;q23.3);MLLT3-KMT2A
AML with t(6;9)(p23;q34.1);DEK-NUP214
AML with inv(3)(q21.3q26.2) or t(3;3)(q21.3;q26.2); GATA2, MECOM

AML (megakaryoblastic) with t(1;22)(p13.3;q13.3);RBM15-MKL1
Provisional entity: AML with BCR-ABL1
AML with mutated NPM1
AML with biallelic mutations of CEBPA
Provisional entity: AML with mutated RUNX1
AML with myelodysplasia-related changes
Therapy-related myeloid neoplasms
AML, NOS
AML with minimal differentiation
AML without maturation
AML with maturation
Acute myelomonocytic Leukemia
Acute Monoblastic/Monocytic Leukemia
Pure erythroid leukemia
Acute Megakaryoblastic Leukemia
Acute Basophilic Leukemia Acute Panmyelosis with Myelofibrosis
Myeloid Sarcoma
Myeloid proliferations related to Down syndrome
Transient Abnormal Myelopoiesis (TAM)
Myeloid Leukemia associated with Down syndrome
Blastic plasmacytoid dendritic cell neoplasm
Acute Leukemia's of ambiguous lineage
Acute undifferentiated Leukemia

Mixed phenotype Acute Leukemia (MPAL) with t(9;22)(q34.1;q11.2); BCR-ABL1
MPAL with t(v;11q23.3); KMT2A rearranged
MPAL, B/myeloid, NOS
MPAL, T/myeloid, NOS
B-lymphoblastic leukemia/lymphoma
B-Lymphoblastic Leukaemia/Lymphoma, NOS
B-Lymphoblastic Leukaemia/Lymphoma with recurrent genetic abnormalities
B-Lymphoblastic Leukaemia/Lymphoma with t(9;22)(q34.1;q11.2);BCR-ABL1
B-Lymphoblastic Leukaemia/Lymphoma with t(v;11q23.3);KMT2A rearranged
B-Lymphoblastic Leukaemia/Lymphoma with t(12;21)(p13.2;q22.1); ETV6-RUNX1
B-Lymphoblastic Leukemia/Lymphoma with hyperdiploidy
B-Lymphoblastic Leukemia/Lymphoma with hypodiploidy
B-Lymphoblastic Leukemia/Lymphoma with t(5;14)(q31.1;q32.3) IL3-IGH
B-Lymphoblastic Leukemia/Lymphoma with t(1;19)(q23;p13.3);TCF3-PBX1
Provisional entity: B-Lymphoblastic Leukemia/Lymphoma, BCR-ABL1–like
Provisional entity: B-Lymphoblastic Leukemia/Lymphoma with iAMP21
T-Lymphoblastic Leukemia/Lymphoma
Provisional entity: Early T-cell precursor Lymphoblastic Leukaemia
Provisional entity: Natural killer (NK) cell Lymphoblastic

Leukaemia/Lymphoma

1.2 Chronic Myeloid Leukaemia (CML)

CML is a myeloproliferative disorder of haematopoietic stem cells (HSC) and arises from the fusion of the *ABL1* gene (Abelson murine leukaemia viral oncogene homology) to *BCR* (breakpoint cluster region) resulting in the *BCR–ABL1* oncogene (Kokate, Dalvi and Mandava, 2015). The fusion of *BCR–ABL1* occurs from reciprocal translocation between chromosomes 9 and 22, t(9;22)(q34;q11), which is termed the Philadelphia chromosome (Ph+), Figure 1.2 (Zhu *et al.*, 2015).

In 1960, Peter Nowell discovered the Ph^+ and named it after the US city (NOWELL and HUNGERFORD, 1960). It is common to find Ph^+ in more than 95% of CML patients (Warmuth, Danhauser-Riedl and Hallek, 1999), however, the Ph^+ can also be found in ALL (Koo, 2011). Although rare in ALL, (less than 5%), the presence of the Ph^+ is considered a very high risk in paediatric patients (Koo, 2011).

The fusion of *BCR–ABL1* generates three distinct proteins (P190, P210 and P230) according to the breakpoints cluster region on *BCR* on chromosome 22. The breakpoint in *ABL1* is usually in exon 2 (Li *et al.*, 1999). The minor breakpoint cluster region (m-*BCR*) occurs between *BCR* exon e1 and *ABL* exon a2 resulting in e1a2 mRNA (Deininger, Goldman and Melo, 2000).

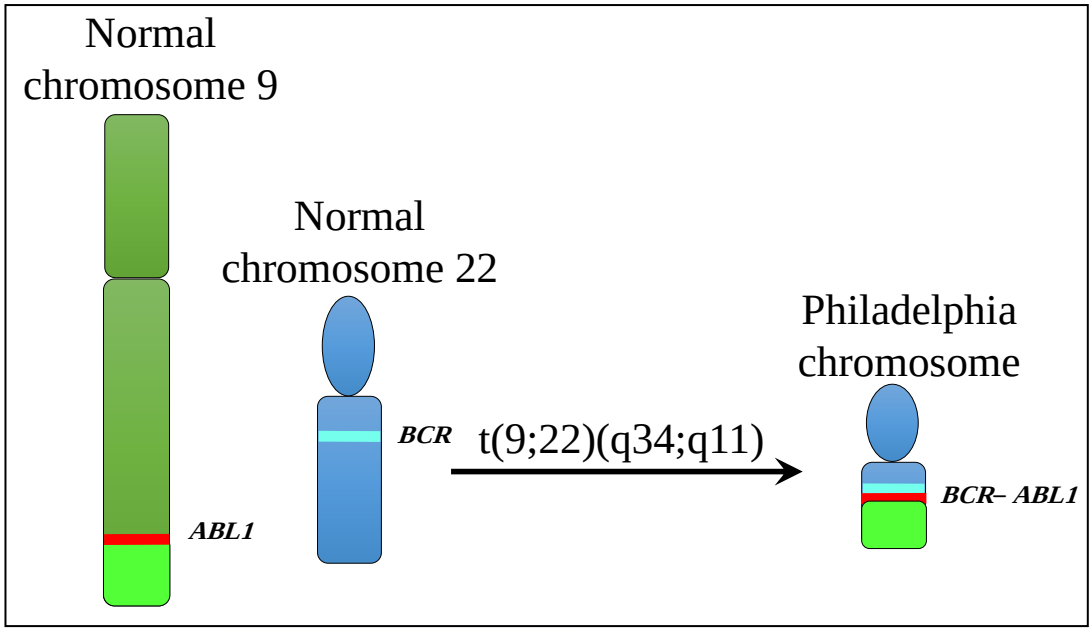

Figure 1.2. The Philadelphia chromosome
The reciprocal translocation between chromosome 9 and 22 fusing *BCR* to *ABL1*, generates the Philadelphia chromosome.

The protein is translated as $P190^{BCR\text{-}ABL}$ and is commonly detected in ALL patients (Uchida *et al.*, 2009). The major breakpoint cluster region (M-*BCR*) lies between *BCR* exons e13 (b2) or e14 (b3) and *ABL* exon a2 to produce b2a2 mRNA or b3a2 mRNA and gives rise to the protein product; $P210^{BCR\text{-}ABL}$ (Bernt and Hunger, 2014; Deininger, Goldman and Melo, 2000). It has been reported that $P210^{BCR\text{-}ABL}$ is commonly detected in CML patients (Uchida *et al.*, 2009). In rare cases of CML, the micro breakpoint cluster region (μ-*BCR*) lies between exons 19 and *ABL* exon a2 producing e19a2 mRNA and the $P230^{BCR\text{-}ABL}$ protein product, Figure 1.3 (Deininger, Goldman and Melo, 2000; Uchida *et al.*, 2009). These different fusion proteins express the same levels of c-ABL tyrosine kinase, however they differ in terms of *BCR* sequence (Sawyers *et al.*, 2002).

CML is characterised by increased the proliferation of immature granulocytic cells line.

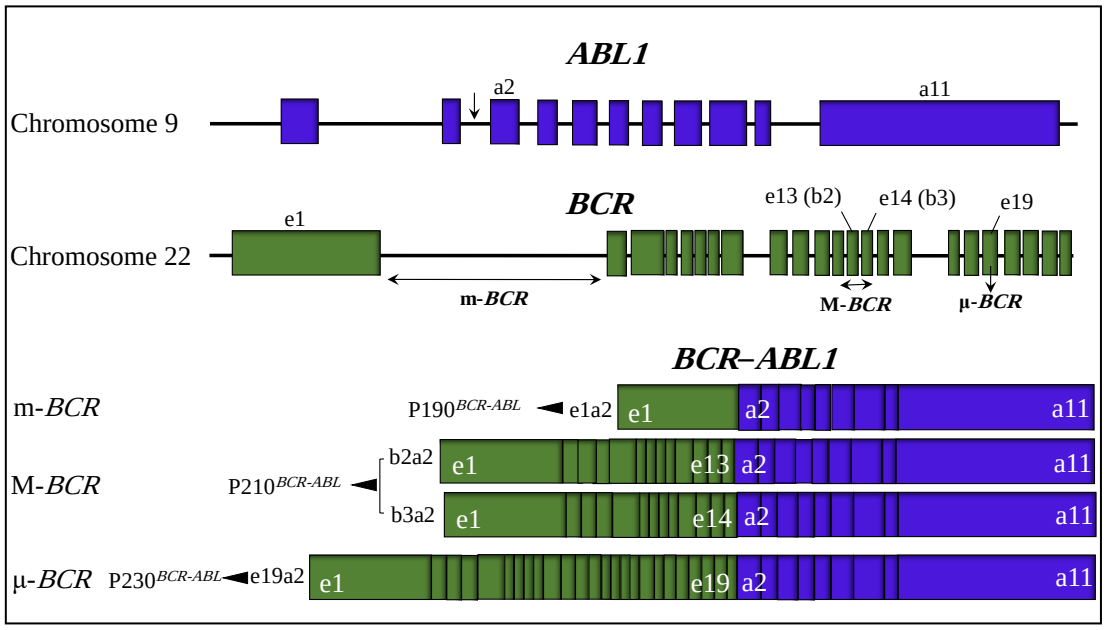

Figure 1.3. The three forms of the *BCR–ABL1* oncogene
The arrows indicate the breakpoints in *ABL1* and *BCR* producing the various breaks. The breakpoint in *ABL1* is in exon a2 while *BCR* breaks at three distinct locations. The minor (m-*BCR*) occurs in fusions with *BCR* exon e1 resulting in e1a2 mRNA and translating as $P190^{BCR-ABL}$, whereas the major (M-*BCR*) results from fusions with *BCR* exon e13 (b2) or e14 (b3) to produce b2a2 mRNA or b3a2 mRNA generating $P210^{BCR-ABL}$. The rare form of CML is the micro (µ-*BCR*) cluster, which is results from fusion with *BCR* exon e19 producing e19a2 mRNA, translating as $P230^{BCR-ABL}$ protein.

The disease progresses from a benign chronic phase (CP) to an accelerated phase (AP) and terminates in blast crisis (BC) (Giles *et al.*, 2004). The progression from CP to BC occurs by continuous activation of *BCR–ABL1* leading to increased cell proliferation, reactive oxygen species (ROS) generation, and activation of DNA damage with impairments in DNA repair, multiple mutations causing genomic instability, gene doubling, translocations and chromosomal breakage, Figure 1.4 (Hehlmann, 2012).

Additional CML genetic abnormalities, other than the *BCR–ABL1* fusion, include a double Ph^+ chromosome, isochromosome i(17q), trisomy 8, trisomy 19, loss of chromosome 9, mutations in tumour-suppressor genes such as *p53*, *INK4A/ARF* and *RB*.

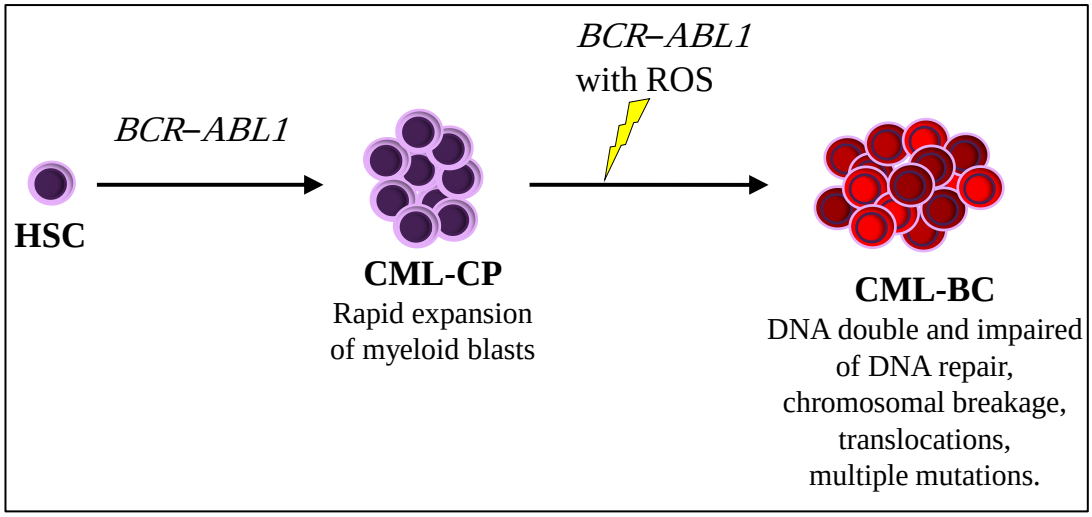

Figure 1.4. The role of *BCR–ABL1* in CML progression to blast crisis (BC)
The fusion of *BCR–ABL1* stimulates cell proliferation in CML-CP accompanied by ROS activation, leading to DNA double breakages, genetic instability, chromosomal breakages, translocations and multiple mutations.

It has been also identified that the RUNX1/MDS1/EVI1 fusion, generated from t(3;21)(q26;q22), and the NUP98/ HOXA9 fusion, generated from t(7;11)(p15;p15), develop CML to BC (Zhao *et al.*, 2012). Previous studies have shown that mutations in *RUNX1* associate with the *BCR–ABL1* fusion promoting the acute myeloid leukaemia transformation of CML (Zhao *et al.*, 2012).

Common symptoms of CML include anaemia, diabetes, infection caused by syphilis and HIV retinopathy, however, vision loss is believed to form the initial diagnosis of CML (Huang and Sanjay, 2011). It is important to monitor disease progression by early diagnosis. Real-time polymerase chain reaction (PCR), flow cytometry, chromosome analysis and fluorescence *in situ* hybridization (FISH) are conventional methods used for clinical diagnosis. Due to the complexity of the techniques and high costs, Xu and co-workers have reported that chemiluminescence was the most effective clinical diagnosis method (Xu *et al.*, 2016). Recent studies have demonstrated that cardiac tamponade is considered the first sign of CML-BC (Huang

et al., 2016). According to WHO the diagnostic criteria for CML are listed in Table 1.3 (Arber *et al.,* 2016).

1.3 CML treatment

In recent decades, the main treatment for CML was cytoreductive chemotherapy such as Busulphan and Hydroxyurea, which controls white blood cell (WBC) counts. However, the disease did not show improvements in the accelerated and blast phase. The survival rate of the therapy ranges from 45 to 58 months (Fausel, 2007). Interferon (IFN) immunotherapy was used in the 1980s and proved as superior to cytoreductive therapy (Deininger *et al.,* 2003) due to the production of a complete haematologic response (CHR) in more than 50% of patients. However, the IFN therapy generates nonspecific immunostimulatory mechanisms, is expensive, inconvenient in terms of IFN injections and it produces intolerant symptoms. The median survival rate was from 60 to 89 months (Fausel, 2007).

Allogeneic bone marrow transplantation (BMT) is the only curative therapy for CML, however, mortality rates increases due to infection, bleeding and developing graft versus host disease (GvHD). Moreover, the difficulty of finding suitable donors limits the use of BMT as a therapy (Jain *et al.*, 2013; Fausel, 2007). Tyrosine kinase inhibitors (TKIs) are the most common treatments for CML; they are highly efficacious, present minimal cytotoxicity and are specific in their targeting of gene mutations. Imatinib mesylate (IM) has become the first-line therapy for CML (Salizzato *et al.*, 2016). IM (also called STI-571) acts as an inhibitor for tyrosine kinase (Brouard *et al.*, 2001). Upon administration of IM, lekaemic cells stop

proliferating and undergo to a process of cell death (apoptosis) (Novak *et al.*, 2015). The chemical structure of IM will be discussed later, (Chapter 2).

The survival percentages for CML patients treated with IM ranges according to the stage of the disease. Patients in CP have an 80% chance of survival. However, in advanced disease stages such as AP and BC, the survival rates drop to 50% and 20%, respectively. Despite IM producing high remission rates and improvements in disease prognosis approximately 20-30% of patients develp resistance to IM over time (Salizzato *et al.*, 2016).

Imatinib resistance allows CML to progress and leads to failures in haematologic responses (CHR). This is due to the insufficient binding of tyrosine kinase inhibitors to the receptor, which is termed primary resistance mechanism. However, the most common resistance mechanism is secondary resistance to imatinib. It develops from point mutations within the BCR-ABL1 kinase domain, thereby reducing the affinity of binding sites (Wieczorek and Uharek, 2016; Bhamidipati *et al.*, 2013). Second generation formulations of imatinib, e.g. dasatinib and nilotinib, decrease resistance and intolerance (Wieczorek and Uharek, 2016).

Table 1.3. Heamatologic/cytogenetic criteria for CML

CP CML
▪ Cytogenetic evidence of Ph^+ chromosome in peripheral blood or bone marrow ▪ Morphology evaluation from bone marrow (BM) aspiration
AP CML (diagnosed if any one or more of the following exist)
▪ Persistent or increase while blood cells (>10 × 10^9/L) unresponsive to therapy ▪ ≥10% of peripheral white blood cells or bone marrow cells are blasts ▪ Peripheral blood basophils ≥20% ▪ Persistent thrombocytopenia (>100 × 10^9/L) unrelated to therapy, or persistent thrombocytosis (>1000 × 10^9/L) unresponsive to therapy ▪ Persistent or increase spleen size (splenomegaly) unresponsive to therapy ▪ Additional genetic abnormalities other than the fusion of *BCR–ABL1* gene
BC CML (diagnosed if any one or more of the following exist)
▪ ≥20% of peripheral blood or BM cells are blasts ▪ Onset lymphoblast in the peripheral blood or BM cells

Each drug is used according to disease stages. Dasatinib has an effective response in the CML chronic phase, accelerated phase and blast phase of the disease. Nilotinib is approved by the US Food and Drug Administration (FDA) and the European Medicines Agency (EMA) for chronic phase and accelerated phase therapy (Rogers *et al.*, 2012). However, nilotinib causes problems in diabetic patients as it raises blood sugar (Rea *et al.*, 2014). Bosutinib and ponatinib modify the disease in cases of relapse or intolerance (Caldemeyer *et al.*, 2016). The main goal of these therapies is to maintain remission and prevent progression of the disease, with high efficacy and minimal toxicity.

Several clinical trials have shown that kinase inhibitor combinations exert an efficacy against most of the mutated forms of the *BCR–ABL1* oncogene (Change *et al.,* 2011). One study suggested that treatment can be advanced cytogenetically and molecularly when combining imatinib and interferon (Fava, Rege-Cambrin and Saglio, 2015). Recent study reported that targeting the CK2 and MEK protein kinases elicit better effects in eliminating CML cells with reducing viability of imatinib resistat CML cells (Salizzato *et al.,* 2016). Another trial found that co-treatment with amiloride and imatinib could be a potential treatment for CML (Chang *et al.,* 2011). These studies suggest incorporating a combinatorial kinase treatment approach could overcome the imatinib resistance.

1.4 Alternative splicing (AS)

Splicing is a cell mechanism whereby introns (non-coding DNA regions) are excised and exons (coding regions) are joined together, Figure 1.5. Alternative splicing generates several mature mRNAs from a single gene, allowing for a diversity in terms of protein expression. In humans, 94% of genes undergo alternative splicing, resulting in the production of functional isoforms, therefore single genes can generate more than one variant mRNA, encoding different proteins (Pan *et al.,* 2008; Wang *et al.,* 2008).

AS was first characterised in the 1970s in adenoviruses (Chow *et al.*, 1977).

Approximately a decade later, researchers discovered that more than one mRNA could be generated from a single immunoglobulin μ gene by alternative splicing (Early *et al.,* 1980). There are several modes of alternative splicing. Approximately

75% of all human genes undergo cassette exon or exon skipping events. Therefore, exon skipping is the most common form of alternative splicing in eukaryotes (Weatheritt, Sterne-Weiler and Blencowe, 2016).

The other types include: 1) alternative 3' splice site selection (3' SS selection), 2) alternative 5' splice site selection (5' SS selection) and 3) intron retention and mutually exclusive exons (Keren, Lev-Maor and Ast, 2010).

Figure 1.5 shows the different AS mechanisms. Exon skipping or cassette exon occurs when exons are spliced out from the transcript with flanking introns. Alternative 3' splice site and 5' splice site selection happens when two or more splice sites are recognised by splice factors at the beginning or end of an exon, respectively. Intron retention occurs when an intron remains in the mRNA transcript while one of two exon remains in the mRNA after splicing, but not both is known as mutually exclusive exons (Cartegni, Chew and Krainer, 2002).

A recent study from Martinez-Montiel and co-workers investigated natural products (actinomycetes, filamentous fungi, and medical plants) that inhibited gene splicing, (Martinez-Montiel *et al.*, 2016). Another study demonstrated the importance of AS in histone methylation and demethylation in neurons (Fiszbein and Kornblihtt, 2016). It has also been reported that suppressing some protein kinases, such as Serine/Arginine splicing factor kinase (SRPK1) affects splicing during angiogenesis (Amin *et al.*, 2011). Therefore, controlling gene expression through protein kinase activity has allowed us to hypothesis that inhibiting SRPK1 and Clk1 could significantly reduce CML progression.

1.5 The regulation of alternative splicing

1.5.1. pre-mRNA splicing

Mature mRNA result from spliced precursor messenger RNAs (pre-mRNAs) at splice sites found at exon-intron junctions consisting of 5’ and 3’ splice site sequences. The sequence of the 3’ splice site has the 3’ splice site itself, a polypyrimidine tract and a branchpoint (BP) sequence. In humans, the 5’ splice site consensus sequence is CAG GURAGU while the 3’ splice site consensus sequence is YAG.

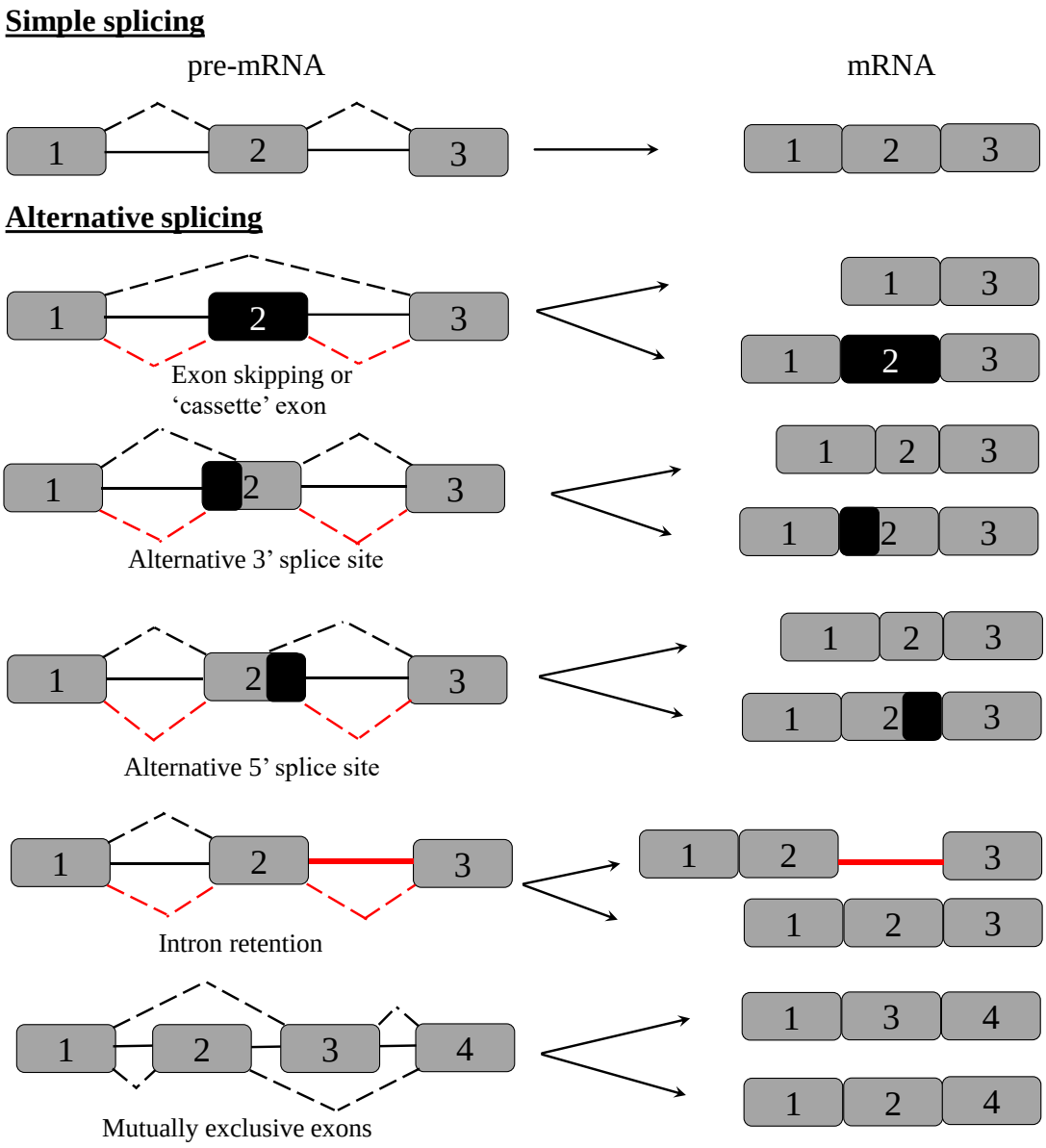

Figure 1.5. The splicing and four basic modes of alternative splicing showing exon skipping, alternative 3' and 5' splice sites, intron retention and mutually exclusive exons
Exons (grey and black rectangles) are connected by introns (black lines). The dotted black lines indicates the alternative splicing patterns and the dotted red lines indicate the splicing patterns. In each model, grey exons are constitutive and black exons are alternative.

The branchpoint has a YNYURAC consensus sequence and a polypyrimidine tract usually has T residues, Figure 1.6. The process of splicing occurs through a major ribonucleoprotein complex called as spliceosome which contains five building

blocks known as small nuclear RNAs (U1, U2, U4, U5 and U6 snRNAs), associated with five small nuclear ribonucleoproteins (U1, U2, U4, U5 and U6 snRNPs).

Some snRNPs interact with pre-mRNA in early spliceosome assembly, while others interact with each other. The types of snRNPs and their interactions are listed in Table 1.4 (de Almeida and O'Keefe, 2015; O'Keefe and Newman, 1998).

It has been shown that proteins, Prp8, Snu114 and Brr2 are associated with U5 snRNA (Nancollis *et al.*, 2013). Any mutation present in U5 snRNA influences the stability of Prp8, thus affecting splicing regulation (Kershaw *et al.*, 2009). Therefore, the U5 snRNP is regarded as the centre of the spliceosome assembly (Nancollis *et al.*, 2013).

The spliceosome assembles on pre-mRNAs through multiple pathways. Firstly, U1 snRNP recognises the 5′ splice site leading to an interaction of U2 snRNP with BP sequences. Next, the U4/U6•U5 tri-snRNPs associates with bound snRNPs and pre-mRNA. Following this, U5 snRNP interacts with the 5′ and 3′ splice site and destabilises the U1 snRNP association. The U5 snRNP binds to the 5′ splice site and U6 associates with U2 snRNPs resulting in the U2/U4/U6 complex. The complex releases U4 snRNP and forms a complex association of U2/U6 snRNP with U2 snRNP at the BP. U6 snRNP interacts with the 5’ splice site, Table 1.4.

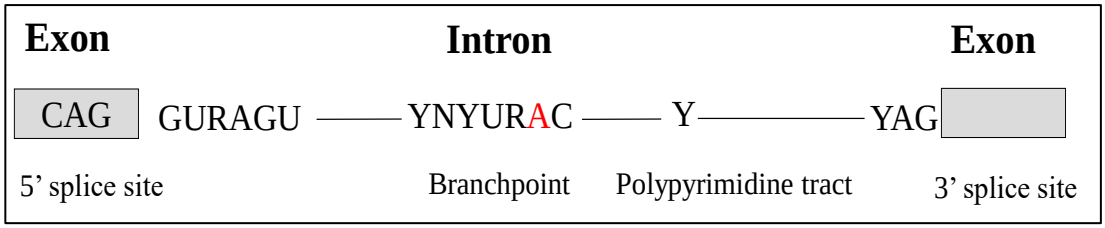

Figure 1.6. Introns start from the GU sequence at the 5′ splice site at the upstream exon
The 3′ splice site has three parts: the branch site (highly conserved adenines), a polypyrimidine tract and a 3′ splice site (AG) sequence at the downstream exon.

Table 1.4. Small nuclear ribonucleoproteins (snRNPs) and their interactions

SnRNPs	Interaction with pre-mRNA	Interaction to other snRNPs
U1	5′ splice site	
U2	Branchpoint	U4/U5•U6 U6 snRNP (late stage of spliceosome assembly)
U4		
U5	5′ and 3′ splice site	
U6		U2 snRNP

Finally, the two exons are re-joined and the intron is removed as a lariat shape. The spliceosome disassembles, splicing components are recycled and the mRNA is exported.

It has been reported that splice factor 1 (SF1), heterodimeric splice factor U2 auxiliary factor (U2AF-35 and U2AF-65), and SR proteins are involved in the

assembly of the spliceosome to regulate alternative splicing (O'Keefe *et al.*, 1994; Rudner *et al.*, 1998).

1.5.2. Serine/arginine-rich proteins as a family of alternative splicing regulators

The serine/arginine-rich proteins (SR proteins) are a large superfamily of nuclear RNA binding proteins (Zhou and Fu, 2013). SR proteins were identified initially in Drosophila in the 1990s and later the proteins SRSF1 and SRSF2 were identified in humans (Manley and Krainer, 2010). The majority of SR proteins share two RNA-binding domains (RNA-recognition motif (RRM) and RRM homologue (RRMH)) and RS domain. Some SR proteins has one RRM and RS domain, such as SC35, SRp20 and SRp54. However, 9G8 is the only SR protein that contains a zinc-knuckle domain instead of an RRMH. The RS domain, however is composed of RS/SR residues that is divided into RS1 and RS2 subdomains. The RS1 subdomain consists of a docking motif and initiation box and its phosphorylated by SRPK1, however, the RS2 is phosphorylated by Clk1, Figure 1.7 (Shepard and Hertel, 2009; Zhou and Fu, 2013). The phosphorylation of SRSF1 by SRPK1 and Clk1 will be discussed in section 1.5.4.3.

A new standardised nomenclature has been suggested for the SR protein family. In humans, nine genes (*SRSF1-7, 9*, and *11*) encode SR proteins which act as splicing factors (Shepard and Hertel, 2009; Vu *et al.*, 2013). In this thesis, the new nomenclature will be used, however for clarity, the previous and recent SR protein names and their domain topologies are shown in Figure 1.8.

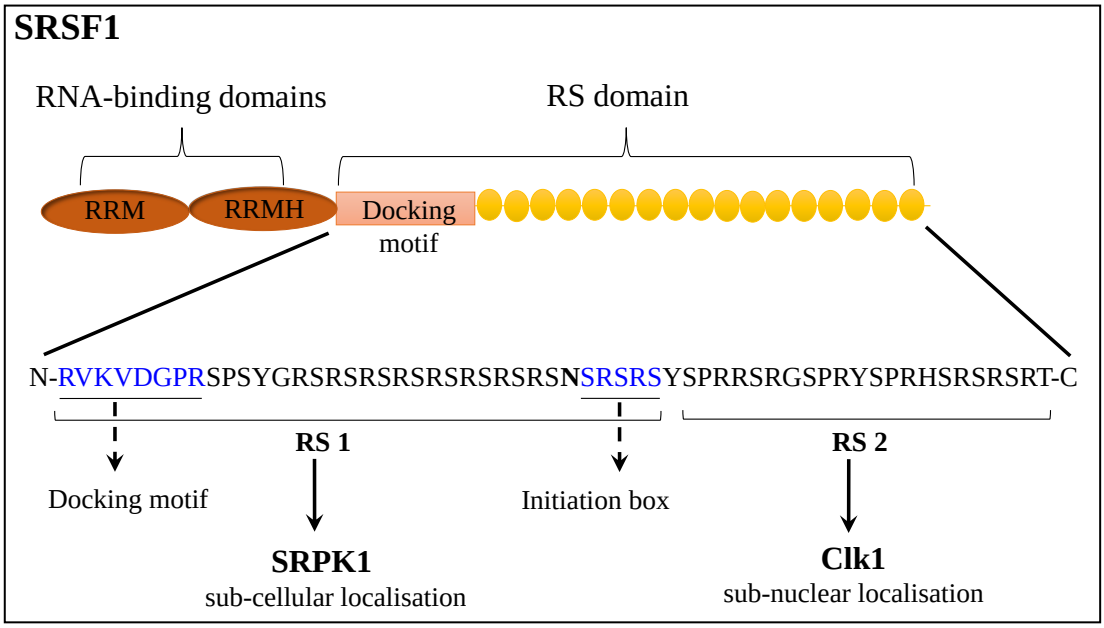

Figure 1.7. The structure of the SR protein (SRSF1)
The domain structure of SR proteins: two RNA-binding domains (RRM and RRMH) and RS domain. The RS domain consists of The RS/SR residues, which is divided into two subdomains (RS1 and RS2). A docking motif and an initiation box in the RS1 domain as shown in blue. RS1 segments are important for SRPK1 phosphorylation. RS2 segments are important for Clk1 phosphorylation.

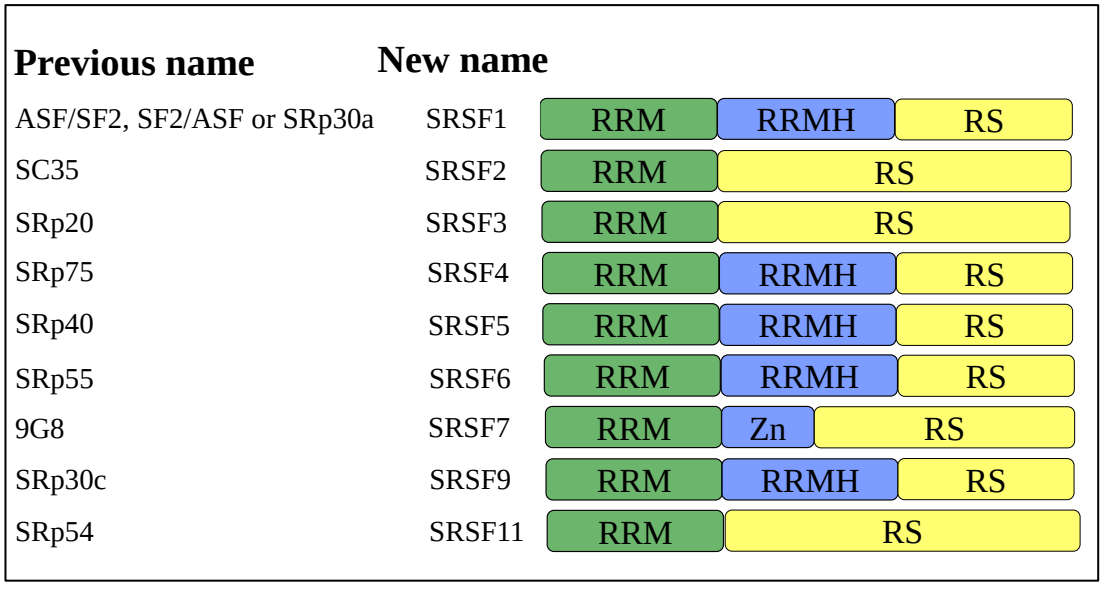

Figure 1.8. The SR protein family
The main domain characteristics of SR proteins structure. RRM (RNA recognition motif); RRMH (RNA recognition motif homology); RS (arginine/serine-rich domain); Zn (Zinc knuckle).

It has been observed that SR proteins interact with other proteins, the SR-related proteins, to regulate splicing. Despite their lack of RRM, SR-related proteins carry RS domains and RNA binding motifs (PWI), or zinc finger motifs (Zn) (Zhou and Fu, 2013). The interaction between SR proteins and SR-related proteins occurs through the RS domains of both proteins, thereby initiating splicing (Shepard and Hertel, 2009). Some examples of SR-related proteins include both subunits of the U2AF heterodimer (U2AF-35 and U2AF-65), U1-70K, and the splicing co-activators SRm 160/300 (Long and Caceres, 2009; Kim *et al.*, 2011).

It has been reported that other domains of SR-related proteins are responsible for enzymatic activities. Clk/Sty1 is an example of another RS domain containing proteins, it contains an RS and kinase domain. However, other RS domains may contain RS domains and motifs characteristic of RNA helicases (DEAH Box), such as hPRP5 (Long and Caceres, 2009).

1.5.3. Functions of SR proteins

1.5.3.1. The role of SR proteins in pre-mRNA splicing

Splicing codes are specific codes by which enable spliceosomes to distinguish between exons and introns in pre-mRNA. The human splicing code depends on the interaction of splicing activators (SR proteins) or splicing repressors (heterogeneous nuclear ribonucleoprotein or hnRNPs) with snRNPs. The splicing activators are found within exons (exonic splicing enhancers, ESEs) or within introns (intronic splicing enhancers, ISEs). The splicing silencer sequences are located within exons (exonic splicing silencers, ESSs) or within introns (splicing silencers, ISSs) (Wu and

Hurst, 2016). There are more than twenty members of hnRNPs, including, hnRNP A1, A2, A3 and hnRNP B1 (Qu *et al.*, 2015).

The functions of SR proteins can be divided into two categories: exon-dependent and exon-independent functions. The exon-dependent functions of SR proteins form interactions between the RS domain of the SR proteins and ESE's facilitating the recruitment of spliceosomal components. For example, interactions between U1-70 snRNP to 5′ splice site from one side and interacting U2AF (U2AF-65 and U2AF-35) to the 3′ splice site from another side (Shepard and Hertel, 2009). The SR proteins bound to ESE's also promote incorporation of the tri-snRNA U4/U6•U5 into the spliceosome, Figure 1.9A (Shepard and Hertel, 2009). SR proteins also function without interaction with exons (exon-independent functions); the U2 snRNP bound to the branchpoint sequence (A) and SR proteins stimulate the interaction of U1 snRNP to 5′ splice site and U2AF to a 3′ splice site. SR proteins also recruit the U4/U6•U5 tri-snRNP into the spliecosome, Figure 1.9B (Shepard and Hertel, 2009).

In addition to the structure of these domains, the activity of SR proteins is related to the RS domain. That was proved by previous study with RS domain lacking SRSF2 (SC35) had no activator effect compared to the SR proteins with RS domain (Dreumont *et al.*, 2010).

It has been also suggested that splicing relies on the specificity of SR protein binding, the location of the interaction and the competitive binding of different SR proteins and competition with other RNA splicing regulators (Zhou and Fu, 2013).

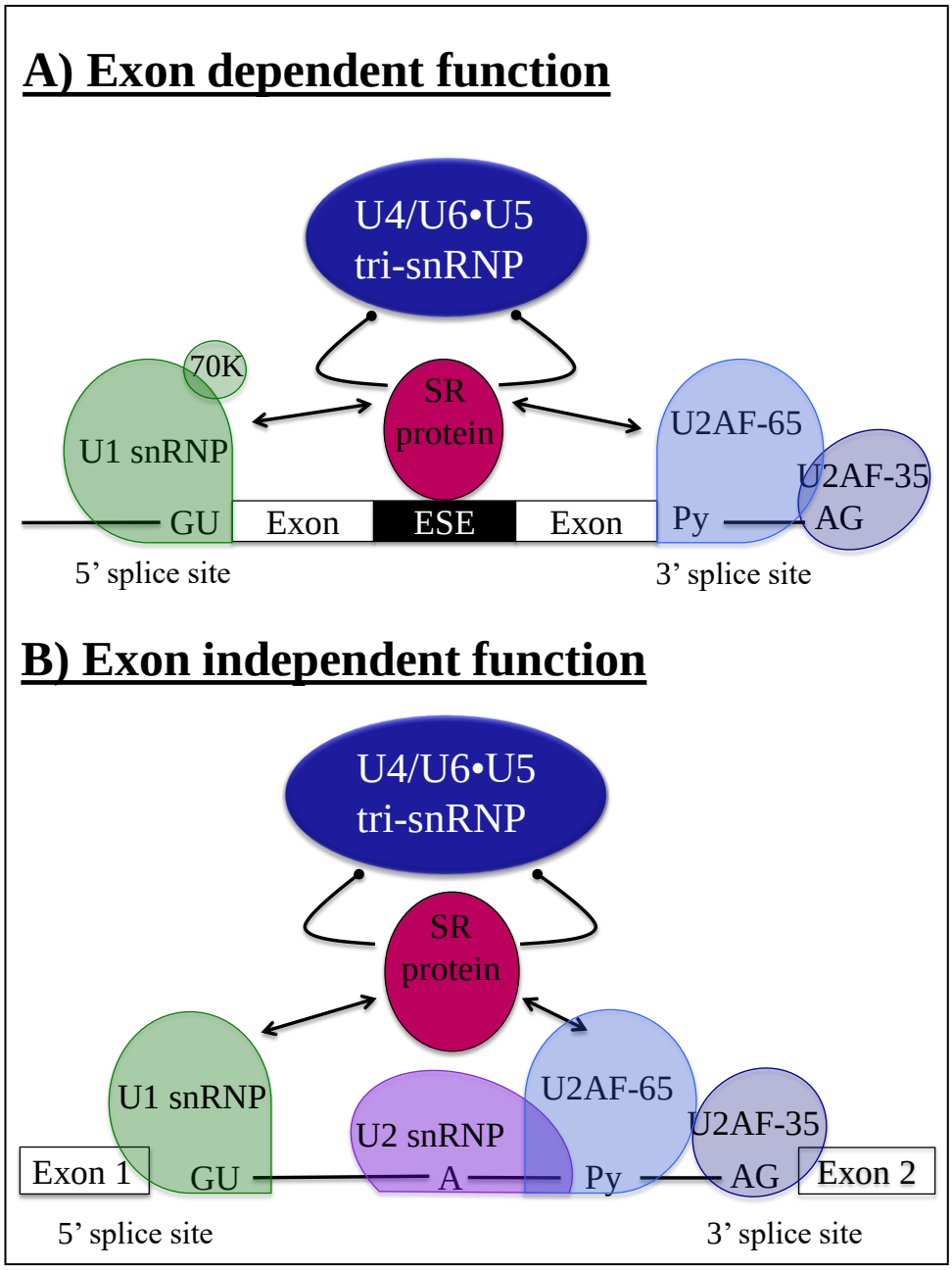

Figure 1.9. Exon dependent and independent mechanisms of splicing activation
A) The exon dependent functions of SR proteins. SR proteins bound to an exonic splicing enhancer (ESE) promote splicing by stabilising bound U1 snRNP to the 5′ splice site and the U2AF to the 3′ splice site. GU sequences are binding sites for the U1 snRNP, while polypryrimidine tracts (Py) and AG sequences are binding sites for the U2AF-65 (the large subunit of the splice factor) and U2AF-35, respectively. The SR proteins bound to ESEs stimulate the incorporation of the tri-snRNA U4/U6•U5 into the spliceosome. B) The exon independent functions of SR proteins. The U2 snRNP bound to the branchpoint (A) and SR proteins promote splicing by activating the interaction of U1 snRNP and U2AF to splice site pairing. U2AF-65 stimulates the binding of U2 snRNP to the branch site. SR proteins are also associated with the recruitment of U4/U6•U5 tri-snRNPs.

1.5.3.2. The role of SR proteins beyond pre-mRNA splicing

SR proteins are not only essential for splicing, but they have important roles in post-transcriptional gene expression through promoting mRNA export. SRSF3 (SRp20) and SRSF7 (9G8) are important key export protein adapters; they enhance mRNA export through the recruitment of the "export receptor Nuclear RNA export factor 1/Tip-associated protein (NXF1/TAP)" (Huang and Steitz, 2005). Both SR proteins also control the shuttling of mRNA into the cytoplasm. Previous studies have shown that SRSF1 interacts with polyribosomes and promoting the translation of luciferase reporters (Michlewski, Sanford and Caceres, 2008).

SR proteins also have key roles in RNA stability, quality control (Zhang and Krainer, 2004) and chromatin interaction (SRSF1 (ASF/SF2) and SRSF3 (SRp20)). These interactions rearrange DNA and arrest the G2/M cell cycle (Loomis *et al.*, 2009). It has been shown that SR proteins can function before splicing; they interact with RNA polymerase II (RNAP II) transcripts, coupling transcription to splicing (Das *et al.,* 2007; Yu and Reed, 2015). Despite the fact that SR proteins are stimulus proteins for splicing, are involved in mRNA export, stability and translation, they can also negatively influence splicing when overexpressed. They specifically target mRNAs by incorporating premature termination codons (PTCs) into sequences, thereby enhancing the nonsense-mediated mRNA decay (NMD) pathway. SR proteins have widespread roles in pre-mRNA mechanisms, therefore it is important to focus on SR protein regulation mechanims to understand their cellular activities in gene expression.

1.5.4. The regulation of SR proteins

1.5.4.1. Post-translational modification of SR proteins

SR proteins can be regulated by multiple enzymatic mechanisms known as post-translational modifications (PTMs) that contribute to the formation of fully mature and functional proteins. Arginine methylation, acetylation and phosphorylation are some of the different types of post-translational modifications. Methylation specifically is important for SR protein and SR-related protein function (Zhou and Fu, 2013).

SRPK1 mediates the phosphorylation of SR proteins leading to the import and accumulation of these proteins at nuclear speckles. Under appropriate phosphorylation states, SR proteins are targeted to nascent pre-mRNAs to activate splicing. For methylation, three methylated arginine residues (R93, R97 and R109) occur in the SR protein SRSF1. These arginines play key roles in controlling the localisation of SRSF1 (Wang, Peterson and Loring, 2014; Zhou and Fu, 2013). Cytoplasmic accumulation of SRSF1 resulting from methylation processing mutations reduces SRSF1 levels in the nucleus, inhibiting the alternative splicing of targeted genes promoting nonsense-mediated (NMD) mRNA decay (Sinha *et al.*, 2010). Furthermore, it has been revealed that some SR proteins are regulated by lysine acetylation through the opposing functions of histone acetyltransferases (HATs) and histone deacetyleases (HDACs) (Edmond *et al.*, 2011).

1.5.4.2. SR specific kinases

The activity of SR proteins is highly regulated by the reversible phosphorylation of serine residues in the RS domain. Several protein kinases have been identified that

phosphorylate SR proteins; the serine/arginine protein kinase family (SRPKs), cycline dependent like kinases (Cdc-like-kinase) or Clk/Sty (also known as Clk1), DNA topoisomerase I and phosphatidylinositol 3-kinase (AKT).

SRPKs are protein kinases that are serine- and arginine-rich and constitute a subfamily of serine-threonine kinases that specifically phosphorylate serine/arginine-rich domains (Daniilidou *et al.*, 2011). SRPK and Clk/Sty family kinases coordinate their activities to regulate SR proteins through specifici interaction with the RS domain of SRSF1 proteins (Zhou and Fu, 2013). The SRPKs phosphorylate SR proteins with high efficiency and specificity. However, the Clk/Sty family are dual specific kinases that phosphorylate serine/threonine and tyrosine residues. Thus, SRPKs phosphorylate SR proteins with a greater efficiency and specificity than Clk/Sty. Despite this, Clk/Sty phosphorylates more residues than SRPKs in the RS domain of SRSF1. Numerous studies have revealed that members of SRPK are responsible for the nuclear import of phosphorylated SRSF1, while Clk/Sty members play key roles in interrupting phosphorylated SRSF1 (Ghosh and Adams, 2011).

Generally, SRPKs are characterised by spacer domains that separating the kinase domains into two lobe forming docking grooves (covered in section 1.5.4.3). Spacer domains are only present in serine/threonine kinases and not in tyrosine kinases, thus Clk phosphorylate SR proteins differently (Zhou and Fu, 2013). Extensive research has revealed that deletion of the spacer domain increase translocation of SRPKs into the nucleus (Ding *et al.*, 2006).

SRPK1, SRPK2, and SRPK3 are examples of alternatively spliced products generated by the SRPK family. SRPK1 is expressed predominantly (Zhou and Fu, 2013) and functions as a tumour suppressor or an oncogene in different cell types (Wang *et al.*, 2014). SRPK2 and SRPK3 are expressed in the nervous system and muscle cells, respectively (Zhou and Fu, 2013). Apart from SRPKs, it is known that Clk/Sty mediates the phosphorylation of SR proteins to activate splicing. Clk/Sty is a member of the LAMMER family of protein kinase. All members of the Clk family (Clk1-4) are localised to the nucleus, unlike SRPKs that are mainly cytoplasm based (Zhou and Fu, 2013). However, SRPKs can mobilise to the nucleus during the M phase of the cell cycle and stimulate aggregation of splice factors (Gaddy *et al.*, 2010).

1.5.4.3. Phosphorylation of SRSF1 recycling for splicing

SRPK1 phosphorylates SRSF1 through a dual-track mechanism combining processive phosphorylation (the kinase attaches to the substrate after each round of phosphorylation) and distributive phosphorylation (where the kinase and substrate dissociate after each round of phosphorylation), Figure 1.10; A and B (Ghosh and Adams, 2011; Shepard and Hertel, 2009). SRPK interacts with the initiation box (Ser221-Ser225) of the RS1 sequence to initiate phosphorylation using processive mechanisms allowing the docking groove of SRPK1 to recognise the docking motif peptide of SRSF1 (Ghosh and Adams, 2011). Some studies have found that the docking motif/docking groove interaction limitats the number of phosphorylated serines and increase the affinity between the SRSF1 and SRPK1 (Ngo *et al.*, 2005).

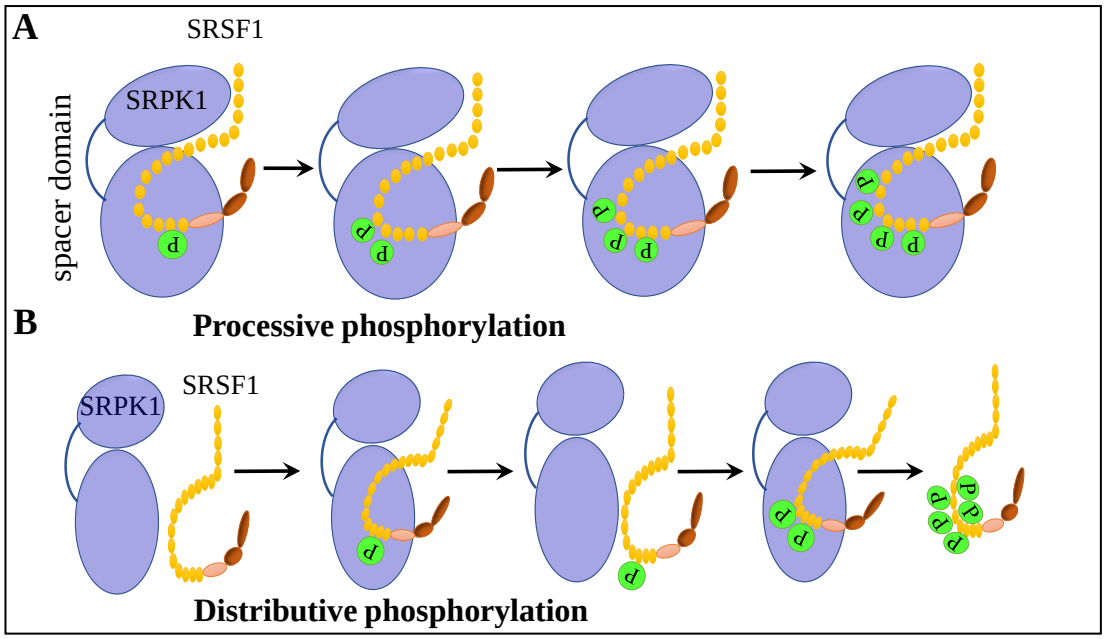

Figure 1.10. The mechanisms of SRSF1 phosphorylation by SRPK1
A. The processive mechanism for phosphorylation. SRPK1 docks at the docking motif of RS1 while the initiation box is activated. The SRPK1 attached to the SRSF1 after each round of phosphorylation without dissociation. **B.** The distributive mechanism by which the SRPK1-SRSF1 dissociate after each round of phosphorylation. Green circles: phosphate groups.

After SRPK1 interacts with SRSF1, phosphorylation of 5-8 of the 12 available serines in the RS1 occurs rapidly and efficiently towards the N-terminal. After phosphorylation, the high affinity between enzyme (SRPK1) and substrate (phosphorylated SRSF1) diminishes and distributive phosphorylation becomes activated (Ghosh and Adams, 2011).

The remaining unphosphorylated serines in RS1 are modified by SRPK1 using a distributive phosphorylated reaction (Ngo *et al.*, 2005). The phosphorylated RS domain translocates SRSF1 from the cytoplasm into the nucleus for storage in nuclear speckles (Naro and Sette, 2013).

Unlike SRPK1, Clk1 lacks a docking groove and phosphorylates the RS domain of SRSF1 randomly. However, Clk1 mediates phosphorylation through the distribution of acidic and basic charges in its shallow area. This charge dispersal causes the interaction of the hypophosphorylated RS domain to become more effective with Clk1 when compared to the unphosphorylated RS domain. Therefore, the pre-phosphorylated RS domain SRPK1 may become the substrate of Clk1.

The overexpression of Clk1 causes the phosphorylation of 7 serines in the SRSF1 RS2 domain, leading to its redistribution from nuclear speckles to active splicing sites, thereby controlling gene expression (Zhou and Fu, 2013; Ghosh and Adams, 2011; Ngo *et al.*, 2005). SR proteins, such as SRSF1, are regulated through the interactions between two families of protein kinases; SRPK1 and Clk1. SRPK1 initiates phosphorylation of SRSF1 to facilitate its nuclear import via protein import receptors known as transportin-SRs (TRN-SR). These phosphorylated SRSF1s are stored in the nuclear speckles for additional phosphorylation by Clk1. Once SRSF1s have been re-phosphorylated, they are released from the nuclear speckles to splice sites (Zhou and Fu, 2013; Ghosh and Adams, 2011). Hyper-phosphorylated SRSF1 binds to pre-mRNA to initiate splicing, leading to the production of different mRNA isoforms from the same gene.

Once splicing is completed, nuclear phosphatases such as protein phosphatase 1 (PP1) and protein phosphatase 2A (PP2A) play important role in dephopsphorylated SRSF1 and export them to the cytoplasm for the next round of phosphorylation and splicing, Figure 1.11 (Ma *et al.*, 2010). It has been reported that PP1 dephosphorylates SRSF1 in a direction toward the C-terminal (Corkery *et al.*, 2015).

Therefore, SRPK1 and Clk1 both play key roles in regulating the activities of SR proteins and gene expression (Zhou and Fu, 2013).

1.5.5. SR proteins, SRPKs and Clk kinase families in cancer

The SR protein SRSF1 is typically described as a proto-oncogene, as there is growing evidence that SRSF1 overexpression is associated with several types of cancer, mainly as a result of changes at the alternative splicing level. More than 50% of genetic mutations lead to the disruption of at least one of the SR proteins (SRSF1, SRSF2, SRSF5, and SRSF6). It has also been reported that SRSF1-3 overexpression was detected found in malignant ovarian tissue, whereas, other SR proteins were elevated in breast cancer. The overexpression of SRSF1 was detected in several solid tumours, such as lung, colon, kidney, liver, pancreas, and breast carcinomas. In addition, overexpression of SRSF1 leads to transformation fibroblasts into immortal rodent fibroblasts forming sacromas in mice unlike other SR proteins, e.g. SRSF2 and SRSF6. That would suggest the important role of SRSF1 in the progression of malignancy (Long and Caceres, 2009).

Specific mutations in SR genes are associated with leukaemia, e.g., mutations of SR3B1, SRSF2, U2AF1, U2AF-65, ZRSR2, SF2A1, SF1 and PRPF40B were found in a wide range of myeloid leukaemias. Specifically, these mutations were detected in ~85% of myelodysplastic syndromes associated with ring sideroblasts (MDS-RS), 55% in chronic myelomonocytic leukaemia, 26% in AML and 7% in primary AML (Lasho *et al.*, 2012; Zhou and Fu, 2013).

The SRPK kinases are upregulated in tumourgenesis, e.g. SRPK1 and SRPK2 were

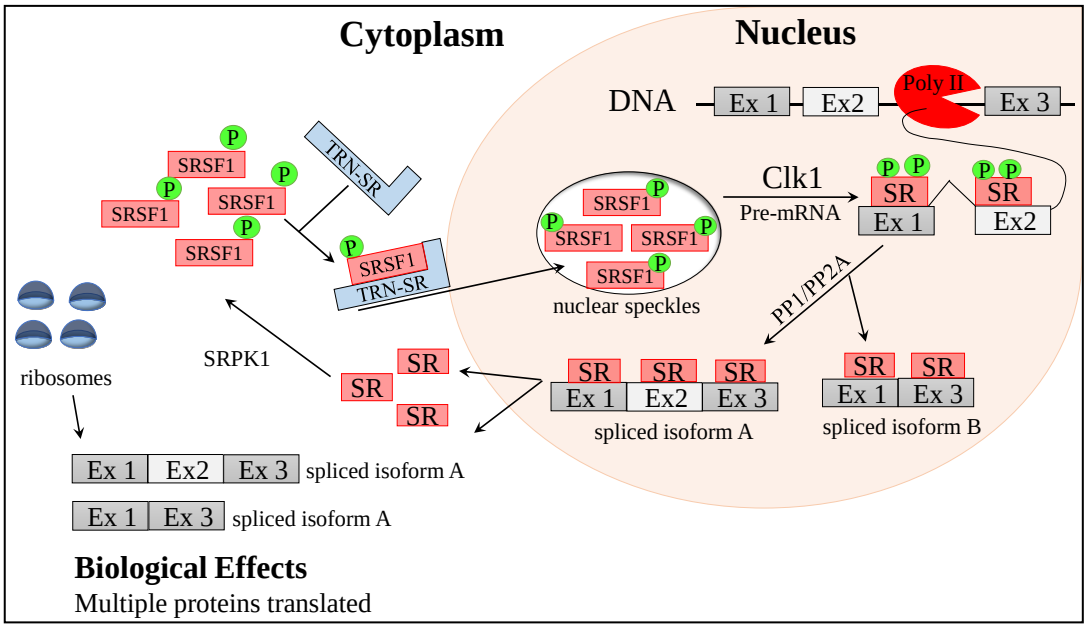

Figure 1.11. The role of SRPK1 and Clk1 kinases in phosphorylation and shuttling SRSF1
SRPK1 phosphorylates SR proteins (SRSF1) and transported into the nucleus by protein import receptors, transportin-SR (TRN-SR). Phosphorylated SRSF1 will be stored in the nuclear speckles. Additional phosphorylation is mediated by Clk1 to induce the release of phosphorylated SRSF1 into the nucleoplasm to regulate splicing. Once splicing is completed, SRSF1s are dephosphorylated by protein phosphatase 1 (PP1) and protein phosphatase 2A (PP2A). Spliced mRNA will be exported for translation and dephosphorylated SRSF1s are recycled for the next round of phosphorylation.

overexpressed in non-small lung cancer due to hyperphosphorylation of SRSF1 and SRSF2 (Zhou and Fu, 2013).

Other studies have shown that elevated SRPK2 occurs in myeloid leukaemia (Jang *et al.*, 2008). In contrast, downregulated SRPK1 was detected in cisplatin-resistant human tumours (Zhou and Fu, 2013). These studies suggest that over- or under regulation of SRPKs are linked to several human malignancies. Apart from SRPKs, it has been shown that all Clk kinase family members are elevated during

erythroleukaemia cell differentiation (Garcia-Sacristan *et al.*, 2005). Indeed, Clk1 is overexpressed in ovarian, breast and prostate cancer (Liu *et al.*, 2013).

Angiogenesis is the formation new blood vessels during embryonic development and growth. The process is regulated by the vascular endothelial growth factor (VEGF), which is an essential angiogenic factor, alternatively spliced by SRSF1 to produce both pro- and anti-angiogenic isoforms (Zeng *et al.*, 2016). The pivotal role of SR proteins in gene expression leads to elevated levels of SRSF1 which in turn increases the production of pro-angiogenic VEGFA isoforms. However, overexpression of SRSF2 and SRSF6 increases VEGFA, anti-angiogenic isoforms (Merdzhanova *et al.*, 2010; Nowak *et al.*, 2008).

Upregulation of SRPK1 has been linked to hyperphosphorylation of SRSF1, leading to increases in the nuclear import of SRSF1 (Nowak *et al.*, 2010). Previous study has observed a shift in splicing towards anti-angiogenic isoform following inhibition SRPK1, SRPIN340, which led to reduce tumour growth in nude mice (Amin *et al.*, 2011). Taken together, these observations suggest that SRPK1 and SRSF1 play important roles in splicing during angiogenesis (Oltean *et al.*, 2012). These findings suggest that targeting the SR protein kinases and/or SR proteins may act as potential therapeutics in treating human cancers.

1.5.6. Receptor Tyrosine Kinases (RTKs) and their roles in cancer

Alternative splicing regulation is important as it increase the functional capacity of a gene. Aberrant splicing events cause alterations in cellular signalling pathways, including tyrosine kinase receptor signalling. As a result, abnormalities in protein

concentration, composition, localisation, activity and irregularity arise potentially leading to disease (Wang *et al.,* 2015) of human receptors tyrosine kinases (RTKs) that comprise twenty subfamilies have been recorded (Lemmon and Schlessinger, 2010). Some of RTKs are listed in Table 1.5.

All RTKs have a similar molecular structures and activation mechanisms. The epidermal growth factor receptor (EGFR), Figure 1.12, is an example of an RTK and is composed of four domains: two extracellular ligand-binding domains (L1 and L2), two cysteine rich domains (CR1 and CR2) and a cytoplasmic region containing six of tyrosine (Y) residues. The mechanism of RTK activation is similar to all 58 proteins. Generally, e.g. the EGFR becomes activated through the binding of its receptor, the epidermal growth factor (EGF). Receptor-mediated activation of EGFR phosphorylates tyrosine residues, which then activate various downstream intracellular signalling pathways, such as (Ras-MAPK and PI3K-mTOR) (Lemmon and Schlessinger, 2010).

In the Ras-MAPK pathway, the phosphorylated tyrosine residues recruit the Sos/Grb2 complex, activating Ras (Dhillon *et al.*, 2007) initiating the Raf/MEK/ERK phosphorylation cascade. Activated ERK translocates to the nucleus, undergroing regulation and further phosphorylation by transcription factors (Roberts and Der, 2007). As RTKs are common to most cell types, the Ras-MAPK pathway is involved in cell growth and proliferation, differentiation, migration, angiogenesis and the suppression of apoptosis (Dhillon *et al.*, 2007).

The PI3K-mTOR pathway is involved in cell growth and survival and is initiated by phosphorylation of RTKs and Ras (Dienstmann *et al.,* 2014).

Table 1.5. The human receptor tyrosine kinases (RTKs)

RTKs	Description	RTKs subfamilies
EGFR	Epidermal growth factor receptor	ErbB
FGFR	Fibroblast growth factor receptor	FGF
InsR	Insulin receptor	Ins
VEGFR	VEGF receptors (vascular endothelial growth factor)	VEGF
HGF	Hepatocyte growth factor receptor (HGF)	Met
MSP	Macrophage-stimulating protein receptor	Met

Activated AKT promotes proliferation signals and apoptosis evasion through the activation of survival factors, such as NF_KB. Additionally, AKT activation influences cell growth through increased mTOR activity and positively regulates the G/S cell cycle (Porta, Paglino and Mosca, 2014).

Constitutive activation of AKT is also caused by overexpression of SRPK1 which cause a titration of pleckstrin homology (PH) domain leucine-rich repeat protein phosphatases (PHLPP) away from AKT leading to AKT activation. Consequently, activated SRPK1 induces SRSF1 phosphorylation leading to cellular transformation and tumorigenesis (Wang *et al.,* 2014).

Frequent activation of EGFR can triggers cancer (breast, gastric and other tumour types) due to its involvement in pathways that promote proliferation, angiogenesis and inhibit apoptosis, therefore it is crucial to target these RTKs in the treatment of different solid and haematological tumours (Roberts and Der, 2007).

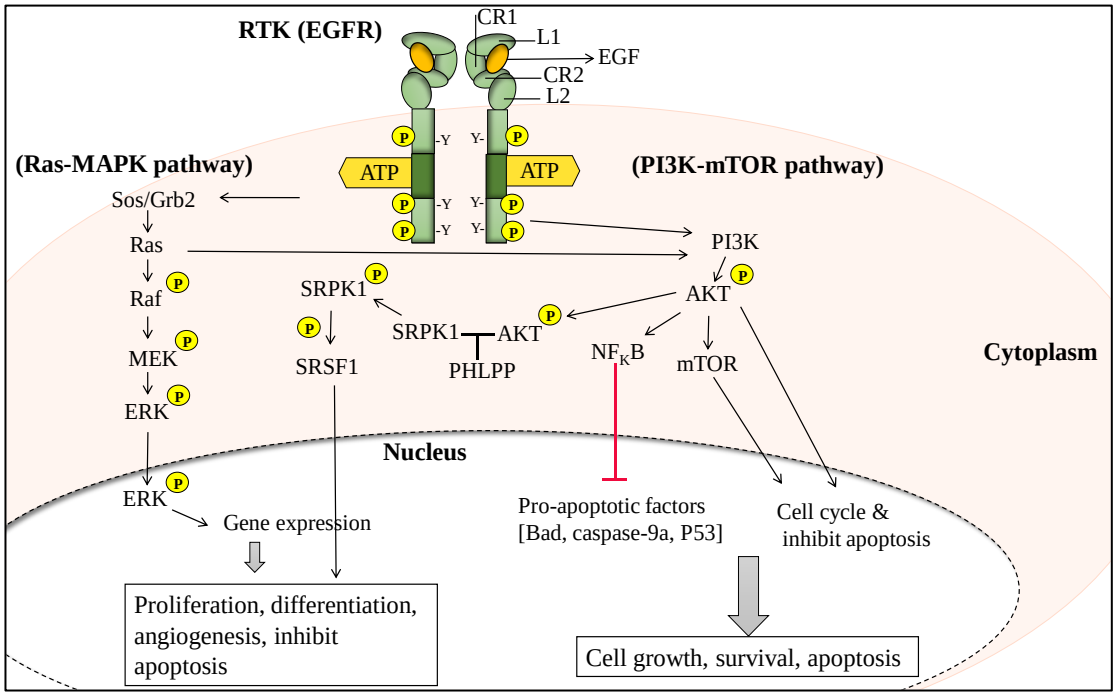

1.12. A schematic representation of the Ras-MAPK and PI3K-mTOR pathways activation by RTKs (EGFR)
The EGFR consists of four domains: two ligand-binding domains (L1 and L2) and two cysteine rich domains (CR1 and CR2) and six tyrosine residues (Y), three are shown for simplicity. The binding of EGF to EGFR activates RTK, which leads to phosphorylate tyrosine residues and trigger intracellular processes. The Ras-MAPK pathway is involved in proliferation, differentiation, angiogensis and suppression apoptosis depending on cell type. In this pathway the activated through Sos/Grb2 complex leading to several phosphorylation towards ERK. The PI3K-mTOR pathway has a potential downstream to inhibit apoptosis and promote cell survival. AKT is phosphorylated through activated PI3K. The overexpression of SRPK1 leads to titrate PHLPP away, thus activation of AKT. Phosphorylated SRPK1 has also a role in phosphorylation SRSF1 downregulating cell proliferation, differentiation and inhibit apoptosis. Abbreviations: EGF, epidermal growth factor; EGFR, epidermal growth factor receptor; Sos, son of sevenless; Grb2, growth factor receptor-bound protein 2; Ras, rat sarcoma viral oncogene homolog; Raf, v-raf murine sarcoma viral oncogene homolog B1; MEK, MAP kinase kinase (MAPKK or MEK or MAPK2); ERK, extracellular signal-regulated kinase; PI3K, phosphatidylinositol 3-kinase; AKT, v-akt murine thymoma viral oncogene homology; mTOR, Mammalian target of rapamycin; NFKB, nuclear factor kappa-light-chain-enhancer of activated B cells; PHLPP, titrate pleckstrin homology (PH) domain leucine-rich repeat protein phosphatases.

EGFR, also known as HER1/erbB-1, is one of four transmembrane receptors of the EGFR family. Inhibiting EGFR by erlotinib in combination with gemcitabine has provided a successful treatment in patients with metastatic pancreatic cancer (Roberts and Der, 2007).

Another important RTK is RON (Recepteur d'Origine Nantais) or the macrophage stimulating protein receptor (MST1R), which belongs to the Met proto-oncogene family. The receptor is involved in cell motility, cell dissociation, adhesion and invasion of extracellular matrices (Batth, Yun and Kumar, 2015a; Kang, Babicky and Lowy, 2014). RON consists of an extracellular domain, a single chain of transmembrane domains and an intracellular tyrosine kinase domain for engagement with c-Met (Leonis, Thobe and Waltz, 2007). Both RON and c-Met are closely related and are activated in response to their ligands: MSP for RON and HGF for c-Met (Zhang *et al.*, 2008a). Mature RON is a heterodimeric protein of disulfide-linked α (35 kDa) and β (145 kDa) subunits, originating from the proteolytic cleavage of a single chain (proMSP) (Wang *et al.*, 2013). The β- subunit is involved in downstream signalling pathways through phosphorylation of tyrosine kinase upon MSP, Figure 1.13. Following RON activation, phosphorylation of the intracellular signalling pathways (Ras-MAPK and PI3K-mTOR) is initiated (Yao *et al.*, 2013).

Under normal phoysiological conditions, RON is expressed at low levels, however, the ΔRON (exon 11 skipped) is highly overexpressed in malignancies, such as gastroesophageal adenocarcinoma (Wang *et al.*, 2013). Generation of oncogenic variants of RON in cancer will be described later.

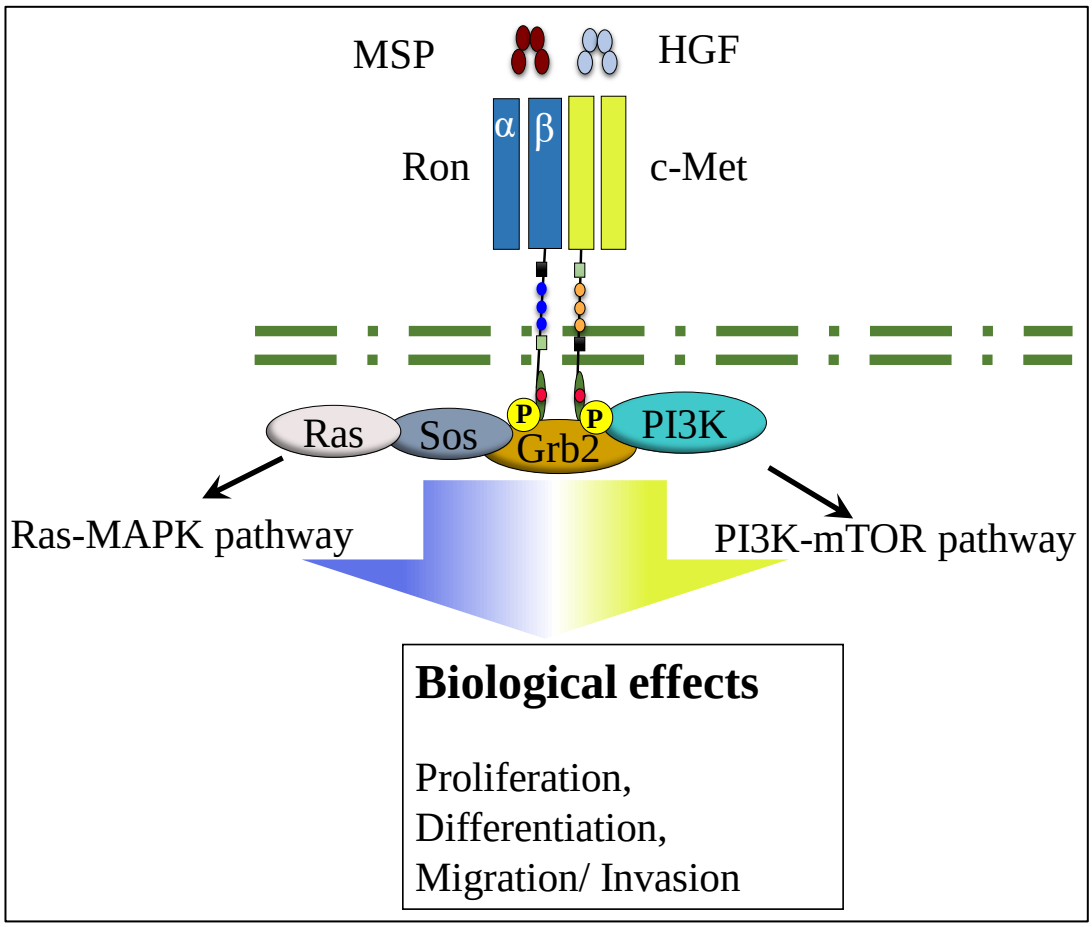

Figure 1.13. RON activation mechanisms and intracellular signalling pathways
MSP activates RON dimerisation through the activation of tyrosine kinase. Upon activation, the tyrosine kinase phosphorylates through the activated β- subunit of RON resulting in Ras-MAPK and PI3K-mTOR stimulation. Cell growth, survival and invasiveness are mediated through the Ras-MAPK pathway. In addition, cell shape, motility, matrix invasion and gene transcription are regulated by the PI3K-mTOR pathway. Abbreviations: Sos, son of sevenless; Grb2, growth factor receptor-bound protein 2; Ras, rat sarcoma viral oncogene homolog; MEK, MAP kinase kinase (MAPKK or MEK or MAPK2); PI3K, phosphatidylinositol 3-kinase; mTOR, Mammalian target of rapamycin.

1.5.7. Splicing activity of non-Receptor tyrosine kinases (*BCR–ABL1*) and their roles in CML

Not only can RTKs able to stimulate the cellular signalling pathways through constitutive activation of tyrosine kinases, but non-receptor tyrosine kinases (nRTKs) also play essential roles in the activation of tyrosine kinases through the fusion of the Bcr-Abl oncoprotein (Naka *et al.*, 2016). Bcr-Abl protein is

predominantly located in the cytoplasm of human haemopoietic lineages, such as myeloid, erythroid and lymphoid cells (Naka *et al.,* 2016). The fusion of Bcr-Abl is associated with the activation of Ras-MAPK and PI3K-mTOR pathways leading to regulate gene transcription, cell proliferation and survival, differentiation and inhibition apoptosis (Gowda *et al.*, 2014; Sheng, Wang and Green, 2009). Clinical trails have shown that proliferation of CML expressing *BCR–ABL1* cells can be suppressed in after inhibition of the Ras-MAPK signalling pathway (Sheng, Wang and Green, 2009). In addition, the Bcr-Abl can activate the Janus kinase (JAK)-signal transducers and downstream to STAT5 through HCK or JAK2, Figure 1.14. Activation of JAK-STAT leads to the suppression of apoptosis (Gowda *et al.*, 2014). However, Bcr-Abl protein can directly activate STAT5 through the haemopoietic cell kinase (Hck) to upregulate the anti-apoptotic isoform Bcl-xL (Bibi *et al.,* 2014; Chai, Nichols and Rothman, 1997; Pene-Dumitrescu *et al.,* 2008). It has been shown that the constitutive activation of tyrosine kinases in *BCR–ABL1* cells, increases the levels of anti-apoptotic signals, including B-cell lymphoma-2 (Bcl-2), B-cell lymphoma extra-large (Bcl-xL) and myeloid cell leukaemia-1 (Mcl-1) (Naka *et al.,* 2016).

The fusion oncogene *BCR–ABL1* resides on the Ph^+ chromosome and initiates CML and was found to play an essential role in the haematopoietic transformation from CML-AP to CML-BC (Chu *et al.*, 2007; O'Hare *et al.*, 2011). Sensitivity to apoptosis inducing agents was also reduced in *BCR–ABL1* associated HL-60. Therefore, the fusion of *BCR–ABL1* in CML causes cells to be more resistant to cytotoxic agents (Amarante-Mendes *et al.*, 1998; Roy *et al.*, 2015).

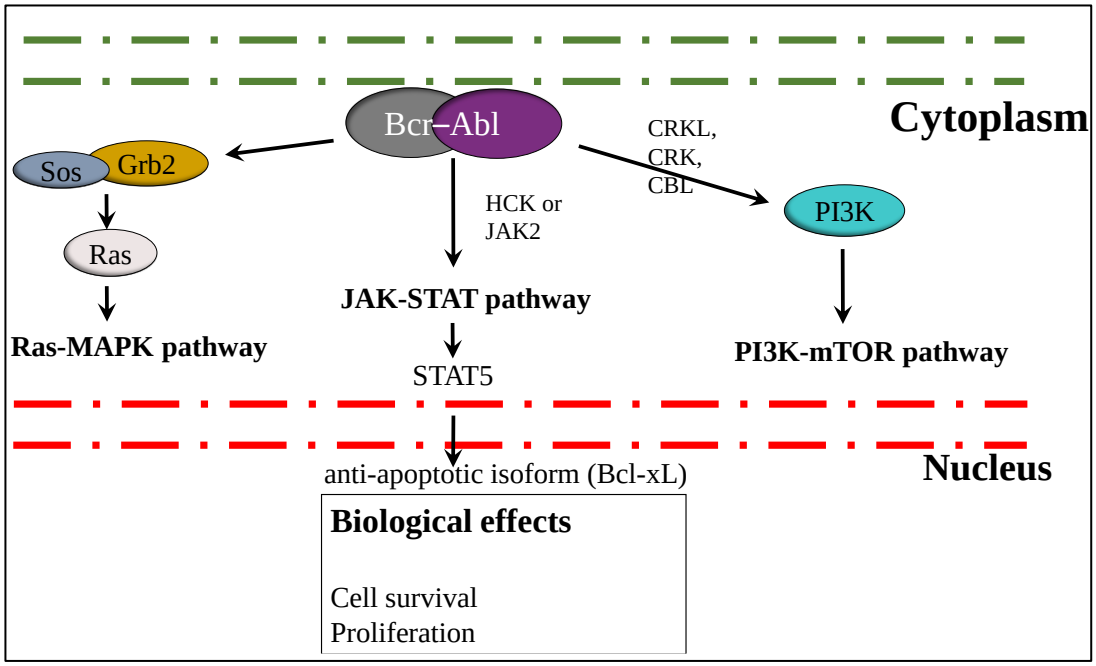

Figure 1.14 The main *BCR–ABL1* intracellular signalling pathways
Constitutive activation of the tyrosine kinase in *BCR–ABL1* in CML. Multiple pathways such as Ras-MAPK, PI3K-mTOR and JAK-STAT are stimulated resulting in suppression of apoptosis, cell survival and proliferation. The fusion of Bcr–Abl oncoprotein activates downstream of Ras-MAPK signalling, the JAK-STAT pathway through HCK or JAK2 and PI3K-mTOR signalling through adaptor proteins, such as CRKL, CRK and CBL. Abbreviations: Sos, son of sevenless; Grb2, growth factor receptor-bound protein 2; Ras, rat sarcoma viral oncogene homolog; MEK, MAP kinase kinase (MAPKK or MEK or MAPK2); JAK, Janus kinase; STAT, signal transducers and activators of transcription.

1.6 Small molecule protein kinase inhibitors as therapeutic agents

In recent years, researchers have been focused on the identification of small molecule inhibitors that target protein kinases in cancer. Of these, the SRPIN340 was found to inhibit SRPK1 leading to the production of the anti-angiogenic VEGF isoform, $VEGF_{165}b$, thereby reducing tumour growth in nude mice (Amin *et al.*, 2011).

The overexpression of SRPK1 or Clk1 has been linked to the increased the phosphorylation of SR factors (Siqueira *et al.*, 2015), increasing protein expression and mediating tumour cell proliferation, Figure 1.15A. SRPIN340 (SR protein

inhibitor 340) and more recently SPHINX (SR protein inhibitor X) function as an ATP-competitive inhibitors that appear to specifically target SRPKs without inhibiting other protein kinases (Siqueira *et al.,* 2015; Fukuhara *et al.,* 2006). Following SR protein phosphorylation inhibition, SR-splicing factors become inhibited and trigger apoptosis in cancer cells, Figure 1.15B. Another strategy inhibits SR protein phosphorylation through a benzothiazol compound (TG003) directed against Clk1 kinase activity, suppressing Clk1-dependent alternative splicing, Figure 1.15B (Fukuhara *et al.,* 2006). More detail on SRPK1 and Clk1 inhibitors will be covered in Chapter 3 and Chapter 4, respectively.

Similarly, the frequent activation of RTKs in cancer has stimulated intensive efforts by clinicians and the pharmaceutical industry to develop inhibitors targeted against tyrosine kinase (TKIs) for cancer treatment. These inhibitors include ATP-competitive imatinib mesylate (IM) that controls the continuous proliferation of cancerous cells in leukaemia (Tamascar and Ramanarayanan, 2009). Imatinib acts as a competitive inhibitor to the adenosine triphosphate (ATP) site on the Bcr-Abl protein fusion. Under normal conditions, ATP binds to the kinase domain on Bcr-Abl casuing phosphorylation and activation of tyrosine residues. However, in a disease state, STI571 or IM binds to the kinase domain blocking phosphorylation and activation of tyrosine residues (Tamascar and Ramanarayanan, 2009), Figure 1.16.

1.6.1. ALTERNATIVE SPLICING IN LEUKAEMIA

1.6.1.1. Alternative splicing of genes involved in apoptosis

Cell death is a natural process whereby old, unwanted and compromised cells are killed. There are several forms of cell death including necrotic cell death and apoptotic cell death. The cell morphology and its molecular features are used to differentiate the type of cell death. Apoptosis or cell suicide is the principle mechanism of cell death (Edinger and Thompson, 2004).

A complex cellular mechanism, apoptosis consists of protein cascades instingating changes in cell structures, resulting in cell shrinkage, nuclear fragmentation (karyorrhexis) and cell death. Apoptosis is more common in eukaryotic cells and is the primary cell death mechanism that can proceed to necrosis in the absent of phagocytosis (Krysko *et al.*, 2008). Necrosis causes the swelling of organelles, leading to cell rupture and spillage of the cellular components causing localised tissue inflammation and immune system involvement (Ziegler and Groscurth, 2004).

Two pathways initiate apoptosis: the intrinsic and extrinsic. The intrinsic pathway is activated in a response to intracellular stress, e.g. DNA damage, oxidative stress and others. The net impact is the release of p53, initiating apoptosis. The Bcl-2 family of proteins produce pro-apoptotic members (Bax, Bid, Bak) and anti-apoptotic members (Bcl-2, Bcl-xL). Under normal physiological conditions, the pro-apoptotic members translocate to the mitochondria and induce permeability of the outer mitochondrial membrane (OMM), and producing pro-apoptotic effectors such as Direct IAP-binding protein with low PI (DIABLO or SMAC), Cytochrome C, apoptosis-inducing factor (AIF) and others.

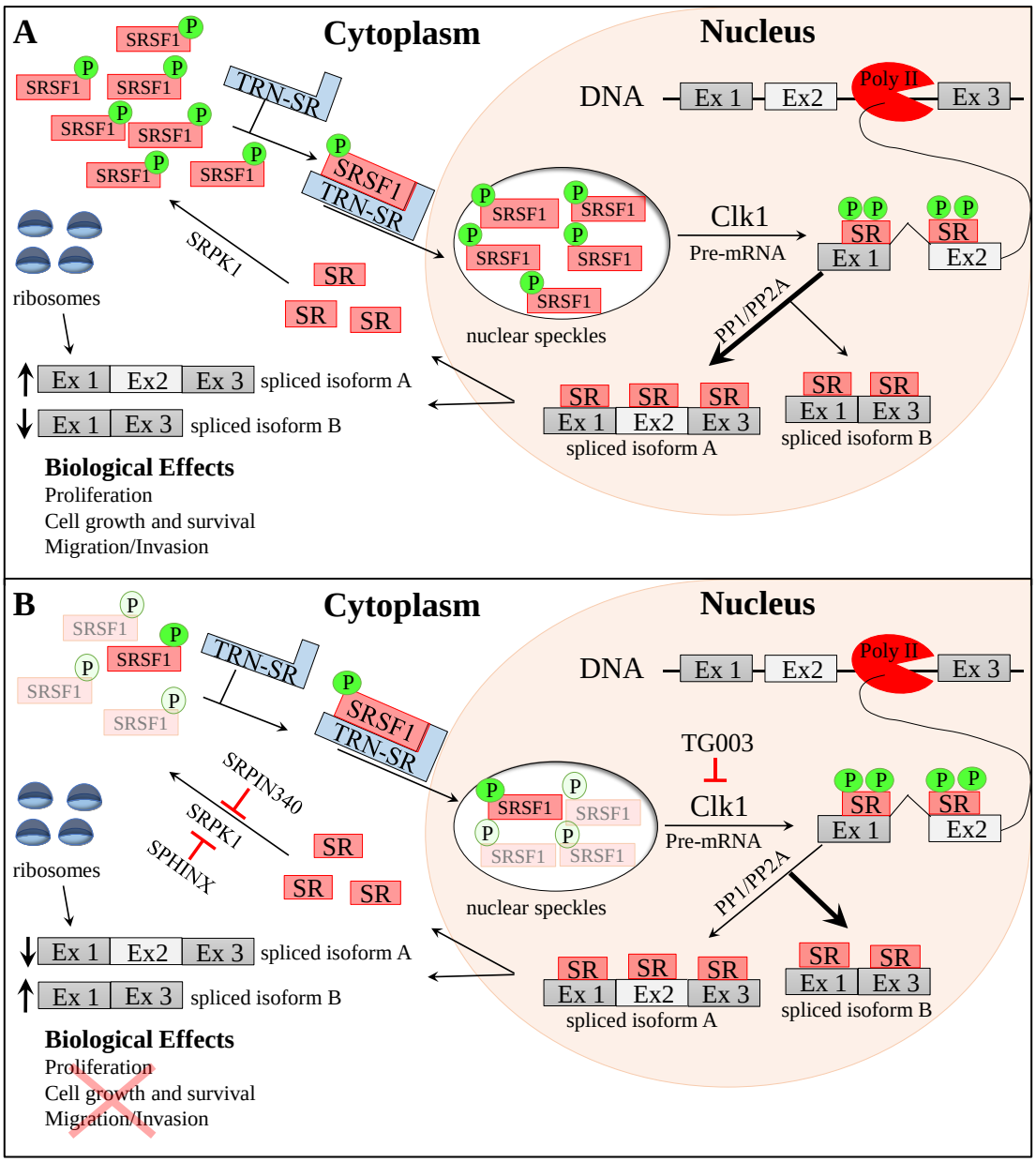

Figure 1.15. The inhibition of SRPK1 or Clk1 by protein kinase inhibitors
A. The overexpression of SRPK1 in cancer increases phosphorylation of SRSF1 that can be stored in nuclear speckles. Further phosphorylation is required by Clk1 to release SRSF1 to splicing sites, increasing the production of mRNA isoform A, triggering increased cell proliferation and delayed apoptosis. **B.** Targeting SRPK1 (SRPIN340 or SPHINX) or Clk1 (TG003) reduces activation of SRSF1 and ultimately switched in splicing, thus increase apoptosis through to up-regulation the expression of isoform B.

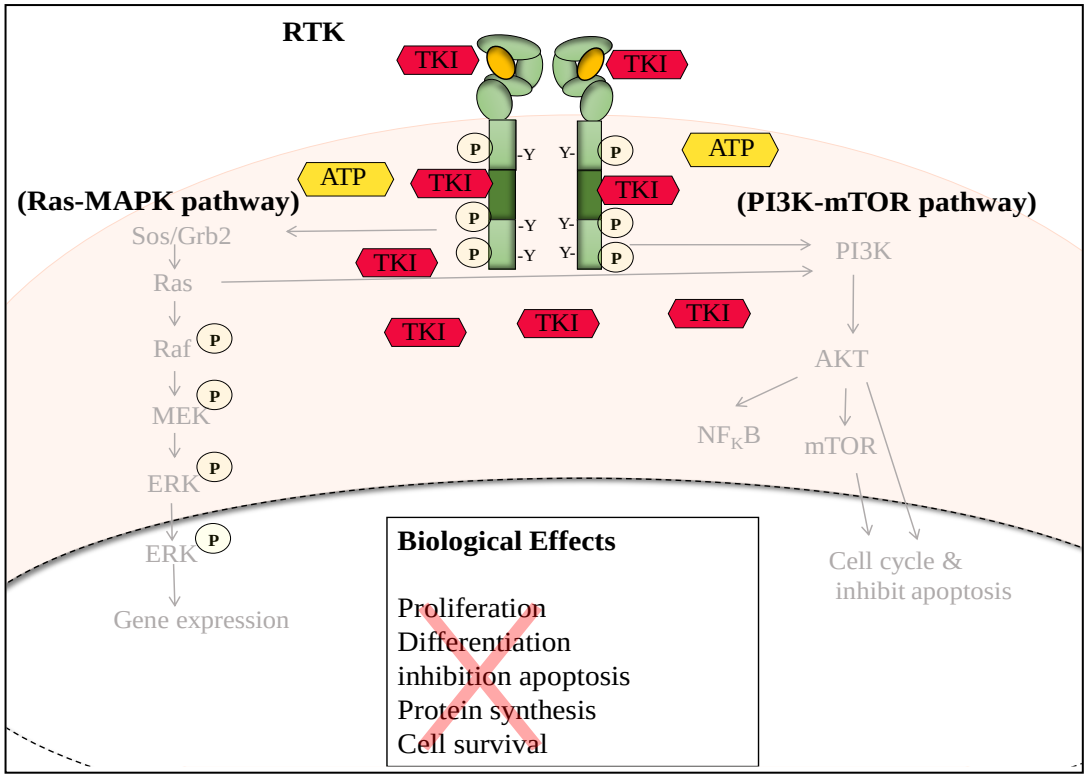

Figure 1.16. The inhibition of the tyrosine kinase receptor by imatinib (IM)
The tyrosine kinase inhibitor (TKI) such as imatinib (IM) blocks activation of receptor tyrosine kinases (RTK) by competing with ATP binding at the kinase domain leading to the inhibition of downstream cellular signalling pathways.

Cytochrome C binds to apoptotic caspase activating factor (APAF-1) forming apoptosomes. Caspase-9 is also activated thereby triggering the apoptosis pathway. Meanwhile, SMAC interacts with inhibitors of apoptosis proteins (IAPs) to inhibit their function and initiate apoptosis (Favaloro *et al.*, 2012).

The extrinsic pathway is mediated by the activation of the TNF receptor superfamily, also called death receptors. The binding of these receptors to their respective ligands leads to the formation of the Death Initiation Signalling Complex (DISC) which triggers a caspase cascade comprising caspase-8 and caspase-3 amongst others. Some cells have sufficient caspase-8 to activate caspase-3 and downstream caspase cascades. However, other cells have limited caspase-8, which would require

mitochondrial amplification (Favaloro *et al.*, 2012). In malignancies, anti-apoptotic factors are overexpressed as a result of desregulation in SR/hnRNP protein expression. This could lead to inhibit apoptosis allowing cancerous cells to survive (Kedzierska and Piekielko-Witkowska, 2017; Placzek *et al.*, 2010).

Caspases are a group of cysteine-aspartic proteases, while caspase-9 is one of the most important intrinsic apoptotic pathway initiators. *CASPASE-9* is located on chromosome 1p36 (Hadano *et al.*, 1999) and is alternatively spliced, generating two protein isoforms (pro- and anti-apoptotic) of opposing function (Vu *et al.*, 2013). These isoforms result from the inclusion or exclusion of a four-exon cassette (exon 3-6), Figure 1.17. In leukaemia, the ratio of caspase-9a/9b isoforms is dys-regulated and occurs through the down-regulation of pro-apoptotic protein isoforms (caspase-9a) and the up-regulation of anti-apoptotic protein isoforms (caspase-9b). Previous studies have suggested that phosphorylation of SR proteins affect *CASPASE-9* splicing. SRSF1 (SRp30a or ASF/SF2) is one of the most important SR proteins involved in the regulation of alternative splicing of *CASPASE-9* (Vu *et al.*, 2013; Shultz *et al.*, 2011).

1.6.1.2. Alternative splicing of other genes involved in leukaemia

The proto-oncogene *RON* (macrophage-stimulating 1 receptor) is located on chromosome 3p21 and has two main splice variants; excluding or including 147 base pairs (bp) of exon 11 in the β-chain (Kang, Babicky and Lowy, 2014). This splicing produces two isoforms: Ron and ΔRon; including or skipping exon 11 respectively. Due to the deletion, ΔRon contains an uneven number of cysteine residues, therefore, these would oligomerise in a dysregulated manner leading to constitutive

activation of RTKs, Figure 1.18. Previous studies have demonstrated increased ΔRon expression in malignancies, such as gastric cancer (Kang, Babicky and Lowy, 2014). Another study found that SRSF1 plays an important role in the alternative splicing of Ron, via the binding to an ESE and enhancing skipping exon 11 (Long and Caceres, 2009). Therefore, inhibiting protein kinases or their splicing factors, such as SRPK1 or SRSF1 may be a potential therapy against leukaemic cells.

Runt-related transcription factor 1 (*RUNX1*), also known as acute myeloid leukaemia 1 (*AML1*) is located on chromosome 21q22. It is a crucial haematopoietic transcription factor and regulates gene expression by binding to specific DNA sequences (Komeno *et al.*, 2014). *RUNX1* encodes α and β subunits of the heterodimeric core binding factor (CBF); the CBFα of which interacts with RUNX1 while the CBFβ subunit is essential for haematopoietic development (Zhao *et al.*, 2012).

RUNX1 is also known as *AML1*, *PEBP2αB* (polymavirus enhancer binding protein 2αB) and *CBFα2* (core-binding factor α2). It generates two isoforms by alternative splicing of exon 6: Runx1 (with exon 6) and ΔRunx1 (without exon 6), Figure 1.19. It has been shown that ΔRunx1 levels are increased in malignancies (Komeno *et al.*, 2014).

AML typically arises from accumulated genetic mutations which are classified according to their role. Class-I-mutations stimulate cell proliferation while class-II-mutations suppress blood cell differentiation. These classes are known as the "two

hit theory" or "multi-hit hypothesis" and was prosposed by Alfred Knudson in 1971 (Knudson, 1971; Wu, Gomes and Sinclair, 2014).

Acute leukaemias are generated from different chromosomal abnormalities, such as: 1) t(8;21)(q22;q22) resulting in the fusion of *RUNX1-ETO* (Runt-related transcription factor 1- eight twenty-one) genes,

2) t(12;21)(p12;q22) resulting in the fusion of *TEL-RUNX1* genes, and 3) t(3;21)(q26;q22) resulting in the fusion of *RUNX1/MDS1/EVI1* genes (Zhao *et al.*, 2012).

However, it has been reported that rare cases of patients with Ph^+ are detected in AML. However, common cases of Ph^+ are found in CML and they are considered as blast phases due to rapid expansion of immature blood cells (blasts) (Bacher *et al.*, 2011). Therefore, co-expression of *RUNX1* with *BCR–ABL1* induces the acute myeloid leukaemia (AML) transformation in CML patients (Zhao *et al.*, 2012), suggesting the importance of evaluating the effect of combinations of ΔRunx1 expression in CML cells.

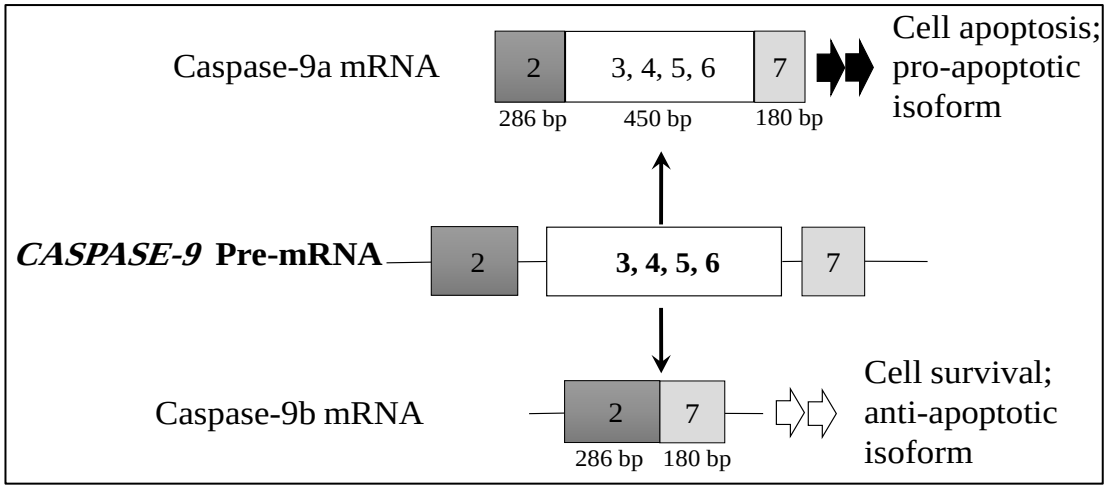

Figure 1.17. The alternative splicing of *CASPASE-9*
The alternative splicing of *CASPASE-9* generates two isoforms: caspase-9a mRNA that includes exons 3, 4, 5 and 6 and caspase-9b mRNA excludes exons 3, 4, 5 and 6.

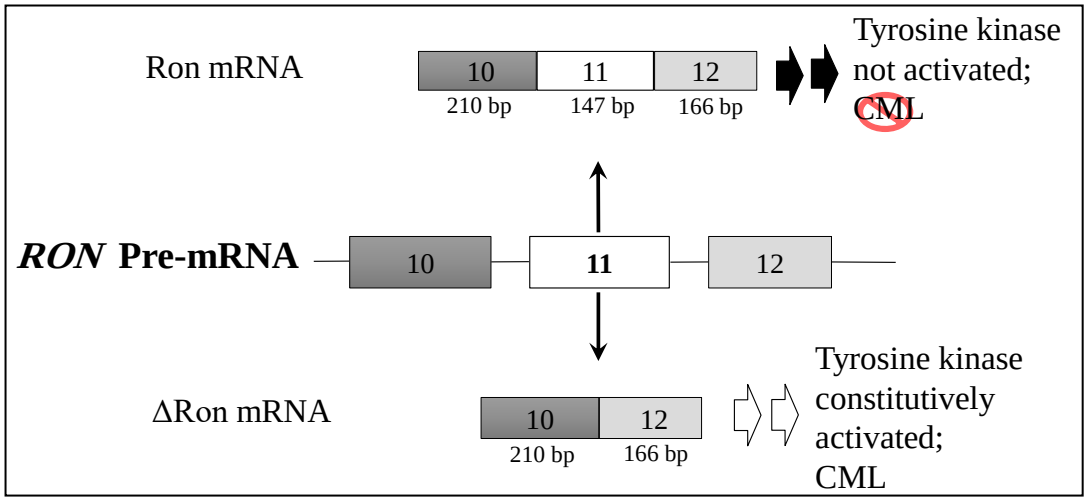

Figure 1.18. The effect of alternative splicing on *RON* (*MST1R*)
The alternative splicing of *RON* generates: Ron and ΔRon protein isoforms including or excluding exon 11, respectively. The expression of ΔRon is increased in malignancies due to the constitutively active tyrosine kinase.

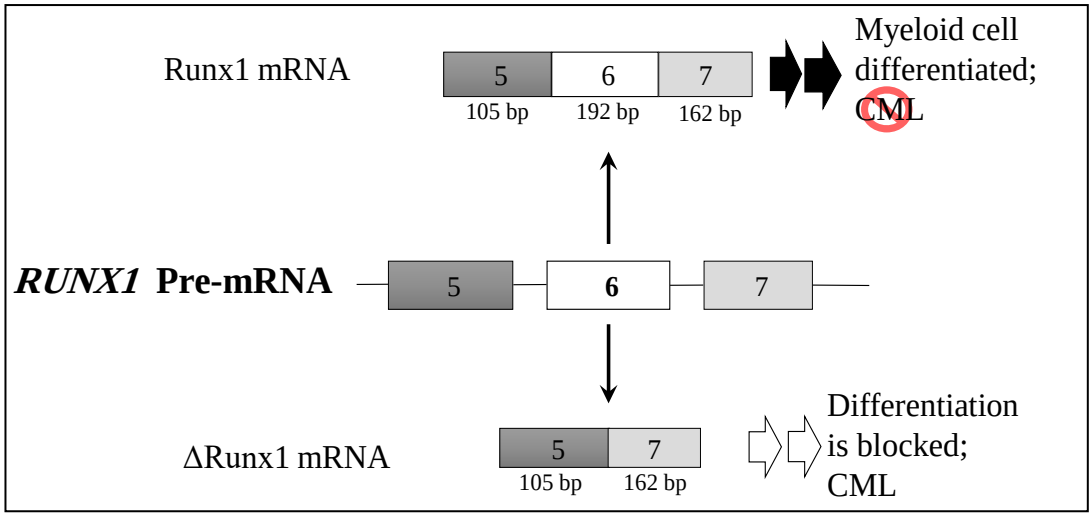

Figure 1.19. *RUNX1* alternatively splicing isoforms
Runx1 and ΔRunx1 isoforms are generated from *RUNX1*. The ΔRunx1 isoform blocks blood cell differentiation resulting in the massive accumulation of immature cells.

1.7 The hypothesis, aim and objectives

SRPK1 and Clk1 regulate the phosphorylation of SRSF1. While SRPK1 plays a direct role importing phosphorylated SRSF1 into the nucleus (Zhou and Fu, 2013), Clk1 has an indirect role whereby it controls the nuclear distribution of SRSF1 at the splicing site (Ghosh and Adams, 2011). As the role of SRPK1 and Clk1 in leukaemia is unclear, this study hypothesised that SRPK1 and Clk1 regulate alternative splicing via SRSF1 phosphorylation in CML.

Targeting SRPK1, Clk1 and SRSF1 through 1) chemical inhibitors, 2) knock-downs using small interfering RNA (siRNA), or 3) establishing a stable knock-down using lentiviral transduction (short hairpin RNA- shRNA) may exert differential expression effects on the alternative splicing of *CASPASE-9, RON,* and *RUNX1* in CML (K562) cells. Studies have shown that co-treatment of IM and amiloride improves CML therapy rather than one agent alone (Change *et al.*, 2011).

Combining kinase inhibitors of TK and SRPK1 or Clk1 inhibitors may provide useful therapeutic options for leukaemia patients.

The specific objectives of this thesis are:

- To investigate how inhibiting or knocking down SRPK1 or SRSF1 switch splicing of *CASPASE-9*, *RON* or *RUNX1* in K562 cells (Chapter 3).
- To investigate how inhibiting or knocking down Clk1 switched splicing of *CASPASE-9*, *RON* or *RUNX1* in K562 cells (Chapter 4).
- To determine the effect of IM alone or in combination with SPHINX or TG003 on the alternative splicing of *CASPASE-9*, *RON* or *RUNX1* in K562 cells (Chapter 5).

CHAPTER 2. MATERIALS AND METHODS

2.1 Cell culture

2.1.1. Cell line Maintenance

All cell lines were purchased from the European Collection of Authenticated Cell Cultures (ECACC, UK). Leukaemic cell lines (Table 2.1) were cultured in 75 cm^2 flasks and grown in RPMI-1640 supplemented with L-glutamine and sodium bicarbonate, 10% (v/v) foetal bovine serum (FBS) and 1% (v/v) penicillin-streptomycin solution P/S (Sigma-Aldrich, UK). All cells were incubated at 37°C in 5% CO_2 and were tested for mycoplasma contamination.

Alternative splicing was analysed following protein kinase inhibition in several leukaemic cell lines (Table 2.1). Of these cell lines, alternative splicing could be demonstrated only in the chronic myeloid leukaemia K562 cell line. Therefore, K562 cell line was chosen for subsequent experiments.

The adherent cell line, PC-3, was u sed as a control in comparing K562 cells treated with si-SRPK1. PC-3 was cultured in Dolbecco's Modified Eagle Medium (DMEM) supplemented with L-glutamine and sodium bicarbonate, 10% (v/v) foetal bovine serum (FBS) and 1% (v/v) penicillin-streptomycin solution P/S (Sigma-Aldrich, UK). When cells reaching confluency, they were also washed with 1 × PBS and incubated with 0.05% trypsin EDTA (Gibco-Invitrogen) to detach. Cells were incubated at 37°C for 5 minutes. Followig detachment, cells were counted and used for further experiments.

Table 2.1. Cell line characteristics

Cell line	**Growth characteristic**	**Molecular feature**
K562	Suspension	CML t(9;22)
KARPAS-45	Suspension	T-cell ALL
MOLT-4	Suspension	T-cell ALL
RPMI-8226	Suspension	Human myeloma
U266	Suspension	Human myeloma
U937	Suspension	Human Caucasian histiocytic lymohoma
HL-60	Suspension	Human Caucasian promyelocytic leukaemia
SUPT-1	Suspension	T-cell ALL

2.1.2. Routine passaging of cells

When cell passaging, suspension cells were stained with trypan blue, counted on a haemocytometer and seeded according to the requirements of each experiment. All media was removed from cells by centrifugation of cells at ≥13,000 × g for 3 minutes. Cells were washed twice with 1 × phosphate buffered saline (PBS).

Adherent cells were also washed with 1 × PBS. Cells were incubated with 0.05% trypsin EDTA (Gibco-Invitrogen) to detach, and incubated at 37°C for 5 minutes. Followning detachment, cells were counted and used for further experiments.

2.1.3. Thawing and freezing of cells

2.1.3.1. Thawing procedure

To defrost cells, cryovials were removed from liquid nitrogen and thawed at 37°C for 1 minute; they were centrifuged at ≥13,000 × g for 3 minutes and cultured in 10 mL appropriate media.

2.1.3.2. Freezing procedure

Suspension cells were grown to > 1 × 10^6 cells/mL, re-suspend in freeze medium (75% RPMI-1640, 20% FBS and 5% dimethyl sulfoxide [DMSO]) and transferred to cryogenic vials. They were then stored at -80°C in a Mr Frosty (Nalgene® Mr Frosty, Sigma-Aldrich, UK), a slow flreezing chamber with isopropanol, for 24 hours before being transferred to liquid nitrogen for long term storage. Adherent cell densities of > 2 × 10^6 cells/mL were re-suspended in 85% FBS and 15% DMSO and treated as above.

2.2 Small molecule inhibitors

K562 cells were treated with protein kinase inhibitors. All small molecules were dissolved in 100% DMSO for stocks and futhre diluted as appropriate in sterile water. K562 cells were treated with protein kinase inhibitors which were dissolved in 100% DMSO (stocks) and further diluted as required required in sterile water. K562 cells were treated with protein kinase inhibitors followed by EGF, to induce the SRPK1 or Clk1-dependent SR activation. As a control, K562 cells were also incubated with 0.02% DMSO to ensure that changes observed in gene expression following treatments were not due to DMSO. More detailed profiling small molecule inhibitors will be covered in later sections.

2.3 RNA extraction and assessment

2.3.1. RNA extraction

Total RNA was extracted from cells using RNeasy® Plus Mini Kit (Qiagen, UK). Initially, 10 μL of β-mercaptoethanol (β-ME) was added to 1 mL Buffer RLT Plus. Cells were washed twice in PBS and appropriate volume of Buffer RLT Plus supplemented with β-ME (Sigma-Aldrich, UK) was added. Harvested cells were mixed by vortexing for 30 seconds. To remove genomic DNA (gDNA), homogenized lysate was transferred to a gDNA spin column placed into a 2 mL collection tube. Genomic DNA removal with these columns is based on a chemical interaction between DNase and homogenized lysates. On-column digestion is more efficient in removing gDNA than in-solution methods. Centrifugation was carried out at ≥9000 × g for 30 seconds. The column was the discarded and the flow-through saved. The RNA was washed by adding one volume of 70% ethanol to the flow-through and mixed by pipetting.

Up to 700 μL from the sample was transferred into RNeasy spin column placed in a 2 mL collection tube. Samples were centrifuged at ≥8000 × g for 15 seconds and the flow-through discarded. Then, 700 μL of Buffer RW1 was added to the RNeasy Mini spin column and centrifuged at ≥8000 × g for 15 seconds. The flow-through was discarded and 500 μL of Buffer RPE was added to the RNeasy spin column. After centrifugation at ≥8000 × g for 15 seconds, the flow-through was discarded. The previous step was repeated twice, and then the spin column was placed in a new 1.5 mL eppendrof. The RNA was eluted twice by adding 30 μL RNase-free water directly to the membrane and stored at -80ºC.

2.3.2. Assessment of RNA yield and quality

RNA purity and concentration was assessed using a Nanodrop 1000A UV spectrophotometer (Thermo Fisher Scientific, USA). Approximately 1 μL of RNA was used and purification determined by calculating the ratio of the sample absorbance at 260/280 nm (A_{260} /A_{280}). The optimal ratio to for pure RNA was 1.8-2.0.

RNA integrity was determined by electrophoresing samples in 2% (w/v) agarose. Agarose (Bioline, UK) was dissolved in 1 × Tris-acetate (TAE) buffer (40 mM TRIS acetate, 10 mM EDTA, PH 8.3) by heating in a microwave. Ethidium bromide (EtBr) (10 mg/mL; Sigma-Aldrich, UK) was added to a final concentration of 3.43 μg/mL. Molten agarose mixture was poured into a gel tray and left to solidify at room temperature for 15 minutes. RNA samples were mixed with DNA loading buffer (Bioline, UK) at a ratio of 4:1 and loaded onto the gel. Electrophoresis was carried out at 90 V for 40 minutes. Gels were visualised and ribosomal RNA (18S and 28S) was detected under UV light using Alpha Innotech instrumentation (FluorchemQ, USA).

2.4 Reverse transcription polymerase chain reaction (RT-PCR)

2.4.1. Primer design

Primers for the genes of interest and reference gene (*CASPASE-9, RON, RUNX1* and *GAPDH*) were designed using the web-based software Primer3Plus, Table 2.2- 2.3. The tool ensured specificity by avoiding cross homologies. Designed primers were blasted using NCBI Probe Database to ensure primer specificity and the absence of

primer-pair formations. Once ordered and delivered (Eurofins MWG Operon, Germany), the primers were tested and confirm specificity by melt-curve analysis using quantitative real-time PCR (qRT-PCR) and 2% agarose gel analysis. Primer specificity was represented as a single peak from the melt curve and a clear band on agarose.

2.4.2. First standard synthesis of cDNA

Approximately 13 μL from total RNA (0.5 - 1 μg) was added to nuclease-free water, mixed with 1 μL of random hexameric primers (0.5 mg/mL) and incubated at 70°C for 5 minutes. Samples were immediately chilled on ice for 2-3 minutes to anneal the primer to targeted sequence. At this point, the samples were supplemented with:

- 5 μL of M-MLV 5x reaction buffer,
- 1.5 μL of dNTP mix,
- 0.5 μL of RNasin Ribonuclease inhibitor,
- 1.0 μL of M-MLV reverse transcriptase and
- 2.0 μL of nuclease free water.

First-strand of cDNA synthesis was performed by incubating the reaction mixture at 37°C for 60 minutes. Resulting cDNA was stored at -20°C until required.

Table 2.2. List of RT-PCR oligonucleotide sequences

Gene	***SRPK1***	***SRSF1***	***CLK1***
Gene name	SRSF protein kinase 1	Serine and arginine rich splicing factor 1	CDC like kinase 1
Accession no.	NM_003137.4	NM_006924.4	NM_001162407.1
Primer sequence	**F:** GGCAATATCGTTCCTTGGAAGTT	**F:** AACAGAGTGGTTGTCTCTGGACT	**F:** TGAATACTATCTTGGGTTTACCGTAT
	R: CACAATGAGCTTGCGAGGCA	**R:** TTCCGTACAAACTCCACGACA	**R:** CGTTTCCTGGTTTTCTGTATCATAT
Alignment	**F:** base 1668 to 1744	**F:** base 570 to 588	**F:** base 1571 to 1601
	R: base 1815 to 1870	**R:** base 589 to 703	**R:** base 1682 to 1687
Amplicon sequence	GGCAATATCGTTCCTTGGAAGTTCTAATC GGATCTGGCTATAATACCCCTGCTGACAT TTGGAGCACGGCATGCATGGCCTTTGAA CTGGCCACAGGTGACTATTTGTTTGAACC TCATTCAGGGGAAGAGTACACTCGAGAT GAAGATCACATTGCATTGATCATAGAACT TCTGGGGAAGGTGCCTCGCAAGCTCATT GTG	AACAGAGTGGTTGTCTCTGGACTGCCTC CAAGTGGAAGTTGGCAGGATTTAAAGGAT CACATGCGTGAAGCAGGTGATGTATGTTA TGCTGATGTTTACCGAGATGGCACTGGT GTCGTGGAGTTTGTACGGAA	TGAATACTATCTTGGGTTTACCGTATTTCCAAC ACACGATAGTAAGGAGCATTTAGCAATGATGG AAAGGATTCTTGGACCTCTACCAAAACATATG ATACAGAAAACCAGGAAACG
Exon	13-15	2-3	10-12
Splice variant	Full transcript	Full transcript	Full transcript
Amplicon length (bp)	203	134	117
Organism	Homo sapiens	Homo sapiens	Homo sapiens
Source	Primer3Plus	Primer3Plus	Primer3Plus

Table 2.2. List of RT-PCR oligonucleotide sequences (cont.)

Gene	***CASPASE-9***	***RON***	***RUNX1***
Gene name	Caspase-9	Macrophage Stimulating 1 Receptor (MST1R)	Runt-related transcription factor 1
Accession no.	NM_001229.3	NM_002447.2	ENST00000431176
Primer sequence	**F:** GCTCTTCCTTTGTTCATC	**F:** CCTGAATATGTGGTCCGAGACCCCCAG	**F:** GCTTCACTCTGACCATCAC
	R: CATCTGGCTCGGGGTTACTGC	**R:** CTAGCTGCTTCCTCCGCCACCAGTA	**R:** GTCGCTGAACGCTGTCAG
Alignment	**F:** base 450 to 633	**F:** base 2743 to 2913	**F:** 21: base 36231727 to 3623192
	R: base 1114 to 1191	**R:** base 3061 to 3226	**R:** 21: base 36164068 to 3616432
Amplicon sequence	GCTCTTCCTTTGTTCATCTCCTGCTTAGAGGACACAGGCCAGGA CATGCTGGCTTCGTTTCTGCGAACTAACAGGCAAGCAGCAAAGT TGTCGAAGCCAACCCTAGAAAACCTTACCCCAGTGGTGCTCAGA CCAGAGATTCGCAAACCAGAGGTTCTCAGACCGGAAACACCCAG ACCAGTGGACATTGGTTCTGGAGGATTTGGTGATGTCGGTGCTC TTGAGAGTTTGAGGGGAAATGCAGATTTGGCTTACATCCTGAGC ATGGAGCCCTGTGGCCACTGCCTCATTATCAACAATGTGAACTT CTGCCGTGAGTCCGGGCTCCGCACCCGCACTGGCTCCAACATCG ACTGTGAGAAGTTGCGGCGTCGCTTCTCCTCGCTGCATTTCATG GTGGAGGTGAAGGGCGACCTGACTGCCAAGAAAATGGTGCTGGC TTTGCTGGAGCTGGCGCAGCAGGACCACGGTGCTCTGGACTGCT GCGTGGTGGTCATTCTCTCTCACGGCTGTCAGGCCAGCCACCTG CAGTTCCCAGGGGCTGTCTACGGCACAGATGGATGCCCTGTGTC GGTCGAGAAGATTGTGAACATCTTCAATGGGACCAGCTGCCCCA GCCTGGGAGGGAAGCCCAAGCTCTTTTTCATCCAGGCCTGTGGT GGGGAGCAGAAAGACCATGGGTTTGAGGTGGCCTCCACTTCCCC TGAAGACGAGTCCCCTGGCAGTAACCCCGAGCCAGATG	CCTGAATATGTGGTCCGAGACCCCCAGGGATGGGTGGCAGG GAATCTGAGTGCCCGAGGGGATGGAGCTGCTGGCTTTACAC TGCCTGGCTTTCGCTTCCTACCCCCACCCCATCCACCCAGT GCCAACCTAGTTCCACTGAAGCCTGAGGAGCATGCCATTAA GTTTGAGTATATTGGGCTGGGCGCTGTGGCTGACTGTGTGG GTATCAACGTGACCGTGGGTGGTGAGAGCTGCCAGCACGAG TTCCGGGGGGACATGGTTGTCTGCCCCCTGCCCCCATCCCT GCAGCTTGGCCAGGATGGTGCCCCATTGCAGGTCTGCGTAG ATGGTGAATGTCATATCCTGGGTAGAGTGGTGCGGCCAGGG CCAGATGGGGTCCCACAGAGCACGCTCCTTGGTATCCTGCT GCCTTTGCTGCTGCTTGTGGCTGCACTGGCGACTGCACTGG TCTTCAGCTACTGGTGGCGGAGGAAGCAGCTAG	GCTTCACTCTGACCATCACTGTCTTCACA ACCGCAAGTCGCCACCTACCACAGAGCCA ATCACAGTGGATGGGCCCCGAGAACCTCC ATCGGCAGAAACTAGATGATCAGACCAAC GAGCTTGTCCTTTTCCGAGCGGCTCAGTC GAGCAGCTGCGGCGCACAGCCATGAGGGT CACACCACCCAGCCCCCACGCCCAACCCT CTCCCTGAACCACTCCACTGCCTTTAACC CCTCAGAGTCAGATGCAGGATACAAGGCA AACCATCCCCACCGTGGTCCTACGATCAC CCAATACCTGGGATCCATTGCCTCTCCTT CACCCAGCAACGCCCATTTCACCTGGACC GCGGCATGACAACCCTCTCTGCAGAACTT TCGACTCTCAACGGCACCCGACCTGACAC AGCGAC
Exon	2-7	10-12	5-8
Splice variant	Caspase-9a: exons 2-7 (742 bp) Caspase-9b: exons 2 and 7 (292 bp)	Ron: exons 10-12 (484 bp) ΔRon: exons 10 and 12 (337 bp)	Runx1: exons 5-8 (482 bp) ΔRunx1: exons 5, 7 and 8 (290 bp
Amplicon length (bp)	742	484	482
Organism	Homo sapiens	Homo sapiens	Homo sapiens
Source	Primer3Plus	Primer3Plus	Primer3Plus

Table 2.3. Reference genes primer information

Gene	***GAPDH***
Gene name	Glyceraldehyde-3-phosphate dehydrogenase
Accession no.	NM_002046
Primer sequence	**F:** ACGGATTTGGTCGTATTGGGC **R:** CTCCTGGAAGATGGTGATGG
Alignment	**F:** base 214 to 217 **R:** base 425 to 425
Amplicon sequence	ACGGATTTGGTCGTATTGGGCGCCTGGTCACCAGGGCTGCTTTTAACTC TGGTAAAGTGGATATTGTTGCCATCAATGACCCCTTCATTGACCTCAAC TACATGGTTTACATGTTCCAATATGATTCCACCCATGGCAAATTCCATG GCACCGTCAAGGCTGAGAACGGGAAGCTTGTCATCAATGGAAATCCCAT CACCATCTTCCAGGAG
Exon	2-5
Amplicon length (bp)	212
Splice variant	Full transcript
Organism	Homo sapiens
Source	Primer3Plus

2.4.3. Standard reverse transcription polymerase chain reaction (RT-PCR)

PCR was performed using sequence specific primers. Each 23 μL PCR reaction contains;

- 5 μL of 5 × Green GoTaq

- 1.5 μL of 25 mM $MgCl_2$

- 0.6 μL of 10 mM dNTP mix

- 0.1 μL of GoTaq Hot Start Polymerase (Promega, UK)

- 10.3 μL of nuclease free water (Sigma-Aldrich, UK)

- 5 μM oligonucleotide primers and,

- 0.5 μL (500-1000 ng) cDNA template.

For negative control amplifications, cDNA was replaced with 0.5 μL nuclease free water. Cycling was performed using a PTC200 DNA engine (MJ RESEARCH,

USA) using the following conditions, Table 2.4. RT-PCR products were store at -20°C until required.

Table 2.4. Thermal cycles for standard PCR conditions

	Conditions	***Temperature (°C)***	***Time (minutes)***
1	Initial Denaturation	94ºC	2:00
2	Denaturation	94ºC	0:30
3	Annealing	60ºC	0:30
4	Extension	72ºC	0:30
5	Repeat Step 2	33 cycles	
6	Final Extension	72ºC	5:00
7	Forever	4ºC	-

2.5 Agarose gel electrophoresis

Agarose gel electrophoresis separated RT-PCR products according to molecular weight. PCR product reactions were electrophoresed in 2% agarose gels with ethidium bromide (EtBr) (10 μg/mL) (Sigma-Aldrich, UK). DNA hyperladder: HyperLadder Π (Bioline, UK) was electrophoresed simultaneously to estimate RT-PCR product sizes. A gel was made and allowed set (as previously described) and an electrophoresis tank filled with 1 × TAE buffer to approximately 2 mm above the gel surface. PCR reaction volumes were loaded and electrophoresis carried out at 100 V for 40 minutes. After electrophoresis, the PCR products were visualised under UV light using Alpha Innotech technology (FluorchemQ, USA).

2.5.1. Normalisation of RT-PCR

To ensure gene expression are alternations were due to treatments alone, gels were analysed using ImageJ software that measured RT-PCR band densities; the data from

which was exported to Statistical Package for the Social Sciences (SPSS) software. The graphs depicted the splice variants from K562 cells, such as Casp9a/9b mRNA ratios. Data were presented as mean ± SE. Statistical differences between treatment groups were compared using one-way ANOVA. *P* values less than or equal to 0.05 were significant (* $P \leq 0.05$).

2.6 Gel extraction and purification of PCR products

To sequence the PCR products, DNA purification following electrophoresis was required. The MiniElute® Gel Extraction kit (Qiagen, UK) was used to extract DNA from gels. Initially, PCR was performed in 23 μL reaction volumes (7 tubes) and pooled together. After electrophoresing the desired band was removed with a sterile scalpel.

DNA Gel elution involved several steps. After weighing the gel, three volume of Buffer QG was added to 1 volume of gel (100 mg of gel ~100 μL). The gel solution was dissolved at 50°C for 10 minutes with periodic vortexing. Once dissolved, one gel volume of isopropanol was added and mixed by inverting. The sample was placed in a MinElute spin column for centrifugation at ≥1000 × g for 1 minute. The flow through was discarded. Buffer PE (500 μL) was added to the MinElute column and incubated at room temperature for 5 minutes. The flow through was discarded after centrifugation at ≥1000 × g for 1 minute. At this point, MinElute columns were placed into clean 1.5 mL Eppendrof tubes. The elution was initiated by adding Buffer EB (30 μL) to the centre of the MinElute membrane, incubating at room temperature for 5 minutes and centrifuging for 2 minutes. The purified cDNA was

analysed on a 1.5% agarose gel and stored at -20°C until sequencing (Eurofins MWG Operon, Germany).

2.7 Methods specific for Chapter 3 and 4

2.7.1. Treatment of K562 cells with protein kinase inhibitors

For inhibition studies, 10 μM of SRPIN340 (N-[2-(1-Piperidinyl)-5-(trifluoromethyl) phenyl] isonicotinamide), has shown to inhibit SRPK1, leading to the suppression of VEGFA in a mouse model (Dong *et al.,* 2013). SRPIN340 is a specific serine/threonine protein kinase inhibitor that suppresses both SRPK1 and SRPK2 expression (Dong *et al.,* 2013). SRPIN349 exerts no inhibitory effects on SRPK1 due to the lack of a lack of a triluorormethyl group, therefore it can be used as a negative control (Gammons *et al.,* 2013).

Alternative splicing was analysed in K562 cells treated with a range of SRPIN340 concentrations. Two concentaions; 10 and 20 μM were used for futher experiments. After a 30 min pre-treatment with selective inhibitors for SRPK1, K562 cells were incubated with 100 ng/mL EGF for 24 hours. K562 cells were also treated with SRPK340/9 and 0.02% of DMSO prior to RNA extraction.

In addition, SPHINX (5-methyl-N-[2-(morpholin-4-yl)-5-(tri-fluoromethyl)phenyl]furan-2-carboxamide) was shown to have similar inhibitory properties to SRPIN340 in relation to SRPK1 suppression. However, SPHINX is a more selective inhibitor SRPK1 function (Gammons *et al.,* 2013). K562 cells were treated with a range of SPHINX concentations (0 to 30 μM) followed by EGF, as previously descriped.

TG003, (Z)-1-(3-Ethyl-5-methoxy-2,3-dihydrobenzothiazol-2-ylidene)-2-propanone is a benzothiazole agent that suppresses Clk1. As a Cdc2-Like Kinase inhibitor, it acts as an ATP-competitive inhibitor for the Clk family. The agent increases skipping of mutated exon 31 of the dystrophin gene, suggesting an important role as a small molecule inhibitor in disease mechanisms (Sakuma, Iida and Hagiwara, 2015).

Another member of the family is TG009. This molecule elicits approximately 400 times weaker inhibition than TG003, therefore it is used as a negative control (Muraki *et al.*, 2004). K562 cells have demonstrated sensitivity to higher concentrations of TG003. Therefore, a range of TG003 concentrations (50 to 150 μM) were chosen and followed by EGF or DMSO treatment, as previously descriped. All inhibitors and their chemical structures were drawn using ChemSketch software (Table 2.5).

Both SRPIN340/349 and TG003/9 were kindly provided by Professor Masatoshi Hagiwara (University of Kyoto, Japan). They were dissolved in 100% DMSO to generate a 50 mM of stock. Further dilutions were prepared in sterile water (Table 2.6).

Table 2.5. List of inhibitors and their chemical structures

Compound	Structure
SRPIN340 (SR protein inhibitor 340)	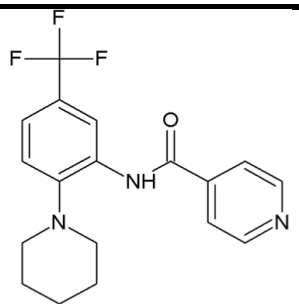
SRPIN349 (Negative SR protein inhibitor 349)	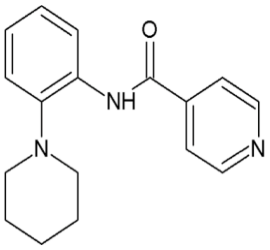
SPHINX (SR protein inhibitor X)	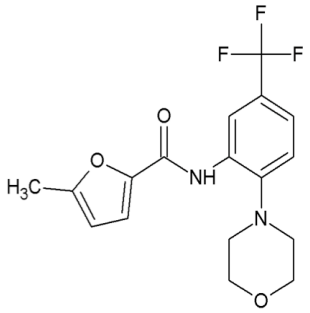
TG003 (Cdc2-Like Kinase 1 inhibitor)	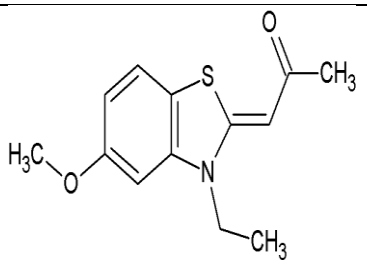
TG009 (Negative Cdc2-Like Kinase 1 inhibitor)	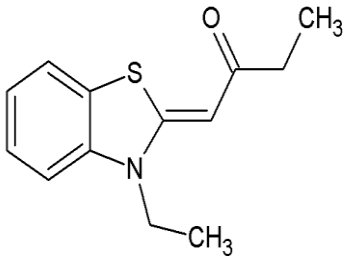

Table 2.6. List of inhibitors and their dilutions

Compound	**Stock concentration**	**Dilution**	**Final concentration μM**
SRPIN340- SRPIN349	50 mM	1:200	10 μM
		1:100	20 μM
SPHINX	50 mM	1:400	5 μM
		1:200	10 μM
		1:100	20 μM
		1:66.6	30 μM
TG003	50 mM	1:40	50 μM
		1:20	100 μM
		1:13.3	150 μM

2.7.2. RNA interference

2.7.2.1. siRNA transfection

Before transfection, K562 cells were cultured overnight with antibiotic free RPMI-1640 media. On the day of transfection, cells were cultured for 2 hours in Opti-MEM® I Reduced Serum Media (Life Technologies, UK), after which they were seeded in 6-well plates at a density of 0.5×10^6. Cells were then transfected with a siGENOME siRNA smartpool of SRPK1, SRSF1 and a siGENOME siRNA pool of Non-targeting (Thermoscientific, UK).

According to the manufacturer's guidelines, 2 mM of the siRNA transfection stock was prepared through dissolving in 1 × siRNA buffer (Thermoscientific, UK) and

further diluted to 100 nM. In two separate tubes, 100 nM siRNA and Dharmfect 2 transfection reagent (increases cell membrane permeability) were diluted in Opti-MEM® I Reduced Serum Media. Incubation of both was carried out at room temperature for 5 minutes followed by gentle pipetting to mix. After this, the transfection mix was prepared by adding the diluted siRNA to the transfection reagent and incubating at room temperature for 20 minutes.

During incubation, Opti-MEM® I medium was removed from the cells and replaced with fresh medium. The cells were transfected with the appropriate volume of transfection mix at a final concentration of 75 nM siRNA and 2 µM Dharmatect 2 reagent per well for 48 - 72 hours. After 4 hours of incubation, the transfection reagent was removed and replaced with antibiotic free medium. All procedures were carried out in technical and biological triplicates.

K562 cells were also seeded in 6-well plate at a density of 0.5×10^6 and transfected with three different CLK1 silencer siRNA and Non-targeting, Chapter 4 (Ambion, UK). The three siRNAs and the Non-targeting siRNA were dissolved as the candidate siRNA of SRPK1 and SRSF1.

2.7.2.2. shRNA transduction

Stable knockdown was of SRPK1 was achieved using SMART vector 2.0 lentiviral shRNA constructs in K562 cells. A puromycin selection cassette ensured the elimination all untransduced cells. To achieve this, the minimal puromycin concentration was determined. K562 cells were cultured in complete medium, in 6-well plate, at 3×10^5 cells per well. The next day, the medium was replaced with

fresh medium supplemented with different puromycin concentrations (0.1 - 10 μg/mL). The cells were incubated at 37°C in 5% CO_2 for 3 to 4 days. Cell proliferation was assessed and medium supplemented with puromycin was replaced every two days. Cells were examined daily and the minimal puromycin concentration that efficiently eliminated all untransduced cells between 4 - 6 days was identified.

For a successful transduction, it was necessary to use a ratio of SMART vector 2.0 that would generate a particular multiplicity of infection (MOI). Different cell lines have different MOIs for establishing stable knockdown of the target genes. shRNA transduction was achieved according to the manufacture's guidelines.

2.7.3. Apoptosis quantification using acridine orange staining

Acridine orange (AO) is a nucleic acid selective stain used in cell-cycle studies. AO is a cationic dye, is membrane permeable and intercalates with the nucleic acids of viable cells to distinguish between apoptosis and necrosis. Apoptosis quantification was carried out using a fluorescence microscope (Nikon Eclipse 80i). K562 cells were plated at a concentration of 20×10^3 cells/mL in 6-well plate, treated with kinase inhibitors and incubated at 37°C in 5% CO_2 for 24 hours. Cells were pelleted at ≥40 × g for 5 minutes and supernatants discarded. The pellet was washed twice with PBS and finally resuspended with 150 μL PBS. Cells were adjusted in the cytofunnel (Fisher Scientific, UK) and centrifuged at ≥20,000 × g for 10 minutes using Cyospin 4 (Thermo Scientific, UK). Slides were removed from cytocentrifuge, air-dried and were fixed with absolute methanol for 10 minutes air dried again.

For staining, slides were immersed in fresh phosphate buffer [0.66% (w/v) potassium phosphate mono- basic + 0.32% (w/v) sodium phosphate dibasic, pH 6.4-6.5)], then stained in AO solution (0.12 mg/mL in phosphate buffer) for 45 seconds. Slides were placed in phosphate buffer for 10 minutes, followed by a further 15 minutes wash in fresh buffer.

After staining and drying, slides were protected from light. For morphology analyses, slides were observed using a fluorescent microscope for up to 30 minutes before fluorescence faded. Nuclei morphology was analysed using a BG-12 excitation filter and 0-530 barrier filter under × 40 objective lens. The criteria for identifying cells were nuclei and micronuclei (DNA) were stained yellow/green and the cytoplasm was stained red. Various stages of apoptotic and necrotic cell dealth were identified in cells treated with SRPIN340 or SPHINX when compared to EGF control. Percentages of viable, apoptotic and necrotic cells were determined in at least 1,000 cells per treatment. All experiments were repeated three times.

2.7.4. APC Annexin V assay

Annexin V:FITC staining detects apoptotic cells in a flow cytometry (BD Biosciences, USA). Annexins binding to phospholipids and Annexin V-FITC binding to phosphatidylserine (PS) is a calcium mediated process. In living cells, PS is located inside the lipid layer, however during apoptosis, phospholipids are exposed extracellularly due to e.g. cell assault. This causes PS stimulation and exposure at the cell surface, Therefore PS and Annexin binding are valuable apoptotic markers.

Before flow cytometric analysis, 1×10^6 of cells were washed twice with cold 1 × PBS and resuspended in 1 × binding buffer. Cells incubated with 5 μL of Annexin V and 5 μL propidium iodide for 15 minutes at room temperature, in the dark. After incubation, 400 μL of 1 × binding buffer was added prior to flow cytometry. Viable cells show no staining, they are APC Annexin V^- or Propidium $Iodide^-$ while poptotic cells are APC Annexin V^+ but Propidium $Iodide^-$. Cells undergoing late apoptosis or already dead from necrosis are APC Annexin V^+ and Propidium $Iodide^+$, Figure 2.1.

2.7.5. Protein analysis

2.7.5.1. Cells harvesting and protein extraction

Proteins were extracted from cells using Radioimmunoprecipitation assay (RIPA) lysis buffer (Sigma-Aldrich, UK). Harvested cells were washed twice with ice-cold

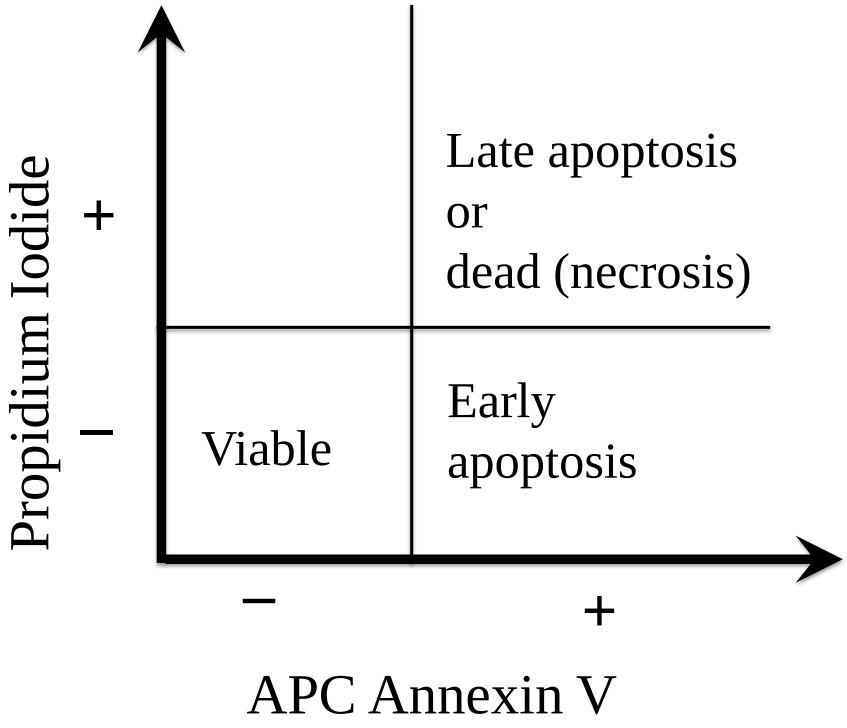

Figure 2.1. Apoptosis by flow cytometry using Annexin V and Propidium Iodide staining

1 × PBS and centrifuged at 3000 × g for 3 minutes to pellet the cells, after which the 1 × PBS was drained and ice-cold lysis buffer (0.5 mL per 5×10^6 cells) added. The RIPA buffer was supplemented with fresh protease and phosphatase inhibitor cocktail (1:1000) (Sigma-Aldrich, UK). Samples were further centrifuged at 4°C for 10 minutes at ~20,000 × g and placed on ice, after which the supernatant (protein) was transferred to a fresh Eppendrof tube and stored at -80° C until use.

2.7.5.2. The pierce™ BCA assay for protein quantification

For protein estimation, dilutions of known concentrations were prepared to generate a standard curve. The protein standard, bovine serum albumin (BSA) (Sigma-Aldrich, UK), was diluted in sterile water to prepare a set of BSA standards, Table 2.7. For each standard, 25 µL was added in triplicates of 96-well plate.

Table 2.7. Preparation of BSA standards

	Volume of diluent (µL)	***Volume of BSA (µL)***	***Final BSA concentration (µg/mL)***
A	700	100 of Stock	250
B	400	400 of vial A dilution	125
C	450	300 of vial B dilution	50
D	400	400 of vial C dilution	25
E	400	100 of vial D dilution	5
F	400	0	Blank

Chilled samples were prepared by mixing 1 part of sample with seven parts of RIPA buffer (1:7, sample: RIPA buffer). For each diluted samples, 25 µL was added to triplicate 96-well plate. Protein quantification was carried out by preparing a working reagent (WR); 50 parts of BCA Reagent A to 1 part BCA reagent B (50:1, A:B). Whole protein content was quantified in triplicate at λ 595/490 nm using Revelation Quicklink software (Opsys Microplate Reader by Dynex Technologies, UK).

2.7.5.3. SDS polyacrylamide gel electrophoresis (SDS-PAGE)

Sodium dodecyl sulfate-polyacrylamide gel electrophoresis (SDS-PAGE) was used to separate proteins according to size in an electric field (electrophoresis). Samples were thawed and 75 µg protein lysates were mixed with 1 × NuPAGE LDS sample buffer (Bio-rad, UK) supplemented with β-mercaptoethanol (1:20) (Sigma-Aldrich, UK) and make up to 20 µL. The mixture was heated to 95°C for 5 minutes prior to loading onto 4-15% Tris-Glycine eXtended (TGX) pre-cast gradient gel. In order to assess molecular weight, pre-stained protein standard markers (Bioline, UK) were loaded into the first lane. The gel was electrophoresed 1 × running buffer (10 × Running Buffer diluted in dH_2O) at 150V for 1 hour. All chemicals are listed in Table 2.8.

Table 2.8. Buffer composition

No	Buffers	Composition
1	10 × Running buffer	144 g Glycine, 30.3 g Tris base, 10 g SDS, 825 mL dH_2O.
2	1 × Running buffer	10% Running buffer (10×), 90% dH_2O.
3	10 × Transfer buffer	144 g Glycine, 30.3 Tris base 825 mL dH_2O.
4	1 × Transfer buffer	10% Transfer buffer (10×), 10% Methanol, 80% dH_2O.
5	10 × TBST	24.23 g Tris base, 80.06 g NaCl, 900 mL dH_2O
6	1 × TBST	100 mL TBST (10×), 10 mL Tween 20, 890 mL dH_2O. Adjust pH to 7.5

2.7.5.4. Western blot analysis

Following gel electrophoresis, gel separated proteins were transferred to polyvinylidene fluoride (PVDF) membrane (GE Healthcare, UK). Membranes were activated by immersing in absolute methanol for 1 minute, and immersing in 1 × transfer buffer (10 × transfer buffer diluted in dH_2O supplemented with 10% methanol) for 10 minutes. A sandwich of sponges, filter papers, gel and PVDF membrane were prepared in a cassette, Figure 2.2. The assembled cassette was placed in 1 × transfer buffer in a transfer tank and protein were transferred at 250V for 1 hour.

After transfer, the unit was dissembled and the PVDF membrane blocked in 5% BSA and 1 × TBST (10 × TBST diluted in dH_2O) at room temperature for 1 hour with constant agitation. Blocking the membrane prevents unspecific binding of antibodies to membranes. Antibodies were diluted in 5% BSA in 1 × TBST, Table 2.9.

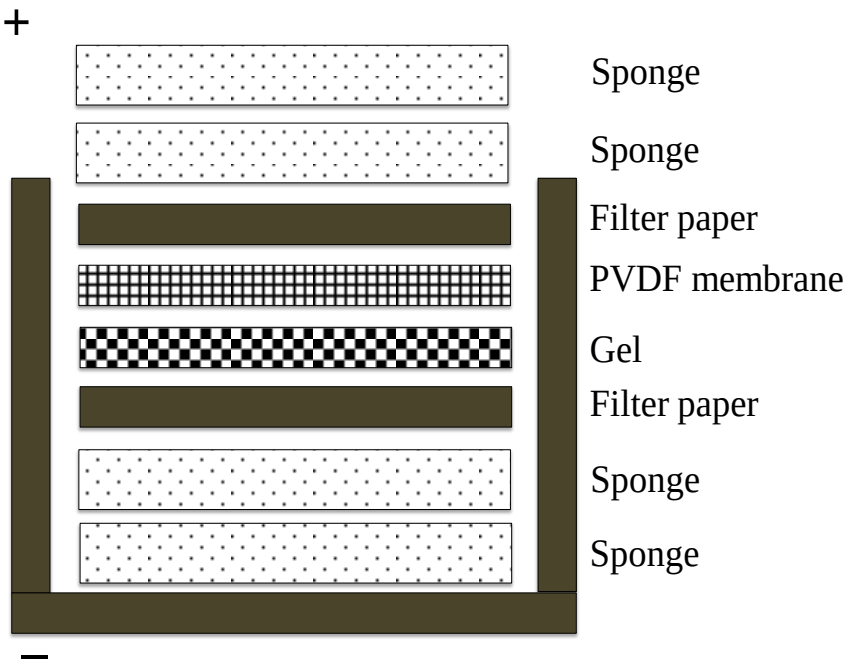

Figure 2.2. Sandwich assembly for protein transfer to PVDF membrane

After blocking, primary antibody was added and incubated overnight at 4°C with gentle agitation. The next day, membranes were washed 3 times with Tween (0.1%) and 1 × TBST for 5 minutes intervals and incubated with a secondary antibody diluted in blocking solution, at room temperature for 30 minutes with constant agitation. The secondary antibody was either anti-rabbit or anti-mouse IgG peroxidase (acts as an antibody-enzyme conjugate), Table 2.9. The membrane was washed 3 times with Tween (0.1%) and 1 × TBST for 5 minutes intervals. Finally, the membrane was incubated with equal amounts of luminol/enhancer and peroxide solutions for 1-4 minutes (Bio-rad, UK). The bound antibody was detected by an Amersham Imager 600 machine.

Table 2.9. Antibodies for Western blotting

Primary antibodies			
Antibody	**Species**	**Concentration/ Dilution**	**Manufacturer**
SRPK1	Mouse	1 µg/mL	Abcam, UK
SRSF1	Rabbit	1 µg/mL	Abcam, UK
CLK1	Rabbit	900 µg/mL	Aviva systems biology, USA
Tubulin – α	Mouse	1:10 000	Sigma-Aldrich, UK
Secondary antibodies			
Polyclonal anti – Rabbit (peroxidase conjugated)	Goat	1:10 000	Sigma-Aldrich, UK
Polyclonal anti – Mouse (Horse radish peroxidase conjugated)	Goat	1:10 000	Santa Cruz Biotechnology, UK

2.7.5.5. Western blot normalisation

ImageJ software was used to quantitatively analyse Western blots. Density values were exported to SPSS to calculate the average and standard error for each sample. The results were normalised against α-tubulin expression and the statistical differences compared with scrambled shRNA (sh-CTRL) or with the si-CTRL cells using one-way ANOVA. *P* values less than or equal to 0.05 were considered significant (* $P \leq 0.05$).

2.8 Methods specific for Chapter 5

2.8.1. Treatment of K562 cells with protein kinase inhibitors

Imatinib Mesylate (IM or STI571) is a tyrosine and serine/threonine protein kinase inhibitor (Selleckchem, UK) which was dissolved in DMSO and stored in 10 mM stocks at -20°C.

Imatinib mesylate (IM) or STI571 (4-[(4-methyl-1-piperazinyl) methyl]-N-[4-methyl-3-[[4-(3-pyridinyl)-2-pyrimidinyl] amino] phenyl] benzamide methanesulfonate (imatinib, Gleevec®; Novartis, Basel, Switzerland), is a tyrosine kinase inhibitor (TKI) of Bcr-Abl in CML (Tamascar and Ramanarayanan, 2009). As a powder (Selleckchem, UK), it was dissolved in DMSO and stored as 10 mM stocks at -20°C. The chemical structure of IM was drawn using ChemSketch software, Table 2.10.

IM has been used as a front-line treatment for multiple cancers, most notably Philadelphia chromosome positive (Ph^+) chronic myeloid leukaemia (CML). The formation of Ph^+ is due to the fusion of Bcr-Abl proteins, resulting in constitutive tyrosine kinase activation. Despite the effectiveness of IM treatments, it induces approximately 98% of gene expression changes when used for one week (Philips *et al.*, 2014).

Other studies have shown that other mutations may occur within the Bcr-Abl kinase domain, causing a reduced affinity for IM binding (Wieczorek and Uharek, 2016; Bhamidipati *et al.*, 2013). It has been suggested that combining protein kinase

inhibitors may provide successful cancer treatments (Dienstmann *et al.*, 2014). For example, a shift in *APAF-1*, *CRK*, and *SURVIVIN* splicing was observed in K562 cells treated with IM and amiloride (Chang *et al.*, 2011). In this regard, the co-administration of IM with other protein kinase inhibitors is required to re-sensitise CML patients to IM.

The International Randomised Study (Yoon *et al.*, 2013; Yeung *et al.*, 2015) recommended IM range of 400 mg/day to 800 mg/day to treat Ph^+ CML patients, depending on the disease stage (Yoon *et al.*, 2013; Yeung *et al.*, 2015). The European Treatment Outcome Study suggested the equivalent concentrations for CML (EUTOS) from mg/day to μg/mL (Table 2.11) (Egorin, Molimard and Mahon 2007). Three different concentrations of IM alone were initially used; 1.0, 1.4 and 2.9 μg/mL. A final dose of 1.0 μg/mL was chosen for subsequent experiments. Cells were treated with 1.0 μg/mL in combinations with SPHINX doses (5 – 20 μM) and TG003 doses (25 – 100 μM).

Table 2.10. The chemical structure of Imatinib

Compound	**Structure**
Imatinib mesylate- IM or STI571 (Tyrosine kinase inhibitor, TKI)	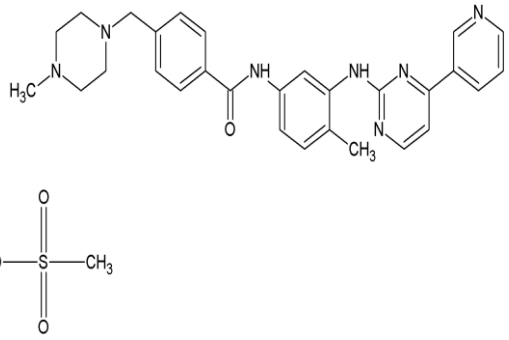

Table 2.11. Imatinib ranges recommended for CML patients

Compound	**Concentrations mg/day**	**Concentrations µg/mL**
Imatinib mesylate- IM or STI571 (Tyrosine kinase inhibitor, TKI)	400 mg/day	1.0 µg/mL
	600 mg/day	1.4 µg/mL
	800 mg/day	2.9 µg/mL

CHAPTER 3. TARGETING SERINE ARGININE-RICH SPLICING FACTOR 1 (SRSF1) AND SERINE ARGININE PROTEIN KINASE-1 (SRPK1) IN A CHRONIC MYELOID LEUKAEMIA CELL LINE

3.1 Introduction

The serine/arginine-rich splicing factor 1 (SRSF1) is a proto-oncogene and is a member of the SR protein family. SRSF1, alternatively known as ASF/SF2 or SF2/ASF, is essential for alternative splicing regulation (Moulton, Gillooly and Tsokos, 2014). SRSF1 is also involved in several functions beyond mRNA splicing, including mRNA stability regulation, translation (Moulton, Gillooly and Tsokos, 2014), nuclear export and nonsense-mediated mRNA decay (Goncalves and Jordan, 2015). Several studies suggested that SRSF1 overexpression in some cancers is down to the dysregulation of alternative splicing in several genes, for example, SRSF1 overexpression was detected in paediatric acute lymphoblastic leukaemia (ALL) (Zou *et al.*, 2012), similarly, it has been suggested that human lung cancer is linked to SRSF1 overexpression by increasing the anti-apoptotic isoforms of 3 genes: *BIN1*, *BIM* and *MCL1* (Das and Krainer, 2014).

Angiogenesis (new blood vessel formation) is regulated by vascular endothelial growth factor A (*VEGFA*). It has been shown that upregulation of SRSF1 increases the production of a splice variant of *VEGFA*, called the pro-angiogenic ($VEGF_{165}$) isoform in a mouse model of retinal neovascularization (Nowak *et al.*, 2010). Another study indicated that SRSF1 overexpression led to the constitutive production of the ΔRon isoform, causing increased cell motility in breast and colon

carcinomas (Long and Caceres, 2009). SRSF1 overexpression also drives transformation of immortal lung cancer cells through increases in the caspase-9b (anti-apoptotic) isoform (Shultz *et al.*, 2011).

SRSF1 phosphorylation is controlled by serine-arginine protein kinase 1 (SRPK1) in order to regulate alternative splicing. Phosphorylated SRSF1 accumulates in the nucleus and is stored in the nuclear speckles (Aubol and Adams, 2011; Czubaty and Piekielko-Witkowska, 2017). It has been speculated that SRPK overexpression is linked to increased regulation of human immunodeficiency virus (HIV) and hepatitis C virus (HCV) (Karakama *et al.*, 2010). Overexpression of SRPK1 has been reported in several malignancies, such as prostate cancer, breast cancer, lung cancer and glioma (Bullock and Oltean, 2017).

Evidence shows that SRPK1 knockdown, or inhibition of its catalytic activity reduces SRSF1 phosphorylation levels, causing shifts in the alternative splicing of several genes, thereby limiting tumour growth (Goncalves *et al.*, 2014; Mavrou and Oltean, 2016; Nowak *et al.*, 2010). Despite these important observations, the precise roles of SRSF1 and SRPK1 in leukaemia remains unclear, therefore targeting SRSF1 and/or SRPK1 and analysing the alternative splicing of e.g. *CASPASE-9, RON,* and *RUNX1* in chronic myeloid leukaemia cells could be enlightening in uncovering disease molecular mechanisms.

Moreover, SRPK1 knockdown limits tumour growth in colon cancer. It also shifts *VEGFA* alternative splicing, increasing the expression of the anti-angiogenic isoform in prostate cancer cells (Mavrou and Oltean, 2016). As SRPK1 regulates alternative

splicing and thus gene expression, it is critical to identify the precise roles SRPK1 or SRSF1 in K562 cells.

3.2 Hypothesis

The inhibition of SRPK1 or its splice factor (SRSF1), either pharmacologically or knockdown affects *CASPASE-9*, *RON* and *RUNX1* alternative splicing in K562 cells. SRPK1 or SRSF1 knockdown was achieved through K562 cell transfection with siRNA or generate stable knockdown using lentiviral transduction (short hairpin RNA–shRNAs).

3.3 Objectives

All experiments were performed in the K562 cell line unless otherwise stated;

- To assess proliferation of cells treated with SRPK1 small molecule inhibitors (Chapter 2, Materials and methods (Table 2.5)), prior to epidermal growth factor (EGF) addition.
- To detect the effect of SRPK1 inhibitors on *CASPASE-9*, *RON* and *RUNX1* alternative splicing in K562 cells followed by EGF or dimethyl sulfoxide (DMSO) (Chapter 2: Materials and methods, section 2.7.1).
- To investigate the effects of SRPK1 inhibitors on cell survival and cell death (apoptosis and necrosis) by acridine orange staining followed by EGF treatment.
- To assess the cellular responses to SRPK1 inhibitors using an Annexin V/PI followed by EGF treatment.

- To generate SRPK1 stable knockdowns with shRNA lentiviral particles and to verify SRPK1 by Western blotting.
- To introduce siRNA against SRPK1 or SRSF1 and confirm knockdown of SRPK1 or SRSF1 expression.
- To confirm SRPK1 siRNA knockdown efficiency in PC-3 cells.
- To detect siRNA SRSF1 effects on *CASPASE-9, RON,* and *RUNX1* alternative splicing.

3.4 Results

3.4.1. SRPK1 and SRSF1 expression in K562 cells

The expression of SRPK1 and SRSF1 (mRNA and protein) in K562 cells was assessed using RT-PCR and Western blotting. Total mRNA was extracted from cells and reverse transcribed to cDNA. Primers, Chapter 2: Materials and methods (Table 2.2), for SRPK1, SRSF1 and GAPDH were used to perform RT-PCR, generating products of 203 bp and 134 bp for SRPK1 and SRSF1, respectively. A GAPDH loading control was also used (212 bp),

Figure 3.1A.

Antibodies that listed in Chapter 2: Materials and methods (Table 2.9) were used for Western blott to assess the protein expression of SRPK1 and SRSF1 producing a 92 kDa band for SRPK1 and a 32 kDa band for SRSF1. A loading control, α-tubulin at (55 kDa) was also used,

Figure 3.1B.

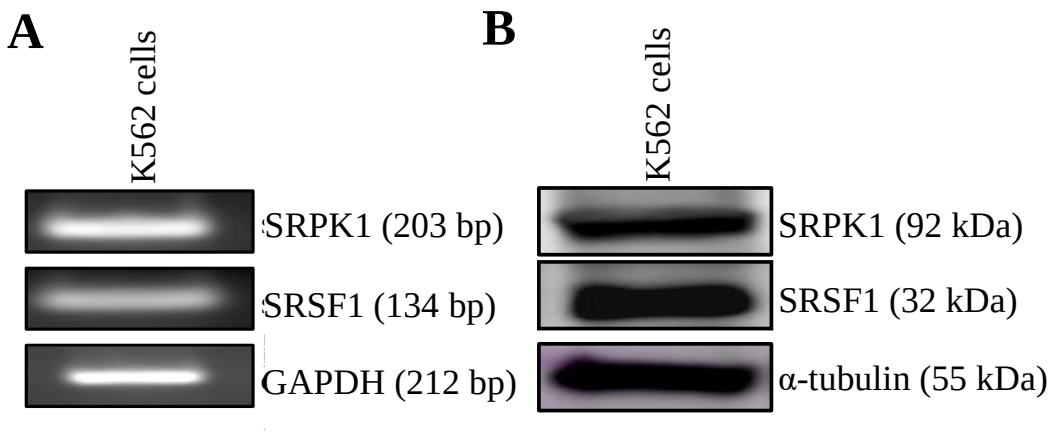

Figure 3.1. SRPK1 and SRSF1 expression in K562 cells
A. RT-PCR producted bands of 203 bp and 134 bp for SRPK1 and SRSF1, respectively. GAPDH yielded a product size of 212 bp and was used as a loading control. **B.** Western blotting generated a protein band of 92 kDa for SRPK1, 32 kDa for SRSF1 and 55 kDa for α-tubulin.

3.4.2. The effects of SRPK1 small molecule inhibitors in K562 cells

3.4.2.1. Proliferation of K562 cells following SRPK1 inhibition

Approximately 1×10^6 K562 cells were used to assess cell proliferation upon SRPK1 inhibition with SRPIN340 or SPHINX. Cells were counted by trypan blue at 24 hours following inhibition and compared to the no treatment 1×10^6 cell control ($n = 3, \pm$ SEM).

The proliferation of cells treated with EGF only (100 ng/mL) was 1.5×10^6. K562 cells were treated with 10 μM SRPIN340 reached 1.6×10^6 ($p = 0.52$) and K562 cells treated with 20 μM SRPIN340 accounted for 1.98×10^6 ($p = 0.11$), one-way ANOVA, Figure 3.2.

K562 cells were also treated with different SPHINX concentrations (Figure 3.3). Cell numbers treated with only EGF (100 ng/mL) were approximately 1.5×10^6, while cell numbers were significantly increased to (2.2×10^6, $p = 0.02$) in those cells treated with 5 μM SPHINX, when compared to 1×10^6 cell control, one-way ANOVA. K562 cells treated with 10 and 30 μM SPHINX were 1.2×10^6 ($p = 0.97$) and 1.3×10^6 ($p = 0.92$) respectively, (one-way ANOVA). However, cell numbers for the 20 μM SPHINX treatment were 1.5×10^6 (one-way ANOVA, $p = 0.74$).

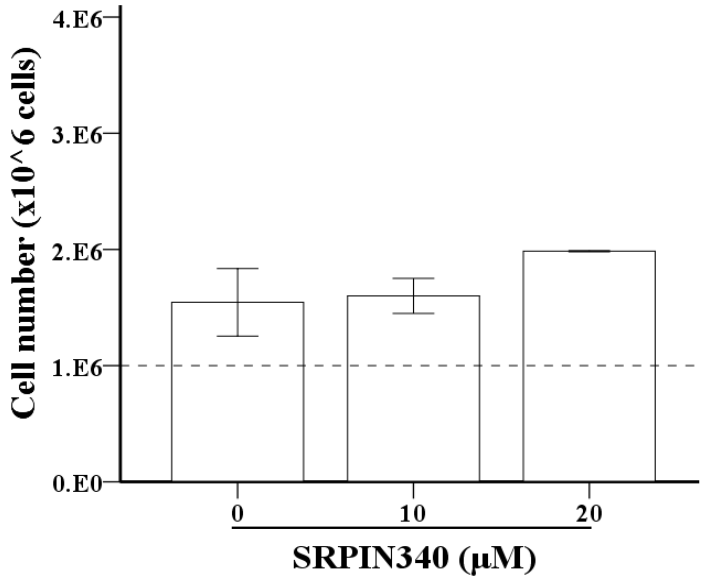

Figure 3.2. K562 proliferation after 24 hour treatment with SRPIN340
Quantitative analysis of K562 cells treated with only 100 ng/mL EGF (0 μM) and 10 and 20 μM SRPIN340 followed by 100 ng/mL EGF. Cells were counted after 24 hours and compared to a 1×10^6 cell control. The bars indicate standard errors (one-way ANOVA). The data represents three independent experiments ($n = 3$).

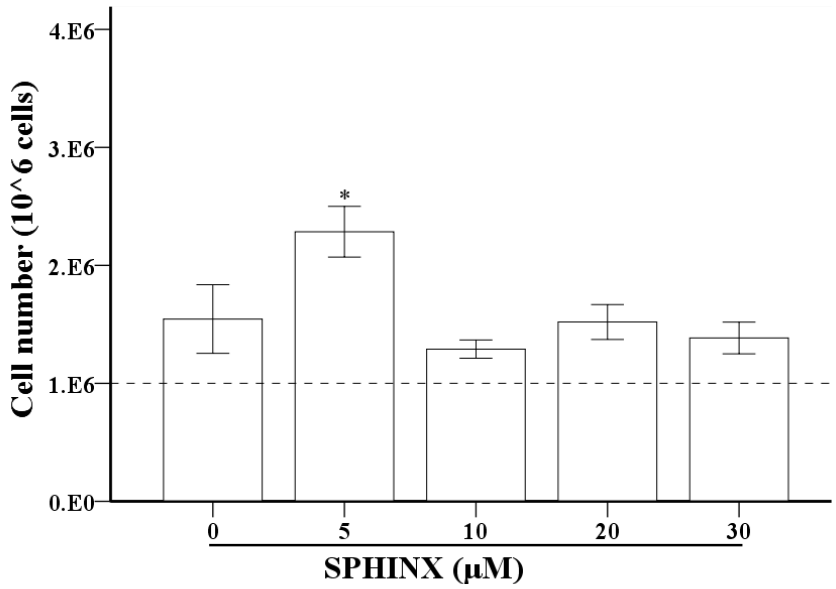

Figure 3.3. K562 proliferation after 24 hour treatment SPHINX
Quantitative analysis of K562 cells treated with only 100 ng/mL EGF (0 μM) and several SPHINX concentrations (5–30 μM) followed by 100 ng/mL EGF. After 24 hours, cells were counted, a 1×10^6 untreated control compared proliferation of SPHINX treated cells. Cell proliferation was significantly increased in those cells treated with 5 μM SPHINX when compared to a 1×10^6 cell control. The bars indicate standard error, * $P \leq 0.05$ (one-way ANOVA). The data represents three independent experiments ($n = 3$).

3.4.2.2. *CASPASE-9* splicing in K562 cells following SRPK1 inhibition

The effects of SRPK1 inhibition on *CASPASE-9* splicing was investigated in K562 cells and compared with cells treated with 0.02% DMSO (DMSO control) or cells treated with 100 ng/mL EGF (EGF control). The caspase-9a/9b expression ratio was quantified using densitometry and ImageJ software.

The expression of the caspase-9b isoform was increased in cells treated with both 10 μM SRPIN340 and 20 μM SRPIN340/9, when compared to the DMSO control

(Figure 3.4B). In Figure 3.4C, the expression ratio of the caspase-9a/b isoform compared to the DMSO control was 1.34, while the expression ratio in cells treated with 10 μM SRPIN340 was 1.15 (p = 0.87, one-way ANOVA). Cells treated with 10 μM SRPIN349 reached the expression ratio of caspase-9a/b isoform to 1.18 (p = 0.93, one-way ANOVA). Furthermore, the caspase-9a/9b expression ratio in cells treated with 20 μM SRPIN340 and 20 μM SRPIN349 were significantly decreased to 0.74 (p = 0.03) and 0.68 (p = 0.02) respectively, when compared to DMSO control (one-way ANOVA), Figure 3.4C. This significant effect, however, is not specific when cells treated with 20 μM SRPIN340 compared to 20 μM SRPIN349 (p = 0.99, one-way ANOVA).

There was no change in splice variant caspase-9a and caspase-9b mRNA expression after SRPIN340 treatment, Figure 3.5B. The expression ratio of caspase-9a/9b isoform in the EGF control was 0.71 while in cells treated with 10 μM SRPIN340, the expression ratio was 0.54 (p = 0.91, one-way ANOVA), Figure 3.5C. However, the ratio of caspase-9a/9b was 0.59 (p = 0.96) in cells treated with 20 μM SRPIN340 (one-way ANOVA), Figure 3.5C.

Cells treated with SPHINX (5–30 μM) showed no obvious changes in splice variant caspase-9a and caspase-9b expression when compared to EGF control, Figure 3.6B. The expression ratio of caspase-9a/9b ratio in cells treated with EGF only (100 ng/mL) was 1.16 while the expression ratio in cells treated with 5 μM SPHINX was 1.24 (p = 0.99, one-way ANOVA). The expression ratio of caspase-9a/9b in cells treated with 10 μM and 20 μM SPHINX were 1.41 (p = 0.81) and 0.98 (p = 0.93),

Figure 3.6C. However, the expression ratio of caspase-9a/9b in cells treated with 30 μM SPHINX was 0.71 (p = 0.26), Figure 3.6C.

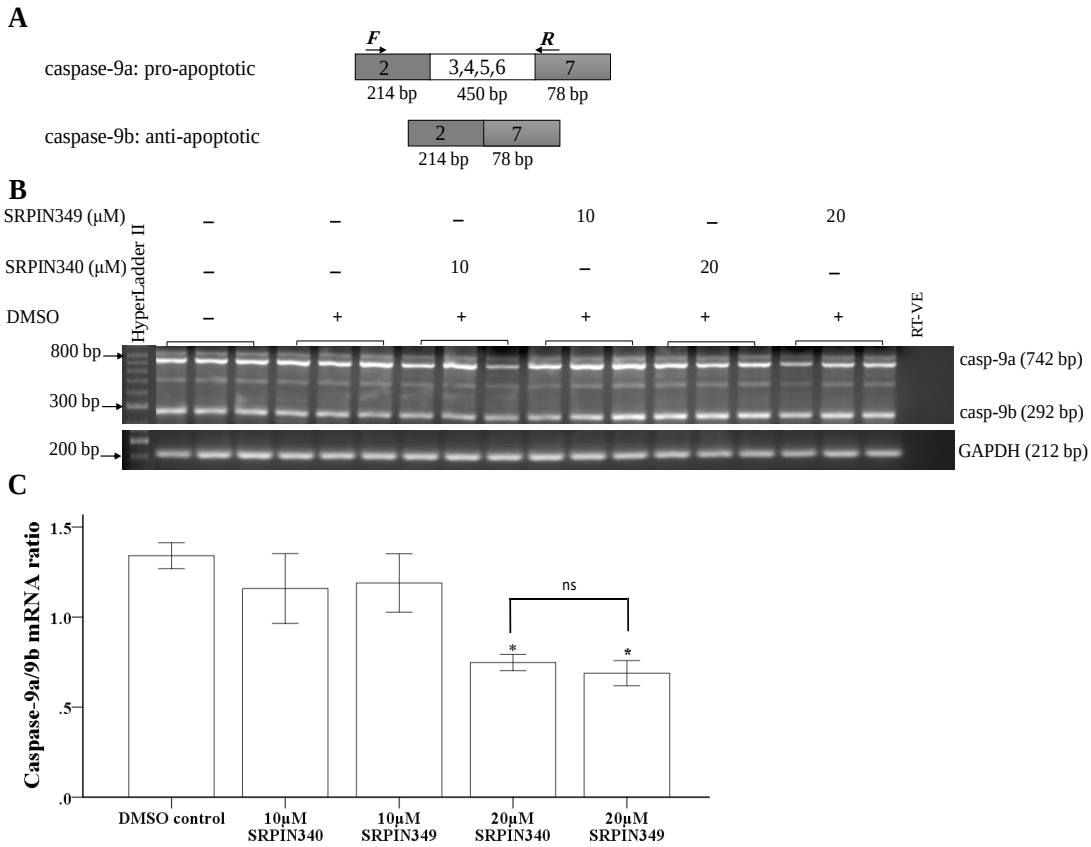

Figure 3.4. SRPK1 inhibition (SRPIN340 and SRPIN349) on *CASPASE-9* alternative splicing

A. *CASPASE-9* showing the two splice variants resulting from inclusion or exclusion of exons 3–6 (caspase-9a and caspase-9b, respectively). Arrows indicate the position of *forward* and *reverse CASPASE-9* primers. **B.** K562 cells were treated with 0.02% DMSO (DMSO control) and two concentrations of SRPIN340/9 were used at 10 and 20 μM followed by (0.02%) DMSO. RT-PCR was performed and bands at 742 bp (casp-9a) and 292 bp (casp-9b) were detected. Intermediate bands at ~ 500 bp represent skipped exons. GAPDH was used as a loading control (212 bp). Each rung of the hyperLadder II represents 100 bp. **C.** Densitometric analysis of caspase-9a/9b isoforms representing the intensity ratio of caspase-9a against caspase-9b. K562 cells treated with SRPIN340 or SRPIN349 were compared with the DMSO control. The caspase-9a/9b ratio was significantly decreased for 20 μM SRPIN340 and SRPIN349 treatments when compared to the DMSO control. However, this significant effect is not specific when cells treated with 20 μM SRPIN340 compared to 20 μM SRPIN349. The bars indicate standard error, * $P \leq 0.05$ (one-way ANOVA). The data represents three independent experiments ($n = 3$).

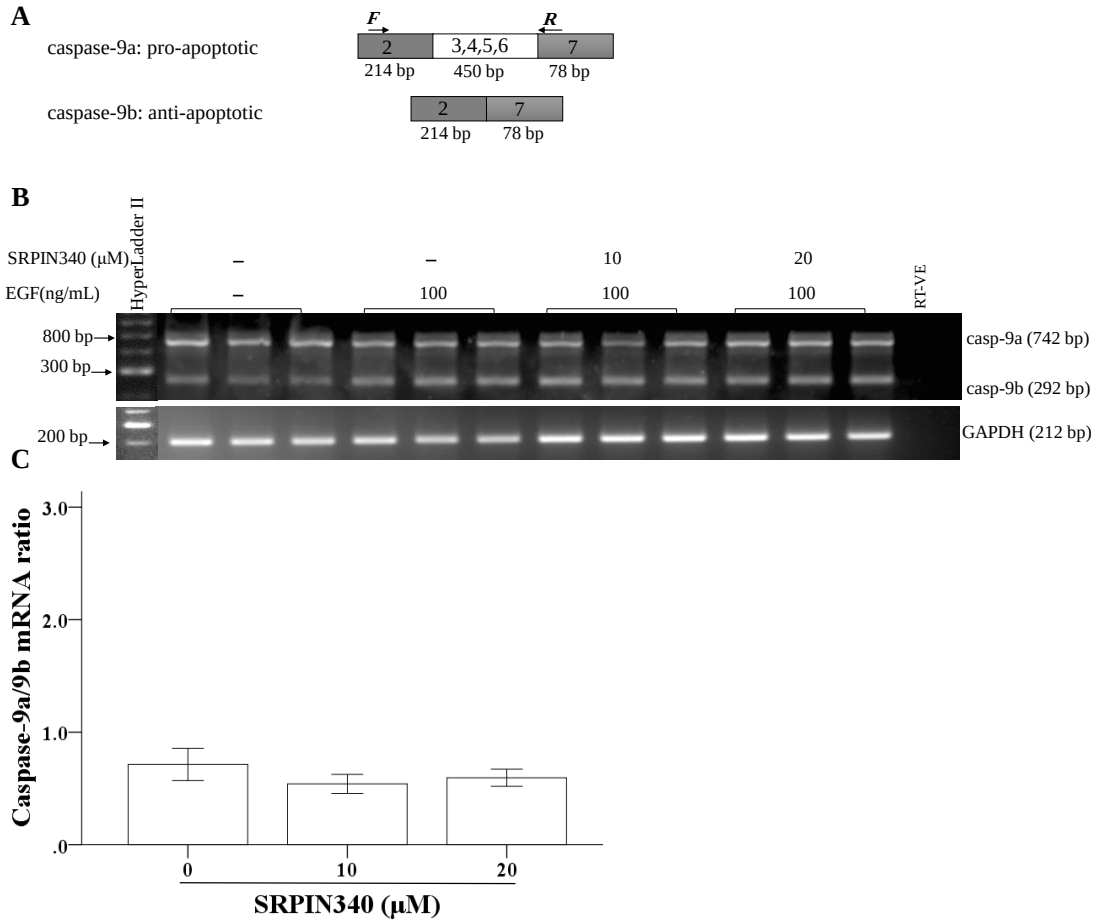

Figure 3.5. SRPK1 inhibition (SRPIN340) on *CASPASE-9* alternative splicing
A. *CASPASE-9* showing the two splice variants resulting from inclusion or exclusion of exons 3–6 (caspase-9a and caspase-9b, respectively). Arrows indicate the positions of *forward* and *reverse CASPASE-9* primers. **B.** K562 cells were treated with only 100 ng/mL EGF (0 μM SRPIN340) and two concentrations of SRPIN340 were used at 10 and 20 μM followed by 100 ng/mL EGF. RT-PCR was performed and bands 742 bp (casp-9a) and 292 bp (casp-9b) were detected and GAPDH was used as a loading control. Intermediate bands at ~ 500 bp represent skipped exons. Each rung of the hyperLadder II represents 100 bp. **C.** Densitometric analysis of caspase-9a/9b isoforms. K562 cells treated with 10 μM and 20 μM SRPIN340 were compared with the EGF control (0 μM SRPIN340). The graph represents the intensity ratio of caspase-9a against caspase-9b. The bars indicate standard error (one-way ANOVA). The data represents three independent experiments (n = 3).

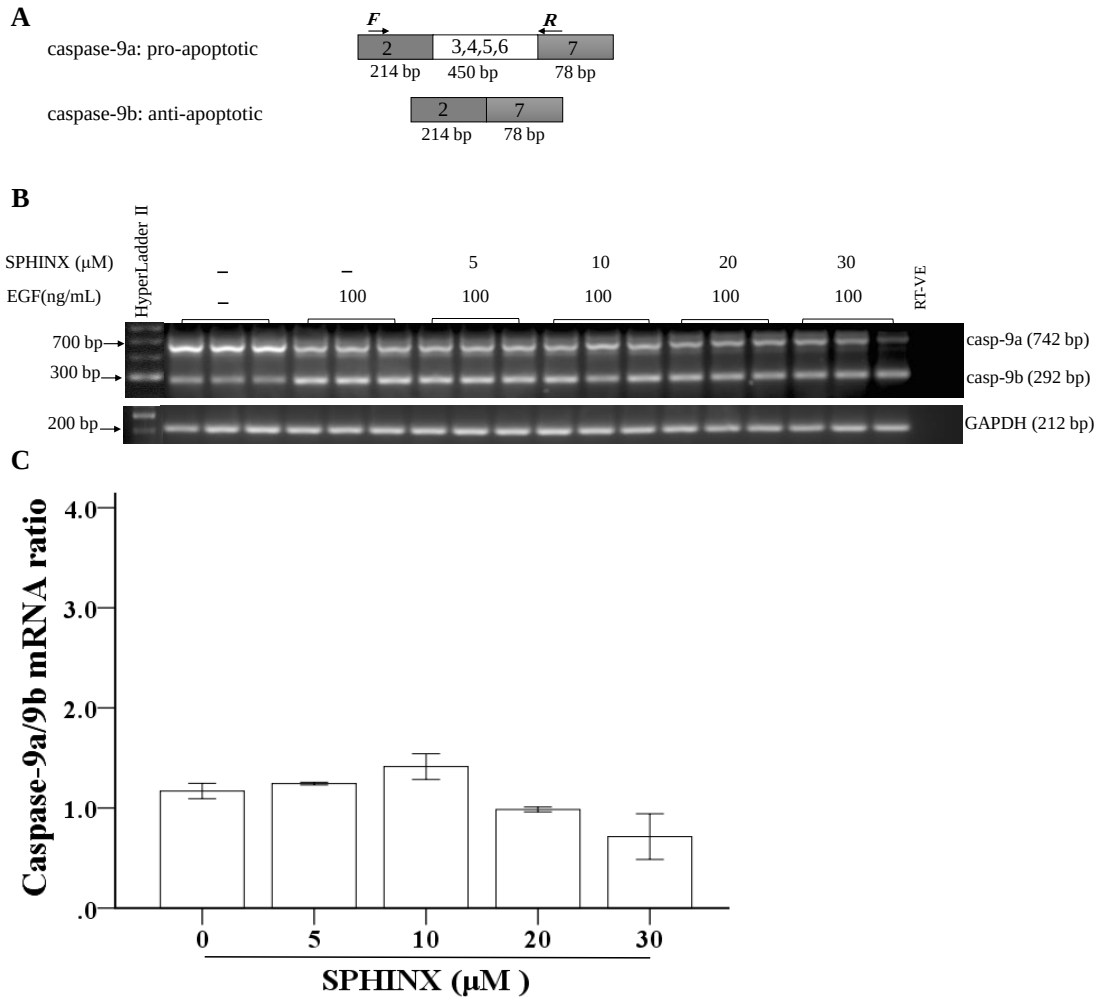

Figure 3.6. SRPK1 inhibition (SPHINX) on *CASPASE-9* alternative splicing
A. *CASPASE-9* showing the two splice variants resulting from inclusion or exclusion of exons 3–6 (caspase-9a and caspase-9b, respectively). Arrows indicate the positions of *forward* and *reverse CASPASE-9* primers. **B.** K562 cells were treated with only 100 ng/mL EGF (0 μM SPHINX) and range concentrations of SPHINX were used (5–30 μM) followed by 100 ng/mL EGF. RT-PCR was performed and bands at 742 bp (caspase-9a) and 292 bp (caspase-9b) were detected. Intermediate bands at ~ 500 bp represent skipped exons. GAPDH was used as a loading control. Each rung of the hyperLadder II represents 100 bp. **C.** Densitometric analysis of caspase-9a/9b isoforms. K562 cells treated with 5–30 μM SPHINX were compared with the EGF control (0 μM SPHINX). The graph represents the intensity ratio of caspase-9a against caspase-9b. The bars indicate standard error (one-way ANOVA). The data represent three independent experiments (n = 3).

3.4.2.2.1 The *CASPASE-9* cDNA amplicon sequence

Four *CASPASE-9* isoforms are produced; however, only two were studied in these studies. *CASPASE-9* mRNA PCR products were isolated from agarose gels and sequenced (Chapter 2). The sequenced *CASPASE-9* was based on the reference sequence at NCBI GenBank (accession number: NM_001229.4). Figure 3.7 and 3.8 show the caspase-9a sequence, including exons 2 - 7 and the caspase-9b sequence, including exons 2 - 7.

5'…CGGGCAGGCTCTGGATCTCGGCGGGATCAGGCCAGGCAGCTGATCATAGATCTGGAGA
CTCGAGGGAGTCAG**GCTCTTCCTTTGTTCATCTCC**TGCTTAGAGGACACAGGCCAGGAC

ATGCTGGCTTCGTTTCTGCGAACTAACAGGCAAGCAGCAAAGTTGTCGAAGCCAACCCT
AGAAAACCTTACCCCAGTGGTGCTCAGACCAGAGATTCGCAAACCAGAGGTTCTCAGA
CCGGAAACACCCAGACCAGTGGACATTGGTTCTGGAGGATTTGGTGATGTCGGTGCTC
TTGAGAGTTTGAGGGGAAATGCAGATTTGGCTTACATCCTGAGCATGGAGCCCTGTGG
CCACTGCCTCATTATCAACAATGTGAACTTCTGCCGTGAGTCCGGGCTCCGCACCCGC
ACTGGCTCCAACATCGACTGTGAGAAGTTGCGGCGTCGCTTCTCCTCGCTGCATTTCAT
GGTGGAGGTGAAGGGCGACCTGACTGCCAAGAAAATGGTGCTGGCTTTGCTGGAGCT
GGCGCAGCAGGACCACGGTGCTCTGGACTGCTGCGTGGTGGTCATTCTCTCTCACGG
CTGTCAGGCCAGCCACCTGCAGTTCCCAGGGGCTGTCTACGGCACAGATGGATGCCCT

GCAGTAACCCCGAGCCAGATGCCACCCCGTTCCAGGAAGGTTTGAGGACCTTCGACCAGC
TGGACGCCATATCTAGTTTGCCCACACCCAGTGACATCTTTGTGTCCTACTCTACTTTCCCA
G…'3

Figure 3.7. The sequence of caspase-9a showing exons 2–7
Sequence analysis of the top band amplified using primers caspase-9F + caspase-9R, showing exon 2, exon 3, exon 4, exon 5, exon 6 and exon 7. In red: forward and reverse primers. Sequence in box is the actual cDNA sequence generated from the caspase-9a PCR product.

5'…CGGGCAGGCTCTGGATCTCGGCGGGATCAGGCCAGGCAGCTGATCATAGATCTGGAGA
CTCGAGGGAGTCAG**GCTCTTCCTTTGTTCATCTCC**TGCTTAGAGGACACAGGC

CAGGACATGCTGGCTTCGTTTCTGCGAACTAACAGGCAAGCAGCAAAGTTGTCGAAGC
CAACCCTAGAAAACCTTACCCCAGTGGTGCTCAGACCAGAGATTCGCAAACCAGAGGT
TCTCAGACCGGAAACACCCAGACCAGTGGACATTGGTTCTGGAGGATTTGGTGATGTC

GTGCTCTTGAGAGTTTGAGGGGAAATGCAGATTTGGCTTACATCCTGAGCATGGAGCCCTG
TGGCCACTGCCTCATTATCAACAATGTGAACTTCTGCCGTGAGTCCGGGCTCCGCACCCGC
ACTGGCTCCAACATCGACTGTGAGAAGTTGCGGCGTCGCTTCTCCTCGCTGCATTTCATGGT
GGAGGTGAAGGGCGACCTGACTGCCAAGAAAATGGTGCTGGCTTTGCTGGAGCTGGCGCA
GCAGGACCACGGTGCTCTGGACTGCTGCGTGGTGGTCATTCTCTCTCACGGCTGTCAGGCC
AGCCACCTGCAGTTCCCAGGGGCTGTCTACGGCACAGATGGATGCCCTGTGTCGGTCGAG
AAGATTGTGAACATCTTCAATGGGACCAGCTGCCCCAGCCTGGGAGGGAAGCCCAAGCTCT

AGCAGAAAGACCATGGGTTTGAGGTGGCCTCCACTTCCCCTGAAGACGAGTCCCCTG

TTTTCATCCAGGCCTGTGGTGGGG
GCAGTAACCCCGAGCCAGATGCCACCCCGTTCCAGGAAGGTTTGAGGACCTTCGACCAGC
TGGACGCCATATCTAGTTTGCCCACACCCAGTGACATCTTTGTGTCCTACTCTACTTTCCCA
G…'3

Figure 3.8. The sequence of caspase-9b showing exons 2–7
Sequence analysis of the top band amplified using primers caspase-9F + caspase-9R, showing exon 2, exon 3, exon 4, exon 5, exon 6 and exon 7. In red: forward and reverse primers. Sequence in box is the actual cDNA sequence generated from the caspase-9b PCR product.

3.4.2.3. *RON* splicing in K562 cells following SRPK1 inhibition

SRPK1 inhibition on *RON* splice isoforms was assessed by RT-PCR and the expression ratio of Ron/ΔRon quantified using ImageJ software. Figure 3.9B, no changes were observed in Ron and ΔRon splice variants in cells treated with SRPIN340 or SRPIN349. In Figure 3.9C, the expression ratio of the Ron/ΔRon isoform in the DMSO control was 0.71, while in K562 cells treated with 10 μM SRPIN340 and 10 μM SRPIN349, the expression ratios were 0.79 (p = 0.64) and 0.76 (p = 0.91), one-way ANOVA. In addition, 20 μM SRPIN340 led to a significant increase in the Ron/ΔRon expression ratio (0.91, p = 0.03), when compared to DMSO control (one-way ANOVA), Figure 3.9C. This elevation, however is not specific when compared to the expression ratio of Ron/ΔRon in cells treated with 20 μM SRPIN349 (0.84, p = 0.23), one-way ANOVA.

Furthermore, there were no statistical changes in Ron and ΔRon splice variant expression in cells treated with 10 and 20 μM SRPIN340, Figure 3.10B. The expression ratio of Ron/ΔRon was 0.73 in K562 cells treated with 100 ng/mL EGF only (0 μM SRPIN340). The expression ratio of Ron/ΔRon in cells treated with 10 μM SRPIN340 and 20 μM SRPIN340 was (0.58, $p = 0.64$) and (0.81, $p = 0.89$), one-way ANOVA), Figure 3.10C.

K562 cells were treated with SPHINX (0 – 30 μM) and *RON* alternative splicing compared to the EGF control, Figure 3.11. RT-PCR showed no changes in *RON* splice variant mRNA expression after SPHINX treatment, Figure 3.11B. The expression ratio of Ron/ΔRon was 0.98 in K562 cells treated with EGF only (100 ng/mL), Figure 3.11C. The expression ratios of Ron/ΔRon in K562 cells treated with 5 and 10 μM SPHINX were (0.85, $p = 0.94$) and (0.86, $p = 0.97$), one-way ANOVA. Additionally, the Ron/ΔRon expression ratios in K562 cells treated with 20 and 30 μM SPHINX were (1.07, $p = 0.98$) and (1.30, $p = 0.32$), one-way ANOVA.

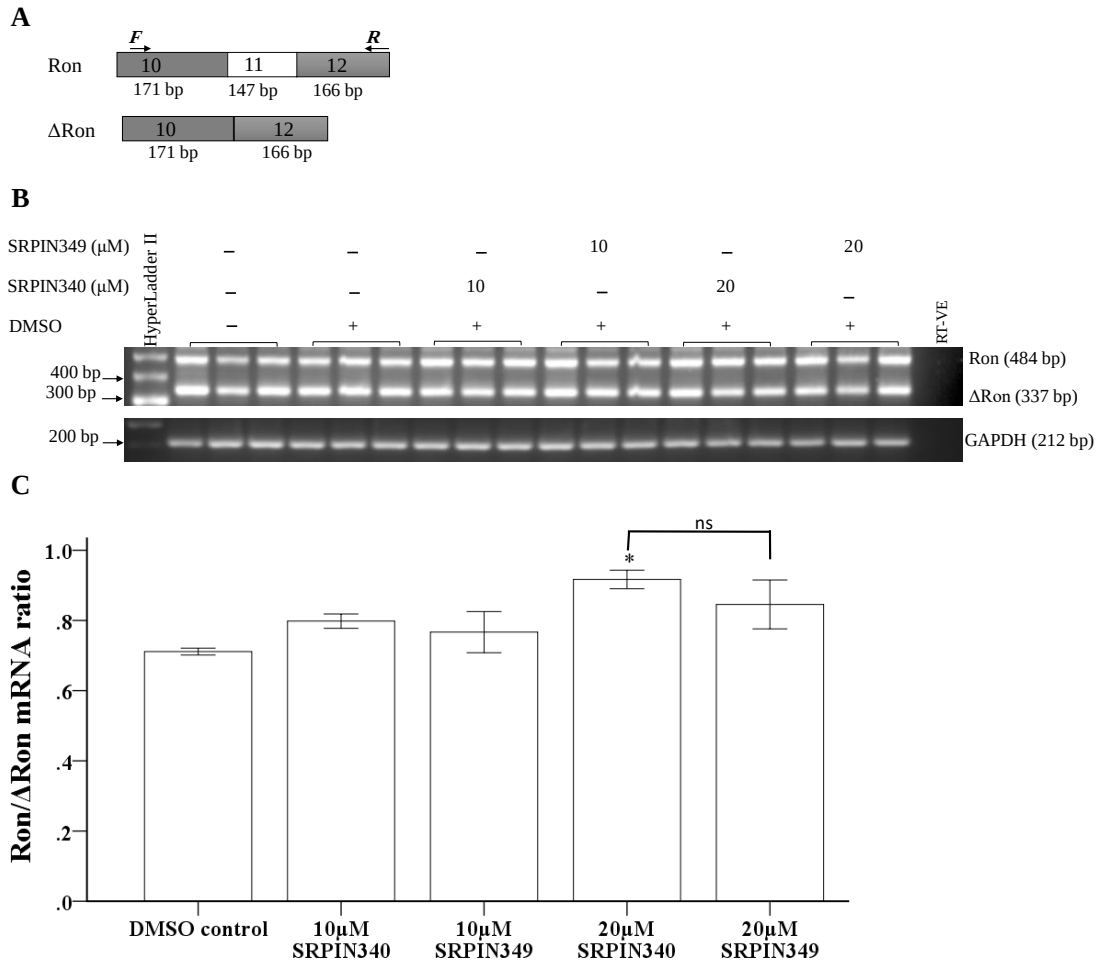

Figure 3.9. SRPK1 inhibition (SRPIN340 and SRPIN349) on *RON* alternative splicing

A. The *RON* gene showing the two splice variants resulting from the inclusion or exclusion of exon 11 (Ron and ΔRon variants, respectively). Arrows indicate the positions of *forward* and *reverse* Ron primers. **B.** K562 cells were treated with 0.02% DMSO (DMSO control) and two concentrations of SRPIN340/9 were used at 10 and 20 μM followed by (0.02%) DMSO. RT-PCR was performed and bands at 484 bp (Ron) and 337 bp (ΔRon) were detected. GAPDH was used as a loading control (212 bp). Each rung of the hyperLadder II represents 100 bp. **C.** Densitometric analysis of Ron/ΔRon isoforms. K562 cells treated with SRPIN340 or SRPIN349 were compared with the DMSO control. The expression ratio of Ron/ΔRon significantly increased for the 20 μM SRPIN340 treatment. However, this significant effect is not specific when the expression ratio of cells treated with 20 μM SRPIN340 compared to 20 μM SRPIN349. The bars indicate standard error, * $P \leq 0.05$ (one-way ANOVA). The data represents three independent experiments (n = 3).

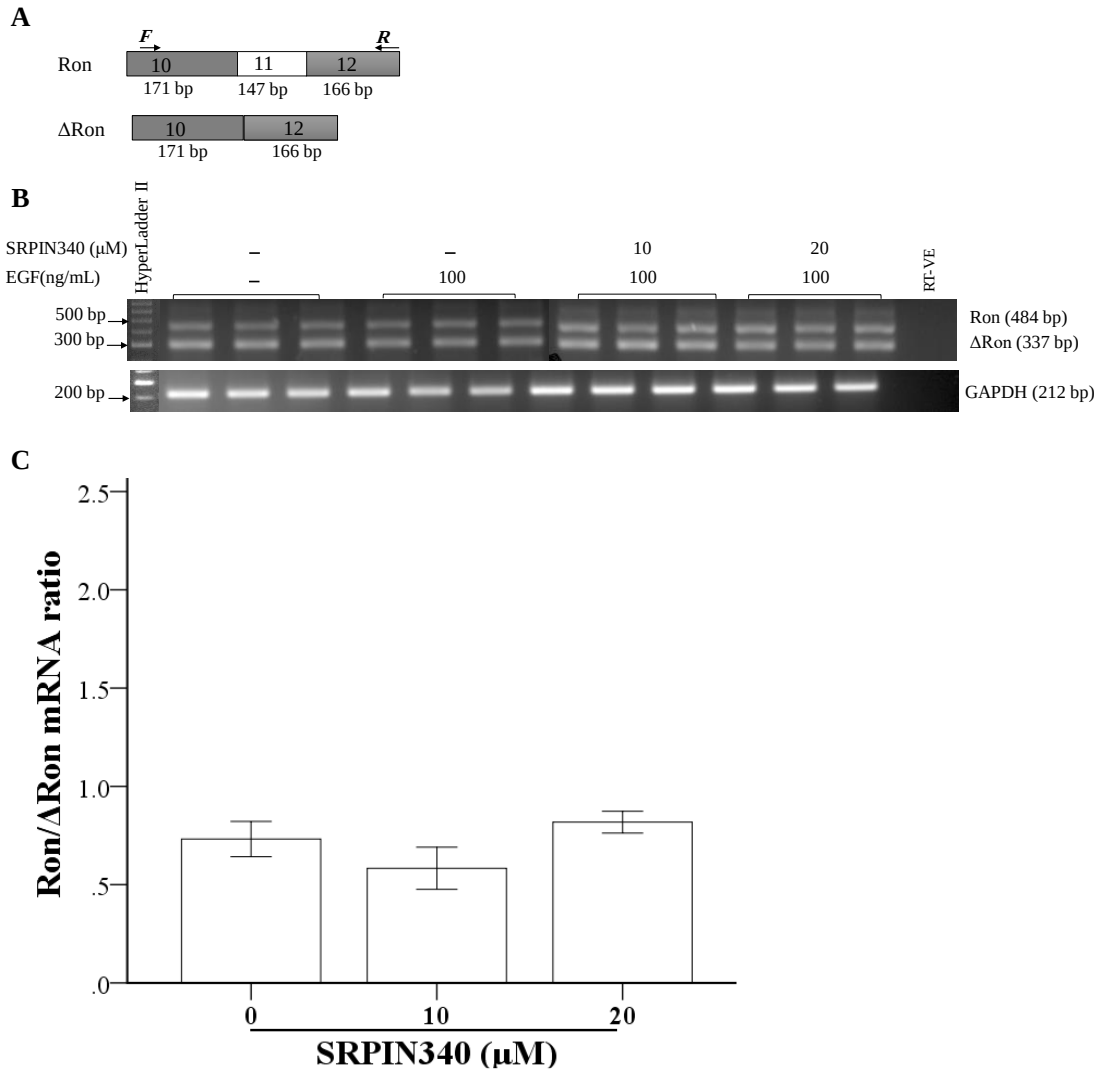

Figure 3.10. SRPK1 inhibition (SRPIN340) on *RON* alternative splicing
A. The *RON* gene showing the two splice variants resulting from inclusion or exclusion of exon 11 (Ron and ΔRon, respectively). Arrows indicate the positions of *forward* and *reverse* Ron primers. **B.** K562 cells were treated with only 100 ng/mL EGF (0 μM SRPIN340) and two concentrations of SRPIN340 were used at 10 and 20 μM followed by 100 ng/mL EGF. RT-PCR was performed and bands at 484 bp (Ron) and 337 bp (ΔRon) were detected. GAPDH was used as a loading control. Each rung of the hyperLadder II represents 100 bp. **C.** Densitometric analysis of Ron/ΔRon isoforms. K562 cells treated with 10 and 20 μM SRPIN340 were compared with the EGF control (0 μM SRPIN340). The graph represents the intensity ratio of Ron against ΔRon. The bars indicate standard error (one-way ANOVA). The data represents three independent experiments (n = 3).

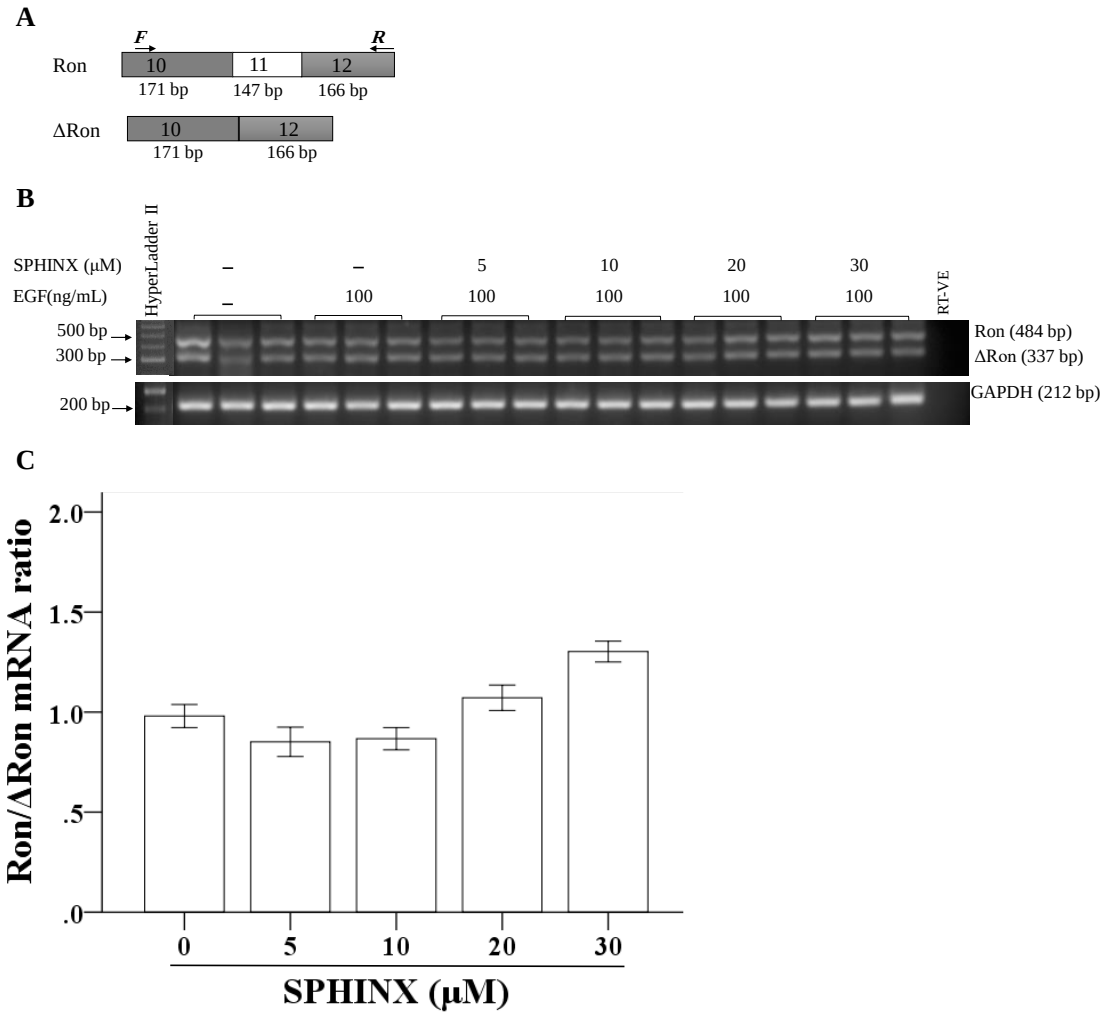

Figure 3.11. SRPK1 inhibition (SPHINX) on *RON* alternative splicing
A. The *RON* gene showing the two splice variants resulting from inclusion or exclusion of exon 11 (Ron and ΔRon, respectively). Arrows indicate the positions of *forward* and *reverse* Ron primers. **B.** K562 cells were treated with only 100 ng/mL EGF (0 μM SPHINX) and range concentrations of SPHINX were used (5–30 μM) followed by 100 ng/mL EGF. RT-PCR was performed and bands at 484 bp (Ron) and 337 bp (ΔRon) were detected. GAPDH was used as a loading control. Each rung of the hyperLadder II represents 100 bp. **C.** Densitometric analysis of Ron/ΔRon isoforms. K562 cells treated with 5–30 μM SPHINX were compared with control cells treated with EGF only (0 μM SPHINX). The graph represents the intensity ratio of Ron against ΔRon. The bars indicate standard error (one-way ANOVA). The data represents three independent experiments (n = 3).

3.4.2.3.1 The *RON* cDNA amplicon sequence

Ron RT-PCR products were sequenced as described previously. The sequenced Ron was based on the NBCI GenBank reference transcription ID_MST1R-001: (ENST00000296474). The Ron isoform sequence includes exons 10–12, Figure 3.12. The ΔRon isoform sequence also includes exons 10 and 12, Figure 3.13.

5'…TGTGAGAGGCAGCTTCCAGAGCAGCAGCTGTGCCGCCTT**CCTGAATATGTGGTCCGAG**
ACCCCCAGGGATGGGTGGCAGGGAATCTGAGTGCCCGA

GGGGATGGAGCTGCTGGCTTTACACTGCCTGGCTTTCGCTTCCTACCCCCACCCCATC
CACCCAGTGCCAACCTAGTTCCACTGAAGCCTGAGGAGCATGCCATTAAGTTTGAGTAT
ATTGGGCTGGGCGCTGTGGCTGACTGTGTGGGTATCAACGTGACCGTGGGTGGTGAG
AGCTGCCAGCACGAGTTCCGGGGGGGACATGGTTGTCTGCCCCCTGCCCCCATCCCTG
CAGCTTGGCCAGGATGGTGCCCCATTGCAGGTCTGCGTAGATGGTGAATGTCATATCC
TGCGTAGACTGGTGCGGCGAGGCGGAGATGCGGTGGCAGAGGACGCTGCTTGCTA

TACTGGTGGCGGAGGAAGCAGCTAG…'3

Figure 3.12. Sequence analysis of the Ron isoform showing exons 10–12
Sequence analysis of the top band amplified using primers Ron-F + Ron-R, showing exon 10, exon 11 and exon 12. In red: forward and reverse primers. Sequence in box is the actual cDNA sequence generated from the Ron PCR product.

5'…TGTGAGAGGCAGCTTCCAGAGCAGCAGCTGTGCCGCCTT**CCTGAATATGTGGTCCGAG**

CCGAGGGGATGGAGCTGCTGGCTTTACACTGCCTGGCTTTCGCTTCCTACCCCCACCC
CATCCACCCAGTGCCAACCTAGTTCCACTGAAGCCTGAGGAGCATGCCATTAAGTTTG

ACCCCCAGGGATGGGTGGCAGGGAATCTGAGTGC
AGTATATTGGGCTGGGCGCTGTGGCTGACTGTGTGGGTATCAACGTGACCGTGGGTGGTGA
GAGCTGCCAGCACGAGTTCCGGGGGGGACATGGTTGTCTGCCCCCTGCCCCCATCCCTGCA

AGGTCTGCGTAGATGGTGAATGTCATATCCTGGGTAGAGTGGTGCGGCCAGGGCCAGA
TGGGGTCCCACAGAGCACGCTCCTTGGTATCCTGCTGCCTTTGCTGCTGCTTGTGGCT
GCACTGGCGACTGCACTGGTCTTCAGC

GCTTGGCCAGGATGGTGCCCCATTGC
TACTGGTGGCGGAGGAAGCAGCTAG…'3

Figure 3.13. Sequence analysis of the ΔRon isoform showing exons 10–12
Sequence analysis of the top band amplified using primers Ron-F + Ron-R, showing exon 10, exon 11 and exon 12. In red: forward and reverse primers. Sequence in box is the actual cDNA sequence generated from the ΔRon PCR product.

3.4.2.4. *RUNX1* splicing in K562 cells following SRPK1 inhibition

RUNX1 splicing was assessed by RT-PCR and Runx1/ΔRunx1 expression ratios quantified by ImageJ software. There were no change in Runx1 and ΔRunx1 mRNA expression after SRPIN340 or SRPIN349 treatment, Figure 3.14B. The expression ratio of Runx1/ΔRunx1 (Figure 3.14C) was 0.96 in K562 cells treated with 0.02% DMSO (DMSO control). The expression ratios in K562 cells treated with 10 μM SRPIN340 and 10 μM SRPIN349 were (0.90, p = 1.00) and (0.78, p = 0.93), one-way ANOVA). Additionally, K562 cells treated with 20 μM SRPIN340 caused 0.57 (p = 0.32) in the expression ratio of Runx1/ΔRunx1, while the 20 μM SRPIN349 treatment caused 0.67 (p = 0.64), one-way ANOVA.

There was no statistical change in *RUNX1* alternative splicing after treatments with 10 and 20 μM SRPIN340, when compared to the EGF control, Figure 3.15B. The expression ratio in cells treated with EGF only (100 ng/mL) was 0.73, while the expression ratio in cells treated with 10 μM SRPIN340 was 0.64 (p = 0.85), one-way ANOVA, Figure 3.15C. Additionally, the expression ratio of Runx1/ΔRunx1 in cells treated with 20 μM SRPIN340 was 0.86 (p = 0.66), one-way ANOVA. Additionally, there were no changes in Runx1/ΔRunx1 splice variant expression in K562 cells treated with SPHINX,

Figure 3.16B. The expression ratio of Runx1/ΔRunx1 treated with EGF only (100 ng/mL) was 0.67, Figure 3.16C. The expression ratios of Runx1/ΔRunx1 in cells treated with 5–30 μM SPHINX were (0.58, p = 0.98), (0.57, p = 0.97), (0.84, p = 0.75) and (0.81, p = 0.85), one-way ANOVA.

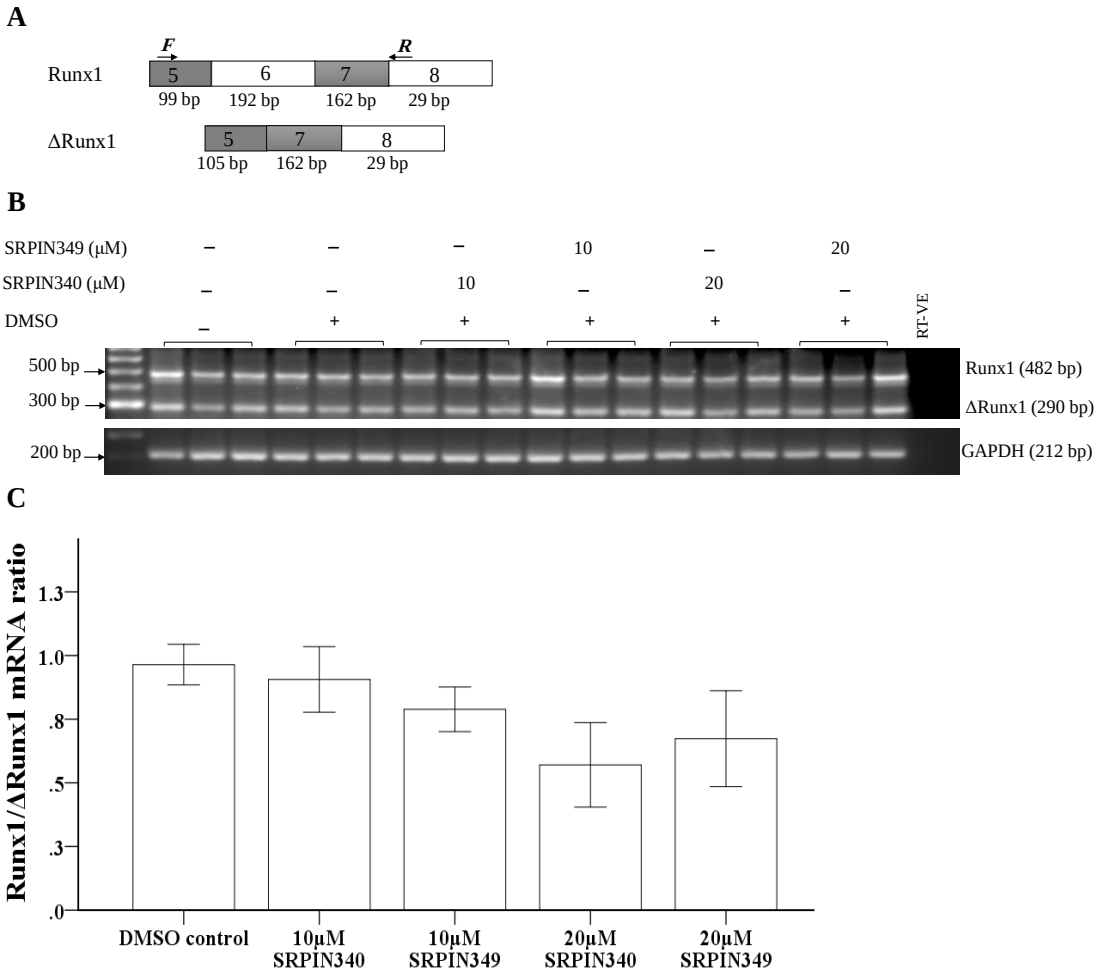

Figure 3.14. SRPK1 inhibition (SRPIN340 and SRPIN349) on *RUNX1* alternative splicing

A. *RUNX1* showing the two splice variants resulting from inclusion or exclusion of exon 6 (Runx1 and ΔRunx1 variants, respectively). Arrows indicate the positions of *forward* and *reverse* Runx1 primers. **B.** K562 cells were treated with 0.02% DMSO (DMSO control) and two concentrations of SRPIN340/9 were used at 10 and 20 μM followed by (0.02%) DMSO. RT-PCR was performed and bands at 482 bp (Runx1) and 290 bp (ΔRunx1) were detected. GAPDH was used as a loading control. Each rung of the hyperLadder II represents 100 bp. **C.** Densitometric analysis of Runx1/ΔRunx1 isoforms. K562 cells treated with SRPIN340 or SRPIN349 were compared with the DSMO control. The bars indicate standard error (one-way ANOVA). The data represents three independent experiments (n = 3).

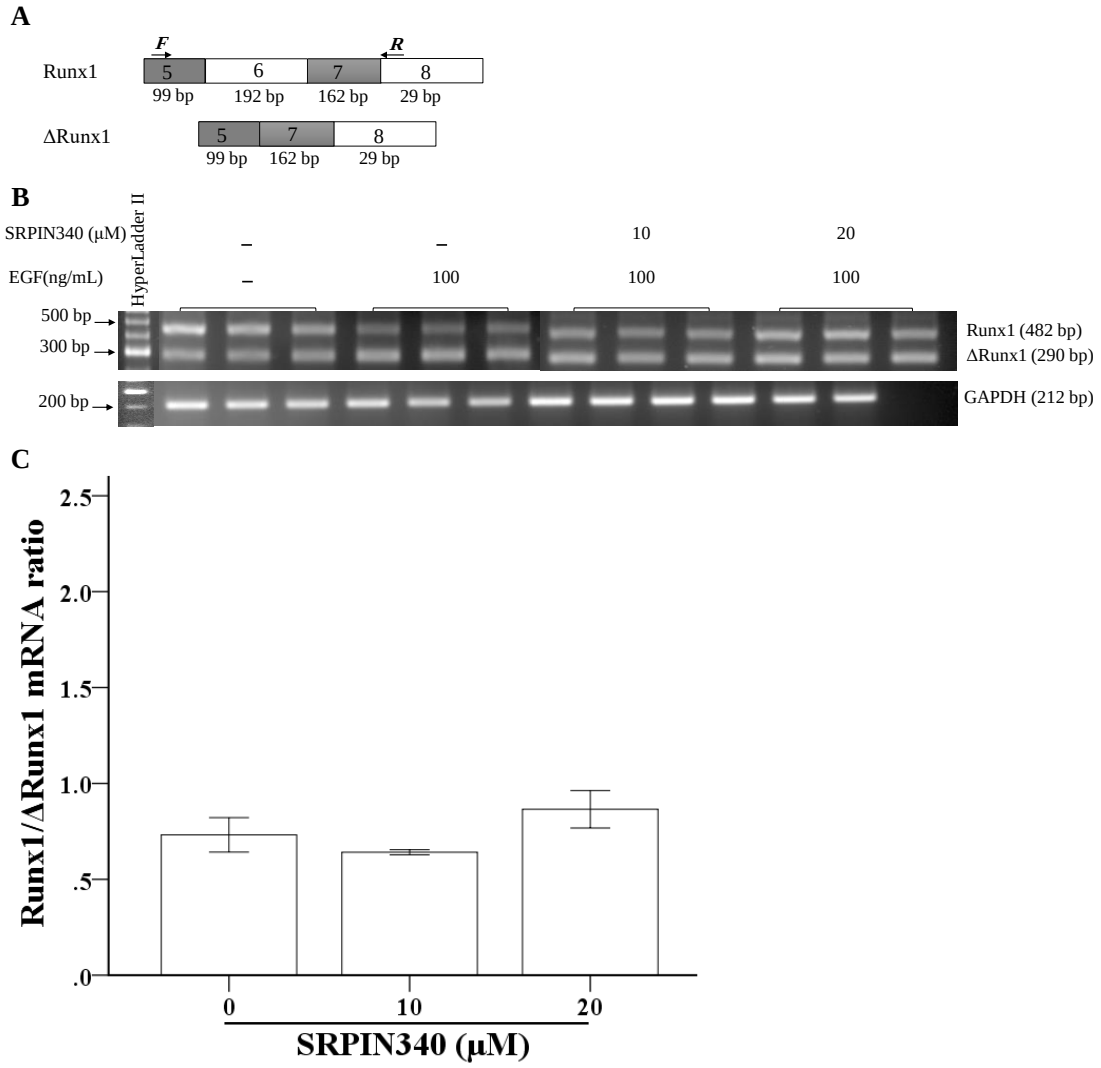

Figure 3.15. SRPK1 inhibition (SRPIN340) on *RUNX1* alternative splicing
A. *RUNX1* showing the two splice variants resulting from inclusion or exclusion of exon 6 (Runx1 and ΔRunx1, respectively). Arrows indicate the positions of *forward* and *reverse* Runx1 primers. **B.** K562 cells were treated with only 100 ng/mL EGF (0 μM SRPIN340) and two concentrations of SRPIN340 were used at 10 and 20 μM followed by 100 ng/mL EGF. RT-PCR was performed and bands at 482 bp (Runx1) and 290 bp (ΔRunx1) were detected. GAPDH was used as a loading control. Each rung of the hyperLadder II represents 100 bp. **C.** Densitometric analysis of Runx1/ΔRunx1 isoforms. K562 cells treated with 10 and 20 μM SRPIN340 were compared with the EGF control (0 μM SRPIN340). The graph represents the intensity ratio of Runx1 against ΔRunx1. The bars indicate standard error (one-way ANOVA). The data represent three independent experiments (n = 3).

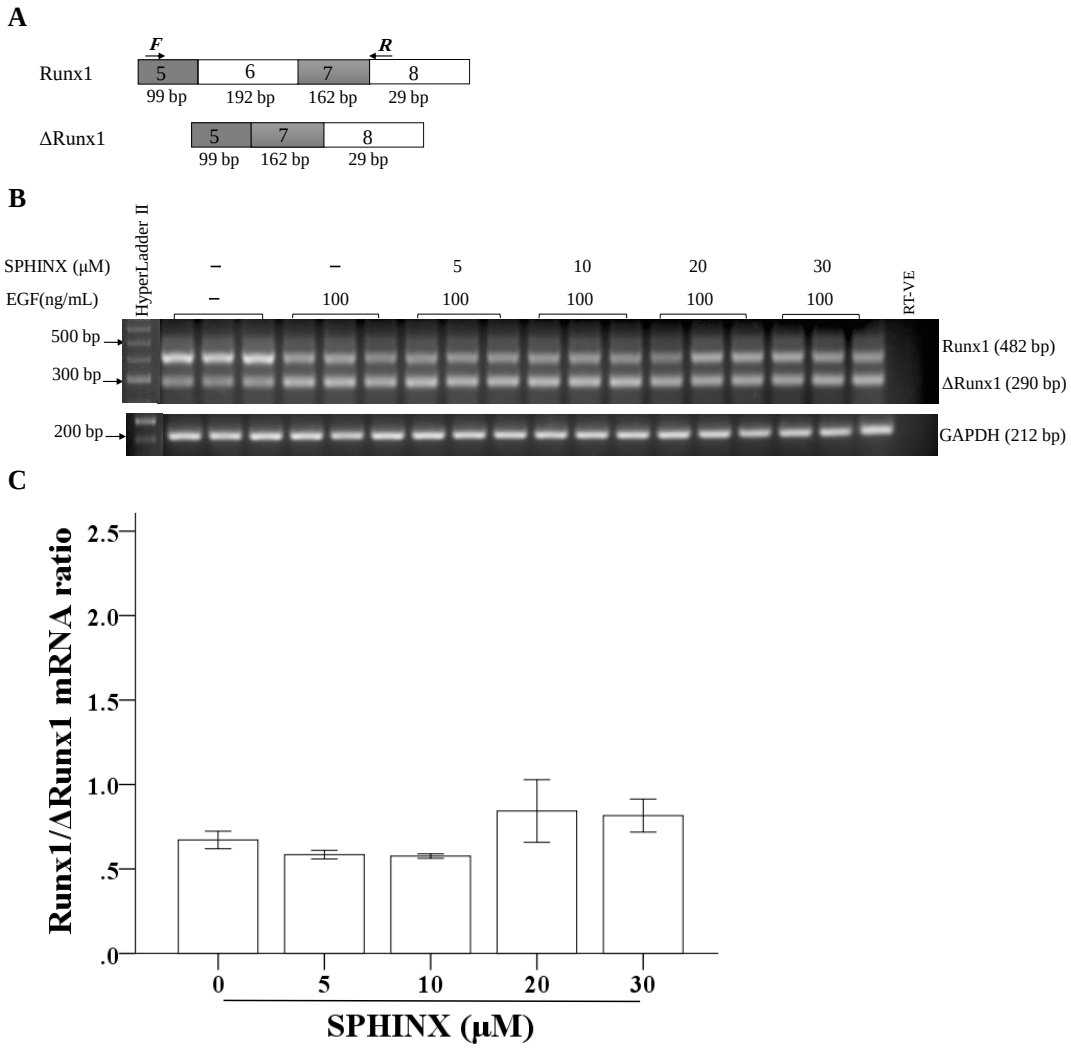

Figure 3.16. SRPK1 inhibition (SPHINX) on *RUNX1* alternative splicing
A. *RUNX1* showing the two splice variants resulting from inclusion or exclusion of exon 11 (Runx1 and ΔRunx1, respectively). Arrows indicate the positions of *forward* and *reverse* Ron primers. **B.** K562 cells were treated with only 100 ng/mL EGF (0 μM SPHINX) and range concentrations of SPHINX were used (5–30 μM) followed by 100 ng/mL EGF. RT-PCR was performed and bands at 482 bp (Runx1) and 290 bp (ΔRunx1) were detected. GAPDH was used as a loading control. Each rung of the hyperLadder II represents 100 bp. **C.** Densitometric analysis of Runx1/ΔRunx1 isoforms. K562 cells treated with 5–30 μM SPHINX were compared with the EGF control (0 μM SPHINX). The graph represents the intensity ratio of Runx1 against ΔRunx1. The bars indicate standard error (one-way ANOVA). The data represents three independent experiments (n = 3).

3.4.2.4.1 The Runx1 cDNA amplicon sequences

Runx1 mRNA sequence was confirmed using NCBI GenBank with Refseq® database: (NG_011402.2). Figure 3.17 shows the Runx1 sequence, including exons 5–7 and part of exon 8.

5'…GGAAAA**GCTTCACTCTGACCATCACTG**TCTTCACAAACCCACCGCAAGTCGCCACCTACCACAGAGCC
ATCAAAATCACAGT

GACATCGGCAGAAACTAGATGATCAGACCAAGAGCTTGTCCTTTTCCGAGCGGCTCAGTGAACTGGAGCAG
CTGCGGCGCACAGCCATGAGGGTCAGCCCACACCACCCAGCCCCCACGCCCAACCCTCGTGCCTCCCTGAA
CCACTCCACTGCCTTTAACCCTCAGCCTCAGAGTCAGATGCAGG
CCGCGCCAGTTCCCCGCGCTGCCCTCCATCTCCGACCCCCGCATGCACTATCCAGGCGCCTTCACCTACTC
CCCGACGCCGGTCACCTCGGGCATCGGCATCGGCATGTCGGCCATGGGCTCGGCCACGCGCTACCACACCT
ACCTGCCGCCGCCCTACCCCGGCTCGTCGCAAGCGCAGGGAGGCCCGTTCCAAGCCAGCTCGCCCTCCTAC
CACCTGTACTACGGCGCCTCGGCCGGCTCCTACCAGTTCTCCATGGTGGGCGGCGAGCGCTCGCCGCCGCG
CATCCTGCCGCCCTGCACCAACGCCTCCACCGGCTCCGCGCTGCTCAACCCCAGCCTCCCGAACCAGAGCG
ACGTGGTGGAGGCCGAGGGCAGCCACAGCAACTCCCCCACCAACATGGCGCCCTCCGCGCGCCTGGAGGAG
GCCGTGTGGAGGCCCTACTGA…'3

Figure 3.18 shows the ΔRunx1 sequence and includes exons 5, 7 and part of exon 8.

5'…GGAAAA**GCTTCACTCTGACCATCACTG**TCTTCACAAACCCACCGCAAG

TCGCCACCTACCACAGAGCCATCAAAATCACAGTGGATGGGCCCCGAGAACCTCGAAGACATCGGCAG
AAACTAGATGATCAGACCAAGAGCTTGTCCTTTTCCGAGCGGCTCAGTGAACTGGAGCAGCTGCGGCG
CACAGCCATGAGGGTCAGCCCACACCACCCAGCCCCCACGCCCAACCCTCGTGCCTCCCTGAACCACT
CCACTGCCTTTAACCCTCAGCCTCAGAGTCAGATGCAGGATACAAGGCAGATCCAACCATCCCCACCG
TGGTCCTACGATCAGTCCTACCAATACCTGGGATCCATTGCCTCTCCTTCTGTGCACCCAGCAACGCC
CATTTCACCTGGACGTGCCAGCGGCATGACAAGCCCGGCCCTCTCTGCAGAACTTTCCAGTCGACTCT
CAACGGCACCC**GACCTGACAGCGTTCAGCGAC**C

CGCGCCAGTTCCCCGCGCTGCCCTCCATCTCCGACCCCCGCATGCACTATCCAGGCGCCTTCACCTACTCC
CCGACGCCGGTCACCTCGGGCATCGGCATCGGCATGTCGGCCATGGGCTCGGCCACGCGCTACCACACCTA
CCTGCCGCCGCCCTACCCCGGCTCGTCGCAAGCGCAGGGAGGCCCGTTCCAAGCCAGCTCGCCCTCCTACC
ACCTGTACTACGGCGCCTCGGCCGGCTCCTACCAGTTCTCCATGGTGGGCGGCGAGCGCTCGCCGCCGCGC
ATCCTGCCGCCCTGCACCAACGCCTCCACCGGCTCCGCGCTGCTCAACCCCAGCCTCCCGAACCAGAGCGA
CGTGGTGGAGGCCGAGGGCAGCCACAGCAACTCCCCCACCAACATGGCGCCCTCCGCGCGCCTGGAGGAGG
CCGTGTGGAGGCCCTACTGA…'3

Figure 3.17. Sequence analysis of Runx1 showing exons 5–8
Sequence analysis of the top band amplified using primers Runx1-F + Runx1-R, showing exon 5, exon 6, exon 7 and exon 8. In red: forward and reverse primers. Sequence in box is the actual cDNA sequence generated from the Runx1 PCR product.

5'…GGAAAA**GCTTCACTCTGACCATCACTG**TCTTCACAAACCCACCGCAAGTCGCCACCTACCACAGAGCC
ATCAAAATCACAGT

GGATGGGCCCCGAGAACCTCGAA

GACATCGGCAGAAACTAGATGATCAGACCAAGAGCTTGTCCTTTTCCGAGCGGCTCAGTGAACTGGAGCAG
CTGCGGCGCACAGCCATGAGGGTCAGCCCACACCACCCAGCCCCCACGCCCAACCCTCGTGCCTCCCTGAA
CCACTCCACTGCCTTTAACCCTCAGCCTCAGAGTCAGATGCAGG

ATACAAGGCAGATCCAACCATCCCCACCGTGGTCCTACGATCAGTCCTACCAATACCTGGGATCCATT
GCCTCTCCTTCTGTGCACCCAGCAACGCCCATTTCACCTGGACGTGCCAGCGGCATGACAAGCCCGGC
CCTCTCTGCAGAACTTTCCAGTCGACTCTCAACGGCACCC**GACCTGACAGCGTTCAGCGAC**

CCGCGCCAGTTCCCCGCGCTGCCCTCCATCTCCGACCCCCGCATGCACTATCCAGGCGCCTTCACCTACTC
CCCGACGCCGGTCACCTCGGGCATCGGCATCGGCATGTCGGCCATGGGCTCGGCCACGCGCTACCACACCT
ACCTGCCGCCGCCCTACCCCGGCTCGTCGCAAGCGCAGGGAGGCCCGTTCCAAGCCAGCTCGCCCTCCTAC
CACCTGTACTACGGCGCCTCGGCCGGCTCCTACCAGTTCTCCATGGTGGGCGGCGAGCGCTCGCCGCCGCG
CATCCTGCCGCCCTGCACCAACGCCTCCACCGGCTCCGCGCTGCTCAACCCCAGCCTCCCGAACCAGAGCG
ACGTGGTGGAGGCCGAGGGCAGCCACAGCAACTCCCCCACCAACATGGCGCCCTCCGCGCGCCTGGAGGAG
GCCGTGTGGAGGCCCTACTGA…'3

Figure 3.18. Sequence analysis of ΔRunx1 showing exons 5–8
Sequence analysis of the top band amplified using primers Runx1-F + Runx1-R, showing exon 5, exon 6, exon 7 and exon 8. In red: forward and reverse primers. Sequence in box is the actual cDNA sequence generated from the ΔRunx1 PCR product.

3.4.2.5. Apoptosis in K562 cells following treatment with SRPK1 inhibitors

3.4.2.5.1 Apoptosis detection using acridine orange

To establish whether SRPK1 inhibition induced apoptosis in K562 cells, acridine orange (AO) was used to distinguish cell survival from cell death (apoptosis or necrosis) according to cell morphological changes.

Cells were treated with doses of SRPIN340 or SPHINX and compared to control cells treated with EGF (100 ng/mL) only, Figure 3.19. Viable cells (VC) with intact plasma membranes and rounded nuclei were present in untreated K562 cells when compared with the EGF control, Figure 3.19A. Apoptosis (Apo) was present in the EGF control and was represented by cell shrinkage, condensation of nuclear chromatin and membrane bound apoptotic bodies, Figure 3.19B. Additionally,

apoptosis was noticed following exposure to 10 μM and 20 μM SRPIN340, Figures 3.19C and D. Fragmentation of nuclear chromatin and apoptotic bodies were observed in cells treated with 5 μM and 30 μM SPHINX, Figures 3.20C and F. Necrosis (NC) denoted by ruptured cell membranes was observed in those cells treated with 10 μM and 20 μM SPHINX, Figures 3.20D and E.

The total number of cells after treatment was not identified, however, at least 1000 cells per treatment were quantified. The percentages of viable, apoptotic and necrotic cells were calculated and compared to the EGF control, Figure 3.21. It was observed that cells treated with 10 μM SRPIN340, for 24 hours, showed reduced apoptosis of 15.3% (p = 0.68) and necrosis of 2% (p = 0.74) when compared with the EGF control (one-way ANOVA), Figure 3.21. Treatment with 20 μM SRPIN340 increased apoptosis to 24.3% (p = 0.74) but decreased necrosis to 3.6% (p = 1.00) when compared to EGF controls (one-way ANOVA). Cell exposures to SPHINX doses (5–30 μM) for 24 hours showed that 5 μM and 30 μM induced apoptosis to 22.3% (p = 0.95) and to 21.3% (p = 0.99) respectively when compared to the EGF control (one-way ANOVA). However, necrosis was reduced in cells treated with 5 μM SPHINX to 1% (p = 0.50), whereas cells treated with 30 μM SPHINX, increased necrosis to 7.6% (p = 0.26) when compared with the EGF control (one-way ANOVA).

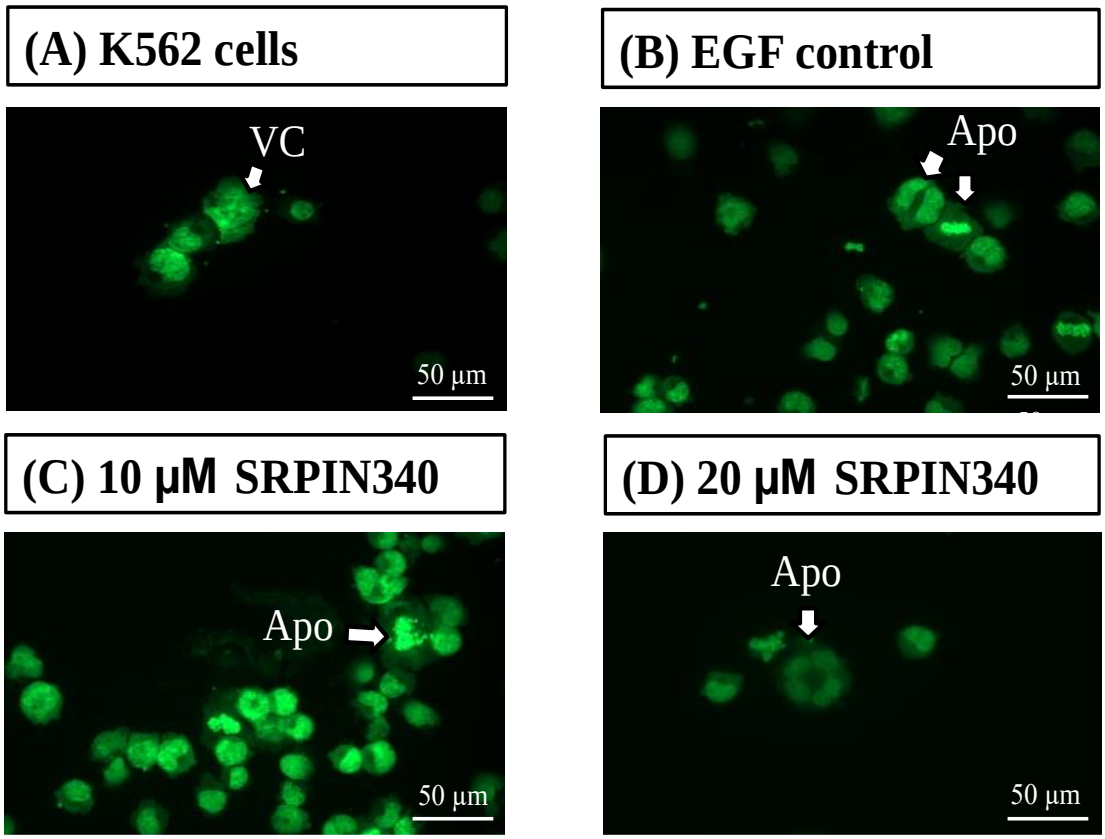

Figure 3.19. Apoptosis and necrosis in kinase inhibited K562 cells
A. Untreated K562 cells were viable (viable cells: VC). **B.** Apoptosis was induced in the EGF control; arrows indicate apoptotic cells with condensed nuclear chromatin and bilobed or fragmented nuclei. **C–D.** Cells treated with 10 µM and 20 µM SRPIN340 increased apoptosis, which was characterised by condensed nuclear chromatin appearing as crescents on the nuclear membrane peripheries, chromatin fragmentation and cytoplasmic condensation. **C.** Arrows show apoptotic cells with fragmented nuclear chromatin and cytoplasmic condensation with cytoplasmic vacuole forming. **D.** Arrows show apoptotic cells with multi-lobed nuclei.

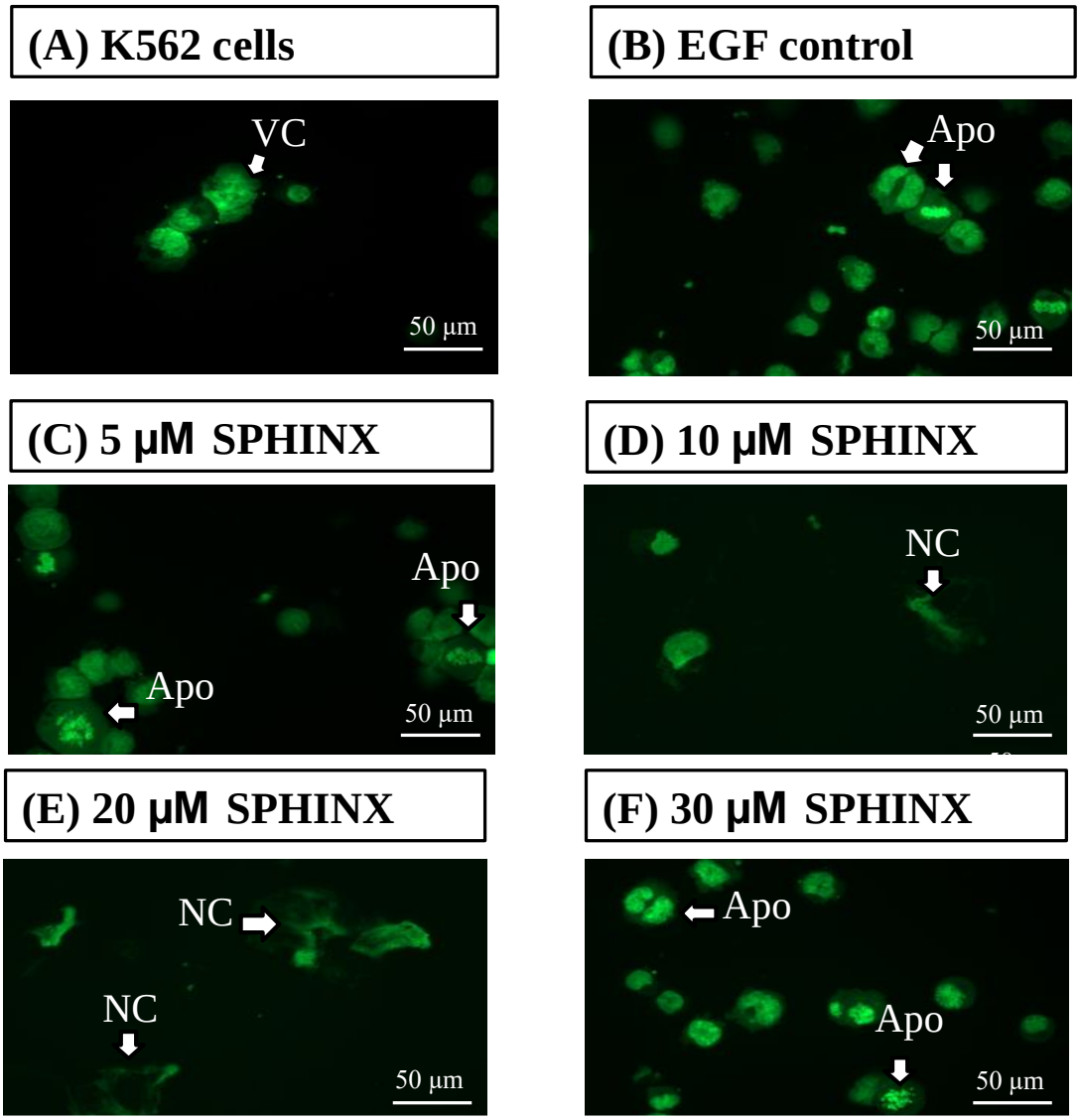

Figure 3.20.Apoptosis and necrosis in kinase inhibited K562 cells
A. Untreated K562 cells were viable (viable cells: VC). **B.** Apoptosis was induced in the EGF control; arrows indicate apoptotic cells with condensed nuclear chromatin and bilobed or fragmented nuclei. **C.** and **F.** Treating K562 cells with 5 µM and 30 µM SPHINX increased apoptosis; arrows indicate apoptotic cells with fragmented chromatin and condensed nuclei. **D.** and **E.** In contrast, cells treated with 10 µM and 20 µM SPHINX induced necrosis with swelling and rupture of the plasma membrane, resulting in the relocation of cytoplasmic contents to the extracellular space. At least 1000 cells per treatment were quantified and assessed.

Cells treated with 10 µM and 20 µM SPHINX revealed significant decreases in apoptosis of up to 3.6% (p = 0.00) and 3% (p = 0.00) when compared with the EGF control (one-way ANOVA). In contrast, cells treated with 10 µM and 20 µM

SPHINX showed significant increases in necrosis of up to 54.6% (p = 0.00) and 69% (p = 0.00) when compared with the EGF control (one-way ANOVA).

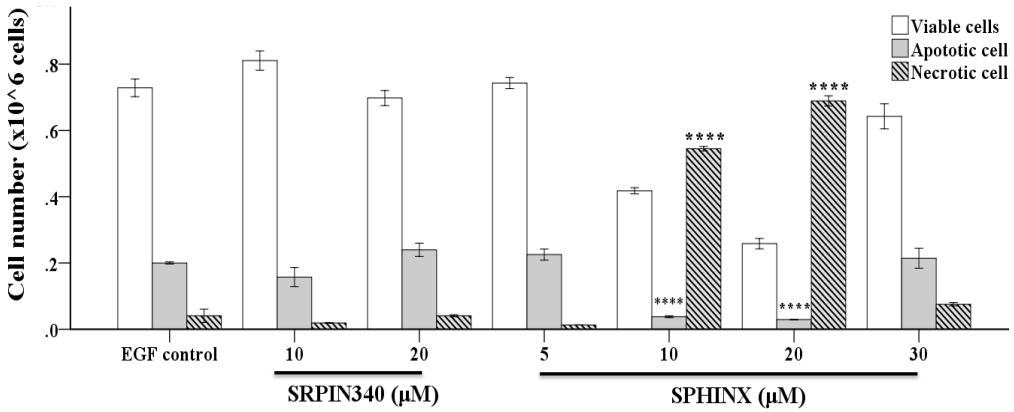

Figure 3.21. Inhibitor treatment of K562 cells showing apoptosis and necrosis
K562 cells were stained with acridine orange following treatments with SRPIN340 (10 μM and 20 μM) or SPHINX (5–30 μM). At least 1,000 cells were assessed. The graph represents the percentage of viable cells (white), apoptotic cells (grey) and necrotic cells (dashed) per treatment. Treatment with 10 μM and 20 μM SPHINX significantly decreased apoptosis and increased necrosis when compared to the EGF control. The bars indicate standard error, **** $P \leq 0.0001$ (one-way ANOVA). The data represents three independent experiments (n = 3).

3.4.2.5.2 Annexin V-FITC/Propidium Iodide apoptosis detection

Annexin V-FITC/PI binding and flow cytometry was performed to investigate early apoptosis stages after treatment with SRPIN340 or SPHINX. In flow cytometric analysis, cells that were Annexin V-FITC positive and PI negative were apoptotic, while cells that were Annexin V-FITC and PI positive were necrotic, Figure 3.22. These results were compared with control cells treated with 100 ng/mL EGF (EGF control) only. Apoptosis within the EGF control population was 0.91% while necrosis was 3.4%, Figure 3.22A.

Apoptotic cells comprised 0.61% under 10 μM SRPIN340 conditions and 0.56% under 20 μM SRPIN340 condition when compared to the EGF control, Figure 3.22B

and C. In contrast, necrotic cells were 4.4% under 10 μM SRPIN340 condition and 5.9% under 20 μM SRPIN340 condition when compared to EGF control. Apoptotic cells treated with 5 μM SPHINX reached to to 0.79%, whereas necrotic cells to 5% in these cells, when compared to the EGF control, Figure 3.22D. Cells treated with 10 μM, 20 μM and 30 μM SPHINX resulted in apoptosis of 0.68%, 0.51% and 0.57% respectively, when compared to the EGF control, Figure 3.22E and G. However, for these conditions; 10 μM, 20 μM and 30 μM SPHINX, necrosis was similar to EGF control (3.0%, 3.7% and 3.2%, respectively).

3.4.3. SRPK1 or SRSF1 knockdown in K562 cells

3.4.3.1. Generating stable SRPK1 knockdown using shRNA in K562 cells

To identify the effects of SRPK1 knockdown on *CASPASE-9, RON* or *RUNX1* splicing, the generation of a stable *SRPK1* knockdown was required. To achieve this, K562 cells were transduced with lentivirus containing shRNA *SRPK1* or scramble shRNA. The SMARTvector 2.0 lentiviral shRNA plasmid expressing a puromycin resistance cassette was used to select transduced cells.

For successful transduction, the minimal puromycin concentration required to eliminate all untransduced cells within seven days, had to be determined, Figure 3.23. Approximately 1×10^6 K562 cells were treated with increased doses (0.66–9 μg/mL) of puromycin. Cells were examined daily. The number of cells in each treatment was calculated and compared with the original 1×10^6 cells.

Cells treated with 0.66 μg/mL puromycin reduced cell numbers to 6.5×10^5 cells/well while 3 μg/mL puromycin reduced cell numbers to 1.8×10^4 cells/well. Subjecting cells to 5, 7 and 9 μg/mL puromycin reduced cell numbers to 1.5×10^4 cells/well. Graphing this data (Figure 3.23) revealed that the 0.66 μg/mL concentration had the minimal visual toxicity, whereas 3 μg/mL had the strongest toxicological effect. Therefore, it was proposed that 1.5 μg/mL puromycin would be the minimal antibiotic concentration to kill all untransduced cells.

Figure 3.24 shows SRPK1 and SRSF1 stable knockdown of SRPK1. K562 cells were transduced with lentivirus targeting SRPK1 or scrambled shRNA (sh-CTRL); 1.5 μg/mL puromycin was added for seven days and protein extracted for Western blotting. Normalisation of SRPK1 and SRSF1 was carried out using the loading control, α-tubulin (75 μg of whole cell lysates).

Figure 3.24A shows SRPK1 expression in stable SRPK1 knockdown cells similar to the sh-CTRL cells. The expression of SRPK1 in cells expressing stable SRPK1-KD was 0.09 (p = 0.94, one-way ANOVA), Figure 3.24B. In contrast, there was a reduction in SRSF1 expression in stable SRPK1-KD cells when compared with sh-CTRL cells, Figure 3.24C. The expression of normalised SRSF1 was 0.87 (p = 0.08) in stabilised SRPK1-KD (one-way ANOVA), Figure 3.24D.

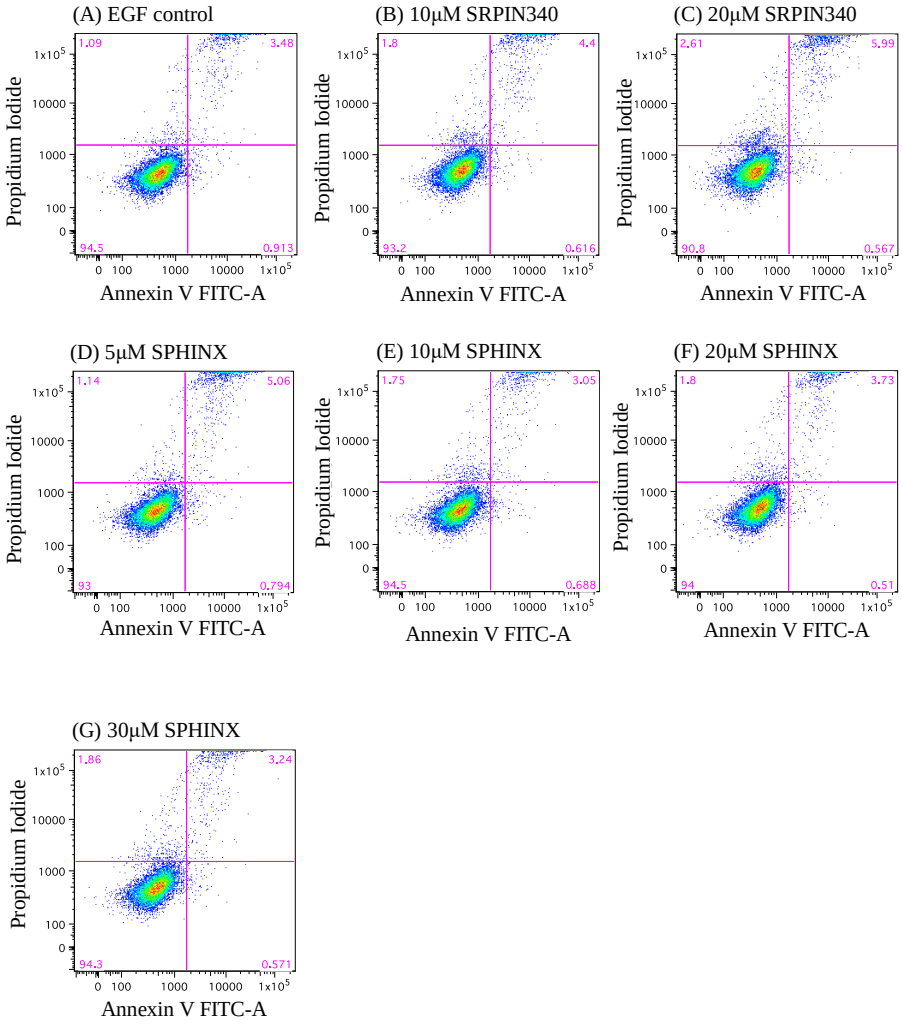

Figure 3.22. Apoptosis and necrosis in treated cells using Annexin V-FITC and Flow Cytometry

Scatterplots of cell death (apoptosis; Annexin V-FITC and necrosis; Annexin V-FITC with propidium iodide) in K562 cells treated with SRPIN340 (10 µM and 20 µM) and SPHINX (5 – 30 µM). **A.** Control K562 cells treated with 100 ng/mL EGF only (EGF control). **B–C.** Cells treated with 10 and 20 µM SRPIN340. **D–G.** Cells treated with 5 – 30 µM. SPHINX. One representative experiment of three is shown.

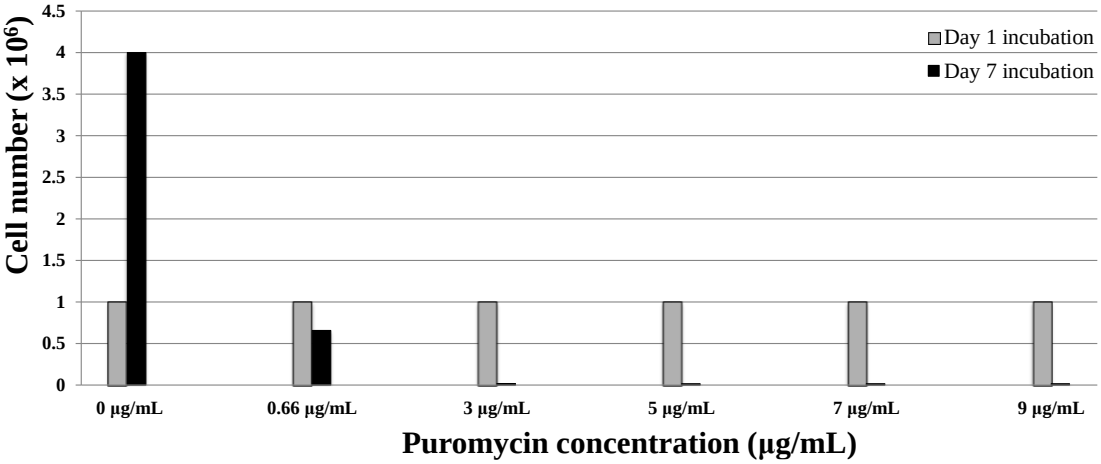

Figure 3.23. The optimal concentration of puromycin to kill untransduced K562 cells

K562 cells (1×10^6 cells/well) were treated with different puromycin concentrations (0.66 – 9 µg/mL) and incubated for seven days. Following this, cell numbers decreased slowly for the 0.66 µg/mL treatment, whereas treatment with 3 µg/mL puromycin dramatically decreased cell numbers when compared to the starting 1×10^6 cells. The results are displayed as mean ± SEM (n = 3).

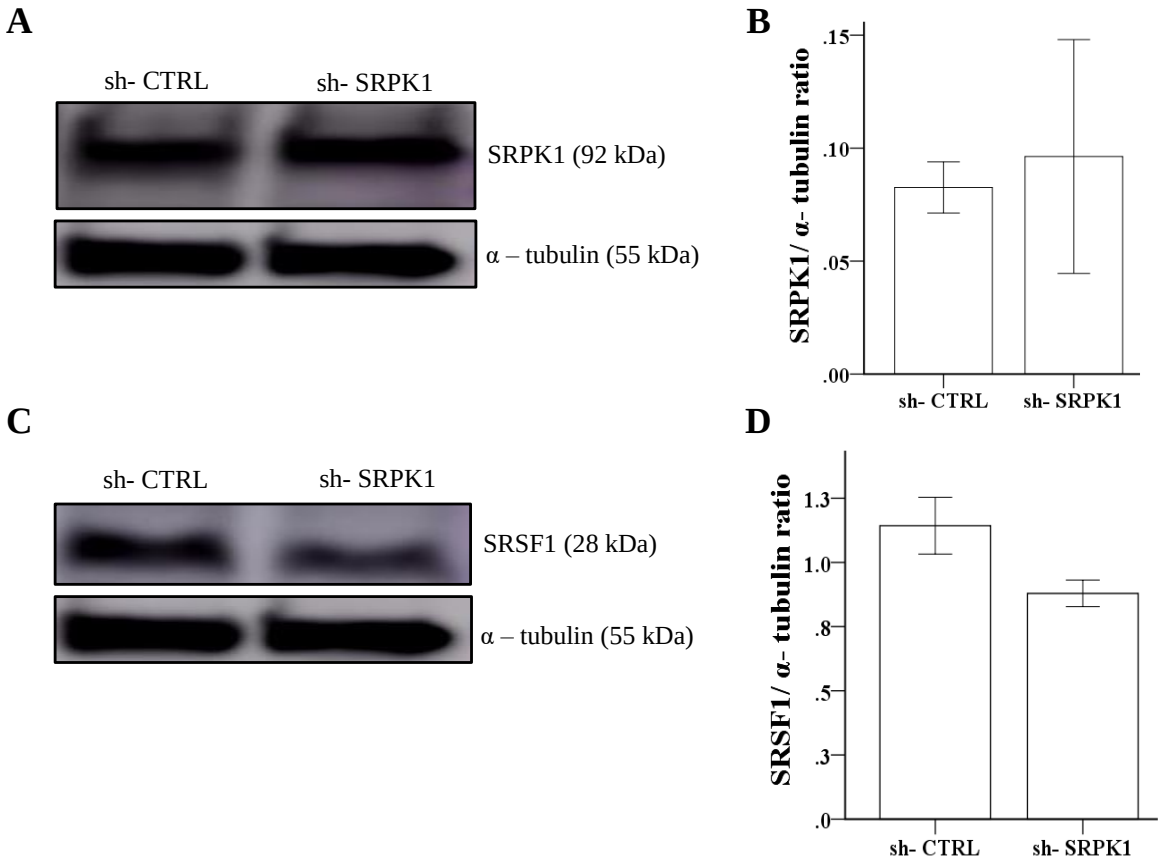

Figure 3.24. The stable knockdown of SRPK1 in K562 cells
A. SRPK1 expression in K562 cells treated with sh-scramble (sh-CTRL) or sh-SRPK1 followed by Western blot analysis using antibodies against SRPK1 and α-tubulin (loading control). SRPK1 was 92 kDa and α-tubulin 55 kDa. **B.** The quantification from replicates with normalisation to α-tubulin (equal loading). **C.** SRSF1 Western blot showing a 28 kDa protein product. **D.** Quantification from replication with normalisation to α-tubulin (equal loading). The transduction of K562 cells with sh-SRPK1 slightly increased SRPK1 expression, whereas it decreased SRSF1 expression. The bars indicate standard error (one-way ANOVA). The data represent three independent experiments (n = 3).

3.4.3.2. The effect of siRNA SRPK1 and SRSF1 knockdown on alternative splicing in K562 cells

Alterations in *CASPASE-9*, *RON* or *RUNX1* splice patterns through SRPK1 or SRSF1 knockdown in K562 cells was assessed. The expression of SRPK1 and SRSF1 was demonstrated using control siRNA (si-CTRL), SRPK1 SMARTpool siGENOME siRNA (si-SRPK1) or SRSF1 SMARTpool siGENOME siRNA (si-SRSF1) in K562 cells, Figures 3.25 and 3.27.

K562 cells were transfected with si-CTRL (75 nM), si-SRPK1 (75 nM) or si-SRSF1 (75 nM) for 48 and 72 hours. Following transfection, Western blotting was carried out, and normalisation of SRPK1 and SRSF1 to α-tubulin (equal loading) was performed (75 μg whole cell lysates). Figures 3.25A and B show SPRK1 expression in cells transfected with si-CTRL (75 nM), si-SRPK1 (75 nM) or si-SRSF1 (75 nM) for 48 hours. There was no difference in SPRK1 expression between si-SRPK1 cells and si-CTRL cells or si-SRSF1 cells and si-CTRL cells, Figure 3.25A. The expression ratio of normalised SRPK1 following si-SRPK1 was 0.64 (p = 0.97) and following si-SRSF1 was 0.70 (p = 0.99, one-way ANOVA), Figure 3.25B.

Furthermore, there was a slight decrease in SPRK1 expression following transfection with si-CTRL (75 nM) or si-SRPK1 (75 nM) after 72 hours, Figure 3.25C. In addition, the SPRK1 expression was observed following transfection with si-SRSF1 (75 nM) after 72 hours. The expression ratio of normalised SRPK1 following si-SRPK1 was 3.39 (p = 0.43) compared with si-CTRL cells. Additionally, cells

transfected with si-SRSF1 was normalised SRPK1 to 3.11 (p = 0.31), one-way ANOVA.

To establish whether higher SRPK1 expression was observed in K562 cells when compared to the prostate cancer cell line (PC-3), PC-3 cells were transfected with si-CTRL (75 nM) or si-SRPK1 (75 nM) for 72 hours. It was observed that SPRK1 expression was reduced in these cells when compared with the si-CTRL control, Figure 3.26A. Similarly, there was a significant reduction in the protein expression ratio of normalised SRPK1 to 0.34 (p = 0.01) when compared to si-CTRL cells (one-way ANOVA), Figure 3.26B.

SRSF1 expression levels, following si-SRPK1 or si-SRSF1 treatment for 48 hours, was observed and compared to si-CTRL cells, Figure 3.27A. The normalised expression ratio of SRSF1 was 1.07 (p = 0.96, one-way ANOVA), Figure 3.27B. At 72 hours post-transfection, there was a decrease in SRSF1 levels in si-SRPK1 cells, and a greater reduction of SRSF1 in si-SRSF1 cells when compared to si-CTRL cells, Figure 3.27C. The protein expression of normalised SRSF1 was 1.14 (p = 0.99) when compared to si-CTRL cells (one-way ANOVA), Figure 3.27D. Down-regulation of SRSF1 at 72 hours' incubation detects a significant reduction in the normalised protein of SRSF1 to 0.42 (p = 0.001) compared with the si-CTRL cells (one-way ANOVA), Figure 3.27D.

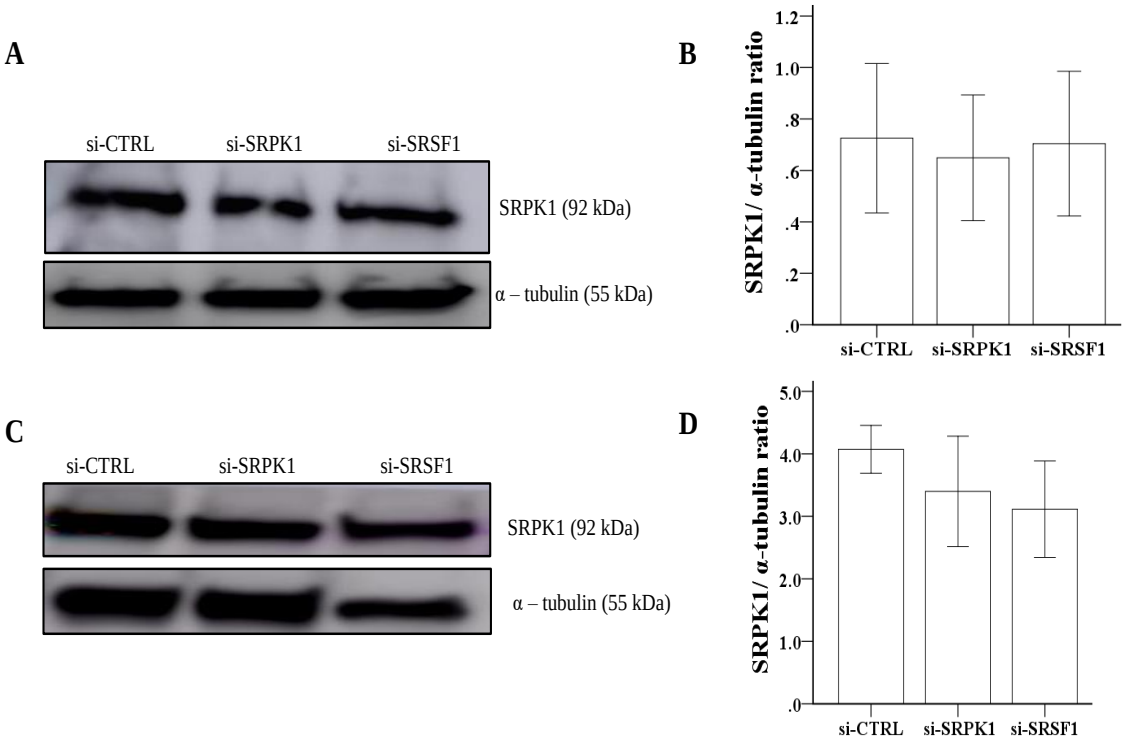

Figure 3.25. siRNA knockdown of SRPK1 and SRSF1 in K562 cells
K562 cells were transfected with si-CTRL (75 nM), si-SRPK1 (75 nM) or si-SRSF1 (75 nM) for 48 and 72 hours' incubation. **A.** SPRK1 expression in transfected cells after 48 hours' incubation. **B.** Expression quantification from three replicates normalised to α-tubulin. **C.** SPRK1 expression in transfected cells after 72 hours. **D.** The normalisation of SRPK1 to α-tubulin. The bars indicate standard error (one-way ANOVA). The data represent three independent experiments (n = 3).

A

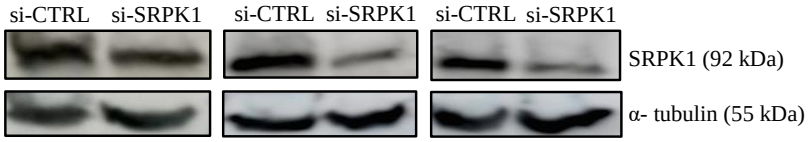

B

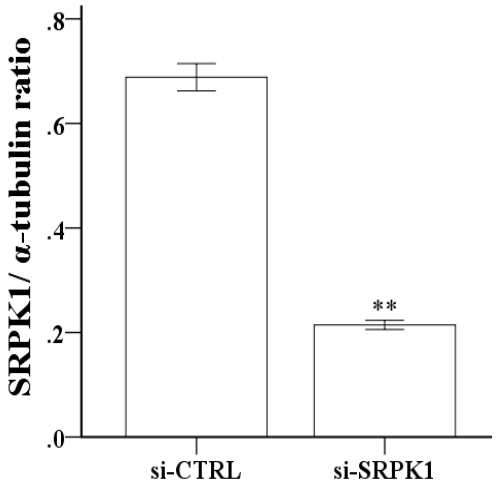

Figure 3.26. siRNA knockdown of SRPK1 in PC-3 cells
PC-3 cells were transfected with si-CTRL (75 nM) or si-SRPK1 (75 nM) for 72 hours. **A.** SRPK1 expression in transfected PC-3 cells after 72 hours. **B.** Quantification ratio of three repeats with normalisation to α-tubulin. SRPK1 levels significantly decreased in si-SRPK1 transfected PC-3 cells (75 nM) for 72 hours. The bars indicate standard error, ** $P \leq 0.01$ (one-way ANOVA). The data represents three independent experiments ($n = 3$).

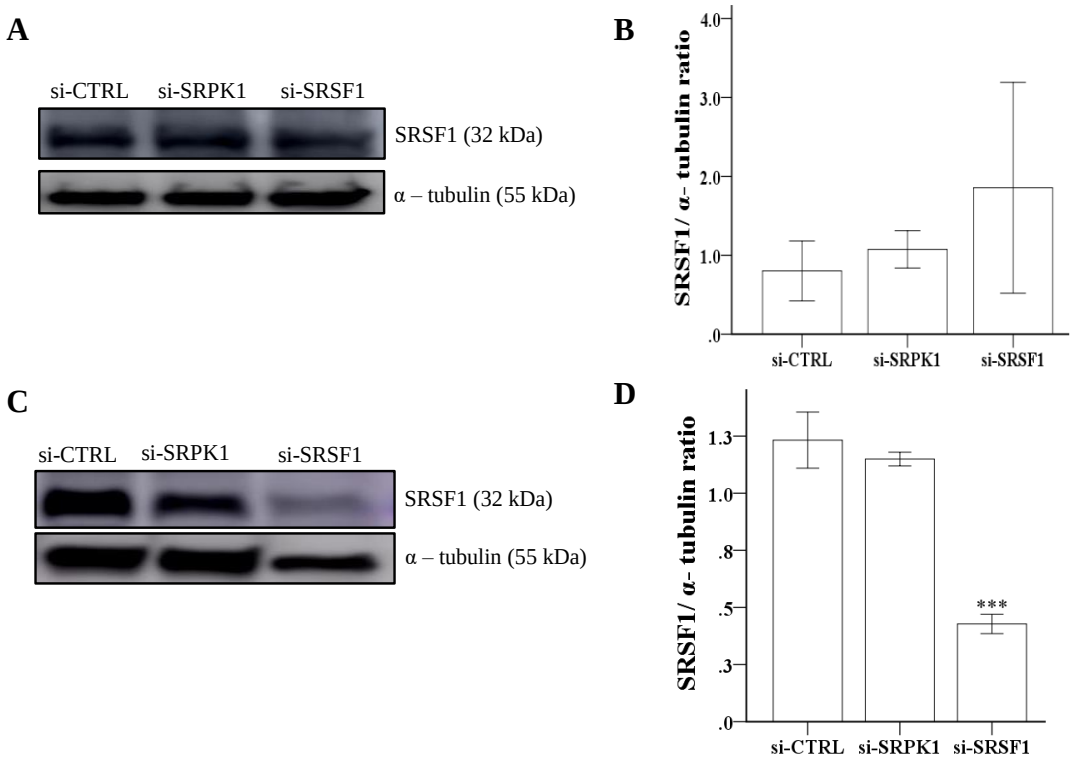

Figure 3.27. siRNA knockdown of SRPK1 and SRSF1 in K562 cells
K562 cells were transfected with si-CTRL (75 nM), si-SRPK1 (75 nM) or si-SRSF1 (75 nM) for 48 and 72 hours. **A.** SRSF1 from transfected cells at 48 hours. **B.** Expression quantification from three replicates normalised to α-tubulin. **C.** SRSF1 expression in transfected cells at 72 hours. **D.** The normalisation of SRPK1 to α-tubulin. SRSF1 was significantly decreased in transfected cells after si-SRSF1 (75 nM) treatment for 72 hours. The bars indicate standard error (one-way ANOVA). The data represent three independent experiments (n = 3).

3.4.3.3. siRNA SRSF1 knockdown and its effect on alternative splicing in K562 cells

SRSF1 knockdown demonstrated how *CASPASE-9*, *RON* and *RUNX1* alternative splicing in K562 cells was affected. Cells were transfected with si-CTRL (75 nM) or si-SRSF1 (75 nM) for 72 hours. For each gene, the expression ratio of splice variants in si-SRSF1 cells was compared to si-CTRL cells and quantified by densitometric analysis using ImageJ software.

3.4.3.3.1 *CASPASE-9* splicing in K562 cells following SRSF1 knockdown

K562 cells transfected with siRNA SRSF1 increased the pro-apoptotic splicing isoform caspase-9a, Figure 3.28B. The effect of si-SRSF1 on *CASPASE-9* mRNA was quantified (Figure 3.28C), showing a slight down- regulation in the expression ratio of caspase-9a/9b to 2.11 ($p = 0.001$) when compared with si-CTRL cells (0.64), one-way ANOVA. This significant effect is not specific when si-SRSF1 cells are compared to untreated K562 cells, Figure 3.28B.

3.4.3.3.1 *RON* splicing in K562 cells following SRSF1 knockdown

The effect of siRNA-SRSF1 on *RON* alternative splicing was examined, Figure 3.29B. Knockdown of SRSF1 resulted in the expression ratio of 0.76 ($p = 0.17$) for Ron/ΔRon when compared to si-CTRL cells (0.40, one-way ANOVA), Figure 3.29C.

3.4.3.3.1 *RUNX1* splicing in K562 cells following SRSF1 knockdown

A down-regulation of expression was noted for Runx1 and ΔRunx1 variants after transfection with si-SRSF1, when compared to si-CTRL cells, Figure 3.30B. The

expression ratio of Runx1/ΔRunx1 in si-SRSF1 cells was 4.71 (p = 0.50), when compared to si-CTRL cells (3.35, one-way ANOVA), Figure 3.30C.

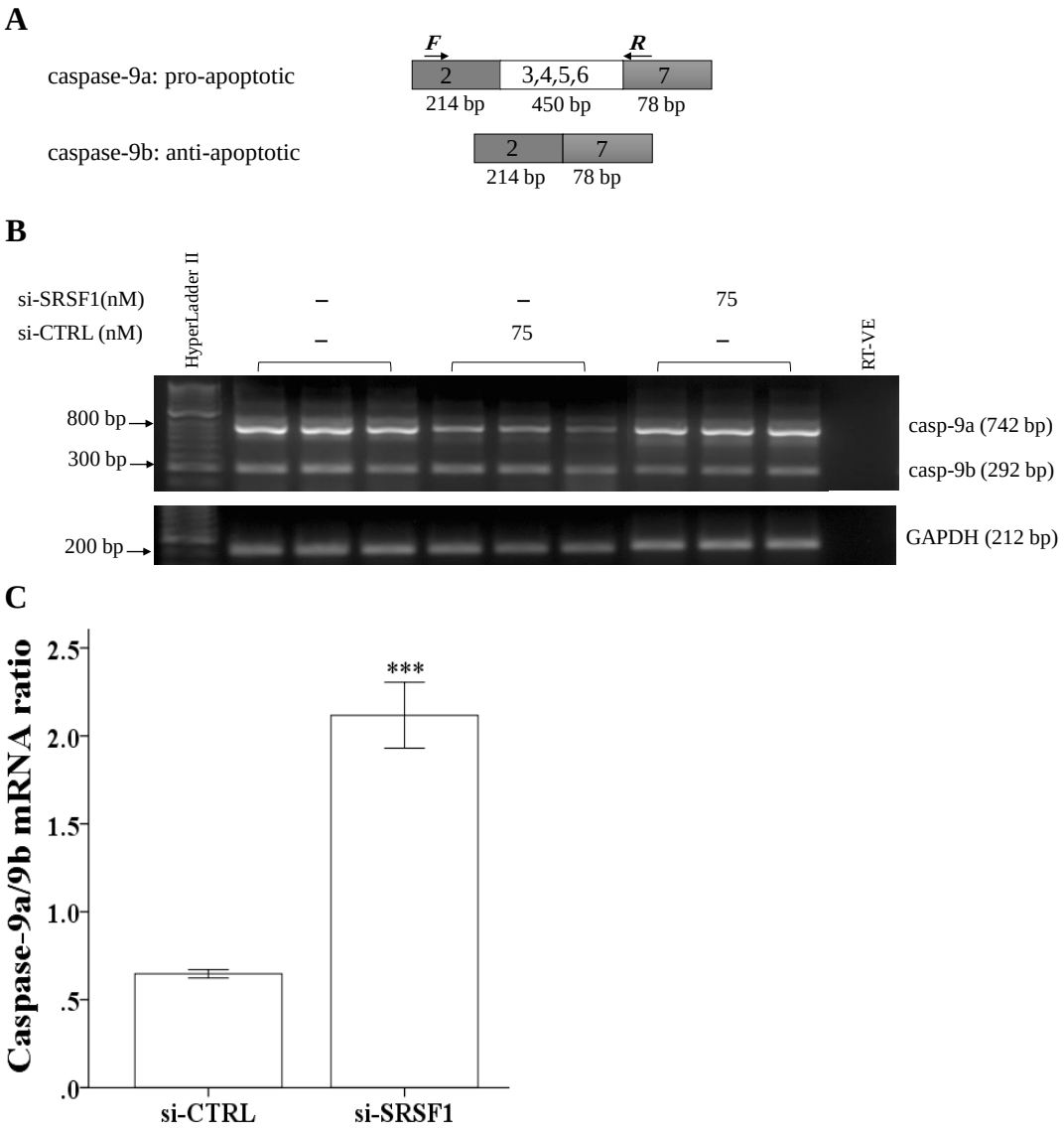

Figure 3.28. siRNA SRSF1 knockdown effects on *CASPASE-9* alternative splicing

A. *CASPASE-9* showing the two splice variants resulting from inclusion or exclusion of exons 3-6 (caspase-9a and caspase-9b, respectively). Arrows indicate the positions of *forward* and *reverse CASPASE-9* primers. **B.** K562 cells transfected with si-CTRL (75 nM), si-SRPK1 (75nM) or si-SRSF1 (75 nM) for 72 hours followed by caspase-9a and caspase-9b RT-PCR. RT-PCR bands at 742 bp (casp-9a) and 292 bp (casp-9b) were detected. GAPDH was used as a loading control (212 bp). Each rung of the hyperLadder II represents 100 bp. Caspase-9a isoform increased in si-SRSF1 cells when compared to si-CTRL cells. This increase is not specific when si-SRSF1 cells compared to untreated K562 cells. **C.** Densitometric analysis of caspase-9a/9b isoforms. K562 cells transfected with si-SRSF1 (75 nM) were compared to si-CTRL (75 nM) cells. The graph represents the intensity ratio of caspase-9a against caspase-9b. The expression ratio of caspase-9a/9b increased in cells transfected with si-SRSF1 (75 nM) after 72 hours. The bars indicate standard error, *** $P \leq 0.001$ (one-way ANOVA). The data represent three independent experiments ($n = 3$).

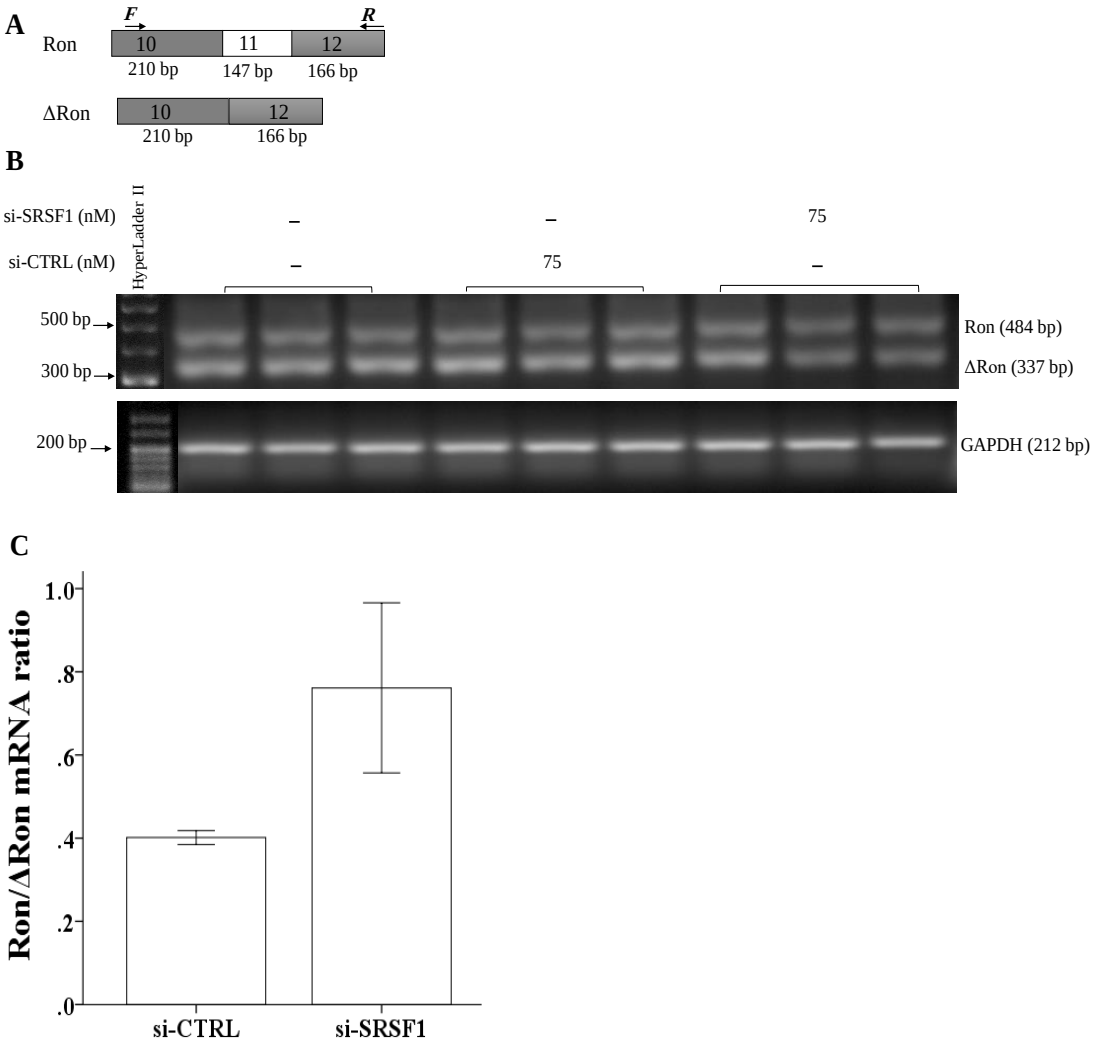

Figure 3.29. siRNA SRSF1 knockdown effects on *RON* alternative splicing
A. The *RON* gene showing the two splice variants resulting from including or excluding exon 11 (Ron and ΔRon variants, respectively). Arrows indicate the positions of forward and reverse Ron primers. **B.** The RT-PCR gel of K562 cells transfected with si-CTRL (75 nM) or si-SRSF1 (75 nM) at 72 hours; 484 bp (Ron) and 337 bp (ΔRon). GAPDH was used as a loading control (212 bp). Each rung of the hyperLadder II represents 100 bp. **C.** Densitometric analysis of Ron/ΔRon isoforms. K562 cells transfected with si-SRSF1 (75 nM) were compared with si-CTRL (75 nM). The graph represents the intensity ratio of Ron against ΔRon. The bars indicate standard error (one-way ANOVA). The data represent three independent experiments (n = 3).

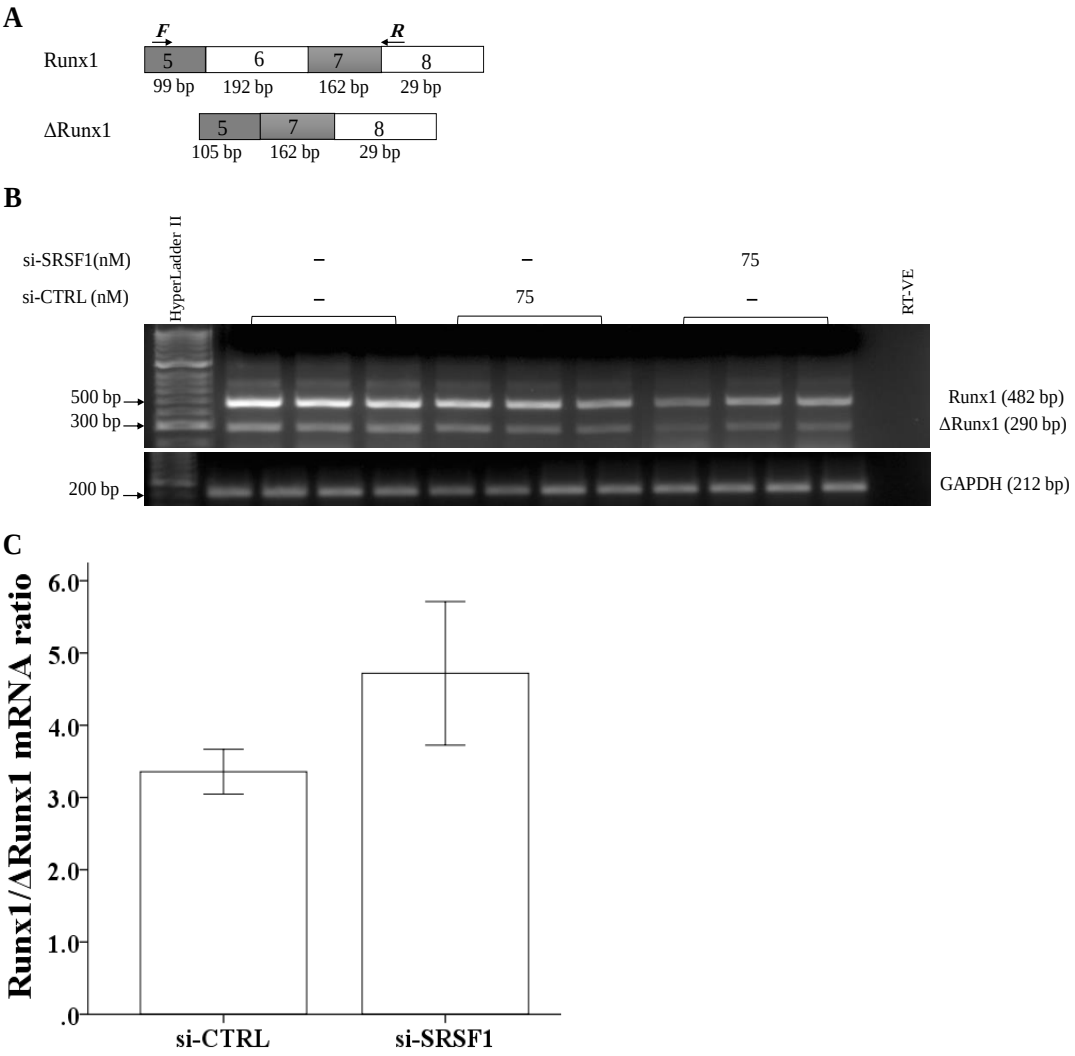

Figure 3.30. siRNA SRSF1 knockdown effects on *RUNX1* alternative splicing
A. *RUNX1* showing the two splice variants resulting from including or excluding exon 6 (Runx1 and ΔRunx1 variants, respectively). Arrows indicate the positions of *forward* and *reverse* Runx1 primers. **B.** RT-PCR gel of K562 cells transfected with si-CTRL (75 nM), si-SRPK1 (75nM) or si-SRSF1 (75 nM) at 72 hours; 482 bp (Runx1) and 290 bp (ΔRunx1). GAPDH was used as a loading control (212 bp). Each rung of the hyperLadder II represents 100 bp. **C.** Densitometric analysis of Runx1/ΔRunx1 isoforms. K562 cells transfected with si-SRPK1 (75nM) or si-SRSF1 (75 nM) were compared to si-CTRL (75 nM). The graph represents the intensity ratio of Runx1 against ΔRunx1. The bars indicate standard error (one-way ANOVA). The data represent three independent experiments (n = 3).

3.5 Discussion

In cancer, SRSF1 dysregulation due to SRPK1 overexpression, affects pre-mRNA alternative splicing, affects gene expression, increases proliferation, invasiveness and inhibition of apoptosis. Therefore targeting SRPK1 using the small molecule inhibitors SRPIN340 or SPHINX is considered a potential therapy against malignancies (Siqueira *et al.*, 2015).

A previous study found that SRPIN340 suppressed viral replication, such as the Sindbis virus, HIV and cytomegalovirus, suggesting that SRPIN340 is an antiviral agent (Karakama *et al.*, 2010). Therefore, it was important to evaluate SRPK1 inhibitors on cancer cell proliferation. A recent study has shown that cell viability was reduced in myeloid and lymphoid leukaemia by SRPIN340 treatment (Siqueira *et al.*, 2015). However, in this study, K562 proliferation was increased following SRPIN340 or SPHINX treatment, suggesting that SRPK1 small molecule inhibitors did not affect K562 cell survival.

SPRK1 overexpression has been reported in several solid tumours, such as colon, breast carcinoma and other types of malignancy (Mavrou *et al.*, 2015). It has been shown that SRPIN340 switched splicing from $VEGF_{165}$ to $VEGF_{165}b$ in human podocytes, resulting in reduced angiogenesis in a mouse model of retinal neovascularisation (Nowak *et al.*, 2010). A recent study indicated that SPHINX effected VEGF splicing and inhibited tumour growth in a mouse model of orthotopic prostate cancer in PC-3 cells (Mavrou *et al.*, 2015).

Studies from several laboratories have investigated the effects of protein kinase inhibition on genes associated with human cancer, as potential targets for therapy. One trial identified that phosphatidylinositol 3-kinase (Akt) inhibition, increased caspase-9a/9b splice isoform ratios in non-small cell lung cancers (Shulz *et al*., 2011). Another trial suggested that thiol-mediated intermolecular disulphide bonding inhibition, resulted in the down-regulation of ΔRon isoforms in human gastric cancer cells (KATO-III) (Collesi *et al*., 1996). Additionally, treatment with the proteasome inhibitor MG13, was shown to reduce ΔRunx1 splice isoforms in human embryonic kidney cells (293T) (Komeno *et al*., 2014). A recent study it has shown that a novel "compound 30" reduced the activity of SRPK through phosphorylation inhibition of SR proteins. It was also found that compound 30 can inhibited the expression of MAP2K1, MAP2K2, VEGF and *RON* oncogenic isoforms (Siqueira *et al*., 2017).

To expand on these findings and investigate the effects of protein kinase inhibitors on alternative splicing, this study investigated the splicing patterns of *CASPASE-9*, *RON* and *RUNX1* in K562 cells where SRPK1 was inhibited. No specific effects were observed on the *CASPASE-9* splice isoform, upon treatment with SRPIN340 and SRPIN349 when compared to DMSO control. Additionally, there were no shifts in *CASPASE-9* splicing in K562 cells treated with SRPIN340 or SPHINX, upon EGF induction of cell signalling.

From cell morphological characteristics, a reduction in apoptosis was observed in the SRPIN340 or SPHINX treatment of K562 cells. Similarly, Annexin V-FITC staining revealed that SRPK1 inhibition reduced apoptosis in K562 cells. These data were in agreement with SRPIN340 reduced effectiveness on myeloid cells as opposed to

lymphoid leukaemia cell lines due to high expression of SRPK1 in myeloid leukaemia (Siqueira *et al.*, 2015). However, a recent study demonstrated the effect of 1-(3,4,5-trihydroxyphenyl)-dodecylbenzoate on apoptosis using both acridine orange and Annexin V staining (Maioral *et al.*, 2016). Although the exact mechanism of action is not clear, p53 and AIF expression were increased in K562 cells treated with this compound. It was also observed that 1-(3,4,5-trihydroxyphenyl)-dodecylbenzoate increased expression of pro-apoptotic Bax in Jurkat cells. These data suggest that 1-(3,4,5-trihydroxyphenyl)-dodecylbenzoate triggers apoptosis in K562 and Jurkat cells, thus reinforcing the compound as an anti-proliferative and cytotoxic inhibitor (Maioral *et al.*, 2016). It was also observed that Jurkat cells are more sensitive to SRPIN340 treatment than K562 cells, due to the higher SRPK1 levels in K562 cells, suggesting that SRPIN340 triggers apoptosis in these cells (Siqueira *et al.*, 2015).

The expression of the Ron isoform was significantly increased in K562 cells when treated with high concentrations of SRPIN340, when compared to DMSO control. This significant effect, however, is not specific when the expression of Ron in K562 cells treated with SRPIN340 is compared to cells treated with SRPIN349. In addition, no shift in *RON* splicing was observed in K562 cells, during SRPK1 inhibition (SRPIN340 or SPHINX followed by EGF addition). Furthermore, there was no switch in *RUNX1* expression towards the Runx1 splice isoform in SRPIN340 treated K562 cells. In contrast, there was a non-significant increase in Runx1 splice isoform expression in SPHINX treated K562 cells.

Overall, no switch in *CASPASE-9*, *RON* or *RUNX1* splicing was observed in cells treated with SRPIN340 or SPHINX. This suggests that selective SRPK1 inhibitors could act differentially on *CASPASE-9, RON* or *RUNX1* splicing in K562 cells. These weak effects on alternative splicing in SPRK1 inhibited K562 cells, could predict activation of other key protein kinases or reflect high SRPK1 levels in K562 cells.

SRPK1 inhibition did not induce apoptosis, nor generate strong effects on *CASPASE-9*, *RON* or *RUNX1* splicing in K562 cells, therefore a SRPK1-knockdown (KD) was investigated to see if it would induce a splicing switch in K562 cells. Recently, a computational strategy was adopted to transduce cells with shRNAs generating stable knockdowns of specific genes. It was observed that generating SRPK1 stable knockdowns, switched the splicing of VEGF towards the $VEGF_{165}b$ isoform in PC-3 cells, resulting in decreased tumour growth in orthotopic prostate cancer mouse models (Mavrou *et al.*, 2015). It has been also found that chimeric antibody target SRPK1 (ChanSRPK1) affects on the level of SRPK1 in lung cancer (Wu *et al.*, 2017). However, in this study, generating stable SRPK1-KDs did not reduce SRPK1, whereas SRSF1 was reduced in K562 cells, confirming an increase of SRPK1 in K562 cells.

Another computational study reported that VEGF alternative splicing was generated by the transfection of SRSF1-KD into podocytes (Amin *et al.*, 2011). A reduction in MNK2b isoform expression was also observed in cells transfected with si-SRSF1 (Karni *et al.*, 2007). Based on these observations, this study investigated whether

SRPK1-KD or SRSF1-KD would affect *CASPASE-9*, *RON* and *RUNX1* alternative splicing in K562 cells.

SRPK1 was not significantly decreased in K562 cells transfected with si-SRPK1 or si-SRSF1 when compared to si-CTRL cells. Despite this, SRPK1 levels were strongly down-regulated in si-SRPK1 transfected PC-3 cells, when compared to si-CTRL cells. This suggests that SRPK1 levels are higher in K562 cells when compared to PC-3 cells. SRSF1 levels were significantly reduced in si-SRSF1 treated K562 cells after 72 hours.

At the mRNA level, there was no clear switch in caspase-9b expression towards the pro-apoptotic splice isoform, caspase-9a, ΔRon towards Ron or in ΔRunx1 expression towards Runx1 in si-SRSF1 treated K562 cells. These data suggest that SRPK1 and SRSF1 are not the regulators the splicing isoforms of these genes.

Taken together, SRPK1 inhibitor treatments appear to react differentially towards the caspase-9, Ron and Runx1 isoforms in K562 cells, suggesting SRPK1 is not the main regulator of *CASPASE-9*, *RON* or *RUNX1* splicing in these cells. The inhibition of SRPK1 may trigger activation of other key protein kinases in these cells. Furthermore, there was no significant reduction of SRPK1 protein in transduced or transfected K562 cells, unlike PC-3 cells, confirming SRPK1 levels are higher in K562 cells. Finally, there was no significant effect on *CASPASE-9* or *RUNX1* splicing in SRSF1-KD treated K562 cells, whereas SRSF1-KD caused a shift in *RON* splicing towards the Ron isoform, suggesting SRPK1 is not the main regulatory kinase in *CASPASE-9* or *RUNX1* splicing in K562 cells.

3.5.1. Conclusion and future directions

This study proposes that SRPK1 inhibition by small molecule inhibitors or shRNA/siRNA knockdown is more effective on splicing in PC-3 cells, but not K562 cells. This suggests one of two scenarios; either SRPK1 levels are higher in some malignancies or it is more resistant in K562 cells.

This study proposes the following research strategies to delineate the precise roles of these regulatory kinases in disease;

1. The evaluation of SRPK1 protein and mRNA levels in other cancer cell lines could provide comparative insights into the action of SRPK1 in K562 cells.
2. Future studies on novel SRPK1 inhibitor development could focus on haematological malignancies.
3. The investigation of the main regulatory protein kinase and its splice factors in K562 cells could provide further insights into therapies with apoptotic activity against leukaemic cells.
4. Additional studies could address the action of the negative control inhibitor (SRPIN349) on SRPK1 in K562 cells.
5. Finally, the generation of stable SRSF1 knockdowns using shRNA technology and lentiviral plasmids could bring about new options in the development of effective drugs for leukaemia.

CHAPTER 4. TARGETING THE SPLICE FACTOR KINASE CLK1 IN A CHRONIC MYELOID LEUKAEMIA CELL LINE

4.1 Introduction

SRSF1 is phosphorylated by SRPK1 and causes nuclear import of SRSF1 into nuclear speckles. Additional phosphorylation, mediated by Cdc2-like kinase 1 (Clk1), induces SRSF1 release from nuclear speckles to regulate pre-mRNA splicing. The discovery of SRPK1 and Clk1 as critical mediators in SRSF1 phosphorylation allowed us to speculate that suppression of these kinases could generate effects on alternative splicing in some malignancies. Clk1 is a dual specificity protein kinase that phosphorylates serine/threonine and tyrosine residues, therefore, Clk1 has an important role in disturbing phosphorylated SRSF1 at splice sites (Ghosh and Adams, 2011).

Increased evidence links Clk1 overexpression to kidney cancer (Dominguez *et al*., 2016). Other studies have suggested that blocking endogenous Clk1 activity by the selective Clk1 inhibitor (TG003) or shRNA knockdown, suppresses the proliferation of HeLa cells (Dominguez *et al*., 2016).

As both SRPK1 and Clk1 phosphorylate SRSF1, we strategised that splicing could be altered following suppression of Clk1 in K562 cells. This approach could prove useful as a therapeutic option for leukaemic patients.

4.2 Hypothesis

The inhibition of Clk1 pharmacologically or through siRNA could affect *CASPASE-9, RON* and *RUNX1* alternative splicing in K562 cells.

4.3 Objectives

- To assess proliferation of K562 cells treated with small molecule inhibitors of Clk1 (Chapter 2: Materials and methods (Table 2.5)), prior to epidermal growth factor (EGF) addition.
- To detect the effects of inhibiting Clk1 on *CASPASE-9, RON* and *RUNX1* alternative splicing in K562 cells followed by EGF or dimethyl sulfoxide (DMSO) treatment (Chapter 2: Materials and methods, section 2.7.1).
- To investigate the effects of inhibiting Clk1 on cell survival and cell death (apoptosis and necrosis) in K562 cells by acridine orange staining followed by EGF treatment.
- To assess the cellular responses to the Clk1 inhibitor (TG003) using an Annexin V/PI assay followed by EGF treatment.
- To introduce small interfering RNAs (siRNA) into K562 cells, targeting Clk1 and to confirm knockdown of Clk1 expression.
- To detect the effects of Clk1 siRNA mediated knockdown on *CASPASE-9, RON* and *RUNX1* alternative splicing in K562 cells.

4.4 Results

4.4.1. Clk1 expression in K562 cells

Clk1 mRNA and protein expression was assessed in K562 cells using RT-PCR and Western blotting.

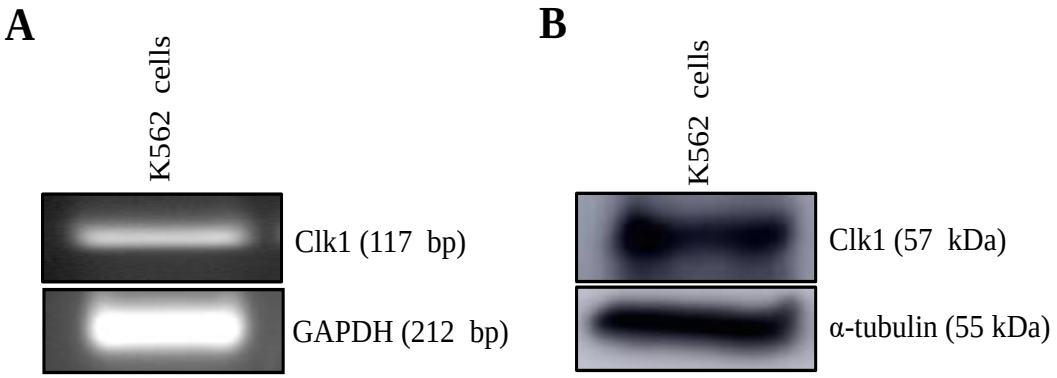

Figure 4.1A shows Clk1 mRNA from K562 cells, whereas Figure 4.1B shows Clk1 protein expression in K562 cells.

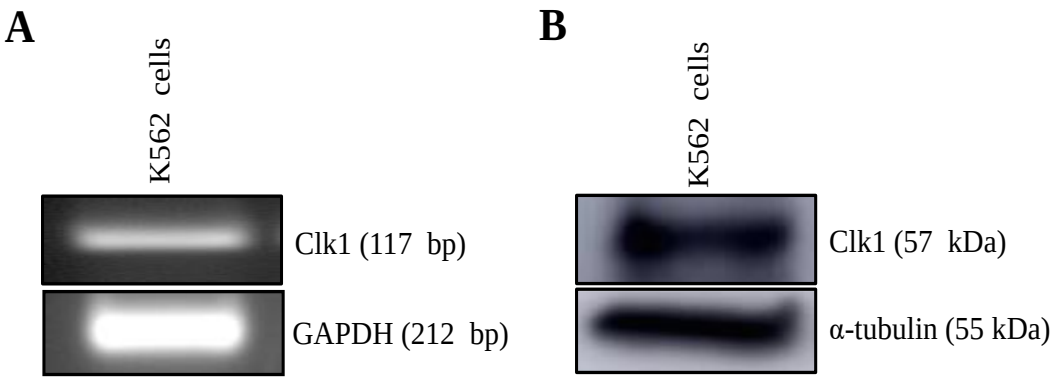

Figure 4.1. Clk1 expression in K562 cells
A. RT-PCR of Clk1 mRNA expression (117 bp) and GAPDH (212 bp). **B.** Western blot showing the expression of Clk1 and α-tubulin. Clk1 is expressed at 57 kDa and α-tubulin at 55 kDa.

4.4.2. The effects of small molecule inhibitors on Clk1 in K562 cells

4.4.2.1. The proliferation of K562 cells following Clk1 inhibition

To investigate the effects of Clk1 inhibition on K562 proliferation, 1×10^6 cells were subjected to TG003 treatment at concentrations of 50, 100 and 150 μM. Equal concentration of EGF (100 ng/mL) was added to all wells. After 24 hours, cells were stained with trypan blue and counted using a haemocytometer. The number of cells was compared with the original 1×10^6 cells and results represented as mean ± SEM ($n = 3$).

In those cells treated with EGF alone (100 ng/mL), cell proliferation was 1.54×10^6. K562 cells were treated with 50 μM TG003 was 1.09×10^6 ($p = 1.00$) when compared to the 1×10^6 cells originally plated (one-way ANOVA), Figure 4.2. Cells treated with 100 μM TG003 yielded 7.35×10^5 ($p = 0.973$), whereas cell proliferation was 5.05×10^5 ($p = 0.728$) in cells treated with 150 μM TG003, when compared to the 1×10^6 cells originally plated (one-way ANOVA). Therefore, it was decided to use 150 μM TG003 concentration to analyse alternative splicing effects in K562 cells.

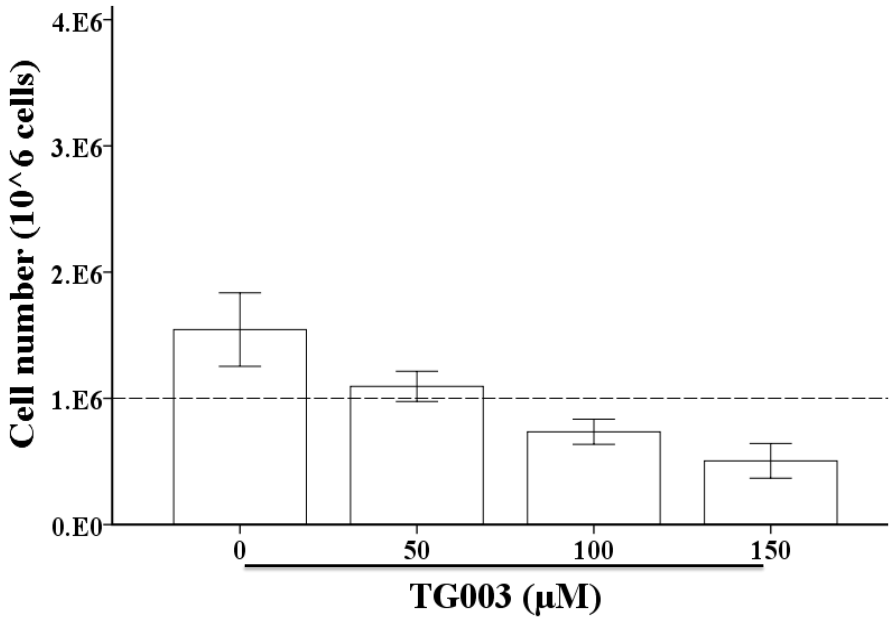

Figure 4.2. K562 cell numbers after TG003 treatment (24 hours)
Quantitative analysis of K562 cells treated with 100 ng/mL EGF (0 μM) only and a range of TG003 concentrations (50 to 150 μM) followed by 100 ng/mL EGF. Cells were counted after 24 hours and compared to a 1×10^6 cell control. The bars indicate

standard error (one-way ANOVA). The data represent three independent experiments (n = 3).

4.4.2.2. *CASPASE-9* splicing in K562 cells following Clk1 inhibition

The effects of Clk1 inhibition on *CASPASE-9* alternative splicing was examined in K562 cells and compared to cells treated with 0.02% DMSO only (DMSO control) or 100 ng/mL EGF (EGF control). The expression ratio of caspase-9a/9b was quantified by densitometric analysis using ImageJ software.

A shift in splicing towards caspase-9a was observed in cells treated with 150 μM TG003 or the negative control inhibitor TG009, when compared to DMSO control, Figure 4.3B. The expression ratio of caspase-9a/9b in DMSO control was 0.63 while cells treated with 150 μM TG003 was 1.21 (p = 0.00). Additionally, the expression ratio of caspase-9a/9b in cells treated with 150 μM TG009 was 1.25 (p = 0.00) when compared to DMSO control (one-way ANOVA), Figure 4.3C. The significant effect in the expression ratio of caspase-9a/b in cells treated 150 μM TG003 is not specific due to the effect is not significant when it's compared to the negatice control inhibitor TG009 (p = 0.98, one-way ANOVA).

Additionally, *CASPASE-9* alternative splicing was analysed in K562 cells treated with different concentrations of TG003 (50, 100 and 150 μM) followed by EGF treatment (100 ng/mL). Treatment of cells with TG003 was compared to cells treated with 100 ng/mL EGF only (control). Figure 4.4B shows the expressions of caspase-9 were reduced in cells treated with higher concentration of TG003 (100 and 150 μM TG003). Figure 4.4C shows the expression ratio of caspase-9a/9b in EGF control

was 1.40 while in cells treated with 50 μM TG003, it was 2.03 (p = 0.13, one-way ANOVA). Interestingly, cells treated with 100 μM TG003 significantly increased the expression ratio of caspase-9a/9b to 2.44 (p = 0.01) when compared to the EGF control (one-way ANOVA). The expression ratio of caspase-9a/9b was 1.90 (p = 0.29) in cells treated with 150 μM TG003 (one-way ANOVA). Caspase-9a and caspase-9b cDNA amplicons were analysed in Chapter 3 (Section 3.4.2.2.1).

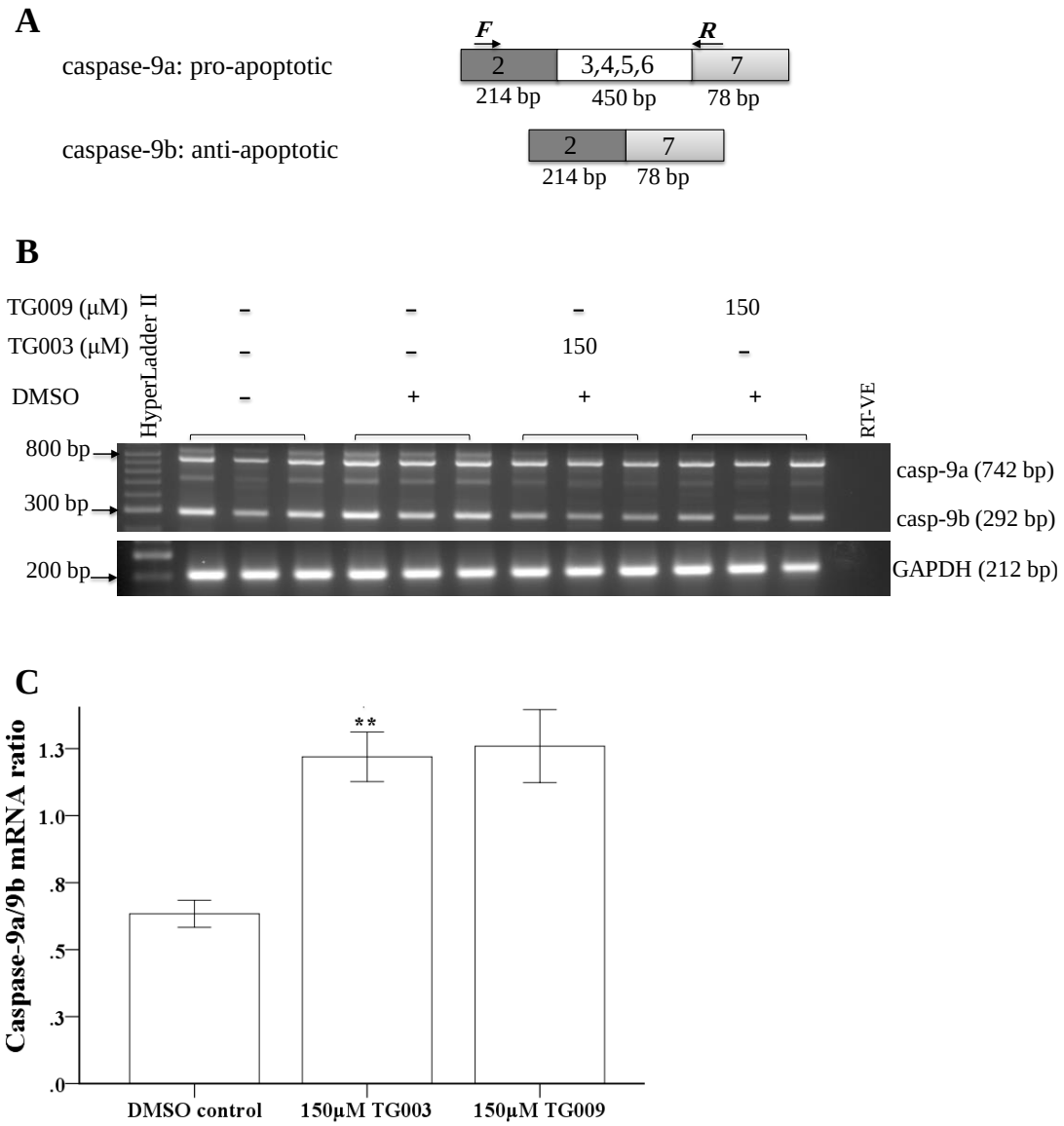

Figure 4.3. Clk1 inhibition on *CASPASE-9* alternative splicing
A. *CASPASE-9* showing the two splice variants resulting from inclusion or exclusion of exons 3–6 (caspase-9a and caspase-9b, respectively). Arrows indicate the positions of *forward* and *reverse* caspase-9 primers. **B.** K562 cells were treated with 0.02% DMSO (DMSO control) and 150 μM TG003/9 followed by 0.02% DMSO. After 24 hours incubation, RT-PCR was performed and bands at 742 bp (casp-9a) and 292 bp (casp-9b) were detected. Intermediate bands at ~ 500 bp represent skipped exons. GAPDH was used as a loading control (212 bp). Each rung of the hyperLadder II represents 100 bp. **C.** Densitometric analysis of caspase-9a/9b isoforms representing the intensity ratio of caspase-9 against caspase-9b. K562 cells treated with TG003 or TG009 were compared with DMSO control. The ratio of caspase-9a/9b significantly increased for 150 μM TG003 and TG009 treatments when compared to DMSO control. However, this significant effect is not specific when cells treated with 150 μM TG003 compared to cells treated with negative control inhibitor (150 μM TG009). The bars indicate standard error, ** $P \leq 0.01$ (one-way ANOVA). The data represent three independent experiments ($n = 3$).

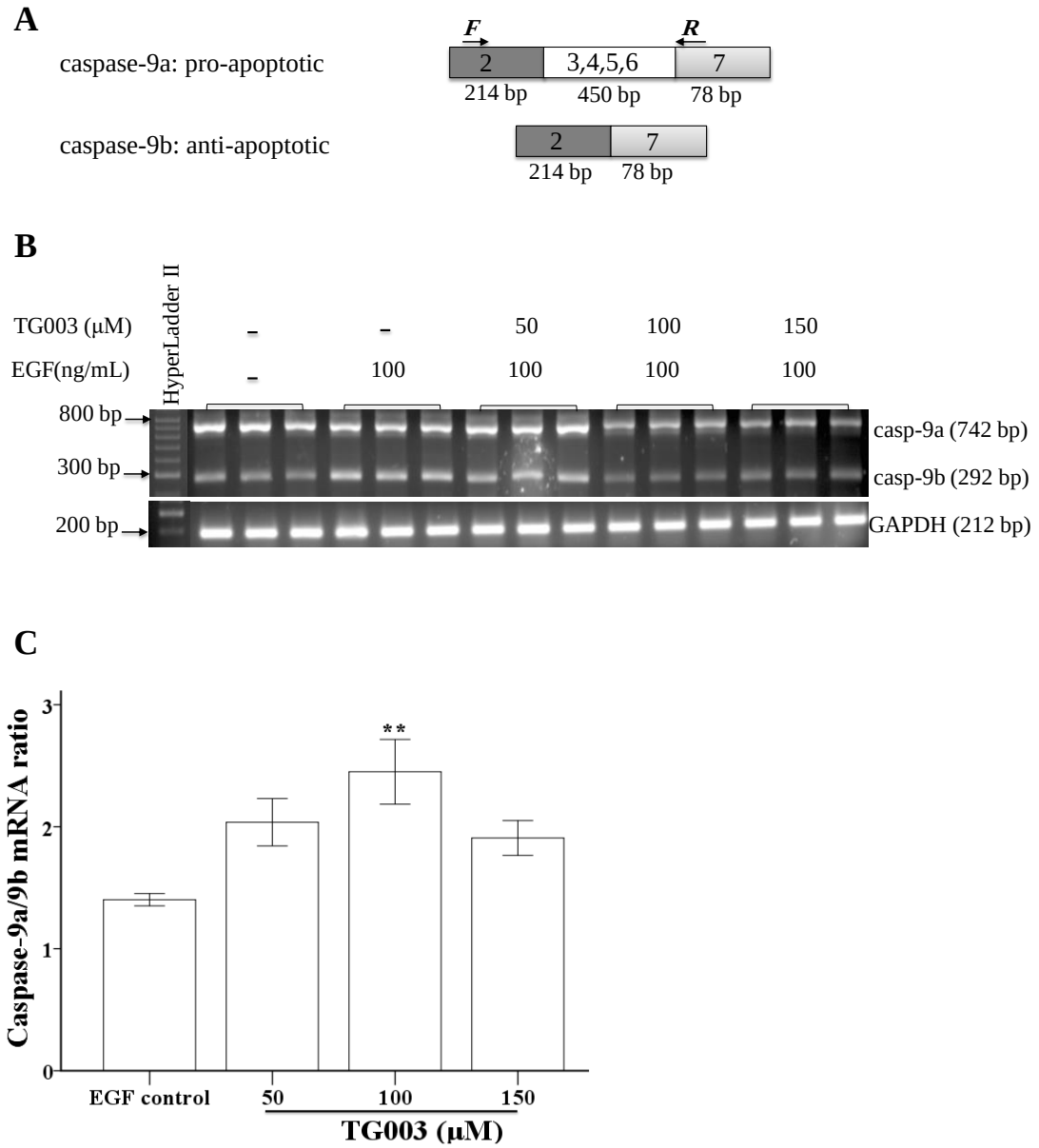

Figure 4.4. Clk1 inhibition on *CASPASE-9* alternative splicing
A. *CASPASE-9* showing the two splice variants resulting from inclusion or exclusion of exons 3–6 (caspase-9a and caspase-9b, respectively). Arrows indicate the positions of *forward* and *reverse* caspase-9 primers. **B.** K562 cells were treated with only 100 ng/mL EGF (0 μM TG003) and three concentrations of TG003 were used at 50, 100 and 150 μM followed by 100 ng/mL EGF. RT-PCR was performed after 24 hours incubation and bands 742 bp (casp-9a) and 292 bp (casp-9b) were detected and GAPDH was used as a loading control. Each rung of the hyperLadder II represents 100 bp. **C.** Densitometric analysis of caspase-9a/9b isoforms. K562 cells treated with TG003 were compared with the EGF control. The graph represents the intensity ratio of caspase-9a against caspase-9b, where the ratio of caspase-9a/9b was significantly increased in the 100 μM TG003 treatment. The bars indicate standard error, ** $P \leq 0.01$ (one-way ANOVA). The data represent three independent experiments ($n = 3$).

4.4.2.3. *RON* splicing in K562 cells following Clk1 inhibition

TG003 effects on *RON* splice isoforms was observed by RT-PCR and the quantification of Ron/ΔRon expression ratios using ImageJ software. There was a switch in *RON* expression towards the Ron splice isoform in cells treated with 150 μM TG003 when compared to EGF control, Figure 4.5B.

Both Ron and ΔRon isoforms were reduced in cells treated with 150 μM TG003 or TG009, Figure 4.5B. The expression ratio of Ron/ΔRon was 1.05 in cells treated with only 0.02% DMSO alone (DMSO control), Figure 4.5C. There was a significant increased in cells treated with 150 μM TG003; 2.58 (p = 0.00) when compared to DMSO control, Figure 4.5C. However, this significant effect is not specific when compared to cells treated with the negative control inhibitor (TG009) (p = 0.07, one-way ANOVA). A significant increase of 1.97 (p = 0.00) was also observed in cells treated with 150 μM TG009, Figure 4.5C.

Ron splice variants were reduced in cells treated with higher concentration of TG003 (150 μM) when compared to EGF control, Figure 4.6B. The expression ratio of Ron/ΔRon was 0.74 in cells treated with only 100 ng/mL EGF (EGF control) while in cells treated with 50 μM TG003 was 1.54 (p = 0.17, one-way ANOVA), Figure 4.6C. The expression ratio of Ron/ΔRon in cells treated with 100 μM TG003 was 1.11 (p = 0.77, one-way ANOVA), Figure 4.6C. However, these results were not statistically significant. There was a significantly increase in the expression ratio of Ron/ΔRon to 1.96 (p = 0.02) after treatment with 150 μM TG003 when compared to

EGF control (one-way ANOVA), Figure 4.6C. Sequences of Ron and ΔRon cDNA amplicons were analysed in Chapter 3 (Section 3.4.2.3.1).

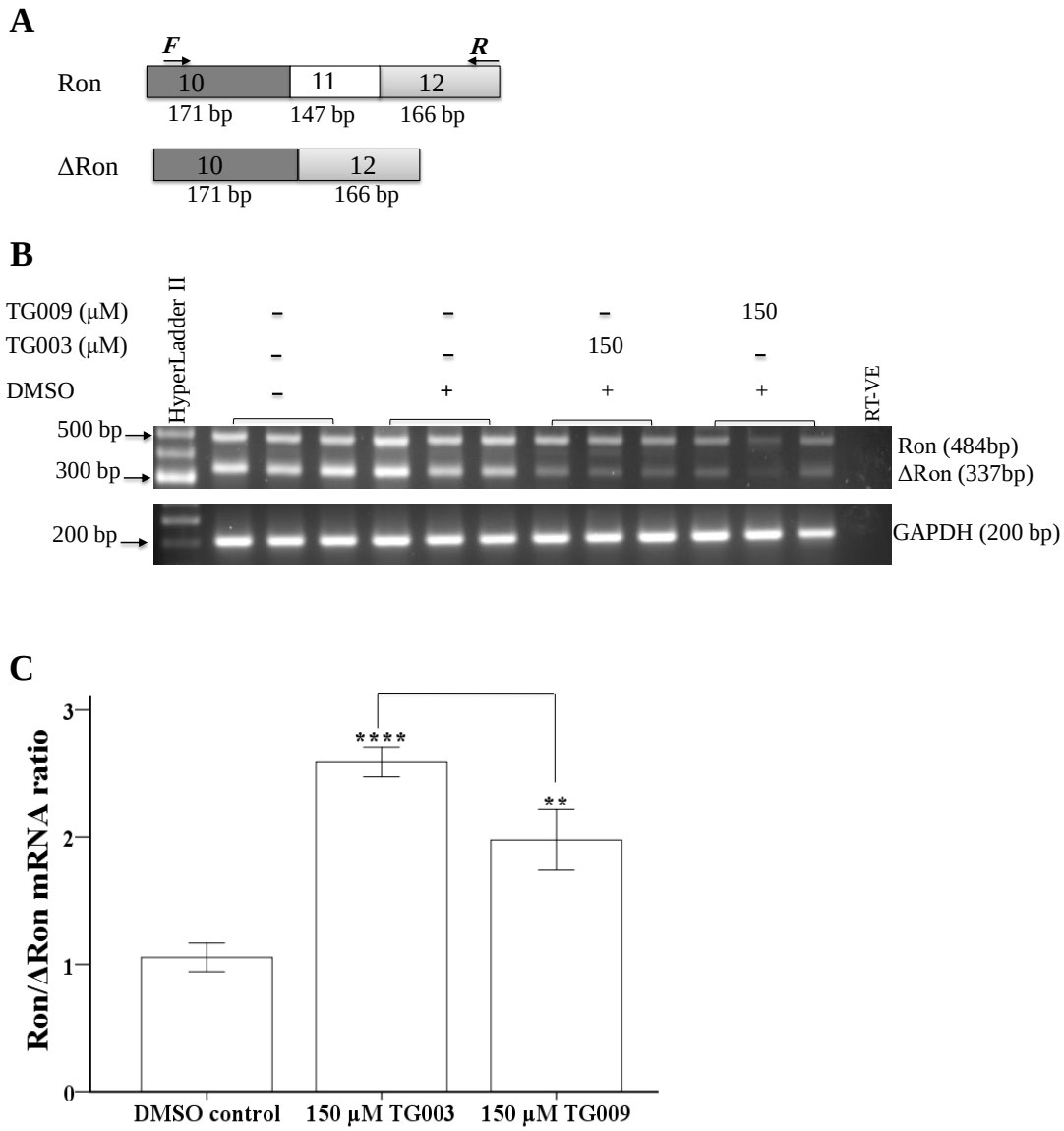

Figure 4.5. Clk1 inhibition on *RON* alternative splicing
A. The *RON* gene showing the two splice variants resulting from the inclusion or exclusion of exon 11 (Ron and ΔRon variants, respectively). Arrows indicate the positions of *forward* and *reverse* Ron primers. **B.** K562 cells were treated with 0.02% DMSO (DMSO control) and 150 μM TG003/9 followed by (0.02%) DMSO for 24 hours. RT-PCR was performed and bands at 484 bp (Ron) and 337 bp (ΔRon) were detected. GAPDH was used as a loading control (212 bp). Each rung of the hyperLadder II represents 100 bp. **C.** Densitometric analysis of Ron/ΔRon isoforms. K562 cells treated with TG003 or TG009 were compared to DMSO control. The ratio of Ron/ΔRon significantly increased in 150 μM TG003 and 150 μM TG009 treatments. However, the significant increased in the expression ratio of Ron/ΔRon in cells treated with 150 μM is not specific when compared to 150 μM TG009. The bars indicate standard error, ** $P \leq 0.01$, **** $P \leq 0.0001$ (one-way ANOVA). The data represent three independent experiments ($n = 3$).

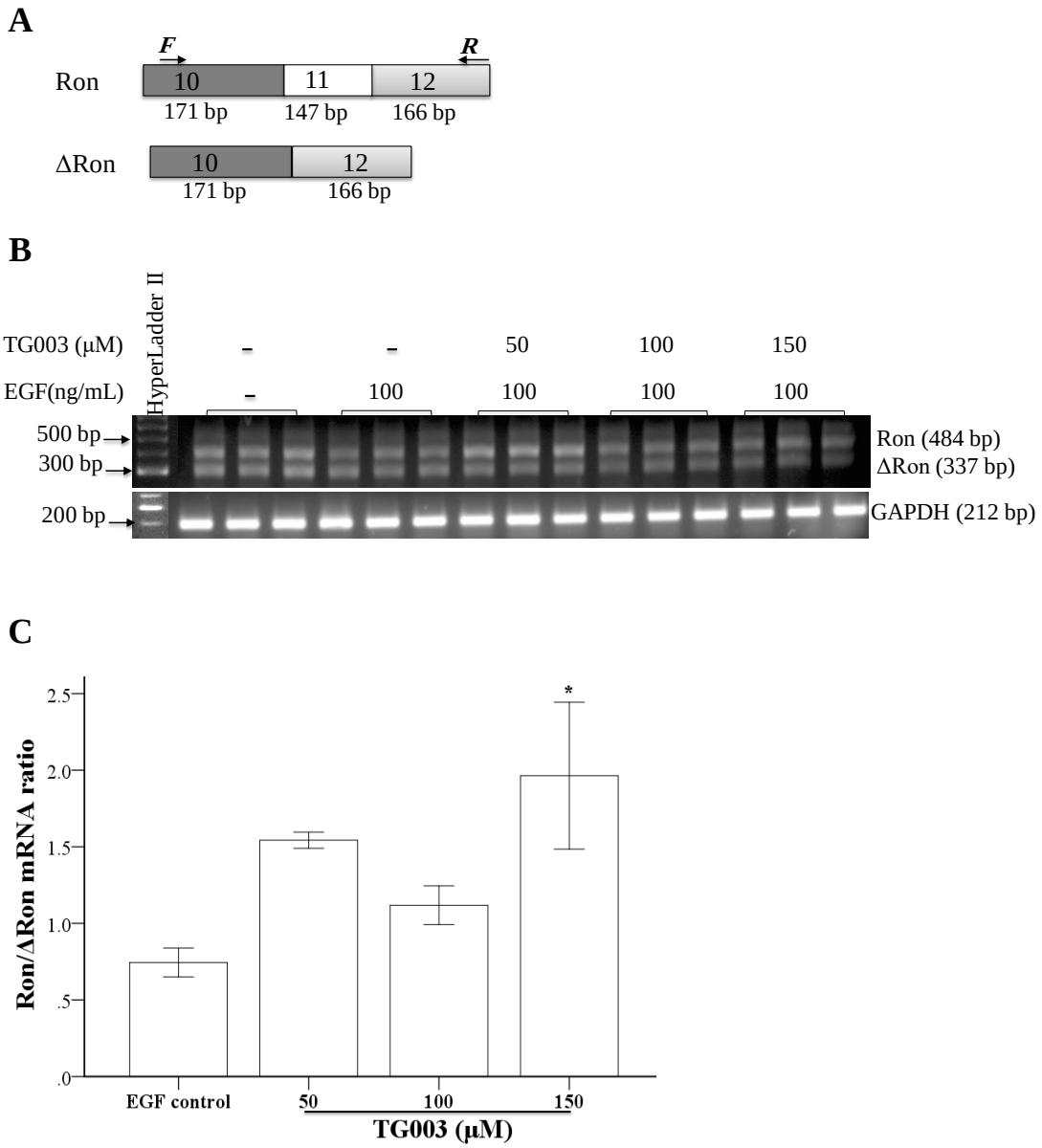

Figure 4.6. Clk1 inhibition on *RON* alternative splicing
A. The *RON* gene showing the two splice variants resulting from including or excluding exon 11 (Ron and ΔRon variants, respectively). Arrows indicate the positions of *forward* and *reverse* Ron primers. **B.** K562 cells were treated with only 100 ng/mL EGF (0 μM TG003) and different concentrations of TG003 were used at 50, 100 and 150 μM followed by 100 ng/mL EGF. After 24 hours incubation, RT-PCR was performed and bands at 484 bp (Ron) and 337 bp (ΔRon) were detected. GAPDH was used as a loading control (212 bp). Each rung of the hyperLadder II represents 100 bp. **C.** Densitometric analysis of Ron/ΔRon isoforms. K562 cells treated with TG003 were compared with EGF control. The ratio of Ron/ΔRon significantly increased in cells treated with 150 μM TG003. The bars indicate standard error, * $P \leq 0.05$ (one-way ANOVA). The data represent three independent experiments ($n = 3$).

4.4.2.4. *RUNX1* splicing in K562 cells following Clk1 inhibition

To assess whether Clk1 inhibition affected *RUNX1* alternative splicing, K562 cells were treated with TG003 and the expression ratio of Runx1/ΔRunx1 were compared to cells treated with only 0.02% DMSO (DMSO control) or 100 ng/mL EGF (EGF control). There was a shift in splicing towards Runx1 in cells treated with 150 μM TG003 and 150 μM TG009, when compared to DMSO control, Figure 4.7B. The expression ratio of Runx1/ΔRunx1 was 1.08 in cells treated with only 0.02% DMSO (DMSO control) (one-way ANOVA), Figure 4.7C. The expression ratio of Runx1/ΔRunx1 in cells treated with 150 μM TG003 was 2.95 (p = 0.17, one-way ANOVA), Figure 4.7C. In addition, the expression ratio of Runx1/ΔRunx1 was significantly increased to 3.71 (p = 0.04) after treatment with 150 μM TG009, when compared to DMSO control, Figure 4.7C..

The Runx1 splice isoform was up-regulated in cells treated with a range of TG003 concentrations (50 to 150 μM) when compared to EGF control, Figure 4.8B. The expression ratio of Runx1/ΔRunx1 was 1.10 in cells treated with only 100 ng/mL EGF (EGF control), Figure 4.8C. The expression ratio of Runx1/ΔRunx1 in cells treated with 50 and 150 μM TG003 were (1.30, p = 0.96) and (1.99, p = 0.10), one-way ANOVA. There was a significant increase in the expression ratio of Runx1/ΔRunx1 to 4.27 (p = 0.00) after treatment with 100 μM TG003 when compared to EGF control (one- way ANOVA), Figure 4.8C. Sequences of Runx1 and ΔRunx1 cDNA amplicons were analysed in Chapter 3 (Section 3.4.2.4.1).

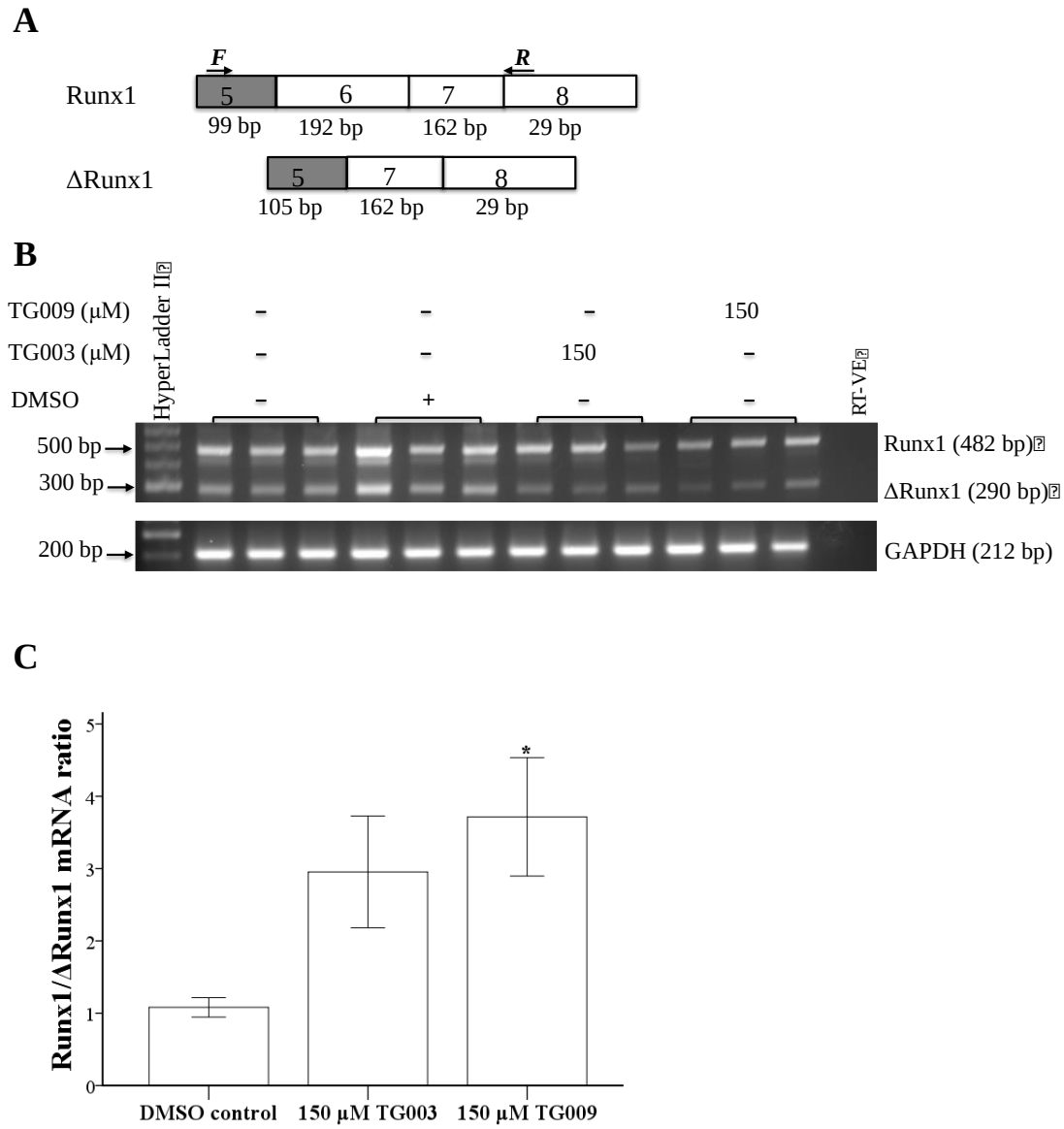

Figure 4.7. Clk1 inhibition on *RUNX1* alternative splicing
A. *RUNX1* showing the two splice variants resulting from including or excluding exon 6 (Runx1 and ΔRunx1 variants, respectively). Arrows indicate the positions of *forward* and *reverse* Runx1 primers. **B.** K562 cells were treated with 0.02% DMSO (DMSO control) and 150 μM TG003/9 followed by (0.02%) DMSO. After 24 hours incubation, RT-PCR was performed and bands at 482 bp (Runx1) and 290 bp (ΔRunx1) were detected. Intermediate bands represent skipped exons. GAPDH was used as a loading control (212 bp). Each rung of the hyperLadder II represents 100 bp. **C.** Densitometric analysis of Runx1/ΔRunx1 isoforms. K562 cells treated with TG003 or TG009 were compared with DMSO control. The ratio of Runx1/ΔRunx1 was significantly increased in cells treated with 150 μM TG009 (negative control inhibitor). The bars indicate standard error (one-way ANOVA). The data represent three independent experiments (n = 3).

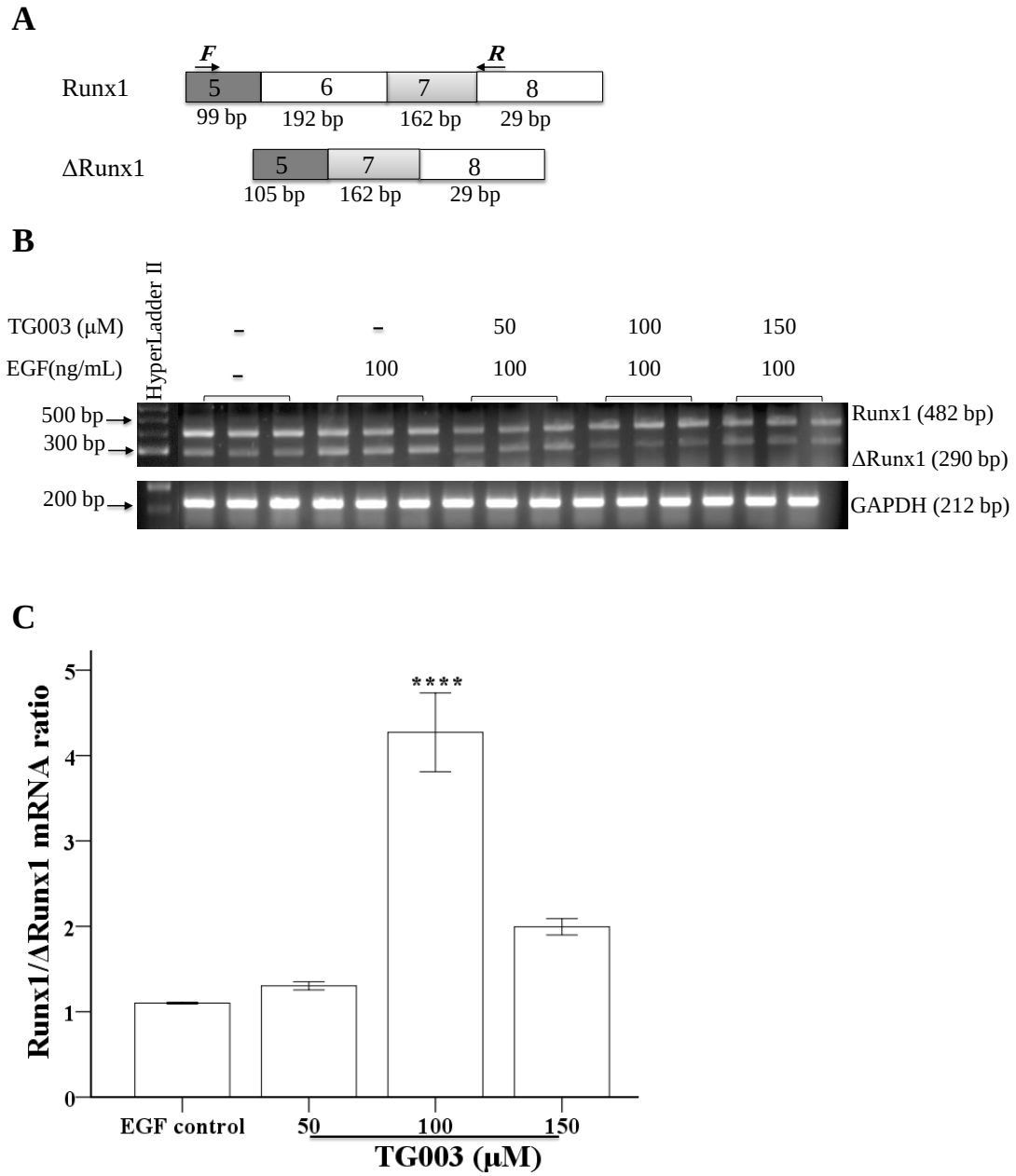

Figure 4.8. Clk1 inhibition on *RUNX1* alternative splicing.
A. *RUNX1* showing the two splice variants resulting from including or excluding exon 6 (Runx1 and ΔRunx1 variants, respectively). Arrows indicate the positions of *forward* and *reverse* Runx1 primers. **B.** K562 cells were treated with only 100 ng/mL EGF (0 μM TG003) and different concentrations of TG003 were used at 50, 100 and 150 μM followed by 100 ng/mL EGF. After 24 hours incubation RT-PCR was performed and bands at 482 bp (Runx1) and 290 bp (ΔRunx1) were detected. GAPDH was used as a loading control (212 bp). Each rung of the hyperLadder II represents 100 bp. **C.** Densitometric analysis of Runx1/ΔRunx1 isoforms. K562 cells treated with TG003 were compared with EGF control (0 μM TG003). The ratio of Runx1/ΔRunx1 was increased in cells treated with 100 μM TG003. The bars indicate standard error, **** $P \leq 0.0001$ (one-way ANOVA). The data represents three independent experiments ($n = 3$).

4.4.2.5. Evaluation of apoptosis and necrosis in K562 cells following treatment with Clk1 inhibitors

4.4.2.5.1 Detection of apoptosis using acridine orange

K562 cells were stained with acridine orange (AO) to observe the presence of apoptosis after Clk1 kinase inhibition. Cell morphological characteristics were assessed to distinguish between cell survival and cell death (apoptosis or necrosis).

K562 cells were treated with TG003 concentations of 0, 50, 100 and 150 μM, Figure 4.9. The cell morphological features of K562 cells after treatment were compared to EGF control cell. Viable cells (VC) were present in K562 cells alone, Figure 4.9A. Apoptotic cells (Apo) were present in the EGF control, Figure 4.9B. Necrotic cells (NC) were present in cells treated with 50 and 100 μM TG003 when compared to EGF control, Figure 4.9C and D. At 150 μM TG003, little apoptosis was observed, Figure 4.9E.

Total cell numbers after treatments were not quantified, however, at 1000 cells were quantified per treatment. The percentage of viable, apoptotic and necrotic cells was calculated and compared to EGF control, Figure 4.10. Apoptosis in cells treated with 50 and 100 TG003 were 11.3% (p = 0.70) and 8.3% (p = 0.65), respectively, when compared to EGF control (one-way ANOVA). There was a siginicant increase in apoptosis of 44% in cin those cells treated with 150 μM TG003 (p = 0.00), Figure 4.10. Moreover, in those cells treated with 50 and 150 μM TG003, necrosis was 8.3% (p = 0.9) and 13.5% (p = 0.07), respectively. However, in cells treated with 100 μM TG003, necrosis was significantly increased to 22.1% (p = 0.02) when compared to EGF control.

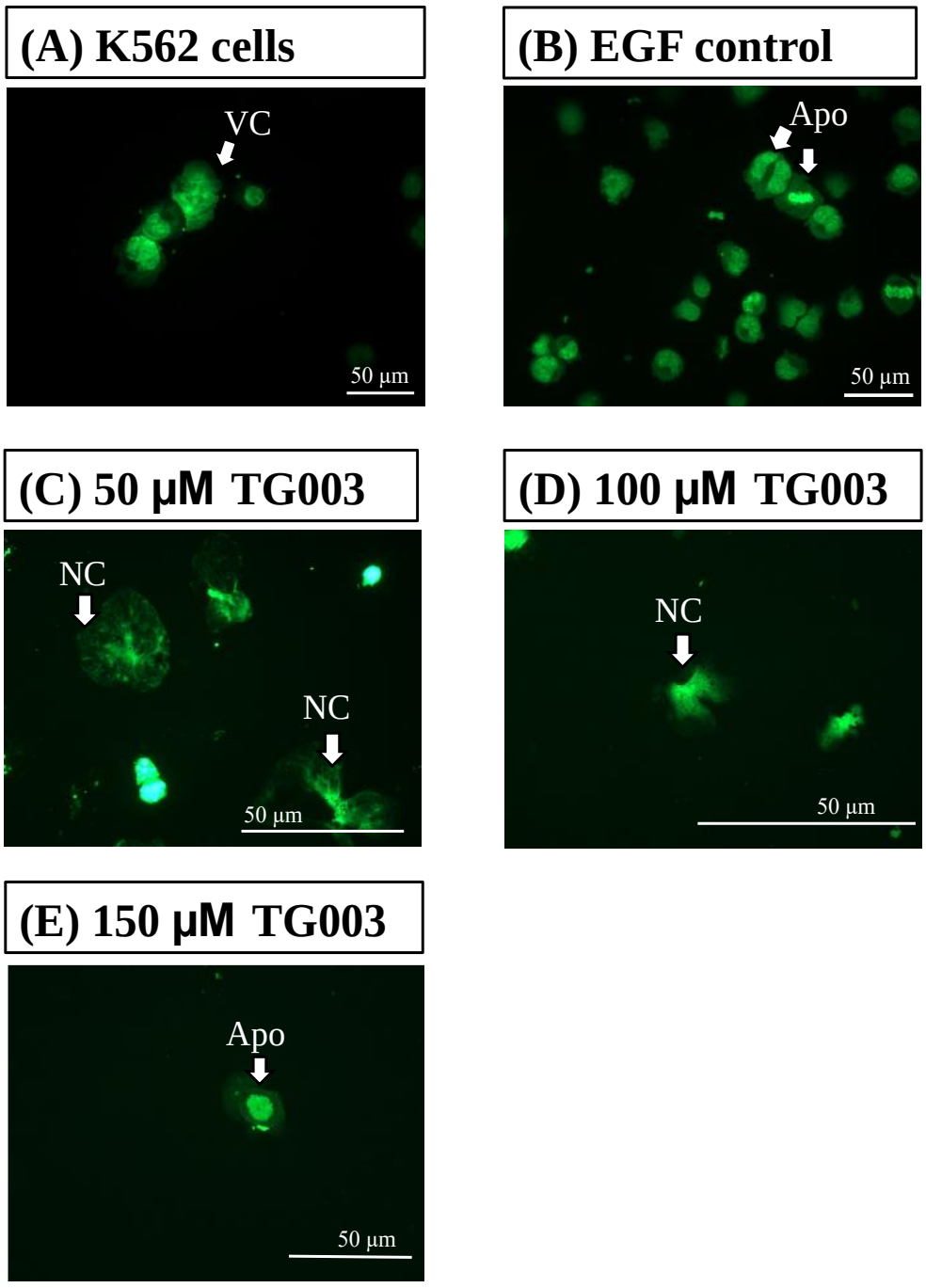

Figure 4.9. Cell death (apoptotic and necrotic) using acridine orange
A. Viable cells (VC) were present in untreated K562 cells. **B.** Apoptosis increased in EGF control cells; arrowheads indicate cells with condensed clear chromatin, bi-lobed and fragmented nuclei. **C**–**D.** Treatment with 50 and 100 µM TG003 induced necrosis; arrowheads show swelling and rupture of the plasma membrane of necrotic cells releasing cytoplasmic contents into the extracellular space. **E.** Apoptotic cells (Apo) with fragmented nuclei and chromatin start to appear at 150 µM TG003. Approximately 1000 cells were quantified per treatment.

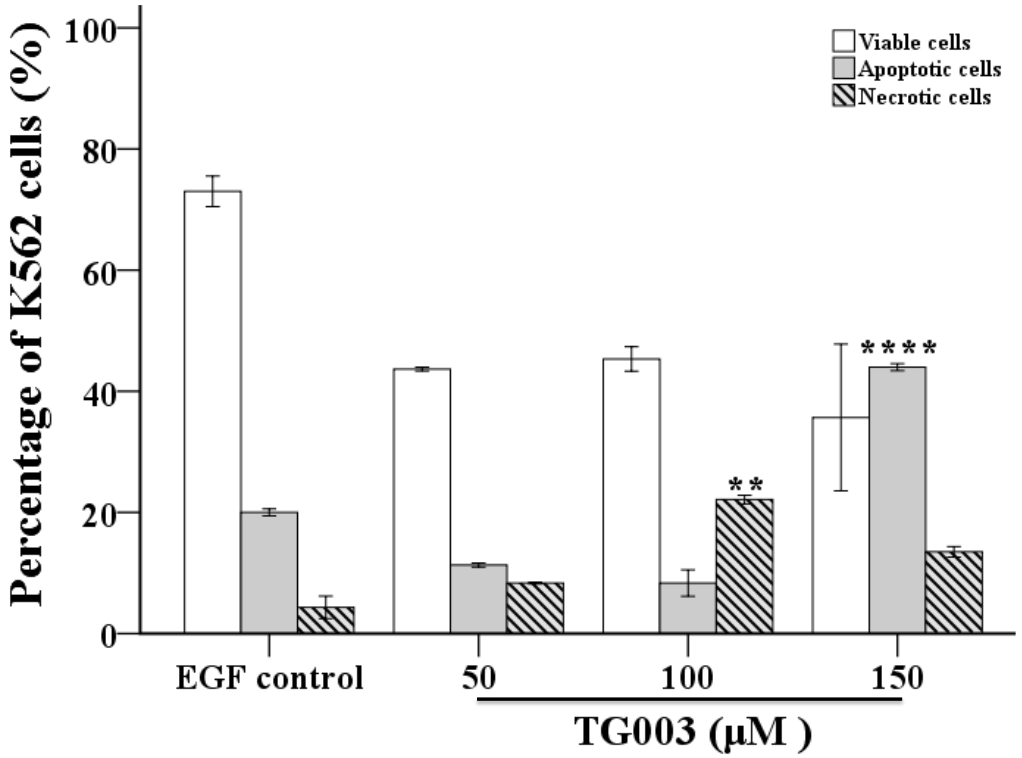

Figure 4.10. Apoptosis and necrosis percentages in inhibitor treated K562 cells
K562 cells were stained with acridine orange following treatment with increasing concentrations of TG003 (50, 100, and 150 μM). At least 1,000 cells were assessed. The graph represents the percentages of viable cells (white bars), apoptotic cells (grey bars) and necrotic cells (dashed bars). Apoptosis was significantly increased in cells treated with 150 μM TG003, necrosis was significantly increased in cells treated with 100 μM TG003 treatment. The bars indicate standard error, ** $P \leq 0.01$, **** $P \leq 0.0001$ (one-way ANOVA). The data represent three independent experiments ($n = 3$).

4.4.2.5.2 Annexin V-FITC apoptosis detection

Apoptosis was identified by flow cytometry and Annexin V-FITC/PI binding. Viable, early apoptotic and late apoptotic (or necrotic) cells were distinguished by flow cytometry. Apoptotic cells were Annexin V-FITC positive and PI negative (Annexin V-FITC$^+$ and PI$^-$), while necrotic cells were Annexin V-FITC positive and PI positive (Annexin V-FITC$^+$ and PI$^+$), Figure 4.11. Apoptosis was observed in EGF control (0.91%) as was necrosis (3.4%), Figure 4.11A. Apoptosis in K562 cells treated with 50 μM TG003 was 0.29%, whereas necrosis was 8.1%, Figure 4.11B. Apoptosis was 0.56% while necrosis was 22.6% in K562 cells treated with 100 μM

TG003, Figure 4.11C. The treatment of cells with 150 µM TG003 resulted 2.3% in apoptosis and 17.2% in necrosis, Figure 4.11D.

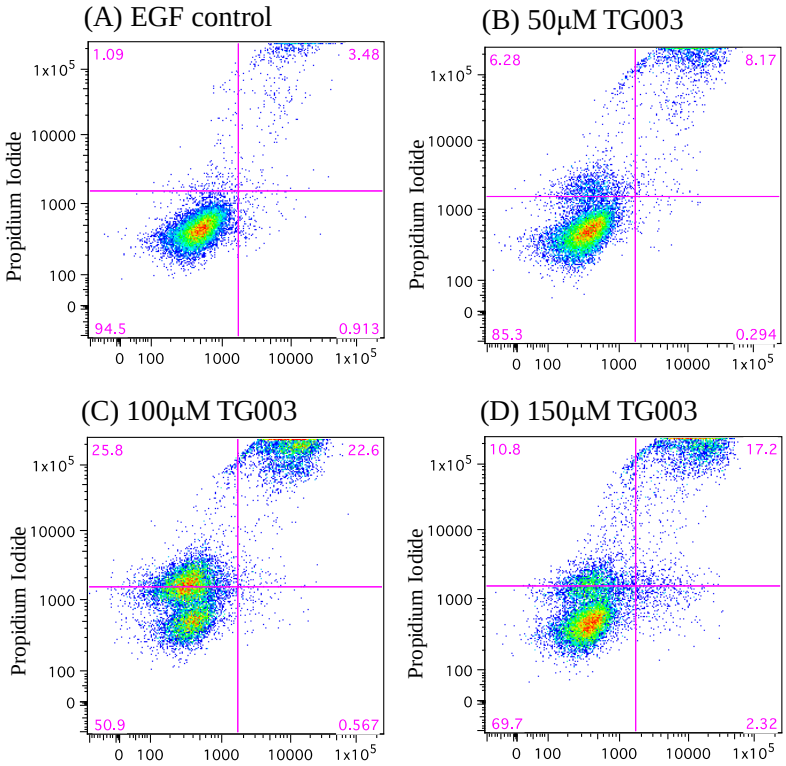

Figure 4.11. Apoptosis and necrosis detection by Flow Cytometry and Annexin V-FITC/PI

Scatterplots of cell death (apoptosis; Annexin V-FITC and necrosis; Annexin V-FITC with propidium iodide) in K562 cells after Clk1 inhibition. **A.** Control K562 cells treated with 100 ng/mL EGF only (EGF control). **B**–**D.** Cells treated with 50, 100 and 150 µM TG003. Apoptosis (Annexin V-FITC$^+$ and PI$^-$) was more than twice as high in cells treated with 150 µM TG003 when compared to EGF controls (values ranged from 0.9 to 2.3%). Necrosis (Annexin V-FITC$^+$ and PI$^+$) was increased in cells treated with 100 µM TG003 when compared to EGF control (values ranged from 3.4 to 22.6%). A representative of three experiments is shown.

4.4.3. siRNA Clk1 knockdown in K562 cells

To investigate the effects of Clk1 kinase activity on *CASPASE-9*, *RON* or *RUNX1* alternative splicing, K562 cells were transfected with Clk1 siRNA to knockdown Clk1 endogenous expression. Cells were transfected with a control (si-CTRL, 75nM) and three different si-Clk1s (si-Clk1-1, si-Clk1-2 and si-Clk1-3, 75 nM) for 72 hours. Following transfection, Clk1 protein expression was determined by Western blot and normalised to α-tubulin (75 μg whole cell lysates), Figure 4.12A-B. The Clk1 knockdown using si-Clk1-1, si-Clk1-2 and si-Clk1-3 produced different Clk1 expression profiles, Figure 4.12A. A decrease in Clk1 expression was observed in cells transfected with si-Clk1-1 and si-Clk1-2 when compared to the si-CTRL cells, however si-Clk1-3 increased Clk1 expression.

The same trend in Clk1 expression was observed after normalisation to α-tubulin. The expression ratio of normalised Clk1 following si-Clk1-1 was 0.91 (p = 0.99) when compared to si-CTRL cells (0.95, one-way ANOVA), Figure 4.12B. There was a significant decrease in the expression ratio of Clk1 in si-Clk1-2 cells to 0.18 (p = 0.01, one-way ANOVA). However, Clk1 expression in si-Clk1-3 was 1.21 (p = 0.59, one-way ANOVA). These results indicate that si-Clk1-2 was the most effective siRNA in knocking down Clk1.

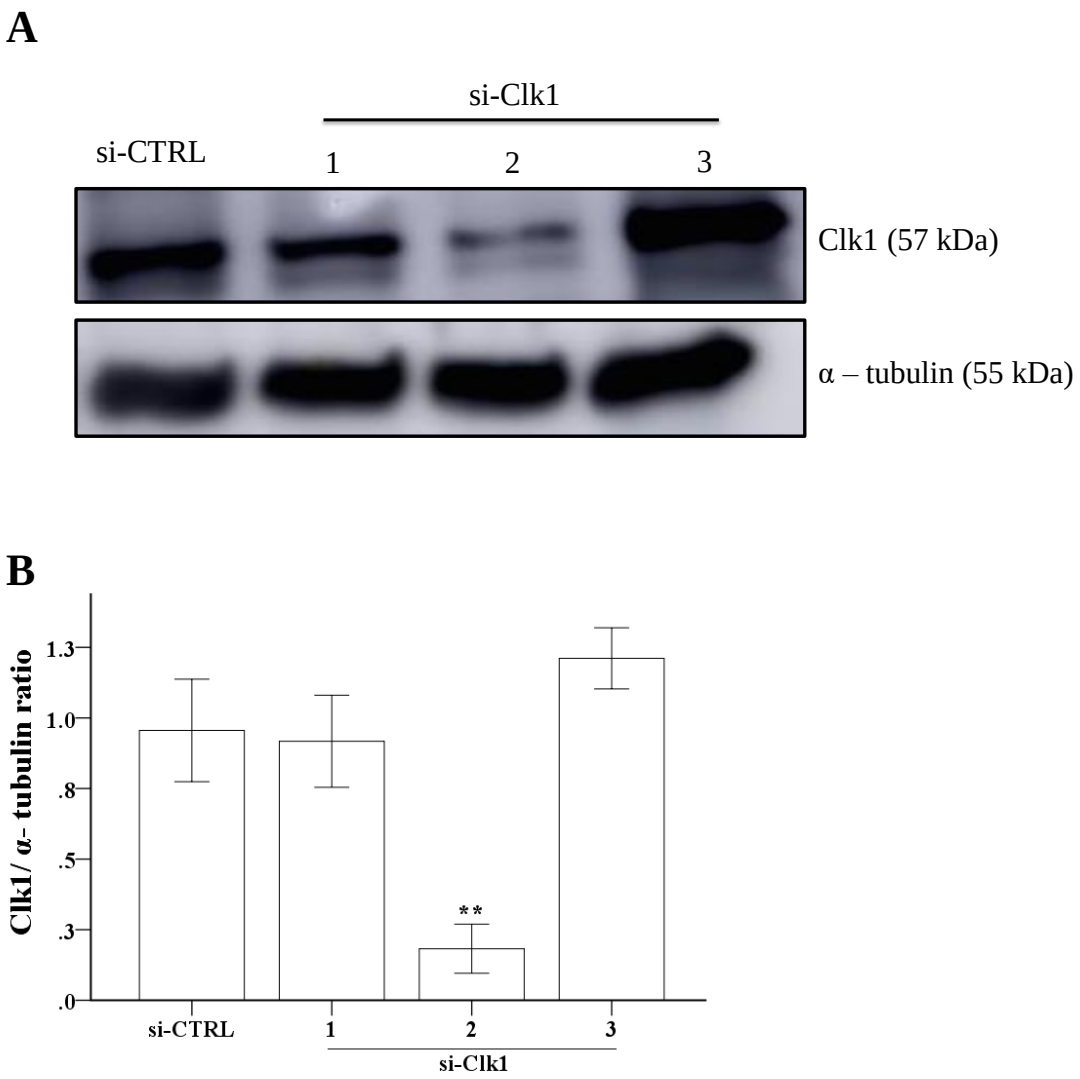

Figure 4.12. siRNA knockdown of Clk1 in K562 cells
K562 cells were transfected with three siRNAs against Clk1 or scrambled control siRNA (si-CTRL). **A.** Cell lysates were extracted at 72 hours post-transfection and immunoblotted against anti-Clk1 and anti-tubulin antibodies, detecting Clk1 at 57 kDa and α-tubulin at 55 kDa. **B.** The normalisation of Clk1 against α-tubulin (three replicates). Transfection of K562 cells with si-Clk1-2 significantly decreased endogenous Clk1 protein levels. The bars indicate standard error (one-way ANOVA). The data represents three independent experiments (n = 3).

4.4.3.1. siRNA Clk1 knockdown effects on alternative splicing in K562 cells

4.4.3.1.1 *CASPASE-9* splicing in K562 cells following Clk1 knockdown

There were no differences in *CASPASE-9* alternative splicing between si-Clk1-2 and si-CTRL cells, Figure 4.13B. The expression ratio of caspase-9a/9b in si-Clk1-2 treated cells to 2.18 (p = 0.88) compared to si-CTRL cells (2.30, one-way ANOVA), Figure 4.13C.

4.4.3.1.1 *RON* splicing in K562 cells following Clk1 knockdown

There was no shift in *RON* splicing in cells transfected with si-Clk1-2, Figure 4.14B. The expression ratio of Ron/ΔRon in si-CTRL cells was 0.81 while in si-Clk1–2 cells was 0.77 (p = 0.64, one-way ANOVA), Figure 4.14C.

4.4.3.1.1 *RUNX1* splicing in K562 cells following Clk1 knockdown

There was a shift in *RUNX1* splicing towards the Runx1 isoform in si-Clk1-2 cells compared to si-CTRL cells, Figure 4.15B. The expression ratio of Runx1/ΔRunx1 isoforms was 1.39 in si-CTRL cells. There was significantly increased in the expression ratio of Runx1/ΔRunx1 in si-Clk1-2 cells (1.61, p = 0.02), one-way ANOVA, Figure 4.15C.

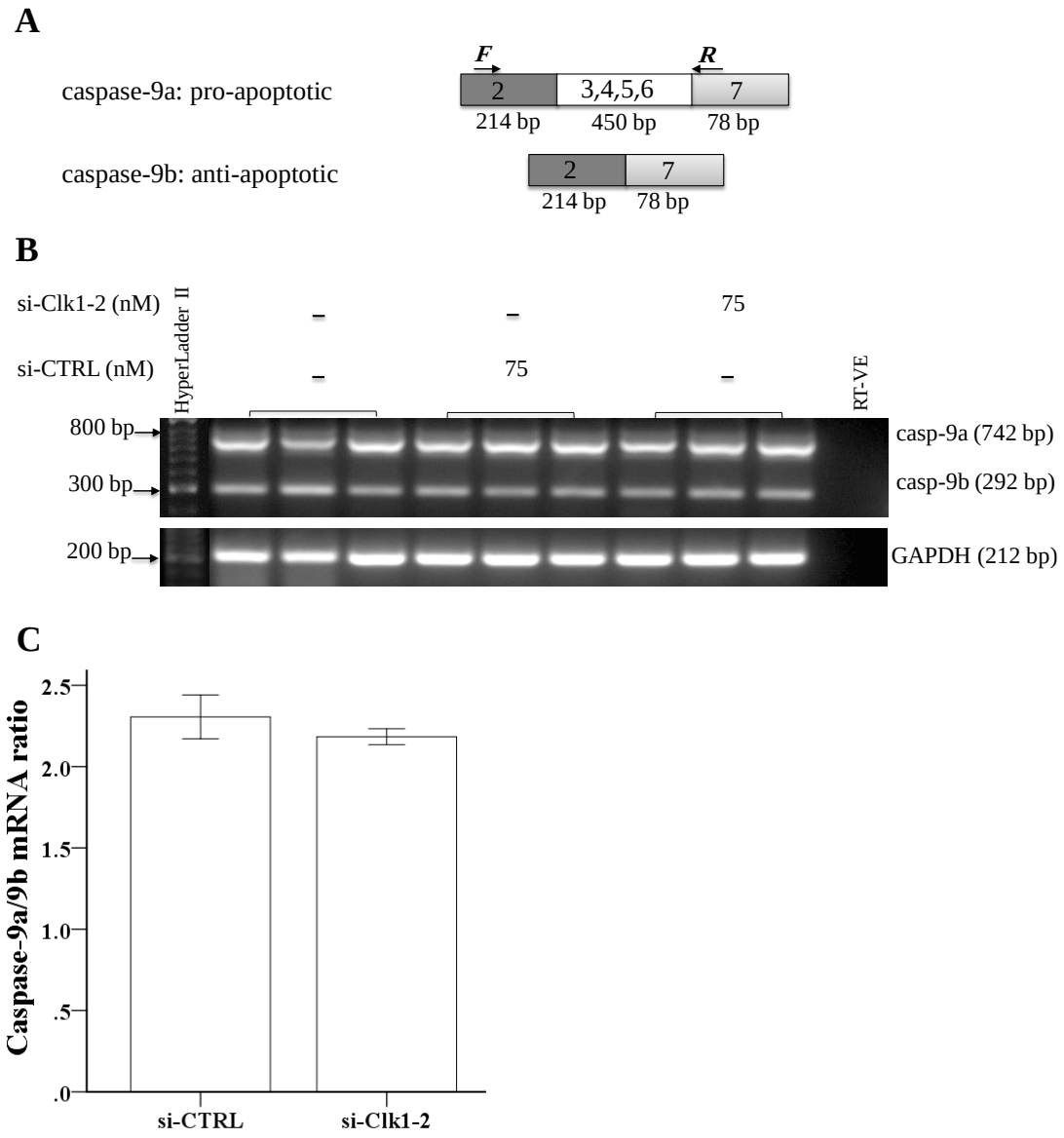

Figure 4.13. siRNA Clk1 knockdown on *CASPASE-9* alternative splicing
A. *CASPASE-9* showing the two splice variants resulting from inclusion or exclusion of exons 3–6 (caspase-9a and caspase-9b, respectively). Arrows indicate the positions of *forward* and *reverse CASPASE-9* primers. **B.** K562 cells were transfected with si-CTRL (75 nM) or si-Clk1-2 (75 nM) for 72 hours before caspase-9a and caspase-9b RT-PCR. PCR bands at 742 bp (casp-9a) and 292 bp (casp-9b) were identified. GAPDH was used as a loading control (212 bp). Each rung of the hyperladder II represents 100 bp. **C.** Densitometric analysis of caspase-9a/9b isoforms. K562 cells transfected with si-Clk1-2 (75 nM) were compared with si-CTRL (75 nM). The graph represents the intensity ratio of caspase-9a against caspase-9b. The bars indicate standard error (one-way ANOVA). The data represents three independent experiments (n = 3).

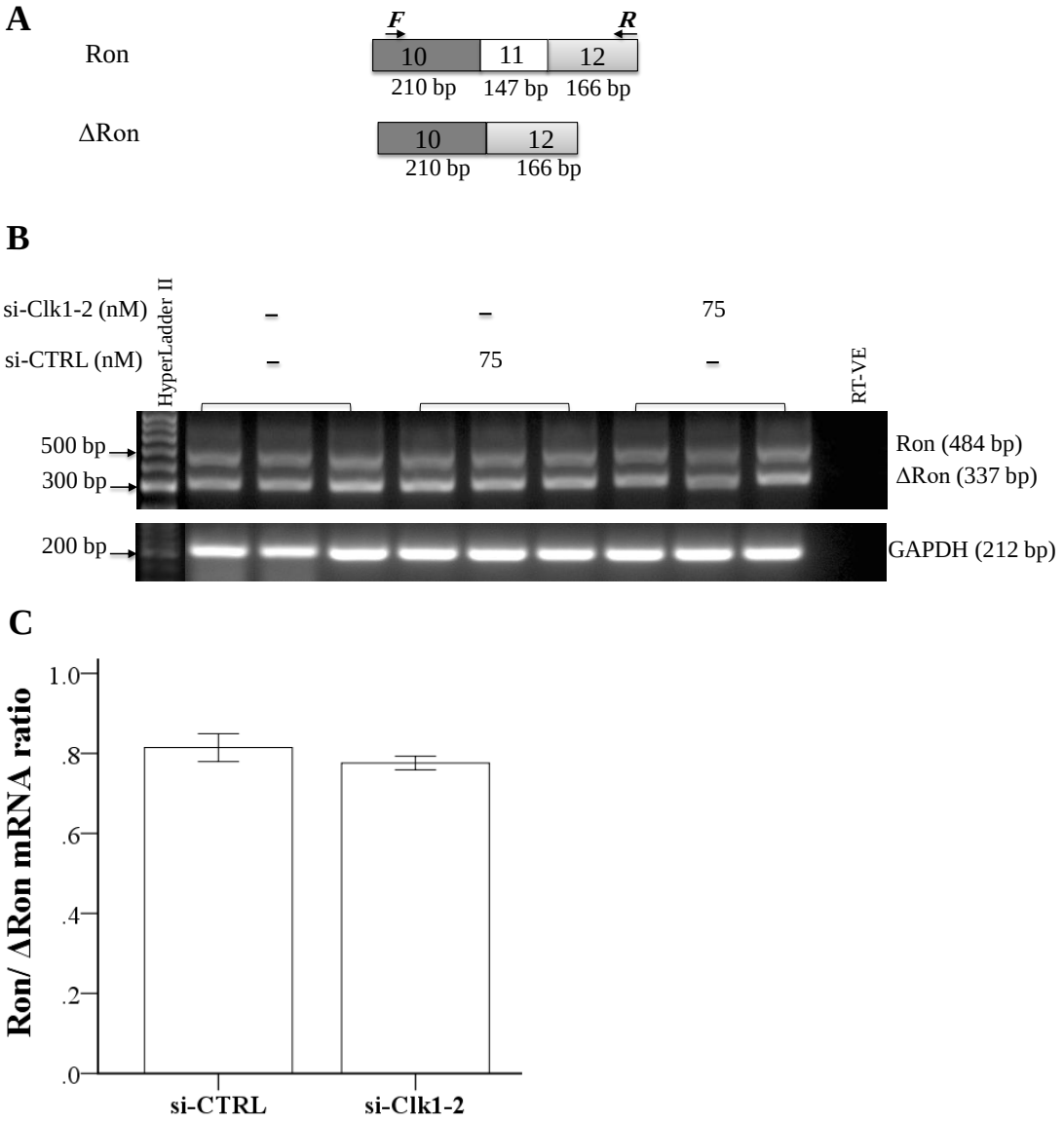

Figure 4.14. siRNA Clk1 knockdown on *RON* alternative splicing
A. The *RON* gene showing the two splice variants resulting from including or excluding exon 11 (Ron and ΔRon variants, respectively). Arrows indicate the positions of forward and reverse Ron primers. **B.** K562 cells were transfected with si-CTRL (75 nM) or si-Clk1-2 (75 nM) for 72 hours before Ron and ΔRon RT-PCR. PCR bands at 484 bp (Ron) and 337 bp (ΔRon) were identified. GAPDH was used as a loading control (212 bp). Each rung of the hyperladder II represents 100 bp. **C.** Densitometric analysis of Ron/ΔRon isoforms. K562 cells transfected with si-Clk1-2 (75 nM) were compared with si-CTRL cells (75 nM). The graph represents the intensity ratio of Ron against ΔRon. The bars indicate standard error, one-way ANOVA. The data represent three independent experiments (n = 3).

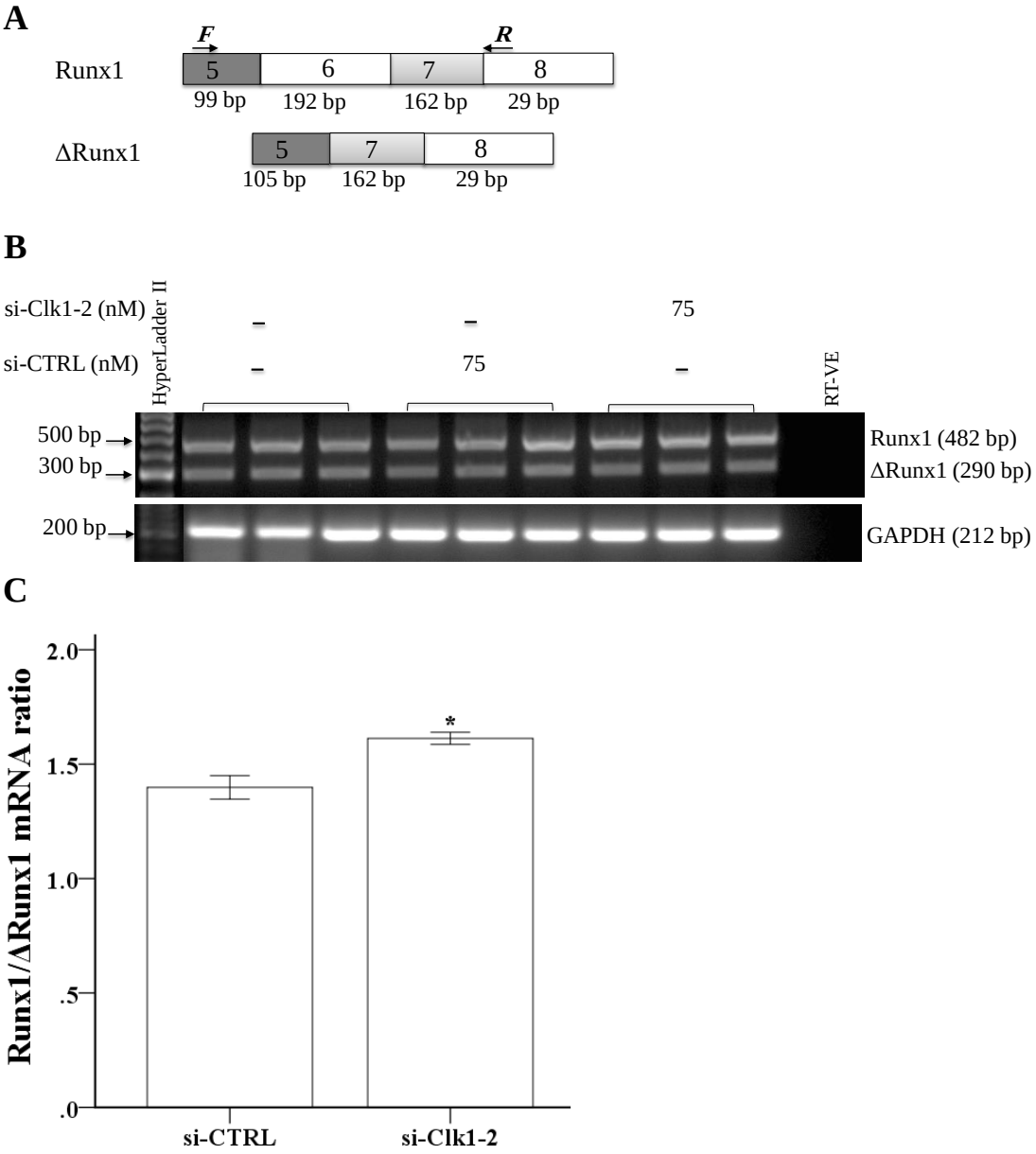

Figure 4.15. siRNA Clk1 knockdown on RUNX1 alternative splicing
A. *RUNX1* showing the two splice variants resulting from including or excluding exon 6 (Runx1 and ΔRunx1 variants, respectively). Arrows indicate the positions of *forward* and *reverse* Runx1 primers. **B.** K562 cells were transfected with si-CTRL (75 nM) or si-Clk1-2 (75 nM) for 72 hours before Runx1 and ΔRunx1 RT-PCR was performed. PCR bands at 482 bp (Runx1) and 290 bp (ΔRunx1) were identified. GAPDH was used as a loading control (212 bp). Each rung of the hyperladder II represents 100 bp. **C.** Densitometric analysis of Runx1/ΔRunx1 isoforms. K562 cells transfected with si-SRSF1 (75nM) were compared with si-CTRL (75 nM). The graph represents the intensity ratio of the Runx1 against ΔRunx1. The ratio of Runx1/ΔRunx1 increased in transfected K562 cells with si-Clk1-2 compared to si-CTRL cells (75 nM). Transfection of K562 cells with si-Clk-2 significantly increased the expression ratio of Runx1/ΔRunx1. The bars indicate standard error, * $P \leq 0.05$ (one-way ANOVA). The data represent three independent experiments (n = 3).

4.5 Discussion

Several protein kinases regulate the phosphorylation of SRSF1, notably SRPK1 and Clk1 (Gosh and Adam, 2011; Liu *et al.*, 2013). Clk1 plays an important role in serine, threonine and tyrosine phosphorylation, thus enhancing or repressing splicing activities (Jain *et al.*, 2014). SRSF1 can effect splice site utilisation, thereby controlling the alternative splicing of many genes, including *CASPASE-9* and *Bcl-x* (Gosh and Adam, 2011).

In previous work, inhibiting Clk1 using KH-CB19 affected pre-mRNA splicing in Alzheimer's disease (Jain *et al.*, 2014). Another investigation suggested that KH-CB20 and KH-CB19 were selective Clk1 inhibitors. Those inhibitors were effective in splicing two tissue factor isoforms, flTF (full-length TF) and asHTF (alternative spliced human TF). In addition, Clk1 inhibition by TG003 resulted in a reduction in phosphorylation of SRp20 in human microvascular endothelial cells (HMEC-1) (Fedorov *et al.*, 2011).

Since Clk1 activation by SRPK1 phosphorylates SRSF1, Clk1 plays an important role in regulating alternative splicing. A recent study found that HeLa, H157 and A549 cell proliferation was dramatically reduced after TG003 or KHCB-19 inhibition or depletion (shRNA) of Clk1 (Dominguez *et al.*, 2016). This Clk1 inhibition or knockdown resulted in the increased expression of CHEK2 exon 9 inclusion leading to defects in mitosis and cell death promotion. It has been observed that inhibiting Clk1 using "compound 21b" blocks EGFR, HDAC1 and p70S6 kinase in cancer cells (ElHady *et al.*, 2017). Another study has designed α-benzylidene-γ-butyrolactone inhibitor targeting several kinases, such as, dual-

specificity tyrosine-regulated kinase 1A (Dyrk1A), Clk1 and CK2. Similarly, it has been also proposed that co-inhibition lipid kinases PI3Kα/γ limit the proliferation of U87MG cells (Mariano, Hartmann and Engel, 2016). Therefore, Clk1 appears to control alternative splicing in malignancies (Dominguez *et al.*, 2016).

The role of Clk1 in some malignancies has been well established, however the literature is lacking on any possible roles in CML. This chapter hypothesises that the Clk1 signalling pathway is important for *CASPASE-9, RON* and *RUNX1* splicing in CML cell models (K562 cells).

In this study, K562 cell proliferation was reduced after treatment with increased concentrations of TG003, in agreement with Dominguez *et al.* (2016) and suggests that TG003 could block K562 cell proliferation. To investigate the effects of protein kinase inhibitors on alternative splicing, the splicing variants of *CASPASE-9*, *RON* and *RUNX1* in K562 cells subjected to Clk1 inhibition was investigated. Due to the significant effect on the expression of the caspase-9a and Ron splice isoforms followed by negative kinase control (TG009), the effect of TG003 treatment is not considered as a specific effect.

Additionally, TG003 treatment followed by EGF, significantly increased expression of the pro-apoptotic (caspase-9a), Ron and Runx1 splice isoforms. Furthermore, cells developed multi-nucleation following incubation with high concentrations of TG003. The increased appearance of multi-nucleation suggests a defect in chromosome segregation or cytokinesis, leading to cell death. These data are in agreement with TG003 evaluation and its impact on K562 apoptosis. Apoptosis increased with

increased concentrations of TG003. Taken together, these data demonstrate that TG003 increased apoptosis in K562 cells and decreased the survival rate of these cells. These data showing also show that blocking endogenous Clk1 activity using TG003, switched splicing from ΔRon to Ron and ΔRunx1 to Runx1 isoforms in K562 cells.

The down-regulation of Clk1 using TG003 or siRNA knockdown was found to decrease mRNA and protein levels of Fas exon 6 exclusion in ovarian cancer cells (Liu *et al.*, 2013). It was also observed that significant reduction in Clk1 protein levels after the transfection of ovarian cancer cells with any of three Clk1 siRNAs (Liu *et al.*, 2013). However, unlike Liu *et al.* (2013), in our study, only si-Clk1-2 significantly reduced Clk1 protein levels in K562 cells, suggesting Clk1 siRNAs exhibit greater efficiency in targeting Clk1 in ovarian cancer than leukaemic cells. Therefore, protein kinase (Clk1) from various types of cancer respond differently.

In this study, no obvious switch in *CASPASE-9* and *RON* splicing was observed after Clk1 knockdown in K562 cells. Intriguingly, Clk1 knockdown significantly shifts *RUNX1* splicing towards Runx1 isoforms in K562 cells. Taken together, TG003 significantly increased caspase-9a, Ron and Runx1 mRNA isoforms in K562 cells. In contrast, K562 cells following Clk1si-RNA knockdown, revealed a switch in splicing in *RUNX1* towards Runx1 isoforms only, suggesting Clk1 could be the main protein kinase regulator of *RUNX1* in K562 cells. No obvious shift in *CASPASE-9* and *RON* splicing in Clk1 si-RNA knockdowns would suggest the activation of other protein kinases for these targets.

4.5.1. Conclusion and future directions

The small molecule inhibitor TG003 reduced K562 cell proliferation. Further analyses are required to assess the effects of TG003 on K562 cell proliferation compared to normal, non-cancerous cells. Treatment of K562 cells with TG003, switched splicing towards the caspase-9a, Ron and Runx1 isoforms. However, Clk1-siRNA depletion caused shifts only in *RUNX1* splicing towards the Runx1 splice isoform in K562 cells. Further experiments are required to identify the main protein kinase regulator for *CASPASE-9* and *RON* and confim the main protein kinase for *RUNX1* in K562 cells.

More comprehensive analyses should address the effects of the negative control inhibitor (TG009) on Clk1 in K562 cells. A thorough understanding of the Clk1 protein kinase in both normal physiological and leukaemic conditions is required as TG009 could prove to be a potential therapeutic target in the treatment of CML.

CHAPTER 5. TARGETING TYROSINE KINASE ALONE OR IN COMBINATION WITH OTHER PROTEIN KINASE INHIBITORS IN CHRONIC MYELOID LEUKAEMIA CELL LINE

5.1 Introduction

The activation of tyrosine kinases are regulated by receptors (RTKs) or non-receptor (nRTKs) tyrosine kinases. *RON* or *recepteur d'origine Nantais* is an RTK while the oncoprotein fusion Bcr-Abl belongs to nRTK family (Batth, Yun and Kumar, 2015b; Naka *et al.*, 2016). Generally, activation of tyrosine kinases promote proliferation, angiogenesis and inhibits apoptosis through the phosphorylation of intracellular signalling pathways (Chapter 1) (Naka *et al.*, 2016). Constitutive activation of tyrosine kinase initiates tumourgenesis, such as that seen in breast, gastric and leukaemia (CML). Therefore, it is crucial to treat different solid and haematological tumours through tyrosine kinase inhibition (TKIs) (Roberts and Der, 2007).

5.2 Hypothesis

To assess the co-treatment of K562 cells with imatinib and SPHINX or TG003 as more effective on *CASPASE-9*, *RON*, and *RUNX1* alternative splicing, than either agent alone.

5.3 Objectives

- To assess proliferation of K562 cells treated with TKI (imatinib) alone or in combination with other protein kinase inhibitors (Table 5.2), prior to epidermal growth factor (EGF) addition.
- To assess the effects of inhibiting TK alone or in combination with other inhibitors on *CASPASE-9, RON* and *RUNX1* alternative splicing in K562 cells.

5.4 Results

5.4.1. The effect of TKI alone or in combination with other protein kinase inhibitors on K562 cells

5.4.1.1. The proliferation of K562 cells following TKI treatment or in combination with other protein kinase inhibitors

To investigate the proliferation of K562 cells following TK inhibition alone or in combination with other protein kinase inhibitors, 1×10^6 cells were used. Cells were treated with inhibitors followed by EGF treatment (100 ng/mL) for 24 hours. Then, cells were stained with trypan blue and counted using a haemocytometer. Cell number were compared to 1×10^6 original cells and the results represented as mean ± SEM (n = 3). Significant reductions in cell numbers treated with IM alone or in combination with SPHINX or TG003 were observed, Figure 5.1.

Cells, treated with the different IM ranges 1, 1.4 and 2.9 μM, were significantly decreased to 6.03×10^5 (p = 0.00), 3.96×10^5 (p = 0.00) and 3.80×10^5 (p = 0.00),

respectively when compared to 1×10^6 cells alone (one-way ANOVA). Treating cells with the IM ranges 1, 1.4 or 2.9 μM in combination with 30 μM Sx, significantly decreased cell numbers to 1.06×10^5 ($p = 0.00$), 5.15×10^4 ($p = 0.00$), and 1.01×10^5 ($p = 0.00$) respectively, when compared to the original 1×10^6 cells (one-way ANOVA). In addition, combining IM with TG003 cause a significant reduction in cell proliferation. Cell numbers treated with 1 μM IM and 100 μM TG003 were 6.3×10^4 ($p = 0.00$) while cell numbers treated with 1.4 μM IM and 100 μM TG003 were 2.1×10^5 ($p = 0.00$), compared to 1×10^6 cells (one-way ANOVA). Similarly, cell numbers were 7.6×10^4 ($p = 0.00$) after combination treatments of IM (2.9 μM) and 100 μM TG003.

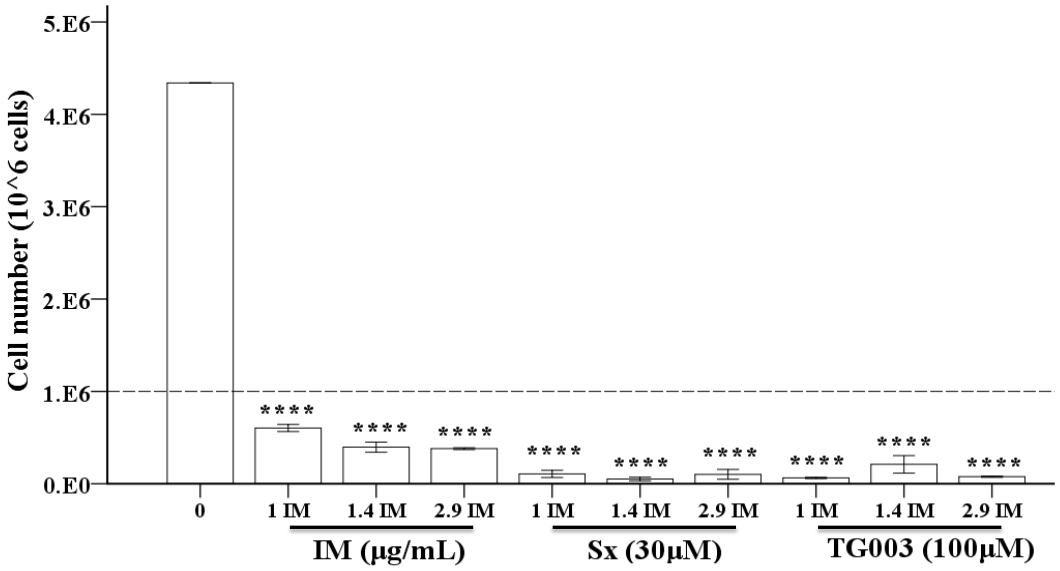

Figure 5.1. K562 cell numbers after treatment with IM alone or in combination with SPHINX or TG003
Quantitative analysis of K562 cell numbers treated with IM (1, 1.4 and 2.9 μg/mL) in combination with 30 μM SPHINX (Sx) or 100 μM TG003 for 24 hours. The y-axis indicates cell numbers versus treatment concentrations. Approximately 1×10^6 cells were used and compared with cells treated with inhibitors. Treatment with only 100 ng/mL EGF (0 μM), range with IM (1, 1.4 and 2.9 μg/mL) following EGF, combined inhibitors of IM and Sx (30 μM) or combined inhibitors of IM and TG003 (100 μM). The bars indicate standard error, **** $P \leq 0.0001$ (one-way ANOVA). The data represents three independent experiments ($n = 3$).

5.4.1.2. *CASPASE-9* splicing in K562 cells following TKI treatment alone or in combination with other protein kinase inhibitors

Inhibiting TK alone or in combination with SRPK1 or Clk1, on *CASPASE-9* alternative splicing was examined in K562 cells and compared to cells treated with 100 ng/mL EGF (EGF control) only. The expression ratio of caspase-9a/9b was quantified by densitometric analysis and ImageJ software.

A switch in the expression of caspase-9b towards the pro-apoptotic splice isoform, caspase-9a was observed in K562 cells, in combination with different TKI (imatinib) concentrations, Figure 5.2B. The expression ratio of caspase-9a/9b was 0.75 in cells treated with only EGF (100 ng/mL), Figure 5.2C. The expression ratio of caspase-9a/9b was significantly increased in cells treated with 1 μg/mL IM to 2.19 (p = 0.001) and in cells treated with 1.4 μg/mL IM to 2.40 (p = 0.00) compared to EGF control cell (one-way ANOVA), Figure 5.2C. There was a significant increase in the expression ratio of caspase-9a/9b in cells treated with 2.9 μg/mL IM to 2.28 (p = 0.00) compared to EGF control (one-way ANOVA).

Additionally, effects on *CASPASE-9* alternative splicing were analysed in K562 cells treated with IM and SPHINX and compared to EGF control. There was a switch in splicing towards the pro-apoptotic splice isoform, caspase-9a, in cells treated with 1 μg/mL IM combined with a range of SPHINX (5–20 μM) concentrations, Figure 5.3B. The expression ratio in cells treated with 100 ng/mL EGF alone was 1.29, Figure 5.3C. The expression ratio of caspase-9a/9b was significantly increased in cells treated with 1 μg/mL IM in combination with 5 and 10 μM SPHINX to 3.53 (p

= 0.01) and to 3.70 (p = 0.00) compared with the EGF control (one-way ANOVA), Figure 5.3C. Treatment of cells with 1 μg/mL IM and 20 μM Sx caused further significant increases in the expression ratio of caspase-9a/9b to 4.31 (p = 0.00) compared to the EGF control (one-way ANOVA). These results were statistically significant.

The effects on *CASPASE-9* alternative splicing was also analysed in K562 cells treated with IM and TG003 and compared to EGF control. There was a shift in splicing towards the caspase-9a isoform in cells treated with 1 μg/mL IM, combined with a range of TG003 (25–100 μM), Figure 5.4B. The expression ratio of caspase-9a/9b was 1.32 in cells treated with EGF alone (100 ng/mL), Figure 5.4C. The mRNA expression ratio of caspase-9a/9b combined with 1 μg/mL IM and 25 μM TG003 was 1.82 (P = 0.53), Figure 5.4C. The expression ratio of caspase-9a/9b in cells treated with 1μg/mL IM in combination with 50 and 100 μM TG003 reached 1.32 (p = 0.99) and 1.03 (p = 0.99), one-way ANOVA.

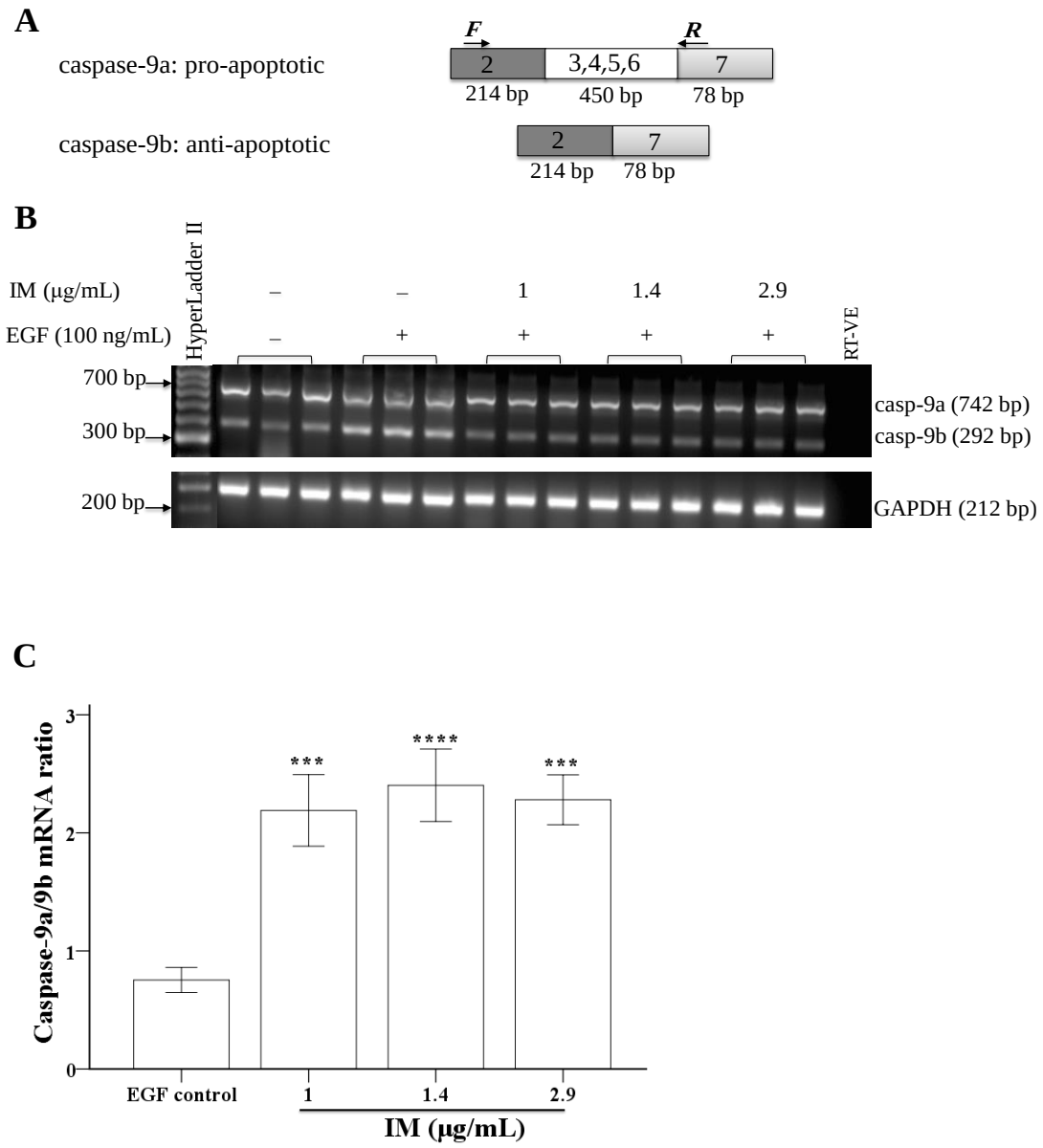

Figure 5.2. TKI effects on *CASPASE-9* alternative splicing
A. *CASPASE-9* showing the two splice variants resulting from inclusion or exclusion of exon 3–6 (caspase-9a and caspase-9b, respectively). Arrows indicate the positions of *forward* and *reverse* caspase-9 primers. **B.** K562 cells treated with only 100 ng/mL EGF (0 µg/mL IM) and three concentrations of IM were used at 1, 1.4 and 2.9 µg/mL followed by 100 ng/mL EGF. RT-PCR was performed after 24 hours incubation and bands at 742 bp (casp-9a) and 292 bp (casp-9b) were detected and GAPDH was used as a loading control (212 bp). Each rung of the hyperLadder II represents 100 bp. **C.** Densitometric analysis of caspase-9a/9b isoforms. K562 cells treated with IM were compared to the EGF control. The graph represents the intensity ratio of the caspase-9a against caspase-9b. As the concentration of IM increased, the ratio of caspase-9a/9b significantly increased compared to the EGF control. The bars indicate standard error, *** $P \leq 0.001$, **** $P \leq 0.0001$ (one-way ANOVA). The data represents three independent experiments ($n = 3$).

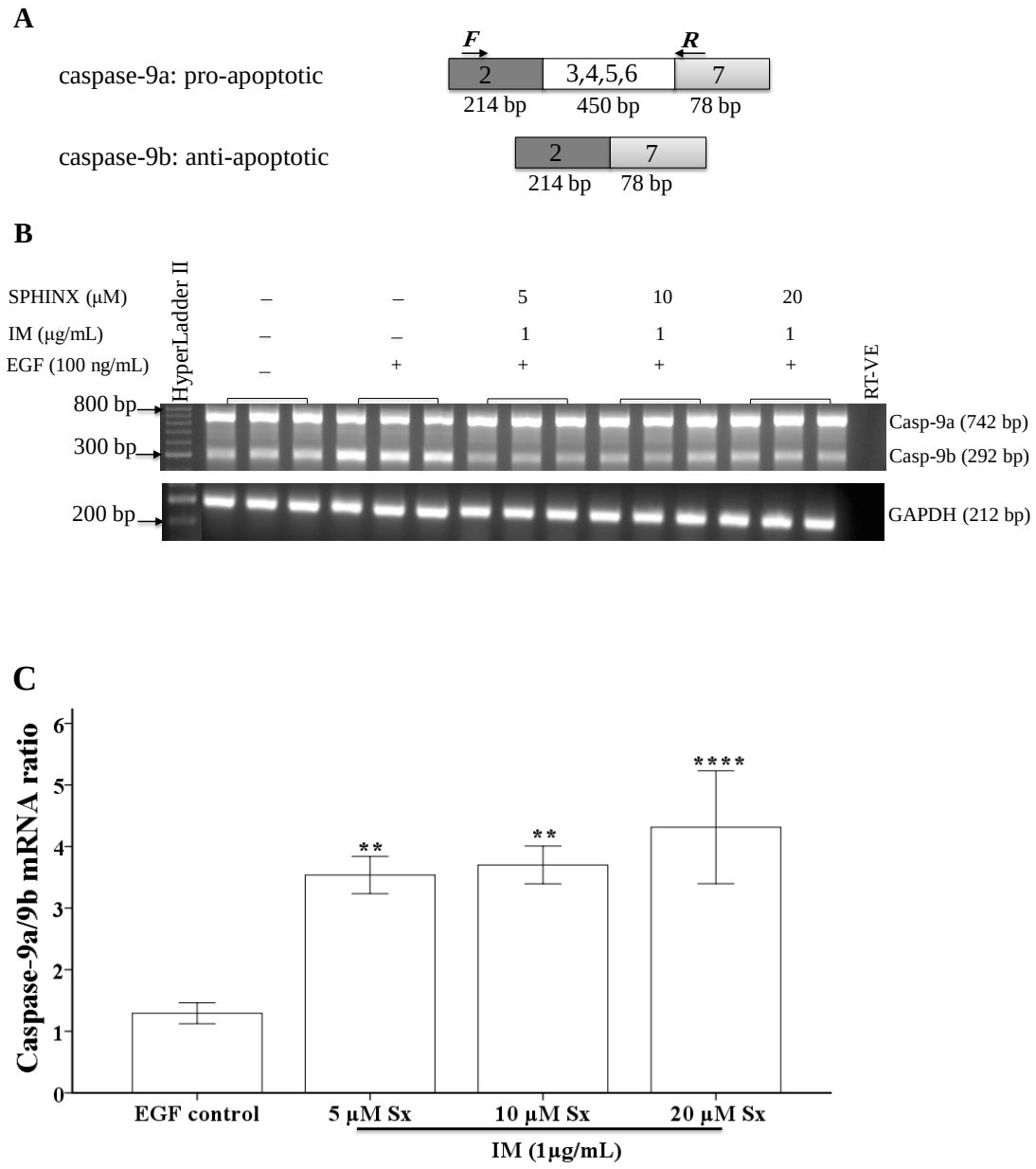

Figure 5.3. TKIs in combination with SRPK1 inhibition on *CASPASE-9* alternative splicing

A. *CASPASE-9* showing the two splice variants resulting from inclusion or exclusion of exon 3–6 (caspase-9a and caspase-9b, respectively). Arrows indicate the positions of *forward* and *reverse* caspase-9 primers. **B.** K562 cells treated with only 100 ng/mL EGF (0 μg/mL IM) and with 1 μg/mL IM in combination with 5–20 μM Sx followed by EGF (100 ng/mL). RT-PCR was performed after 24 hours incubation and bands at 742 bp (casp-9a) and 292 bp (casp-9b) were detected. GAPDH was used as a loading control (212 bp). Each rung of the hyperLadder II represents 100 bp. **C.** Densitometric analysis of caspase-9a/9b isoforms. K562 cells treated with IM were compared to the EGF control. The graph represents the intensity ratio of the caspase-9a against caspase-9b. The expression ratio of caspase-9a/9b significantly increased for the 1 μg/mL IM treatment with increased Sx concentration. The bars indicate standard error, ** $P \leq 0.01$, **** $P \leq 0.0001$ (one-way ANOVA). The data represents three independent experiments ($n = 3$).

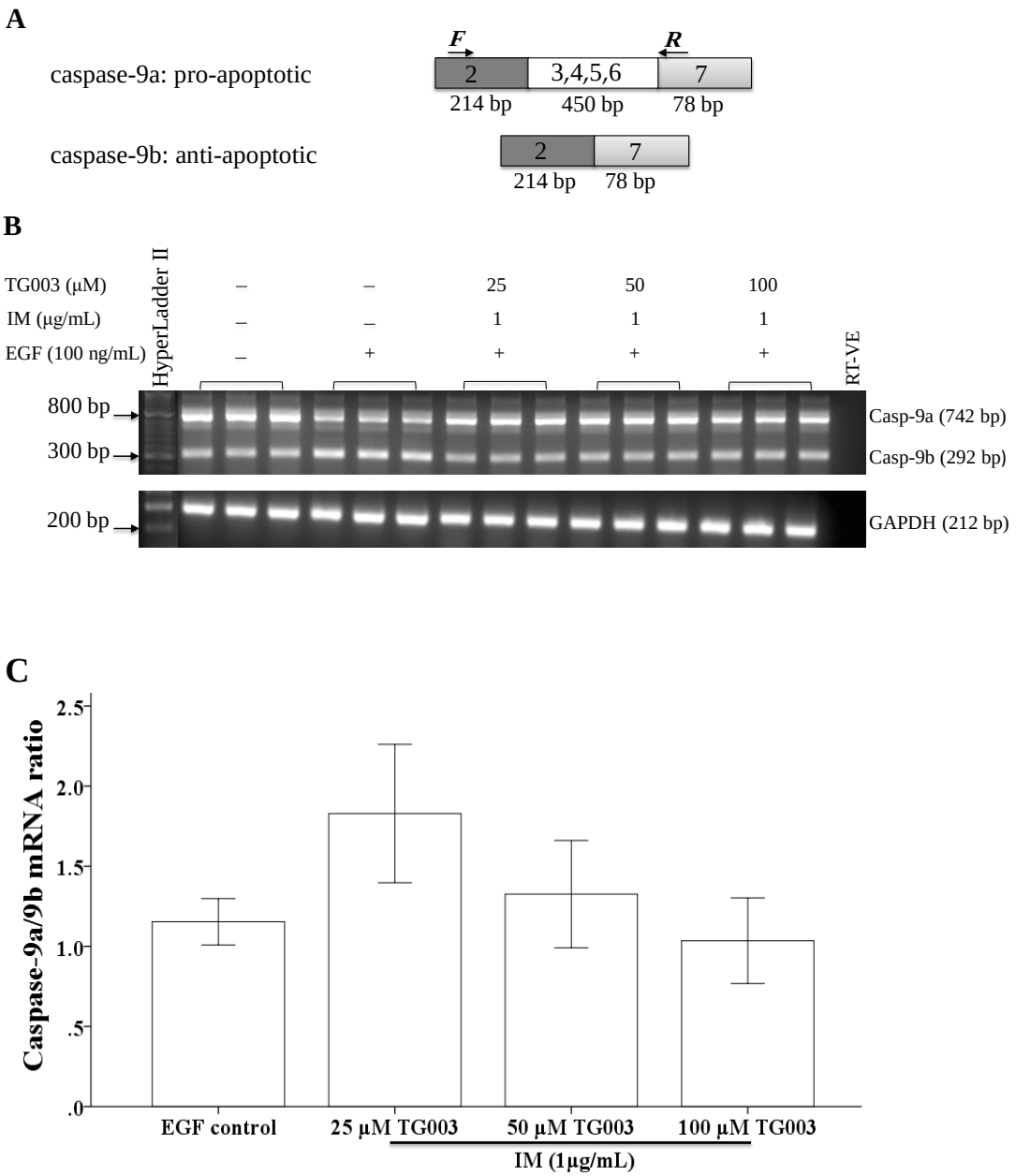

Figure 5.4. TKIs in combination with Clk1 inhibitor on *CASPASE-9* alternative splicing

A. *CASPASE-9* showing the two splice variants resulting from inclusion or exclusion of exon 3–6 (caspase-9a and caspase-9b, respectively). Arrows indicate the positions of *forward* and *reverse* caspase-9 primers. **B.** K562 cells treated with only 100 ng/mL EGF (0 μg/mL IM) and with 1 μg/mL IM in combination with (25–100 μM) TG003 followed by EGF (100 ng/mL). RT-PCR was performed and bands at 742 bp (casp-9a) and 292 bp (casp-9b) were detected. Intermediate bands represent skipped exons. GAPDH was used as a loading control (212 bp). Each rung of the hyperLadder II represents 100 bp. **C.** Densitometric analysis of caspase-9a/9b isoforms. K562 cells treated with IM were compared with the EGF control. The graph represents the intensity ratio of caspase-9a against caspase-9b. The bars indicate standard error (one-way ANOVA). The data represents three independent experiments (n = 3).

5.4.1.3. *RON* splicing in K562 cells following TKI treatment alone or in combination with other protein kinase inhibitors

IM alone or in combination with SPHINX or TG003 on *RON* splice isoforms was investigated by RT-PCR and quantified using ImageJ software.

A range of IM concentrations reduced Ron and ΔRon splice isoforms in K562 cells compared to the EGF control, Figure 5.5B. The expression ratio of Ron/ΔRon was 1.12 in cells treated with 100 ng/mL EGF alone, Figure 5.5C. The expression ratio of Ron/ΔRon in cells treated with 1 μg/mL IM significantly reduced to 0.46 (p = 0.00) while 1.4 μg/mL IM caused further significant reduction to 0.27 (p = 0.00) compared with EGF control (one-way ANOVA). At 2.9 μg/mL IM, the expression ratio of Ron/ΔRon was significantly reduced to 0.15 (p = 0.00) compared with EGF control (one-way ANOVA).

Combining IM and Sx down-regulated both Ron and ΔRon splice isoforms in cells treated with 5 and 10 μM Sx, Figure 5.6B. The expression ratio of Ron/ΔRon was 0.98 in cells treated with 100 ng/mL EGF alone, Figure 5.6C. The expression ratio of Ron/ΔRon in cells treated with 1 μg/mL IM in combination with 5 μM SPHINX was significantly reduced to 0.46 (p = 0.00) when compared to the EGF control (one-way ANOVA). The expression ratios of Ron/ΔRon in cells treated with 1 μg/mL IM in combination with 10 and 20 μM SPHINX were 0.67 (p = 0.08) and 0.83 (p = 0.71), one-way ANOVA.

Co-treatment of IM and higher doses of TG003 (100 μM) were found to down-regulate both Ron and ΔRon splice isoforms in K562 cells, Figure 5.7B. The expression ratio of Ron/ΔRon was 1.01 in cells treated with 100 ng/mL EGF alone, Figure 5.7C. The expression ratio of Ron/ΔRon in cells treated with 1 μg/mL IM and 25 μM TG003 revealed significant increases of 1.56 (p = 0.00) when compared with the EGF control (one-way ANOVA). The expression ratio of Ron/ΔRon in cells treated with 1 μg/mL IM and 50 μM TG003 was 1.14 (p = 0.53), one-way ANOVA. In contrast, treatment of cells with 1 μg/mL IM and 100 μM TG003 caused a significant reduction in the expression ratio of Ron/ΔRon to 0.68 (p = 0.02), one-way ANOVA.

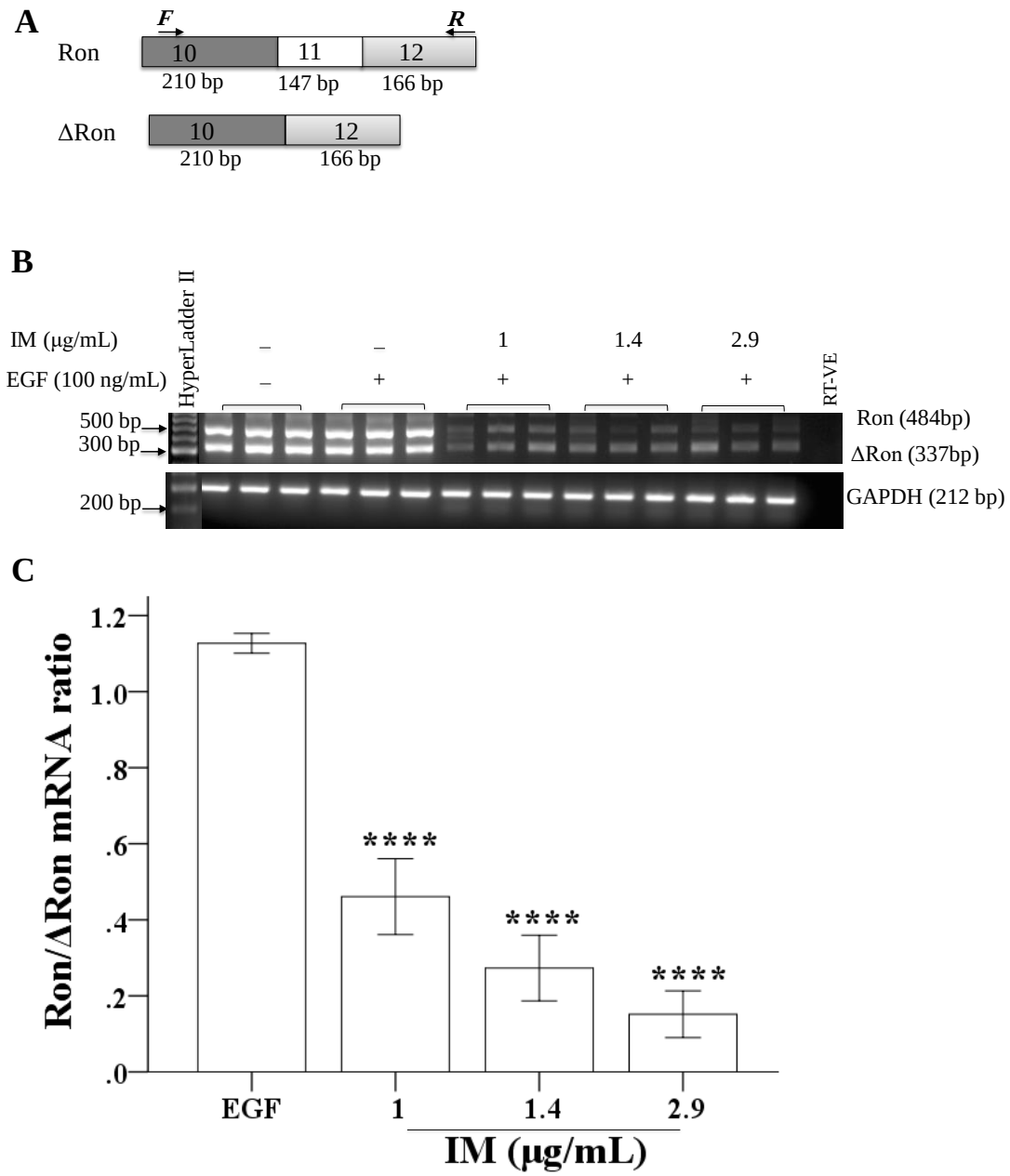

Figure 5.5. TKI effects on *RON* alternative splicing

A. The *RON* gene showing the two splice variants resulting from inclusion or exclusion of exon 11 (Ron and ΔRon variants, respectively). Arrows indicate the positions of *forward* and *reverse* Ron primers. **B.** K562 cells treated with only 100 ng/mL EGF (0 μg/mL IM) and three concentrations of IM were used at 1, 1.4 and 2.9 μg/mL followed by 100 ng/mL EGF. RT-PCR was performed after 24 hours incubation and bands at 484 bp (Ron) and 337 bp (ΔRon) were detected. GAPDH was used as a loading control (212 bp). Each rung of the hyperLadder II represents 100 bp. **C.** Densitometric analysis of Ron/ΔRon isoforms. K562 cells treated with IM were compared to the EGF control. The ratio of Ron/ΔRon decreased in cells treated with 1–2.9 μg/mL IM. The bars indicate standard error (one-way ANOVA). The data represents three independent experiments (n = 3).

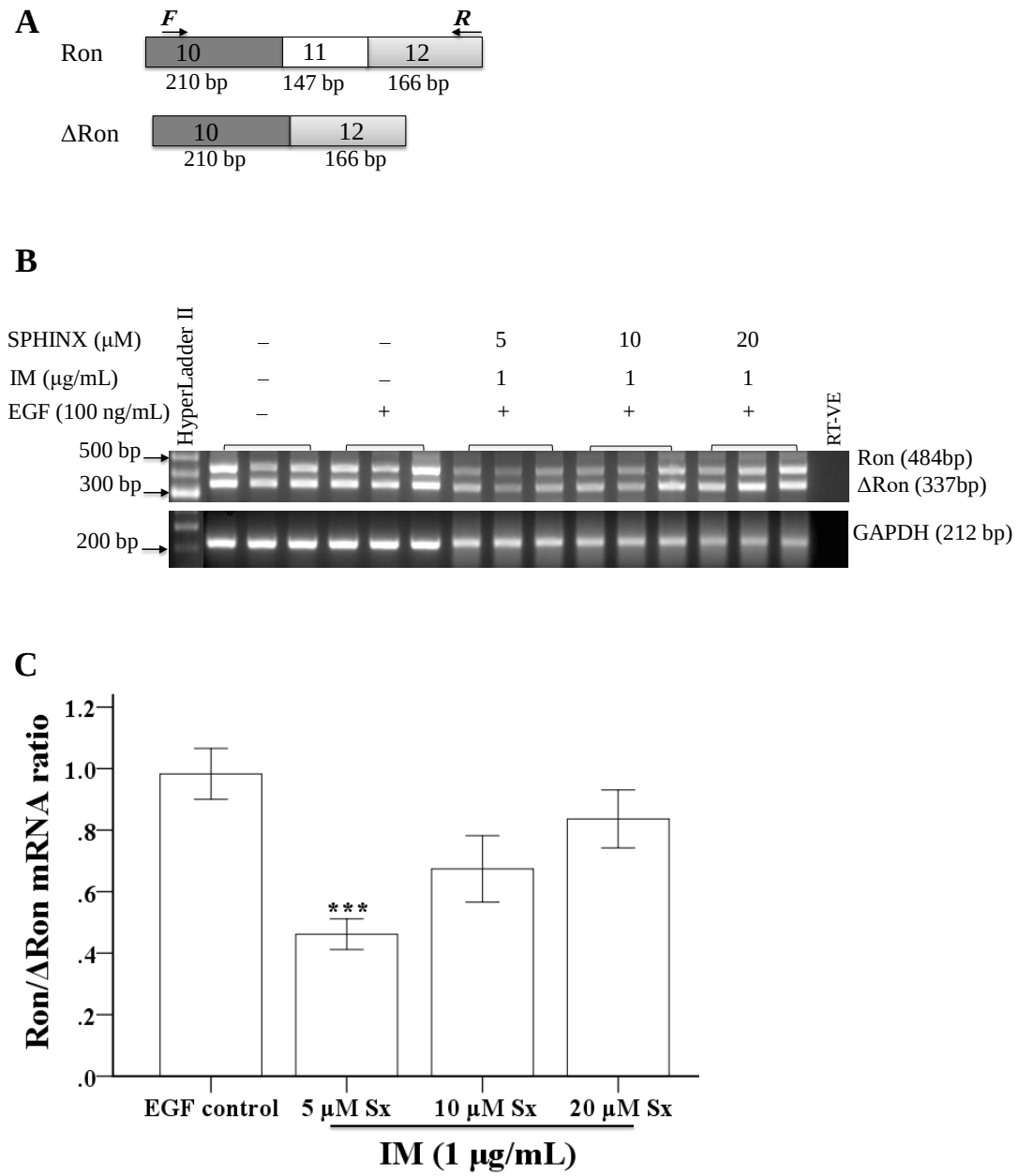

Figure 5.6. TKIs in combination with SRPK1 inhibitors on *RON* alternative splicing

A. The *RON* gene showing the two splice variants resulting from inclusion or exclusion of exon 11 (Ron and ΔRon variants, respectively). Arrows indicate the positions of *forward* and *reverse* Ron primers. **B.** K562 cells treated with only 100 ng/mL EGF (0 μg/mL IM) and with 1 μg/mL IM in combination with (5–20 μM) Sx followed by EGF (100 ng/mL). RT-PCR was performed after 24 hours incubation and bands at 484 bp (Ron) and 337 bp (ΔRon) were detected. GAPDH was used as a loading control (212 bp). Each rung of the hyperLadder II represents 100 bp. **C.** Densitometric analysis of Ron/ΔRon isoforms. K562 cells treated with IM combined with Sx were compared with the EGF control. The graph represents the intensity ratio of Ron against ΔRon. The ratio of Ron/ΔRon significantly decreased in cells treated with 1 μg/mL IM and 5 μM Sx. The bars indicate standard error, *** $P \leq 0.001$ (one-way ANOVA). The data represents three independent experiments ($n = 3$).

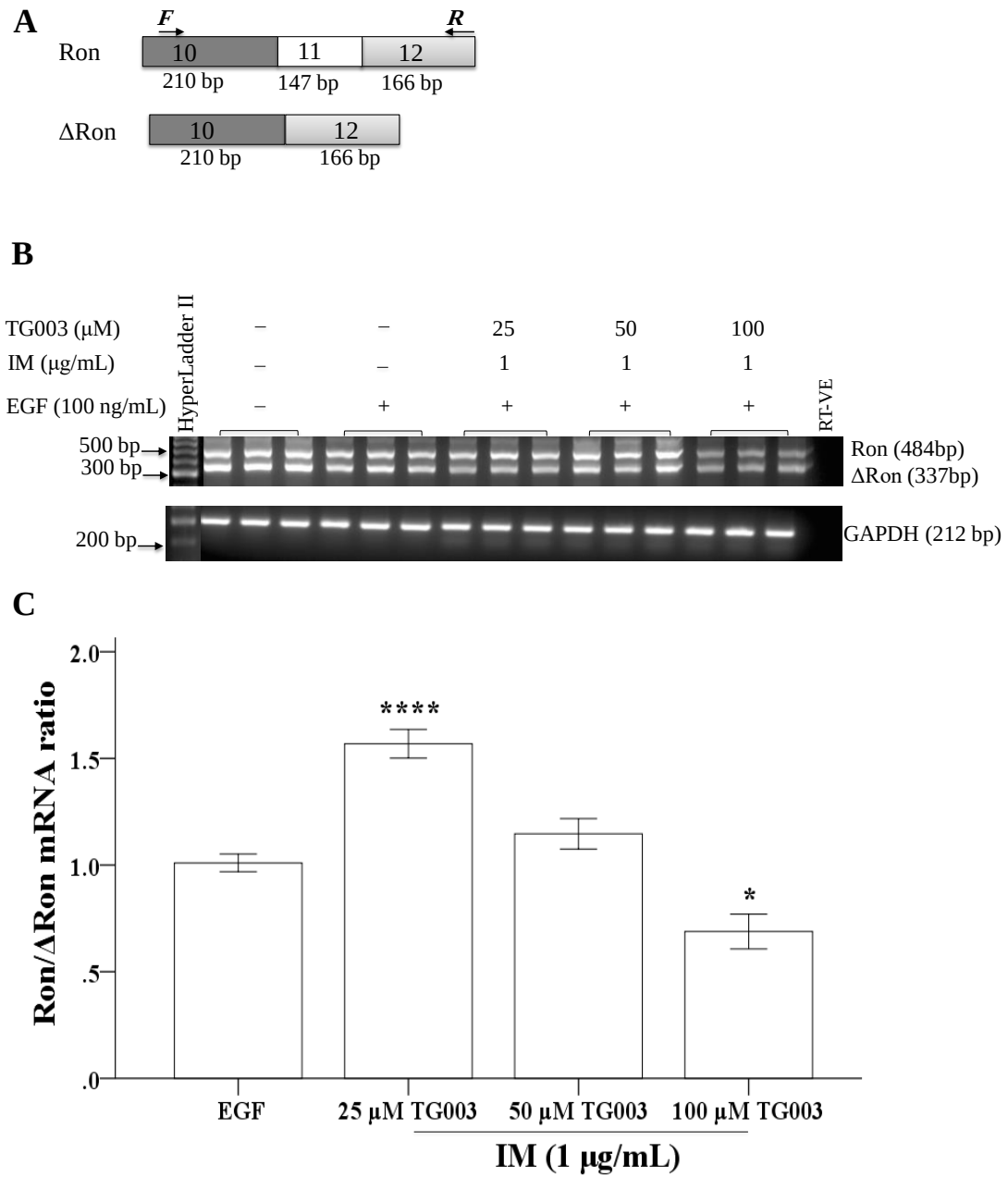

Figure 5.7. TKIs in combination with the Clk1 inhibitor on *RON* alternative splicing

A. The *RON* gene showing the two splice variants resulting from the inclusion or exclusion of exon 11 (Ron and ΔRon variants, respectively). Arrows indicate the positions of *forward* and *reverse* Ron primers. **B.** K562 cells treated with only 100 ng/mL EGF (0 μg/mL IM) and with 1 μg/mL IM in combination with (25–100 μM) TG003 followed by EGF (100 ng/mL). RT-PCR was performed after 24 hours incubation and bands at 484 bp (Ron) and 337 bp (ΔRon) were detected. GAPDH was used as a loading control (212 bp). Each rung of the hyperLadder II represents 100 bp. **C.** Densitometric analysis of Ron/ΔRon isoforms. K562 cells treated with IM combined with TG003 were compared with the EGF control. The ratio of Ron/ΔRon significantly increased in cells treated with 1 μg/mL IM and 25 μM TG003. The graph represents the intensity ratio of Ron against ΔRon. The bars indicate standard error, ** $P \leq 0.01$ (one-way ANOVA). The data represents three independent experiments ($n = 3$).

5.4.1.4. *RUNX1* splicing in K562 cells following TKI treatment alone or in combination with other protein kinase inhibitors

RUNX1 alternative splicing was assessed following treatment with IM alone or in combination with SPHINX or TG003 in K562 cells. There was no effect on ΔRunx1 expression in cells treated with three doses of IM (1, 1.4 and 2.9 μg/mL), Figure 5.8B. The expression ratio of Runx1/ΔRunx1 was 0.75 in cells treated with only 100 ng/mL EGF, Figure 5.8C. The expression ratio of Runx1/ΔRunx1 in cells treated with 1 μg/mL IM was 0.60 (p = 0.98), one-way ANOVA. Additionally, treatment with 1.4 and 2.9 μg/mL IM resulted in expression ratios of 0.93 (p = 0.96) and 0.94 (p = 0.95) for Runx1/ΔRunx1, Figure 5.8C.

Additionally, *RUNX1* splice isoforms were assessed in K562 cells treated with IM alone or in combination with Sx. There were no effects on *RUNX1* splice variants, Figure 5.9B. The expression ratio of Runx1/ΔRunx1 was 0.87 in cells treated with 100 ng/mL EGF alone, Figure 5.9C. The expression ratio of Runx1/ΔRunx1 in cells treated with 1 μg/mL IM and 5 μM Sx (ratio = 0.96, p = 0.99) compared with EGF control (one-way ANOVA), Figure 5.9C. The expression ratio of Runx1/ΔRunx1 in cells treated with 1 μg/mL IM and 10 μM Sx was almost identical to the EGF control (ratio = 0.88, p = 1.00, one-way ANOVA). At a higher concentration of Sx (20 μM), in combination with 1 μg/mL IM, an increase in the expression ratio of Runx1/ΔRunx1 to 1.12 (p = 0.78) was observed when compared with the EGF control (one-way ANOVA).

Furthermore, there was no change in *RUNX1* alternative splicing in cells treated with IM and TG003, Figure 5.10B. The expression ratio of Runx1/ΔRunx1 was 0.86 in cells treated with only 100 ng/mL, Figure 5.10C. The expression ratio of Runx1/ΔRunx1 in cells treated with 1μg/mL IM and TG003 (25 and 50 μM) were 0.99 (p = 0.95) and 0.99 (p = 0.96), one-way ANOVA. In addition, the expression ratio of Runx1/ΔRunx1 in cells treated with 1 μg/mL IM and TG003 (100 μM). to 1.04 (p = 0.96) and 1.06 (p = 0.87) compared with EGF control (one-way ANOVA).

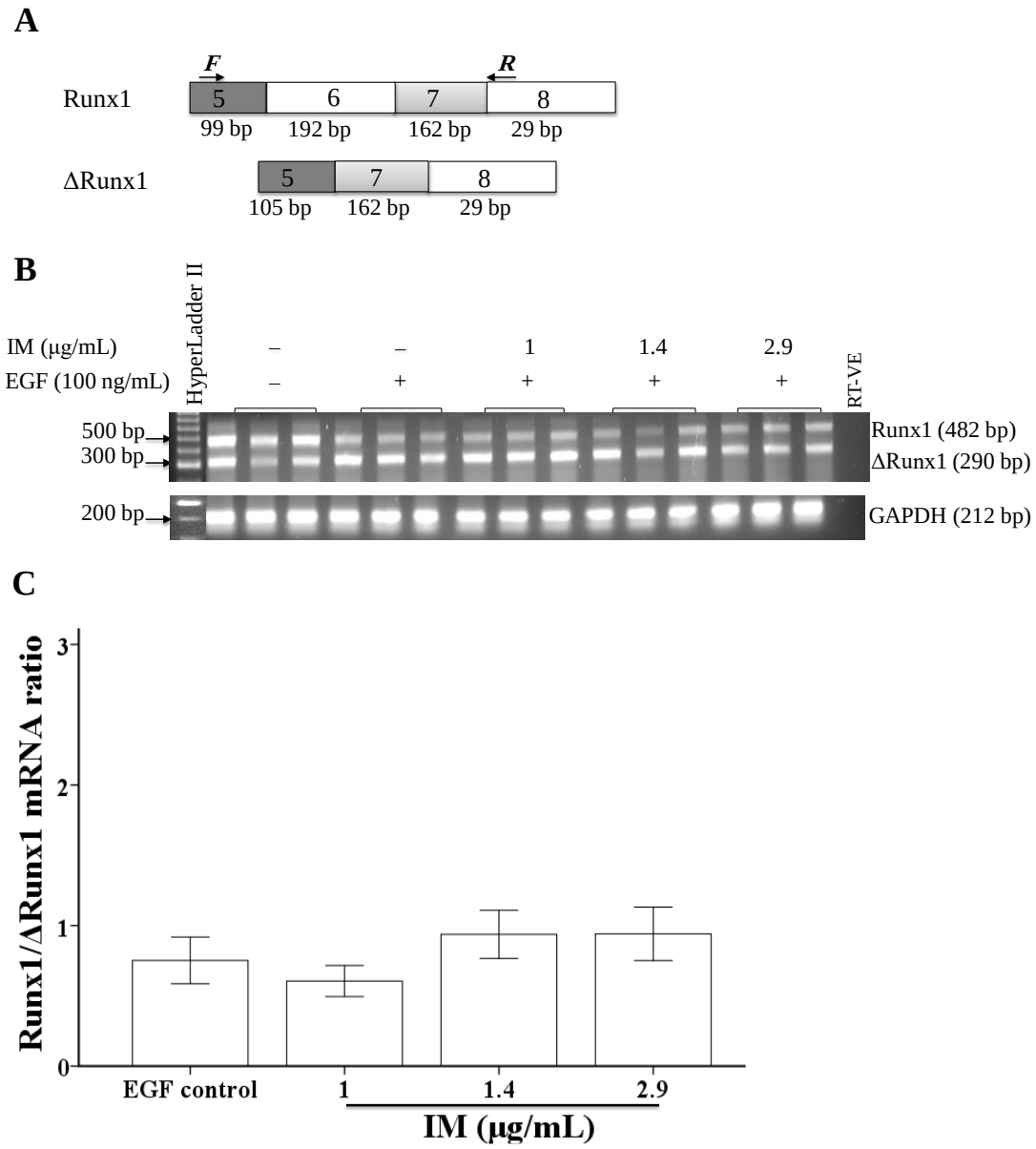

Figure 5.8. TKI effects on *RUNX1* alternative splicing
A. *RUNX1* showing the two splice variants resulting from including or excluding exon 6 (Runx1 and ΔRunx1 variants, respectively). Arrows indicate the positions of *forward* and *reverse* Runx1 primers. **B.** K562 cells treated with only 100 ng/mL EGF (0 μg/mL IM) and three concentrations of IM were used at 1, 1.4 and 2.9 μg/mL followed by 100 ng/mL EGF. RT-PCR was performed after 24 hours incubation and bands at 482 bp (Runx1) and 290 bp (ΔRunx1) were detected. GAPDH was used as a loading control (212 bp). Each rung of the hyperLadder II represents 100 bp. **C.** Densitometric analysis of Runx1/ΔRunx1 isoforms. K562 cells treated with IM were compared with the EGF control. The bars indicate standard error (one-way ANOVA). The data represents three independent experiments (n = 3).

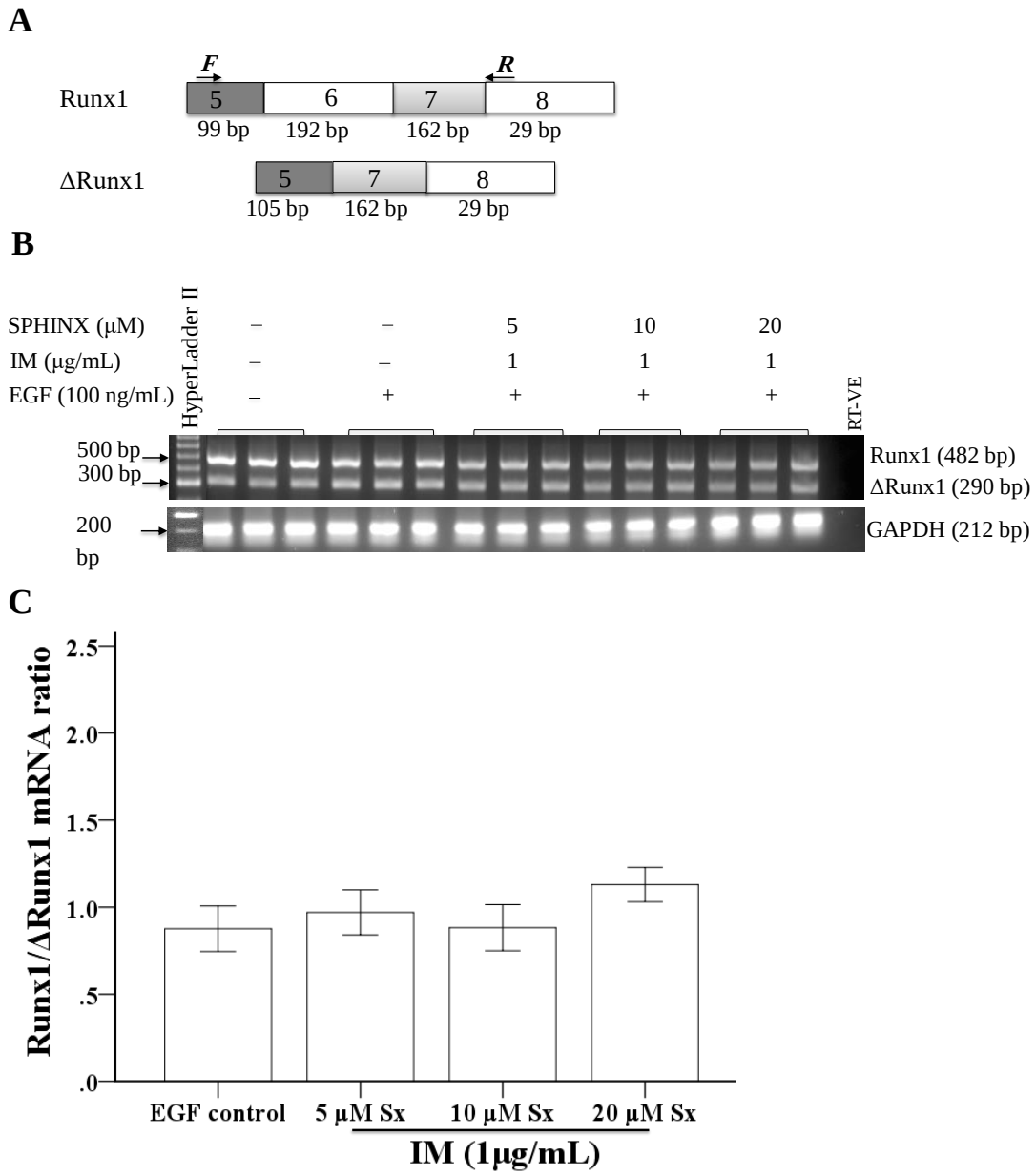

Figure 5.9. TKI in combination with SRPK1 inhibition on *RUNX1* alternative splicing

A. *RUNX1* showing the two splice variants resulting from including or excluding of exon 6 (Runx1 and ΔRunx1 variants, respectively). Arrows indicate the positions of *forward* and *reverse* Runx1 primers. **B.** K562 cells treated with only 100 ng/mL EGF (0 μg/mL IM) and with 1 μg/mL IM in combination with (5–20 μM) Sx followed by EGF (100 ng/mL). RT-PCR was performed after 24 hours incubation and bands at 482 bp (Runx1) and 290 bp (ΔRunx1) were detected. GAPDH was used (212 bp). Each rung of the hyperLadder II represents 100 bp. **C.** Densitometric analysis of Runx1/ΔRunx1 isoforms. K562 cells treated with IM combined with SPHINX were compared with the EGF control. The graph represents the intensity ratio of Runx1 against ΔRunx1. The bars indicate standard error (one-way ANOVA). The data represents three independent experiments (n = 3).

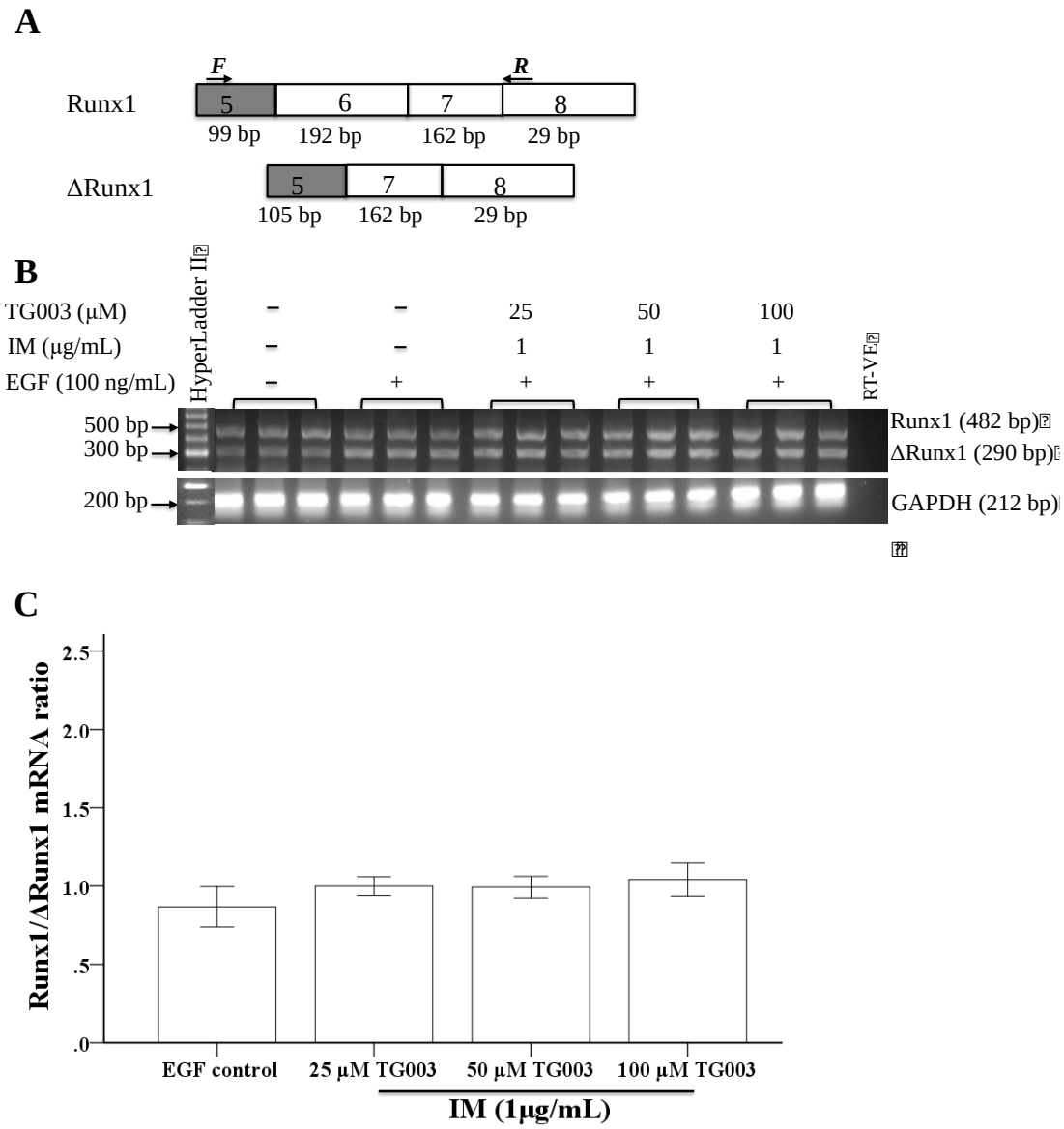

Figure 5.10. TKIs in combination with CLK1 inhibition on *RUNX1* alternative splicing

A. *RUNX1* showing the two splice variants resulting from including or excluding exon 6 (Runx1 and ΔRunx1 variants, respectively). Arrows indicate the positions of *forward* and *reverse* Runx1 primers. **B.** K562 cells treated with only 100 ng/mL EGF (0 μg/mL IM) and with 1 μg/mL IM in combination with (25–100 μM) TG003 followed by EGF (100 ng/mL). RT-PCR was performed after 24 hours incubation and bands at 484 bp (Ron) and 337 bp (ΔRon) were detected. GAPDH was used as a loading control (212 bp). Each rung of the hyperLadder II represents 100 bp. **C.** Densitometric analysis of Runx1/ΔRunx1 isoforms. K562 cells treated with IM combined with TG003 were compared with the EGF control. The graph represents the intensity ratio of Runx1 against ΔRunx1. The bars indicate standard error (one-way ANOVA). The data represents three independent experiments (n = 3).

5.5 Discussion

Reducing IM binding site affinity in CML enhances disease treatment through the co-targeting of protein kinases (Change *et al.*, 2011; Henkes *et al.*, 2008). A recent study has shown that multi-targeting of spleen tyrosine kinase (SYK) and oncogenic FLT3 kinase has a potential effect in acute myeloid leukaemia (AML) (Weisberg *et al.*, 2017). In contrast, it has been suggested that suppressing Ax1 using a single agent (TP-0903) would overcome the AML resistance (Park *et al.*, 2015). Other studies found that targeting STAT3/5 alone or in a combination with Janus kinase 1/2 (JAK1/2) has a potential effect on adenoviral transgene expression (Akinfenwa *et al.*, 2017).

To develop these observations, this study investigated the effects of IM alone or in combination with SPHINX (SRPK1 inhibitor) or TG003 (Clk1 inhibitor) on *CASPASE-9*, *RON*, and *RUNX1* alternative splicing in K562 cells. To achieve this, it was important to evaluate K562 cell proliferation upon treatment with IM alone or in combination with other protein kinase inhibitors. In previous work, rapid reductions in K562 and BaF3/*Bcr-Abl*T315I proliferation was observed in cells treated with amiloride in combination and IM (Change *et al.*, 2011). In addition, cell proliferation was reduced by co-treatment with rapamycin and everolimus (mTOR inhibitors) in CML cell lines. It has been suggested that rapamycin, combined with IM, acts synergistically and improves CML therapy (Henkes, van der Kuip and Aulitzky, 2008). This suggests that Bcr-Abl kinase activity plays an important role in CML cell lines. In accordance with previous studies, this study showed that K562 cell proliferation was significantly reduced following IM treatment alone, similar to co-

treatment with Sx or TG003. This demonstrates that co-inhibitors affect K562 cell survival.

It has been recently reported that cells treated with Hedgehog (Hh) inhibitor (Vismodegib) and autophagic inhibitor chloroquine (CQ), stimulated apoptosis of both IM sensitive or resistant Bcr-Abl^{+} CML cells (Zeng *et al.*, 2015). It has been shown that increasing apoptosis may re-sensitise CML cells to cancer therapy. Renne *et al.*, (2005) investigated six RTKs in Hodgkin/Reed-Sternberg (HRS) cell lines, one of which *RON,* was aberrantly expressed. Therefore, IM could be a promising therapeutic for HL patients (Renne *et al.*, 2005). It was also shown that combining IM with arsenic trioxide exerted effects on mice with myeloproliferative neoplasms (MPNs) (Philips *et al.*, 2014).

Expanding on previous published data, this study observed *CASPASE-9, RON* and *RUNX1* alternative splicing, following TK inhibition alone or in combination with SRPK1 or TG003 inhibition in K562 cells. There was a clear switch in splicing form towards the pro-apoptotic splice isoform, caspase-9a in K562 cells treated with IM alone or in combination with Sx. This could be due to the inhibition of TK pathways via IM-mediated apoptosis. However, co-treatment of IM and TG003 caused non-specific effects on the expression of caspase-9 in K562 cells.

In addition, the treatment of cells with IM alone inhibited expression of all Ron isoforms. As *RON* is an RTK, inhibiting TKs would exert strong effects on the expression of Ron isoforms in K562 cells. A switch from Ron expression towards the ΔRon splice isoform was seen in cells co-treated with IM and Sx and suggests

that SRPK1 is overexpressed in K562 cells, or inhibiting SRPK1 may trigger other protein kinase activation leading to increased cell motility and migration for *RON* in K562 cells. In contrast, K562 cells treated with IM and low TG003 doses increased Ron isoform levels, suggesting that Clk1 could be the primary protein kinase regulator for *RON* splicing in K562 cells.

It is noteworthy to observe the resistance of *RUNX1* splicing to IM alone or in combination with Sx or TG003 in K562 cells. This observation suggests that TKs are not directly involved in *RUNX1* splicing/regulation in K562 cells. Similarly, it may be that inhibiting SRPK1 or Clk1 in combination with TKIs, activated unknown protein kinases which compensate for the loss of SRPK1 or Clk1 activity.

5.5.1. Conclusion and future directions

The data has indicated that co-targeting the tyrosine kinases, SRPK1 or Clk1 induced the expression of caspase-9a isoform in K562 cells. Further assays will confirm elevated levels of apoptosis in K562 cells treated with IM and Sx or TG003. This research strategy could enhance the development of a therapy against resistant or persistent CML progenitors. Another important finding is the enhancement of cell migration and invasion for *RON* after treatment with IM and Sx in K562 cells. In contrast, the combination of IM and TG003 limited K562 cell migration and invasion.

Additionally, the expression of Runx1 and ΔRunx1 splice isoforms were resistant following IM alone or in combination with SPHINX or TG003. It is therefore important to identify the main regulator protein kinase for *RUNX1* in K562 cells.

CHAPTER 6. CONCLUSIONS AND FUTURE PERSPECTIVES

Although IM has become a successful and powerful therapy for CML, patients develop resistance over time (Salizzato *et al.*, 2016). Allogenic bone marrow transplantation is the only curative therapy, however survival rates are low due to infection, bleeding, GvHD and difficulties in finding suitable donors (Jain *et al.*, 2013; Fausel, 2007). This study has provided important insight on *CASPASE-9*, *RON* and *RUNX1* alternative splicing in K562 cells, upon targeting protein kinases and splice factors.

6.1 K562 cell proliferation following protein kinase inhibiton

A number of studies have suggested that small molecule inhibitors of SRPK1 or Clk1 reduce cell proliferation rates in tumour cell lines (Dominguez *et al.*, 2016; Siqueira *et al.*, 2015). Other studies have demonstrated that co-treatment with inhibitors, decrease cell proliferation rates in CML cells (Henkes, van der Kuip and Aulitzky, 2008; Change *et al.*, 2011). In this study, the inhibitors, SRPIN340 or SPHINX did not suppress K562 cell proliferation, suggesting that inhibiting SRPK1 may trigger the activation of other compensatory protein kinases in K562 cells. It also suggests that K562 cells express high levels of SRPK1 or that there is a high level of resistance to SRPK1 in K562 cells.

TG003 or IM treatments reduced cell proliferation in K562 cells. Co-treatment of IM with Sx or TG003 strongly reduced K562 proliferation, suggesting that Clk1 or TKs play important roles in K562 cell proliferation. It also suggests that TKI treatment in

combination with SRPK1 or Clk1 inhibitors, induced significant reduction in proliferation of K562 cells.

6.2 *CASPASE-9* splicing in K562 cells following protein kinase inhibiton

Inhibiting phosphorylation of Akt by sulforaphene induces apoptosis in lung cancer (Yang *et al.*, 2016). In this study, the inhibitors, SRPIN340 or SPHINX were shown no effect in the *CASPASE-9* splice isoform in K562 cells. This confirms high SRPK1 levels or stimulation of other protein kinase after inhibiting SRPK1 in K562 cells. However, TG003 induced apoptosis through increasing pro-apoptotic isoforms in K562 cells, suggesting *CASPASE-9* may be regulated by Clk1.

It was also shown that IM treatment alone or in combination with Sx increased pro-apoptotic isoform in K562 cells. However, cells treated with IM in a combination with TG003, resulted in non-specific effect on apoptosis in K562 cells. This would indicate that TKs contribute to regulation of apoptosis and that a combination of kinase inhibitors can trigger apoptosis in K562 cells, thus potentially inhibiting transformation to a malignant state. According to cell morphological characteristics, apoptosis was decreased during SRPIN340 or SPHINX treatment. Annexin V staining confirmed that SRPIN340 or Sx reduced apoptosis in K562 cells, as shown in Figure 6.1.

6.3 *RON* splicing in K562 cells following protein kinase inhibition

Smith *et al.* (2013) observed that SRSF1 regulates the expression of ΔRon in breast and gastric carcinoma (Smith *et al.,* 2013), while the RON/c-Met dual kinase

inhibitor suppressed ΔRon expression in colon cancer cell lines (Zhang *et al.*, 2008b). Since constitutive activation of the ΔRon isoform is regulated through SRSF1 phosphorylation, it was therefore relevant to target SRPK1 or Clk1 signalling to down regulate SRSF1 proto-oncogenic activity in K562 cells. No switch in *RON* splicing was observe in K562 cells treated with SRPIN340 or SPHINX followed by EGF addition.

In contrast, treatment with TG003 increased Ron expression when compared to the EGF control. As Ron is an RTK, TK inhibition through IM alone has a strong effect on the production of Ron isoforms through inhibiting both Ron and ΔRon isoforms in K562 cells. K562 cells treated with combinations of IM and Sx increased ΔRon splice isoform expression. SRPK1 inhibition did not switch *RON* splicing, while combinations of SRPK1 and TK inhibitors increased ΔRon splice isoform expression. This therefore confirms high levels of SRPK1 in K562 cells. In contrast, combinations of IM and TG003 increased Ron isoform expression in K562 cells. Combinations of kinase inhibitors such as IM and TG003 exhibited a more effective shift in *RON* splicing towards Ron isoforms, than either agent alone, as shown in Figure 6.1.

6.4 *RUNX1* splicing in K562 cells following protein kinase inhibition

It was reported that ΔRunx1 splice isoforms control heamatopoietic progenitor clonogenicity (Wang *et al.,* 2009). Evidence shows that ERK1/2 serine/threonine kinases play important roles in the regulation and splicing of *RUNX1* (Wang *et al.*,

2009), while others reported that arginine methyltransferase 1 (PRMT1) was the main *RUNX1* regulator (Mizutani *et al.,* 2015).

In this study, SRPIN340 or Sx did not cause a shift in *RUNX1* splicing in K562 cells. Treatment with TG003 increased expression of the Runx1 isoform in K562 cells, suggesting Clk1 directly affects *RUNX1* splicing. In addition, IM alone or in combination with the kinase inhibitors IM with SPHINX or TG003 had no clear effect on *RUNX1* splicing. Taken together, inhibiting SRPK1 or TKs, either alone or in combination wih IM generated weak splicing effects, suggesting these protein kinases may not be directly involved in *RUNX1* splicing in K562 cells, as shown in Figure 6.1.

6.5 The knockdown of SRPK1 and Clk1 in K562 cells

The splice site selection of *VEGF* is regulated by SRSF1, which is phosphorylated by SRPK1 (Nowak *et al.,* 2010). According to a recent report, a significant switch was observed in *VEGF* splicing towards the $VEGF_{165}b$ splice isoform following SRPK1 knockdown, resulting in decreased tumour growth in orthotopic mouse models of prostate cancer (Mavrou *et al.,* 2015).

In this study, no SRPK1 expression reduction was observed, while SRSF1 was reduced in K562 cells, generated from a stable knockdown of SRPK1. There was no significant reduction in SRPK1 in K562 cells, generated from an siRNA knockdown of SRPK1. However, in PC-3 cells, an si-SRPK1 knockdown strongly reduced SRPK1. In our hands, it would appear that SRPK1 knockdown in K562 cells elicited very little phenotypic, molecular and protein expression alterations, whereas in PC-3

cells, profound effects on SRPK1 protein expression were observed, suggesting high SRPK1 expression levels in K562 cells.

In addition, there were significant reductions in SRSF1 in K562 cells, in combination with siRNA SRSF1 knockdown. Equally, there were no switches in *CASPASE-9*, *RUNX1* or *RON* splicing in K562 cells, in combination with SRSF1 knockdown. These observations suggest that SRSF1 may not be the main splice factor for *CASPASE-9*, *RUNX1* or *RON* splice isoforms in K562 cells.

As Clk1 distributes phosphorylated SRSF1to splice sites, this study has determined that Clk1 plays a role in *CASPASE-9*, *RON* and *RUNX1* alternative splicing in siRNA knockdown of Clk1 in K562 cells. Three different siRNA successfully reduced Clk1 levels in ovarian cancer cell lines (Liu *et al.*, 2013).

In comparison to these findings, one siRNA significantly reduced Clk1 levels in K562 cells, predicting that cell-signalling pathways in ovarian cancer cells are different to CML. At the mRNA level, no shifts in *CASPASE-9* and *RON* splicing were seen in K562 cells, in combination with Clk1 knockdown. This suggests that Clk1 knockdown could stimulate other protein kinases. In contrast, Clk1 knockdown caused a significant switch in *RUNX1* splicing towards the Runx1 isoform, suggesting that Clk1 exerts direct effects on *RUNX1* alternative splicing in K562 cells, as shown in Figure 6.1.

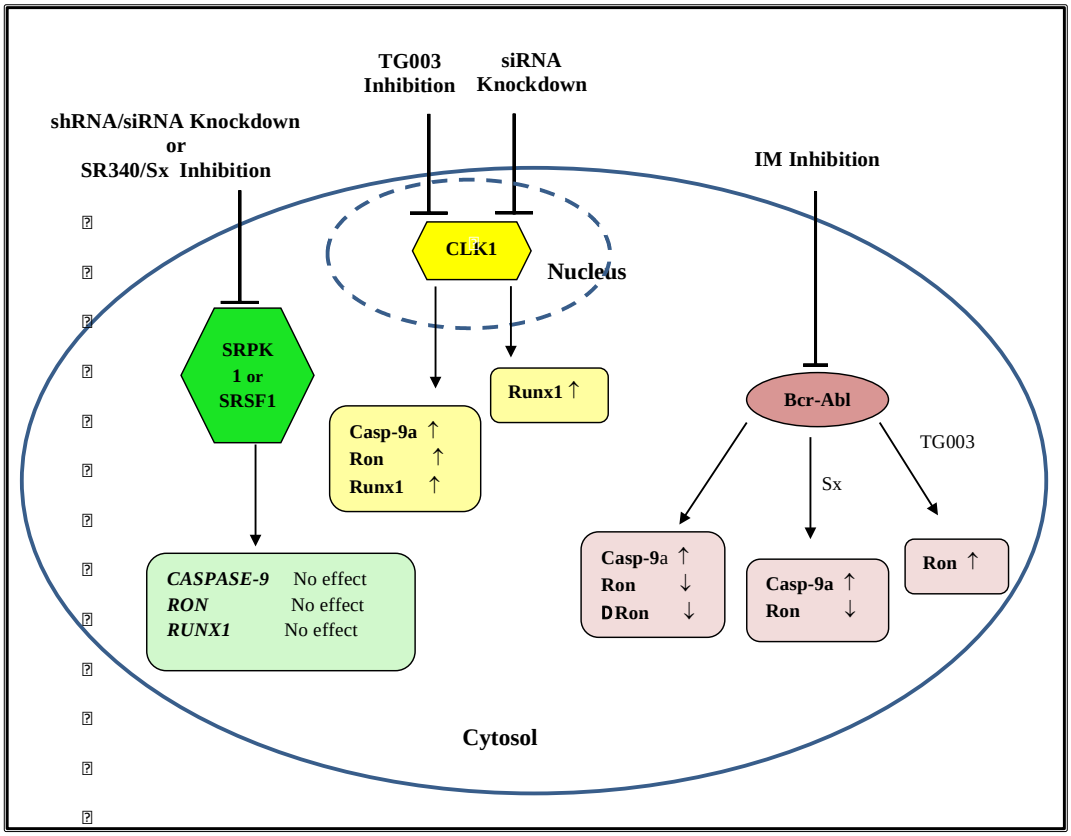

Figure 6.1. Schematic diagram of the kinase inhibitors inducing alternative splicing in K562 cells alone or in a combination with imatinib (IM).
Targeting SRPK1 or SRSF1 through inhibition (SRPIN340 or Sx) or knockdown (siRNA or shRNA) had no significant effects on the alternative splicing of *CASPASE-9*, *RON* and *RUNX1* in K562 cells. Inhibiting Clk1 with selective inhibitor (TG003) resulted in increased expression of caspase-9a, Ron and Runx1 splice isoforms, while, knockdown of Clk1 only increased the levels of Runx1 splicing isoform in K562 cells. Inhibiting tyrosine kinase with imatinib (IM) increased apoptosis and decreased both Ron and ΔRon splice isoforms. Co-treatment of cells with IM and Sx increased the production of caspase-9a and ΔRon splice isoforms. K562 cells treated with IM and TG003 leads to increased levels of Ron only. Abbreviations: Casp: caspase, Sx: SPHINX, IM: imatinib.

6.6 Conclusions and future perspectives

SRPK1 and Clk1 are protein kinases that regulate SRSF1 phosphorylation in mammalian cells (Zhou and Fu, 2013). While SRPK1 plays a direct role in importing phosphorylated SRSF1 into the nucleus, Clk1 has an indirect role whereby it controls SRSF1 nuclear distribution to splice sites (Zhou and Fu, 2013).

The work presented here proposed the following hypothesis; the targeting of SRPK1 or Clk1 along with the splice factor (SRSF1) through inhibition or knockdown, could affect *CASPASE-9*, *RON* and *RUNX1* alternative splicing in K562 cells. These observations may provide the basis for useful therapeutic options for leukaemic patients.

Future research directions may focus on comparing SRPK1 levels in K562 cells to other haematological malignancies and solid cancers. Research could investigate *CASPASE-9*, *RON* and *RUNX1* alternative splicing following SRPK1 knockdown in K562 cells.

In terms of therapy, it will be important to ascertain if combining inhibitors is a more efficient therapy than single inhibitor use. Evaluating these strategies would provide useful alternative therapeutic options in overcoming IM resistance in leukaemic patients.

CHAPTER 7. REFERENCES

Akinfenwa, P.Y., Bond, W.S., I1defonso, C.J., Hurwitz, M.Y. and Hurwitz, R.L. (2017) Versican G1 Domain Enhances Adenoviral-Medated Transgene Expression and Can Be Modulated by Inhibitors of the Janus Kinase (JAK)/STAT and Src Family Kinase Pathways. *The Journal of Biological Chemistry*, pp.jbc-M116.

Amarante-Mendes, G.P., McGahon, A.J., Nishioka, W.K., Afar, D.E., Witte, O.N. and Green, D.R. (1998) Bcl-2-independent Bcr-Abl-mediated resistance to apoptosis: protection is correlated with up regulation of Bcl-xL. *Oncogene*. 16 (11), pp.1383-1390.

Amin, E.M., Oltean, S., Hua, J., Gammons, M.V., Hamdollah-Zadeh, M., Welsh, G.I., Cheung, M.K., Ni, L., Kase, S., Rennel, E.S., Symonds, K.E., Nowak, D.G., Royer-Pokora, B., Saleem, M.A., Hagiwara, M., Schumacher, V.A., Harper, S.J., Hinton, D.R., Bates, D.O. and Ladomery, M.R. (2011) WT1 mutants reveal SRPK1 to be a downstream angiogenesis target by altering VEGF splicing. *Cancer Cell*. 20 (6), pp.768-780.

Aubol, B.E. and Adams, J.A. (2011) Applying the brakes to multisite SR protein phosphorylation: substrate-induced effects on the splicing kinase SRPK1. *Biochemistry*. 50 (32), pp.6888-6900.

Arber, D.A., Orazi, A., Hasserjian, R., Thiele, J., Borowitz, M.J., Le Beau, M.M., Bloomfield, C.D., Cazzola, M. and Vardiman, J.W. (2016) The 2016 revision to the World Health Organization classification of myeloid neoplasms and acute leukemia. *Blood*. 127 (20), pp.2391-2405.

Bacher, U., Haferlach, T., Alpermann, T., Zenger, M., Hochhaus, A., Beelen, D.W., Uppenkamp, M., Rummel, M., Kern, W., Schnittger, S. and Haferlach, C. (2011) Subclones with the t(9;22)/BCR-ABL1 rearrangement occur in AML and seem to cooperate with distinct genetic alterations. *British Journal of Haematology*. 152 (6), pp.713-720.

Batth, I.S., Yun, H. and Kumar, A.P. (2015) Recepteur d'origine nantais (RON), more than a kinase: Role in castrate-resistant prostate cancer. *Molecular Carcinogenesis*. 54 (10), pp.937-946.

Bernt, K.M. and Hunger, S.P. (2014) Current concepts in pediatric Philadelphia chromosome-positive acute lymphoblastic leukemia. *Frontiers in Oncology*. 4 pp.54.

Bhamidipati, P.K., Kantarjian, H., Cortes, J., Cornelison, A.M. and Jabbour, E. (2013) Management of imatinib-resistant patients with chronic myeloid leukemia. *Therapeutic Advances in Hematology*. 4 (2), pp.103-117.

Bibi, S., Arslanhan, M.D., Langenfeld, F., Jeanningros, S., Cerny-Reiterer, S., Hadzijusufovic, E., Tchertanov, L., Moriggl, R., Valent, P. and Arock, M. (2014)

Co-operating STAT5 and AKT signaling pathways in chronic myeloid leukemia and mastocytosis: possible new targets of therapy. *Haematologica*. 99 (3), pp.417-429.

Brouard, M.C., Prins, C., Mach-Pascual, S. and Saurat, J.H. (2001) Acute generalized exanthematous pustulosis associated with STI571 in a patient with chronic myeloid leukemia. *Dermatology (Basel, Switzerland)*. 203 (1), pp.57-59.

Bullock, N. and Oltean, S. (2017) The many faces of SRPK1. *The Journal of Pathology*. 241 (4), pp.437-440.

Buza-Vidas, N., Antonchuk, J., Qian, H., Mansson, R., Luc, S., Zandi, S., Anderson, K., Takaki, S., Nygren, J.M., Jensen, C.T. and Jacobsen, S.E. (2006) Cytokines regulate postnatal hematopoietic stem cell expansion: opposing roles of thrombopoietin and LNK. *Genes & Development*. 20 (15), pp.2018-2023.

Caldemeyer, L., Dugan, M., Edwards, J. and Akard, L. (2016) Long-Term Side Effects of Tyrosine Kinase Inhibitors in Chronic Myeloid Leukemia. *Current Hematologic Malignancy Reports*. 11 (2), pp.71-79.

Cancer Research UK (2016) *Chronic Myeloid Leukaemia (CML) Statistics.* Available from: http://www.cancerresearchuk.org/health-professional/cancer-statistics/statistics-by-cancer-type/leukaemia-cml [Accessed 2016].

Cartegni, L., Chew, S.L. and Krainer, A.R. (2002) Listening to silence and understanding nonsense: exonic mutations that affect splicing. *Nature Reviews.Genetics*. 3 (4), pp.285-298.

Chai, S.K., Nichols, G.L. and Rothman, P. (1997) Constitutive activation of JAKs and STATs in BCR-Abl-expressing cell lines and peripheral blood cells derived from leukemic patients. *Journal of Immunology (Baltimore, Md.: 1950)*. 159 (10), pp.4720-4728.

Chang, W.H., Liu, T.C., Yang, W.K., Lee, C.C., Lin, Y.H., Chen, T.Y. and Chang, J.G. (2011) Amiloride modulates alternative splicing in leukemic cells and resensitizes Bcr-AblT315I mutant cells to imatinib. *Cancer Research*. 71 (2), pp.383-392.

Chow, L.T., Gelinas, R.E., Broker, T.R. and Roberts, R.J. (1977) An amazing sequence arrangement at the 5' ends of adenovirus 2 messenger RNA. *Cell*. 12 (1), pp.1-8.

Chu, S., Li, L., Singh, H. and Bhatia, R. (2007) BCR-tyrosine 177 plays an essential role in Ras and Akt activation and in human hematopoietic progenitor transformation in chronic myelogenous leukemia. *Cancer Research*. 67 (14), pp.7045-7053.

Collesi, C., Santoro, M.M., Gaudino, G. and Comoglio, P.M. (1996) A splicing variant of the RON transcript induces constitutive tyrosine kinase activity and an invasive phenotype. *Molecular and Cellular Biology*. 16 (10), pp.5518-5526.

Corkery, D.P., Holly, A.C., Lahsaee, S. and Dellaire, G. (2015) Connecting the speckles: Splicing kinases and their role in tumorigenesis and treatment response. *Nucleus (Austin, Tex.)*. 6 (4), pp.279-288.

Czubaty, A. and Piekielko-Witkowska, A. (2017) Protein Kinases that phosphorylate splicing factors: Roles in cancer development, progression and possible therapeutic options. *The International Journal of Biochemistry & Cell Biology*. S1357-2725(17), pp.30122-X.

Daniilidou, M., Tsolaki, M., Giannakouros, T. and Nikolakaki, E. (2011) Detection of elevated antibodies against SR protein kinase 1 in the serum of Alzheimer's disease patients. *Journal of Neuroimmunology*. 238 (1-2), pp.67-72.

Das, R., Yu, J., Zhang, Z., Gygi, M.P., Krainer, A.R., Gygi, S.P. and Reed, R. (2007) SR proteins function in coupling RNAP II transcription to pre-mRNA splicing. *Molecular Cell*. 26 (6), pp.867-881.

Das, S. and Krainer, A.R. (2014) Emerging functions of SRSF1, splicing factor and oncoprotein, in RNA metabolism and cancer. *Molecular Cancer Research : MCR*. 12 (9), pp.1195-1204.

de Almeida, R.A. and O'Keefe, R.T. (2015) The NineTeen Complex (NTC) and NTC-associated proteins as targets for spliceosomal ATPase action during pre-mRNA splicing. *RNA Biology*. 12 (2), pp.109-114.

Deininger, M.W., Goldman, J.M. and Melo, J.V. (2000) The molecular biology of chronic myeloid leukemia. *Blood*. 96 (10), pp.3343-3356.

Deininger, M.W. and Druker, B.J. (2003) Specific targeted therapy of chronic myelogenous leukemia with imatinib. *Pharmacological Reviews*. 55 (3), pp.401-423.

Dhillon, A.S., Hagan, S., Rath, O. and Kolch, W. (2007) MAP kinase signalling pathways in cancer. *Oncogene*. 26 (22), pp.3279-3290.

Dienstmann, R., Rodon, J., Serra, V. and Tabernero, J. (2014) Picking the point of inhibition: a comparative review of PI3K/AKT/mTOR pathway inhibitors. *Molecular Cancer Therapeutics*. 13 (5), pp.1021-1031.

Ding, J.H., Zhong, X.Y., Hagopian, J.C., Cruz, M.M., Ghosh, G., Feramisco, J., Adams, J.A. and Fu, X.D. (2006) Regulated cellular partitioning of SR protein-specific kinases in mammalian cells. *Molecular Biology of the Cell*. 17 (2), pp.876-885.

Dominguez, D., Tsai, Y.H., Weatheritt, R., Wang, Y., Blencowe, B.J. and Wang, Z. (2016) An extensive program of periodic alternative splicing linked to cell cycle progression. *eLife*. 5 pp.10.7554/eLife.10288.

Dong, Z., Noda, K., Kanda, A., Fukuhara, J., Ando, R., Murata, M., Saito, W., Hagiwara, M. and Ishida, S. (2013) Specific inhibition of serine/arginine-rich protein kinase attenuates choroidal neovascularization. *Molecular Vision*. 19 pp.536-543.

Dreumont, N., Hardy, S., Behm-Ansmant, I., Kister, L., Branlant, C., Stevenin, J. and Bourgeois, C.F. (2010) Antagonistic factors control the unproductive splicing of SC35 terminal intron. *Nucleic Acids Research*. 38 (4), pp.1353-1366.

E1Hady, A.K., Abdel-Halim, M., Abadi, A.H. and Engel, M. (2017) Development of Selective Clk1 and -4 Inhibitors for Cellular Depletion of Cancer-Relevant Proteins. Journal of Medicinal Chemistry. 60 (13), pp.5377-5391.

Early, P., Rogers, J., Davis, M., Calame, K., Bond, M., Wall, R. and Hood, L. (1980) Two mRNAs can be produced from a single immunoglobulin mu gene by alternative RNA processing pathways. *Cell*. 20 (2), pp.313-319.

Edinger, A.L. and Thompson, C.B. (2004) Death by design: apoptosis, necrosis and autophagy. *Current Opinion in Cell Biology*. 16 (6), pp.663-669.

Edmond, V., Moysan, E., Khochbin, S., Matthias, P., Brambilla, C., Brambilla, E., Gazzeri, S. and Eymin, B. (2011) Acetylation and phosphorylation of SRSF2 control cell fate decision in response to cisplatin. *The EMBO Journal*. 30 (3), pp.510-523.

Egorin M.J., Molimard M. and Mahon F.X / Novartis Oncology, 2007. *Imatinib blood level testing: a new initiative in the era of targeted therapy for Ph+ CML*. EUTOS: European Treatment and Outcome Study.

Fausel, C. (2007) Targeted chronic myeloid leukemia therapy: Seeking a cure. *American Journal of Health-System Pharmacy : AJHP : Official Journal of the American Society of Health-System Pharmacists*. 64 (24 Suppl 15), pp.S9-15.

Fava, C., Rege-Cambrin, G. and Saglio, G. (2015) The choice of first-line chronic myelogenous leukemia treatment. *Annals of Hematology*. 94 Suppl 2 pp.S123-31.

Favaloro, B., Allocati, N., Graziano, V., Di Ilio, C. and De Laurenzi, V. (2012) Role of apoptosis in disease. *Aging*. 4 (5), pp.330-349.

Fedorov, O., Huber, K., Eisenreich, A., Filippakopoulos, P., King, O., Bullock, A.N., Szklarczyk, D., Jensen, L.J., Fabbro, D., Trappe, J., Rauch, U., Bracher, F. and Knapp, S. (2011) Specific CLK inhibitors from a novel chemotype for regulation of alternative splicing. *Chemistry & Biology*. 18 (1), pp.67-76.

Fiszbein, A. and Kornblihtt, A.R. (2016) Histone methylation, alternative splicing and neuronal differentiation. *Neurogenesis (Austin, Tex.)*. 3 (1), pp.e1204844.

Fortunel, N.O., Hatzfeld, A. and Hatzfeld, J.A. (2000) Transforming growth factor-beta: pleiotropic role in the regulation of hematopoiesis. *Blood*. 96 (6), pp.2022-2036.

Fukuhara, T., Hosoya, T., Shimizu, S., Sumi, K., Oshiro, T., Yoshinaka, Y., Suzuki, M., Yamamoto, N., Herzenberg, L.A., Herzenberg, L.A. and Hagiwara, M. (2006) Utilization of host SR protein kinases and RNA-splicing machinery during viral replication. *Proceedings of the National Academy of Sciences of the United States of America*. 103 (30), pp.11329-11333.

Gaddy, C.E., Wong, D.S., Markowitz-Shulman, A. and Colberg-Poley, A.M. (2010) Regulation of the subcellular distribution of key cellular RNA-processing factors during permissive human cytomegalovirus infection. *The Journal of General Virology*. 91 (Pt 6), pp.1547-1559.

Gammons, M.V., Fedorov, O., Ivison, D., Du, C., Clark, T., Hopkins, C., Hagiwara, M., Dick, A.D., Cox, R., Harper, S.J., Hancox, J.C., Knapp, S. and Bates, D.O. (2013) Topical antiangiogenic SRPK1 inhibitors reduce choroidal neovascularization in rodent models of exudative AMD. *Investigative Ophthalmology & Visual Science*. 54 (9), pp.6052-6062.

Garcia-Sacristan, A., Fernandez-Nestosa, M.J., Hernandez, P., Schvartzman, J.B. and Krimer, D.B. (2005) Protein kinase clk/STY is differentially regulated during erythroleukemia cell differentiation: a bias toward the skipped splice variant characterizes postcommitment stages. *Cell Research*. 15 (7), pp.495-503.

Ghosh, G. and Adams, J.A. (2011) Phosphorylation mechanism and structure of serine-arginine protein kinases. *The FEBS Journal*. 278 (4), pp.587-597.

Giles, F.J., Cortes, J.E., Kantarjian, H.M. and O'Brien, S.M. (2004) Accelerated and blastic phases of chronic myelogenous leukemia. *Hematology/Oncology Clinics of North America*. 18 (3), pp.753-74, xii.

Goncalves, V. and Jordan, P. (2015) Posttranscriptional Regulation of Splicing Factor SRSF1 and Its Role in Cancer Cell Biology. *BioMed Research International*. 2015 pp.287048.

Gowda, R., Madhunapantula, S.V., Kuzu, O.F., Sharma, A. and Robertson, G.P. (2014) Targeting multiple key signaling pathways in melanoma using leelamine. *Molecular Cancer Therapeutics*. 13 (7), pp.1679-1689.

Gross, S., Rahal, R., Stransky, N., Lengauer, C. and Hoeflich, K.P. (2015) Targeting cancer with kinase inhibitors. *The Journal of Clinical Investigation*. 125 (5), pp.1780-1789.

Hadano, S., Nasir, J., Nichol, K., Rasper, D.M., Vaillancourt, J.P., Sherer, S.W., Beatty, B.G., Ikeda, J.E., Nicholson, D.W. and Hayden, M.R. (1999) Genomic organization of the human caspase-9 gene on Chromosome 1p36. 1-p36.3. *Mammalian Genome : Official Journal of the International Mammalian Genome Society*. 10 (7), pp.757-760.

Hehlmann, R. (2012) How I treat CML blast crisis. *Blood*. 120 (4), pp.737-747.

Henkes, M., van der Kuip, H. and Aulitzky, W.E. (2008) Therapeutic options for chronic myeloid leukemia: focus on imatinib (Glivec, Gleevectrade mark). *Therapeutics and Clinical Risk Management*. 4 (1), pp.163-187.

Hoffbrand, A.V., Catovsky, D., Tuddenham, E.G.D. and Green, A.R. (2011) *Postgraduate Haematology*. 6th ed. West Sussex, UK: Blackwell Publishing Ltd.

Huang, Y. and Steitz, J.A. (2005) SRprises along a messenger's journey. *Molecular Cell*. 17 (5), pp.613-615.

Huang, P.K. and Sanjay, S. (2011) Visual Disturbance as the first Symptom of Chronic Myeloid Leukemia. *Middle East African Journal of Ophthalmology*. 18 (4), pp.336-338.

Huang, C.T., Yu, S.H., Chen, Y.H. and Lin, S.F. (2016) Cardiac tamponade as a symptom of the blast crisis of chronic myeloid leukemia. *The Kaohsiung Journal of Medical Sciences*. 32 (3), pp.160-161.

Jain, P., Das, V.N., Ranjan, A., Chaudhary, R. and Pandey, K. (2013) Comparative study for the efficacy, safety and quality of life in patients of chronic myeloid leukemia treated with Imatinib or Hydroxyurea. *Journal of Research in Pharmacy Practice*. 2 (4), pp.156-161.

Jain, P., Karthikeyan, C., Moorthy, N.S., Waiker, D.K., Jain, A.K. and Trivedi, P. (2014) Human CDC2-like kinase 1 (CLK1): a novel target for Alzheimer's disease. *Current Drug Targets*. 15 (5), pp.539-550.

Jang, S.W., Yang, S.J., Ehlen, A., Dong, S., Khoury, H., Chen, J., Persson, J.L. and Ye, K. (2008) Serine/arginine protein-specific kinase 2 promotes leukemia cell proliferation by phosphorylating acinus and regulating cyclin A1. *Cancer Research*. 68 (12), pp.4559-4570.

Jones, D.(.). (2010) *Neoplastic Hematopathology Experimental and Clinical Approaches*. 1st ed. Human Press.

Kang, C.M., Babicky, M.L. and Lowy, A.M. (2014) The RON receptor tyrosine kinase in pancreatic cancer pathogenesis and its potential implications for future targeted therapies. *Pancreas*. 43 (2), pp.183-189.

Karakama, Y., Sakamoto, N., Itsui, Y., Nakagawa, M., Tasaka-Fujita, M., Nishimura-Sakurai, Y., Kakinuma, S., Oooka, M., Azuma, S., Tsuchiya, K., Onogi, H., Hagiwara, M. and Watanabe, M. (2010) Inhibition of hepatitis C virus replication by a specific inhibitor of serine-arginine-rich protein kinase. *Antimicrobial Agents and Chemotherapy*. 54 (8), pp.3179-3186.

Karni, R., de Stanchina, E., Lowe, S.W., Sinha, R., Mu, D. and Krainer, A.R. (2007) The gene encoding the splicing factor SF2/ASF is a proto-oncogene. *Nature Structural & Molecular Biology*. 14 (3), pp.185-193.

Kedzierska, H. and Piekielko- Witkowska, A., (2017) Splicing factors of SR and hnRNP families as regulators of apoptosis in cancer. *Cancer Letters*. 396 pp.53-65.

Kershaw, C.J., Barrass, J.D., Beggs, J.D. and O'Keefe, R.T. (2009) Mutations in the U5 snRNA result in altered splicing of subsets of pre-mRNAs and reduced stability of Prp8. *RNA (New York, N.Y.)*. 15 (7), pp.1292-1304.

Kim, Y.D., Lee, J.Y., Oh, K.M., Araki, M., Araki, K., Yamamura, K. and Jun, C.D. (2011) NSrp70 is a novel nuclear speckle-related protein that modulates alternative pre-mRNA splicing in vivo. *Nucleic Acids Research*. 39 (10), pp.4300-4314.

Knudson, A.G., Jr (1971) Mutation and cancer: statistical study of retinoblastoma. *Proceedings of the National Academy of Sciences of the United States of America*. 68 (4), pp.820-823.

Kokate, P., Dalvi, R. and Mandava, S. (2015) A complex three-way translocation with deletion of the TP53 gene in a blast crisis chronic myeloid leukemia patient. *Journal of Cancer Research and Therapeutics*. 11 (4), pp.1037-1482.144372.

Komeno, Y., Yan, M., Matsuura, S., Lam, K., Lo, M.C., Huang, Y.J., Tenen, D.G., Downing, J.R. and Zhang, D.E. (2014) Runx1 exon 6-related alternative splicing isoforms differentially regulate hematopoiesis in mice. *Blood*. 123 (24), pp.3760-3769.

Koo, H.H. (2011) Philadelphia chromosome-positive acute lymphoblastic leukemia in childhood. *Korean Journal of Pediatrics*. 54 (3), pp.106-110.

Krysko, D.V., Vanden Berghe, T., Parthoens, E., D'Herde, K. and Vandenabeele, P. (2008) Methods for distinguishing apoptotic from necrotic cells and measuring their clearance. *Methods in Enzymology*. 442 pp.307-341.

Lasho, T.L., Jimma, T., Finke, C.M., Patnaik, M., Hanson, C.A., Ketterling, R.P., Pardanani, A. and Tefferi, A. (2012) SRSF2 mutations in primary myelofibrosis: significant clustering with IDH mutations and independent association with inferior overall and leukemia-free survival. *Blood*. 120 (20), pp.4168-4171.

Lemmon, M.A. and Schlessinger, J. (2010) Cell signaling by receptor tyrosine kinases. *Cell*. 141 (7), pp.1117-1134.

Leonis, M.A., Thobe, M.N. and Waltz, S.E. (2007) Ron-receptor tyrosine kinase in tumorigenesis and metastasis. *Future Oncology (London, England)*. 3 (4), pp.441-448.

Li, S., Ilaria, R.L.,Jr, Million, R.P., Daley, G.Q. and Van Etten, R.A. (1999) The P190, P210, and P230 forms of the BCR/ABL oncogene induce a similar chronic myeloid leukemia-like syndrome in mice but have different lymphoid leukemogenic activity. *The Journal of Experimental Medicine*. 189 (9), pp.1399-1412.

Liu, Y., Conaway, L., Rutherford Bethard, J., Al-Ayoubi, A.M., Thompson Bradley, A., Zheng, H., Weed, S.A. and Eblen, S.T. (2013) Phosphorylation of the alternative mRNA splicing factor 45 (SPF45) by Clk1 regulates its splice site utilization, cell migration and invasion. *Nucleic Acids Research*. 41 (9), pp.4949-4962.

Long, J.C. and Caceres, J.F. (2009) The SR protein family of splicing factors: master regulators of gene expression. *The Biochemical Journal*. 417 (1), pp.15-27.

Loomis, R.J., Naoe, Y., Parker, J.B., Savic, V., Bozovsky, M.R., Macfarlan, T., Manley, J.L. and Chakravarti, D. (2009) Chromatin binding of SRp20 and ASF/SF2 and dissociation from mitotic chromosomes is modulated by histone H3 serine 10 phosphorylation. *Molecular Cell*. 33 (4), pp.450-461.

Ma, C.T., Ghosh, G., Fu, X.D. and Adams, J.A. (2010) Mechanism of dephosphorylation of the SR protein ASF/SF2 by protein phosphatase 1. *Journal of Molecular Biology*. 403 (3), pp.386-404.

Maioral, M.F., Bubniak, L.D., Marzarotto, M.A., De Moraes, A.C., Leal, P., Nunes, R., Yunes, R.A. and Santos-Silva, M.C. (2016) Molecular Cytotoxic Mechanisms of 1-(3,4,5-Trihydroxyphenyl)-dodecylbenzoate in Human Leukemia Cell Lines. *Indian Journal of Pharmaceutical Sciences*. 78 (1), pp.120-128.

Mamman, A.I., Yusuf, A.J., Aminu, S., Sheikh, T.L. and Hassan, D.A. (2009) Severe depression following a-interferon usage in a patient with chronic myeloid leukemia. *African Health Sciences*. 9 (1), pp.54-56.

Manley, J.L. and Krainer, A.R. (2010) A rational nomenclature for serine/arginine-rich protein splicing factors (SR proteins). *Genes & Development*. 24 (11), pp.1073-1074.

Mariano, M., Hartmann, R.W. and Engel, M. (2016) Systematic diversification of benzylidene heterocycles yields novel inhibitor scaffolds selective for Dyrk1A, Clk1 and CK2. *European Journal of Medicinal Chemistry*. 112 pp.209-216.

Martinez-Montiel, N., Rosas-Murrieta, N.H., Martinez-Montiel, M., Gaspariano-Cholula, M.P. and Martinez-Contreras, R.D. (2016) Microbial and Natural Metabolites That Inhibit Splicing: A Powerful Alternative for Cancer Treatment. *BioMed Research International*. 2016 pp.3681094.

Mavrou, A., Brakspear, K., Hamdollah-Zadeh, M., Damodaran, G., Babaei-Jadidi, R., Oxley, J., Gillatt, D.A., Ladomery, M.R., Harper, S.J., Bates, D.O. and Oltean, S. (2015) Serine-arginine protein kinase 1 (SRPK1) inhibition as a potential novel targeted therapeutic strategy in prostate cancer. *Oncogene*. 34 (33), pp.4311-4319.

Mavrou, A. and Oltean, S. (2016) SRPK1 inhibition in prostate cancer: A novel anti-angiogenic treatment through modulation of VEGF alternative splicing. *Pharmacological Research*. 107 pp.276-281.

Merdzhanova, G., Gout, S., Keramidas, M., Edmond, V., Coll, J.L., Brambilla, C., Brambilla, E., Gazzeri, S. and Eymin, B. (2010) The transcription factor E2F1 and the SR protein SC35 control the ratio of pro-angiogenic versus antiangiogenic isoforms of vascular endothelial growth factor-A to inhibit neovascularization in vivo. *Oncogene*. 29 (39), pp.5392-5403.

Michlewski, G., Sanford, J.R. and Caceres, J.F. (2008) The splicing factor SF2/ASF regulates translation initiation by enhancing phosphorylation of 4E-BP1. *Molecular Cell*. 30 (2), pp.179-189.

Mizutani, S., Yoshida, T., Zhao, X., Nimer, S.D., Taniwaki, M. and Okuda, T. (2015) Loss of RUNX1/AML1 arginine-methylation impairs peripheral T cell homeostasis. *British Journal of Haematology*. 170 (6), pp.859-873.

Morooka, S., Hoshina, M., Kii, I., Okabe, T., Kojima, H., Inoue, N., Okuno, Y., Denawa, M., Yoshida, S., Fukuhara, J., Ninomiya, K., Ikura, T., Furuya, T., Nagano, T., Noda, K., Ishida, S., Hosoya, T., Ito, N., Yoshimura, N., Hagiwara, M. (2015) Identification of a Dual Inhibitor of SRPK1 and CK2 That Attenuates Pathological Angiogenesis of Macular Degeneration in Mice. *Molecular Pharmacology*. 88 (2), pp.316-325.

Morrison, S.J., Uchida, N. and Weissman, I.L. (1995) The biology of hematopoietic stem cells. *Annual Review of Cell and Developmental Biology*. 11 pp.35-71.

Moulton, V.R., Gillooly, A.R. and Tsokos, G.C. (2014) Ubiquitination regulates expression of the serine/arginine-rich splicing factor 1 (SRSF1) in normal and systemic lupus erythematosus (SLE) T cells. *The Journal of Biological Chemistry*. 289 (7), pp.4126-4134.

Muraki, M., Ohkawara, B., Hosoya, T., Onogi, H., Koizumi, J., Koizumi, T., Sumi, K., Yomoda, J., Murray, M.V., Kimura, H., Furuichi, K., Shibuya, H., Krainer, A.R., Suzuki, M. and Hagiwara, M. (2004) Manipulation of alternative splicing by a newly developed inhibitor of Clks. *The Journal of Biological Chemistry*. 279 (23), pp.24246-24254.

Naka, K., Ishihara, K., Jomen, Y., Jin, C.H., Kim, D.H., Gu, Y.K., Jeong, E.S., Li, S., Krause, D.S., Kim, D.W., Bae, E., Takihara, Y., Hirao, A., Oshima, H., Oshima, M., Ooshima, A., Sheen, Y.Y., Kim, S.J. and Kim, D.K. (2016) Novel oral transforming growth factor-beta signaling inhibitor EW-7197 eradicates CML-initiating cells. *Cancer Science*. 107 (2), pp.140-148.

Nancollis, V., Ruckshanthi, J.P., Frazer, L.N. and O'Keefe, R.T. (2013) The U5 snRNA internal loop 1 is a platform for Brr2, Snu114 and Prp8 protein binding during U5 snRNP assembly. *Journal of Cellular Biochemistry*. 114 (12), pp.2770-2784.

Naro, C. and Sette, C. (2013) Phosphorylation-mediated regulation of alternative splicing in cancer. *International Journal of Cell Biology*. 2013 pp.151839.

Ngo, J.C., Chakrabarti, S., Ding, J.H., Velazquez-Dones, A., Nolen, B., Aubol, B.E., Adams, J.A., Fu, X.D. and Ghosh, G. (2005) Interplay between SRPK and Clk/Sty kinases in phosphorylation of the splicing factor ASF/SF2 is regulated by a docking motif in ASF/SF2. *Molecular Cell*. 20 (1), pp.77-89.

Novak, M., Zegura, B., Baebler, S., Stern, A., Rotter, A., Stare, K. and Filipic, M. (2015) Influence of selected anti-cancer drugs on the induction of DNA double-strand breaks and changes in gene expression in human hepatoma HepG2 cells. *Environmental Science and Pollution Research International*.

Nowak, D.G., Woolard, J., Amin, E.M., Konopatskaya, O., Saleem, M.A., Churchill, A.J., Ladomery, M.R., Harper, S.J. and Bates, D.O. (2008) Expression of pro- and anti-angiogenic isoforms of VEGF is differentially regulated by splicing and growth factors. *Journal of Cell Science*. 121 (Pt 20), pp.3487-3495.

Nowak, D.G., Amin, E.M., Rennel, E.S., Hoareau-Aveilla, C., Gammons, M., Damodoran, G., Hagiwara, M., Harper, S.J., Woolard, J., Ladomery, M.R. and Bates, D.O. (2010) Regulation of vascular endothelial growth factor (VEGF) splicing from pro-angiogenic to anti-angiogenic isoforms: a novel therapeutic strategy for angiogenesis. *The Journal of Biological Chemistry*. 285 (8), pp.5532-5540.

NOWELL, P.C. and HUNGERFORD, D.A. (1960) Chromosome studies on normal and leukemic human leukocytes. *Journal of the National Cancer Institute*. 25 pp.85-109.

O'Hare, T., Deininger, M.W., Eide, C.A., Clackson, T. and Druker, B.J. (2011) Targeting the BCR-ABL signaling pathway in therapy-resistant Philadelphia chromosome-positive leukemia. *Clinical Cancer Research : An Official Journal of the American Association for Cancer Research*. 17 (2), pp.212-221.

O'Keefe, R.T., Mayeda, A., Sadowski, C.L., Krainer, A.R. and Spector, D.L. (1994) Disruption of pre-mRNA splicing in vivo results in reorganization of splicing factors. *The Journal of Cell Biology*. 124 (3), pp.249-260.

O'Keefe, R.T. and Newman, A.J. (1998) Functional analysis of the U5 snRNA loop 1 in the second catalytic step of yeast pre-mRNA splicing. *The EMBO Journal*. 17 (2), pp.565-574.

Oltean, S., Gammons, M., Hulse, R., Hamdollah-Zadeh, M., Mavrou, A., Donaldson, L., Salmon, A.H., Harper, S.J., Ladomery, M.R. and Bates, D.O. (2012) SRPK1 inhibition in vivo: modulation of VEGF splicing and potential treatment for multiple diseases. *Biochemical Society Transactions*. 40 (4), pp.831-835.

Pan, Q., Shai, O., Lee, L.J., Frey, B.J. and Blencowe, B.J. (2008) Deep surveying of alternative splicing complexity in the human transcriptome by high-throughput sequencing. *Nature Genetics*. 40 (12), pp.1413-1415.

Park, I.K., Mundy-Bosse, B., Whitman, S.P., Zhang, X., Warner, S.L., Bearss, D.J., Blum, W., Marcucci, G. and Caligiuri, M.A. (2015) Receptor tyrosine kinase Ax1 is required for resistance of leukemic cells to FLT3-targeted therapy in acute myeloid leukemia. *Leukemia*. 29 (12), pp.2382-2389.

Pene-Dumitrescu, T., Peterson, L.F., Donato, N.J. and Smithgall, T.E. (2008) An inhibitor-resistant mutant of Hck protects CML cells against the antiproliferative and apoptotic effects of the broad-spectrum Src family kinase inhibitor A-419259. *Oncogene*. 27 (56), pp.7055-7069.

Philips, S.T., Hildenbrand, Z.L., Oravecz-Wilson, K.I., Foley, S.B., Mgbemena, V.E. and Ross, T.S. (2014) Toward a therapeutic reduction of imatinib refractory myeloproliferative neoplasm-initiating cells. *Oncogene*. 33 (46), pp.5379-5390.

Placzek, W.J., Wei, J., Kitada, S., Zhai, D., Reed, J.C. and Pellecchia, M. (2010) A survey of the anti-apoptotic Bcl-2 subfamily expression in cancer types provides a platform to predict the efficacy of Bcl-2 antagonists in cancer therapy. *Cell Death & Disease*. 1 pp.e40.

Porta, C., Paglino, C. and Mosca, A. (2014) Targeting PI3K/Akt/mTOR Signaling in Cancer. *Frontiers in Oncology*. 4 (64) pp.64.

Qu, X.H., Liu, J.L., Zhong, X.W., Li, X.I. and Zhang, Q.G. (2015) Insights into the roles of hnRNP A2/B1 and AXL in non-small cell lung cancer. *Oncology Letters*. 10 (3), pp.1677-1685.

Rea, D., Mirault, T., Cluzeau, T., Gautier, J.F., Guilhot, F., Dombret, H. and Messas, E. (2014) Early onset hypercholesterolemia induced by the 2nd-generation tyrosine kinase inhibitor nilotinib in patients with chronic phase-chronic myeloid leukemia. *Haematologica*. 99 (7), pp.1197-1203.

Renne, C., Willenbrock, K., Kuppers, R., Hansmann, M.L. and Brauninger, A. (2005) Autocrine- and paracrine-activated receptor tyrosine kinases in classic Hodgkin lymphoma. *Blood*. 105 (10), pp.4051-4059.

Roberts, P.J. and Der, C.J. (2007) Targeting the Raf-MEK-ERK mitogen-activated protein kinase cascade for the treatment of cancer. *Oncogene*. 26 (22), pp.3291-3310.

Rogers, G., Hoyle, M., Thompson Coon, J., Moxham, T., Liu, Z., Pitt, M. and Stein, K. (2012) Dasatinib and nilotinib for imatinib-resistant or -intolerant chronic myeloid leukaemia: a systematic review and economic evaluation. *Health Technology Assessment (Winchester, England)*. 16 (22), pp.1-410.

Roy, M., Sarkar, R., Mukherjee, A. and Mukherjee, S. (2015) Inhibition of crosstalk between Bcr-Abl and PKC signaling by PEITC, augments imatinib sensitivity in chronic myelogenous leukemia cells. *Chemico-Biological Interactions*. 242 pp.195-201.

Rudner, D.Z., Breger, K.S., Kanaar, R., Adams, M.D. and Rio, D.C. (1998) RNA binding activity of heterodimeric splicing factor U2AF: at least one RS domain is required for high-affinity binding. *Molecular and Cellular Biology*. 18 (7), pp.4004-4011.

Sakuma, M., Iida, K. and Hagiwara, M. (2015) Deciphering targeting rules of splicing modulator compounds: case of TG003. *BMC Molecular Biology*. 16 pp.16-015-0044-6.

Salizzato, V., Borgo, C., Cesaro, L., Pinna, L.A. and Donella-Deana, A. (2016) Inhibition of protein kinase CK2 by CX-5011 counteracts imatinib-resistance

preventing rpS6 phosphorylation in chronic myeloid leukaemia cells: new combined therapeutic strategies. *Oncotarget*. 7 (14), pp.18204.

Sawyers, C.L., Hochhaus, A., Feldman, E., Goldman, J.M., Miller, C.B., Ottmann, O.G., Schiffer, C.A., Talpaz, M., Guilhot, F., Deininger, M.W., Fischer, T., O'Brien, S.G., Stone, R.M., Gambacorti-Passerini, C.B., Russell, N.H., Reiffers, J.J., Shea, T.C., Chapuis, B., Coutre, S., Tura, S., Morra, E., Larson, R.A., Saven, A., Peschel, C., Gratwohl, A., Mandelli, F., Ben-Am, M., Gathmann, I., Capdeville, R., Paquette, R.L. and Druker, B.J. (2002) Imatinib induces hematologic and cytogenetic responses in patients with chronic myelogenous leukemia in myeloid blast crisis: results of a phase II study. *Blood*. 99 (10), pp.3530-3539.

Shao, L., Wang, Y., Chang, J., Luo, Y., Meng, A. and Zhou, D. (2013) Hematopoietic stem cell senescence and cancer therapy-induced long-term bone marrow injury. *Translational Cancer Research*. 2 (5), pp.397-411.

Sheng, Z., Wang, S.Z. and Green, M.R. (2009) Transcription and signalling pathways involved in BCR-ABL-mediated misregulation of 24p3 and 24p3R. *The EMBO Journal*. 28 (7), pp.866-876.

Shepard, P.J. and Hertel, K.J. (2009) The SR protein family. *Genome Biology*. 10 (10), pp.242-2009-10-10-242. Epub 2009 Oct 27.

Shultz, J.C., Goehe, R.W., Murudkar, C.S., Wijesinghe, D.S., Mayton, E.K., Massiello, A., Hawkins, A.J., Mukerjee, P., Pinkerman, R.L., Park, M.A. and Chalfant, C.E. (2011) SRSF1 regulates the alternative splicing of caspase 9 via a novel intronic splicing enhancer affecting the chemotherapeutic sensitivity of non-small cell lung cancer cells. *Molecular Cancer Research : MCR*. 9 (7), pp.889-900.

Sinha, R., Allemand, E., Zhang, Z., Karni, R., Myers, M.P. and Krainer, A.R. (2010) Arginine methylation controls the subcellular localization and functions of the oncoprotein splicing factor SF2/ASF. *Molecular and Cellular Biology*. 30 (11), pp.2762-2774.

Siqueira, R.P., Barbosa Ede, A., Poleto, M.D., Righetto, G.L., Seraphim, T.V., Salgado, R.L., Ferreira, J.G., Barros, M.V., de Oliveira, L.L., Laranjeira, A.B., Almeida, M.R., Junior, A.S., Fietto, J.L., Kobarg, J., de Oliveira, E.B., Teixeira, R.R., Borges, J.C., Yunes, J.A. and Bressan, G.C. (2015) Potential Antileukemia Effect and Structural Analyses of SRPK Inhibition by N-(2-(Piperidin-1-yl)-5-(Trifluoromethyl)Phenyl)Isonicotinamide (SRPIN340). *PloS One*. 10 (8), pp.e0134882.

Siqueira, R.P., Barros, M.V.A., Barbosa, E.A.A., Onofre, T.S., Goncalves, V.H.S., Pereira, H.S., Silva Junior, A., de Oliveira, L.L., Almeida, M.R., Fietto, J.L.R., Teixeira, R.R. and Bressan, G.C. (2017) Trifluoromethyl arylamides with antileukemia effect and intracellular inhibitory activity over serine/arginine-rich protein kinases (SRPKs). *European Journal of Medicinal Chemistry*. 134 pp.97-109.

Tamascar, I. and Ramanarayanan, J. (2009) Targeted treatment of chronic myeloid leukemia: role of imatinib. *OncoTargets and Therapy*. 2 pp.63-71.

Uchida, N., Hanawa, H., Dan, K., Inokuchi, K. and Shimada, T. (2009) Leukemogenesis of b2a2-type p210 BCR/ABL in a bone marrow transplantation mouse model using a lentiviral vector. *Journal of Nippon Medical School = Nippon Ika Daigaku Zasshi*. 76 (3), pp.134-147.

Vu, N.T., Park, M.A., Shultz, J.C., Goehe, R.W., Hoeferlin, L.A., Shultz, M.D., Smith, S.A., Lynch, K.W. and Chalfant, C.E. (2013) hnRNP U enhances caspase-9 splicing and is modulated by AKT-dependent phosphorylation of hnRNP L. *The Journal of Biological Chemistry*. 288 (12), pp.8575-8584.

Wang, E.T., Sandberg, R., Luo, S., Khrebtukova, I., Zhang, L., Mayr, C., Kingsmore, S.F., Schroth, G.P. and Burge, C.B. (2008) Alternative isoform regulation in human tissue transcriptomes. *Nature*. 456 (7221), pp.470-476.

Wang, L., Huang, G., Zhao, X., Hatlen, M.A., Vu, L., Liu, F. and Nimer, S.D. (2009) Post-translational modifications of Runx1 regulate its activity in the cell. *Blood Cells, Molecules & Diseases*. 43 (1), pp.30-34.

Wang, M.H., Zhang, R., Zhou, Y.Q. and Yao, H.P. (2013) Pathogenesis of RON receptor tyrosine kinase in cancer cells: activation mechanism, functional crosstalk, and signaling addiction. *Journal of Biomedical Research*. 27 (5), pp.345-356.

Wang, P., Zhou, Z., Hu, A., Ponte de Albuquerque, C., Zhou, Y., Hong, L., Sierecki, E., Ajiro, M., Kruhlak, M., Harris, C., Guan, K.L., Zheng, Z.M., Newton, A.C., Sun, P., Zhou, H. and Fu, X.D. (2014) Both decreased and increased SRPK1 levels promote cancer by interfering with PHLPP-mediated dephosphorylation of Akt. *Molecular Cell*. 54 (3), pp.378-391.

Wang, Y.C., Peterson, S.E. and Loring, J.F. (2014) Protein post-translational modifications and regulation of pluripotency in human stem cells. *Cell Research*. 24 (2), pp.143-160.

Wang, Y., Liu, J., Huang, B.O., Xu, Y.M., Li, J., Huang, L.F., Lin, J., Zhang, J., Min, Q.H., Yang, W.M. and Wang, X.Z. (2015) Mechanism of alternative splicing and its regulation. *Biomedical Reports*. 3 (2), pp.152-158.

Warmuth, M., Danhauser-Riedl, S. and Hallek, M. (1999) Molecular pathogenesis of chronic myeloid leukemia: implications for new therapeutic strategies. *Annals of Hematology*. 78 (2), pp.49-64.

Weatheritt, R.J., Sterne-Weiler, T. and Blencowe, B.J. (2016) The ribosome-engaged landscape of alternative splicing. *Nature Structural & Molecular Biology*. 23 (12), pp.1117-1123.

Weisberg, E.L., Puissant, A., Stone, R., Sattler, M., Buhrlage, S.J., Yang, J., Manley, P.W., Meng, C., Buonopane, M., Daley, J.F., Lazo, S., Wright, R., Weinstock, D.M., Christie, A.L., Stegmaier, K. and Griffin, J.D. (2017) Characterization of midostaurin as a dual inhibitor of FLT3 and SYK and potentiation of FLT3 inhibiton against FLT3-ITD-driven leukemia harbouring activated SYK kinase. *Oncotarget*.

Wieczorek, A. and Uharek, L. (2016) Management of Chronic Myeloid Leukemia Patients Resistant to Tyrosine Kinase Inhibitors Treatment. *Biomarker Insights*. 10 (Suppl 3), pp.49-54.

Wu, F., Li, J., Du, X., Zhang, W., Lei, P. and Zhang, Q. (2017) Chimeric antibody targeting SRPK-1 in the treatment of non-small cell lung cancer by inhibiting growth, migration and invasion. *Molecular Medicine Reports*. 16 (2), pp.2121-2127.

Wu, L.E., Gomes, A.P. and Sinclair, D.A. (2014) Geroncogenesis: metabolic changes during aging as a driver of tumorigenesis. *Cancer Cell*. 25 (1), pp.12-19.

Wu, X. and Hurst, L.D. (2016) Determinants of the Usage of Splice-Associated cis-Motifs Predict the Distribution of Human Pathogenic SNPs. *Molecular Biology and Evolution*. 33 (2), pp.518-529.

Xiao, Y., Ramiscal, J., Kowanetz, K., Del Nagro, C., Malek, S., Evangelista, M., Blackwood, E., Jackson, P.K. and O'Brien, T. (2013) Identification of preferred chemotherapeutics for combining with a CHK1 inhibitor. *Molecular Cancer Therapeutics*. 12 (11), pp.2285-2295.

Xu, Y., Bian, X., Sang, Y., Li, Y., Li, D., Cheng, W., Yin, Y., Ju, H. and Ding, S. (2016) Bis-three-way junction nanostructure and DNA machineries for ultrasensitive and specific detection of BCR/ABL fusion gene by chemiluminescence imaging. *Scientific Reports*. 6 pp.32370.

Yang, M., Wang, H., Zhou, M., Liu, W., Kuang, P., Liang, H. and Yuan, Q. (2016) The natural compound sulforaphene, as a novel anticancer reagent, targeting PI3K-AKT signaling pathway in lung cancer. *Oncotarget*. 7 (47), pp.76656-76666.

Yao, H.P., Zhou, Y.Q., Zhang, R. and Wang, M.H. (2013) MSP-RON signalling in cancer: pathogenesis and therapeutic potential. *Nature Reviews.Cancer*. 13 (7), pp.466-481.

Yeh, J.J., Routh, E.D., Rubinas, T., Peacock, J., Martin, T.D., Shen, X.J., Sandler, R.S., Kim, H.J., Keku, T.O. and Der, C.J. (2009) KRAS/BRAF mutation status and ERK1/2 activation as biomarkers for MEK1/2 inhibitor therapy in colorectal cancer. *Molecular Cancer Therapeutics*. 8 (4), pp.834-843.

Yeung, D.T., Osborn, M.P., White, D.L., Branford, S., Braley, J., Herschtal, A., Kornhauser, M., Issa, S., Hiwase, D.K., Hertzberg, M., Schwarer, A.P., Filshie, R., Arthur, C.K., Kwan, Y.L., Trotman, J., Forsyth, C.J., Taper, J., Ross, D.M., Beresford, J., Tam, C., Mills, A.K., Grigg, A.P., Hughes, T.P. and Australasian Leukaemia and Lymphoma Group (2015) TIDEL-II: first-line use of imatinib in CML with early switch to nilotinib for failure to achieve time-dependent molecular targets. *Blood*. 125 (6), pp.915-923.

Yoon, S., Ryu, M.H., Yoo, C., Beck, M.Y., Ryoo, B.Y. and Kang, Y.K. (2013) Imatinib plasma monitoring-guided dose modification for managing imatinib-related toxicities in gastrointestinal stromal tumor patients. *Journal of Korean Medical Science*. 28 (8), pp.1248-1252.

Zeng, X., Zhao, H., Li, Y., Fan, J., Sun, Y., Wang, S., Wang, Z., Song, P. and Ju, D. (2015) Targeting Hedgehog signaling pathway and autophagy overcomes drug resistance of BCR-ABL-positive chronic myeloid leukemia. *Autophagy*. 11 (2), pp.355-372.

Zeng, F.C., Zeng, M.Q., Huang, L., Li, Y.L., Gao, B.M., Chen, J.J., Xue, R.Z. and Tang, Z.Y. (2016) Downregulation of VEGFA inhibits proliferation, promotes apoptosis, and suppresses migration and invasion of renal clear cell carcinoma. *OncoTargets and Therapy*. 9 pp.2131-2141.

Zhang, Z. and Krainer, A.R. (2004) Involvement of SR proteins in mRNA surveillance. *Molecular Cell*. 16 (4), pp.597-607.

Zhang, C.C. and Lodish, H.F. (2008) Cytokines regulating hematopoietic stem cell function. *Current Opinion in Hematology*. 15 (4), pp.307-311.

Zhang, Y., Kaplan-Lefko, P.J., Rex, K., Yang, Y., Moriguchi, J., Osgood, T., Mattson, B., Coxon, A., Reese, M., Kim, T.S., Lin, J., Chen, A., Burgess, T.L. and Dussault, I. (2008) Identification of a novel recepteur d'origine nantais/c-met small-molecule kinase inhibitor with antitumor activity in vivo. *Cancer Research*. 68 (16), pp.6680-6687.

Zhao, L.J., Wang, Y.Y., Li, G., Ma, L.Y., Xiong, S.M., Weng, X.Q., Zhang, W.N., Wu, B., Chen, Z. and Chen, S.J. (2012) Functional features of RUNX1 mutants in acute transformation of chronic myeloid leukemia and their contribution to inducing murine full-blown leukemia. *Blood*. 119 (12), pp.2873-2882.

Zhou, Z. and Fu, X.D. (2013) Regulation of splicing by SR proteins and SR protein-specific kinases. *Chromosoma*. 122 (3), pp.191-207.

Zhu, B., Zhang, J., Chen, J., Li, C. and Wang, X. (2015) Molecular biological characteristics of the recruitment of hematopoietic stem cells from bone marrow niche in chronic myeloid leukemia. *International Journal of Clinical and Experimental Pathology*. 8 (10), pp.12595-12607.

Ziegler, U., and Groscurth, P. (2004) Morphological features of cell death. *News in Physiological Sciences: An International Journal of Physiology Produced Jointly by the International Union of Physiological Sciences and the American Physiological Society*. 19 pp.124-128.

Zou, L., Zhang, H., Du, C., Liu, X., Zhu, S., Zhang, W., Li, Z., Gao, C., Zhao, X., Mei, M., Bao, S. and Zheng, H. (2012) Correlation of SRSF1 and PRMT1 expression with clinical status of pediatric acute lymphoblastic leukemia. *Journal of Hematology & Oncology*. 5 pp.42.

List of oral and poster presentations

1. Oral presentations

- **Alabouh, H.**, Ladomery, M., Oltean, S., Morse, R., (2012) *Alternative splicing in Leukaemia*. **School of Physiology, Pharmacoloy & Neuroscience** University of Bristol, UK on November 3rd, 2012.

- **Alabouh, H.**, Ladomery, M., Oltean, S., Morse, R., (2015) *Regulation of alternative splicing in leukaemia through targeting protein kinases SRPK1 and CLK1*. **Centre for Research in Biosciences Seminar** UWE, Bristol, UK on June 27th, 2015.

2. Poster presentations

- **Alabouh, H.**, Ladomery, M., Morse, R., Oltean, S., (2014) *Regulation of the alternative splicing of genes involved in leukaemia by the splice factor kinase CLK1* **Centre for Research in Biosciences Seminar** UWE, Bristol, UK on January 19th, 2014.

- **Alabouh, H.**, Ladomery, M., Oltean, S., Morse, R., (2015) *The effect of inhibiting the splice factor kinase Clk1 on alternative splicing in K562 cells*. **19th Congress of the European Hematology Association**, Italy on April 29th, 2015.

  *Abstract published

- **Alabouh, H.**, Morse, R., Ladomery, M., Oltean, S., (2014) *Regulation of the alternative splicing of genes involved in leukaemia through the splice factor kinase CLK1 and SRPK1* **EEM Annual meeting**, Lancester, UK on July 6st- 10th 2014.

- **Alabouh, H.**, Ladomery, M., Oltean, S., Morse, R., (2015) *Alternative splicing in CML*. **Non coding RNA conference: New mechanisms and approaches** Boston, USA on May 19th, 2015.

- **Alabouh, H.**, Ladomery, M., Oltean, S., Morse, R., (2016) *Regulation of the alternative splicing of genes involved in leukaemia through the splice factor kinase CLK1 and SRPK1*. **Ideogenesis: the birth of ideas conference** Manchester, UK on October 15th- 16th 2016.